

Quantum-Optical Control Techniques for Atomic Motional States

Von der Fakultät für Mathematik und Physik
der Gottfried Wilhelm Leibniz Universität Hannover
zur Erlangung des Grades

Doktor der Naturwissenschaften
-Dr. rer. nat.-

genehmigte Dissertation
von

Dipl.-Phys. Sönke Schmidt

geboren am 08.09.1982 in Bremerhaven

Erschienen im Jahre

2012

Referent: Prof. Dr. A. Ruschhaupt

Korreferent: Prof. Dr. J. G. Muga

Tag der Promotion: 05.07.2012

Abstract

The present thesis titled “Quantum-Optical Control Techniques for Atomic Motional States” resides in the area of theoretical quantum optics and derives proposals for the development of new laser-based techniques to control and manipulate atoms more efficiently. Such methods are of great interest for various reasons. They allow insights into fundamental physical phenomena and provide important tools in the field of quantum information processing. Moreover, they are an essential premise for atom laser generation and find applications in metrology or interferometry.

Based on their respective objectives, the derived proposals can be divided into three main parts that we now briefly state.

Velocity reduction: One technique to reduce the velocity of atoms in a pulse is based on their reflection from a potential barrier moving in the same direction, which in the following will therefore also be called (atom-)mirror. For a given velocity a classical particle is stopped if the mirror moves with half the particle’s velocity. However, we show that even if the velocity is unknown, a classical particle can be stopped with a mirror moving along a trajectory proportional to a square-root in time. This trajectory can then be used to efficiently slow atoms in a pulse, where the velocities are possibly broadly distributed. This proposal is studied both in one and two dimensions and we demonstrate that it is successful in the classical as well as in the quantum mechanical framework.

Trapping and cooling: Motivated by these results we show that a setup consisting of an atom diode, i.e. a “one-way barrier” for atoms, and a mirror, which have fixed distance and both move along a trajectory proportional to the square-root in time, can be used to trap and cool atoms in a pulse. The atom diode introduces an irreversible step due to spontaneous emission and the atoms become trapped between diode and mirror after passing the former. The acceleration leads to a velocity reduction due to repeated reflections of the atoms. Choosing the distance between diode and mirror appropriately gives rise to a phase-space compression and cooling of the trapped ensemble. We study this setup both in a classical and a quantum mechanical framework and show how it could be realized in principle.

State transfer: Another important technique to control the atomic state is the adiabatic change of the system parameters, which ensures that the state remains an instantaneous eigenstate of the Hamiltonian for all times. However, in many applications it is often preferable that the respective processes are performed as fast as possible, for example to reduce decoherence effects or to improve repetition rates. This objective is in conflict with the fidelity of such a process, since the adiabatic approximation loses its validity for decreasing process times. We propose protocols, with which the initial state can be transferred to the desired final state as in a perfect adiabatic process, but in very short time. The results of applications, for example the cooling of non-interacting atoms via expansion of a harmonic trap or the transport of a Bose-Einstein condensate, show a significant improvement and were already implemented experimentally.

Keywords: laser-based control techniques, atomic motional states, shortcuts to adiabaticity

Schlagworte: laserbasierte Kontrollverfahren, atomare Bewegungszustände, Abkürzungen zur Adiabaticität

Zusammenfassung

Die vorliegende Dissertation mit dem Titel “Quantenoptische Kontrollverfahren für Atomare Bewegungszustände” ist im Bereich der theoretischen Quantenoptik angesiedelt und beinhaltet Vorschläge zur Entwicklung neuer laserbasierter Verfahren zur effizienteren Kontrolle und Manipulation von Atomen. Solche Techniken sind aus einer Vielzahl von Gründen von großem Interesse. Sie ermöglichen Einsicht in fundamentale physikalische Phänomene und sind ein wichtiges Werkzeug im Bereich der Quanteninformationsverarbeitung. Ferner sind sie eine notwendige Voraussetzung für die Entwicklung eines Atom-Lasers und finden Anwendungen in der Metrologie sowie der Interferometrie. Basierend auf ihren jeweiligen Anwendungszielen können diese Vorschläge in drei Hauptbereiche eingeteilt werden und werden anhand dieser kurz dargestellt.

Geschwindigkeitsreduktion: Ein Verfahren zur Verringerung der Geschwindigkeit von Atomen in einem Puls basiert darauf, dass sie von einer in dieselbe Richtung bewegten Potentialbarriere reflektiert werden, die im Folgenden deshalb auch (Atom-) Spiegel genannt wird. Bei gegebener Geschwindigkeit wird ein klassisches Teilchen gestoppt, wenn sich der Spiegel mit der Hälfte dieser Geschwindigkeit bewegt. Wir zeigen darüberhinaus, dass mit einem Spiegel der sich entlang einer Trajektorie proportional zur Quadratwurzel der Zeit bewegt, sogar ein klassisches Teilchen mit unbekannter Geschwindigkeit gestoppt wird. Diese Trajektorie kann dazu verwendet werden, um Atome in einem Puls mit einer breiten Geschwindigkeitsverteilung effizient zu verlangsamen. Dieses Verfahren wird sowohl in einer als auch in zwei Dimensionen untersucht und wir demonstrieren, dass es im Rahmen einer klassischen sowie einer quantenmechanischen Beschreibung erfolgreich angewendet werden kann.

Fangen und kühlen: Motiviert durch diese Ergebnisse zeigen wir, dass eine Anordnung bestehend aus einer Atom-Diode, d.h. einer “Einbahnstraße” für Atome, und einem Spiegel, die einen festen Abstand zueinander haben und sich beide entlang einer Trajektorie proportional zur Quadratwurzel der Zeit bewegen, zum Fangen und Kühlen von Atomen in einem Puls verwendet werden kann. Die Atom-Diode sorgt für einen irreversiblen Schritt durch spontane Emission und die Atome werden zwischen Diode und Spiegel gefangen nachdem sie erstere passiert haben. Die Beschleunigung führt zu einer Geschwindigkeitsreduktion aufgrund wiederholter Reflexion der Atome. Wird der Abstand zwischen Diode und Spiegel geeignet gewählt, so führt dies zu einer Phasenraumkompression und zur Kühlung des gefangenen Ensembles. Wir untersuchen diesen Aufbau sowohl in einem klassischen als auch einem quantenmechanischen Rahmen und zeigen, wie sich dieses Verfahren prinzipiell realisieren ließe.

Zustandsüberführung: Ein anderes wichtiges Verfahren zur Kontrolle des atomaren Zustandes ist die adiabatische Änderung der Systemparameter, die sicherstellt, dass der Zustand für alle Zeiten ein momentaner Eigenzustand des Hamiltonoperators bleibt. In vielen Anwendungen wünscht man jedoch eine möglichst kurze Prozesszeit, um zum Beispiel Dekohärenzeffekte zu reduzieren oder Wiederholungsraten zu steigern. Dies liegt im Widerstreit mit der Güte eines solchen Prozesses, da die adiabatische Approximation für kürzer werdende Prozesszeiten ihre Gültigkeit verliert. Wir stellen Protokolle vor, mit denen sich der Anfangszustand wie in einem perfekt adiabatischen Prozess ohne Abweichungen in den gewünschten finalen Zustand überführen lässt, jedoch in sehr kurzer Zeit. Die Ergebnisse für Anwendungen, wie der Kühlung nicht wechselwirkender Atome durch Expansion einer harmonischen Falle sowie dem Transport eines Bose-Einstein-Kondensates, zeigen eine deutliche Verbesserung und wurden bereits experimentell umgesetzt.

Acknowledgement

It is almost in the nature of such an extensive project like a PhD thesis that one is indebted to a great number of people, without whom it would have been far less successful or even not realisable at all. It is also to be feared that various people, who would deserve at least a written word of gratitude, remain unnamed. I apologize in advance to all of them and hope that they feel adressed nonetheless.

I thank my supervisor Prof. Dr. Andreas Ruschhaupt, who not only introduced me to an interesting topic, but who also accompanied me during my progress all the time. Whenever I had questions or got into an impasse I could be assured of his help.

Furthermore, I thank Prof. Dr. Reinhard Werner, both for his supervision and help in every respect, as well as giving me the opportunity to work in a group for which, especially due to his leadership, it is hard to find the likes not only in scientific, but also in human terms.

With this in mind I also thank the other group members, who create an amazing working atmosphere, and especially I thank Prof. Dr. Tobias Osborne, on whose help I could rely when it was necessary.

I am also indebted to Prof. Dr. Gonzalo Muga for the exceedingly interesting and prolific collaboration, which is mirrored in all results in this thesis, as well as his hospitality and the wonderful time I was allowed to spend in Bilbao.

This gratitude naturally extends to his group, which made it hard for me to leave Bilbao again. Muchas gracias.

Furthermore, I thank Jörg Duhme, Torsten Franz, Florian Richter, Fabian Transchel and Sarah Harrison, who took it upon them to read this thesis and made me aware of smaller and larger problems. Your contributions to this work were invaluable.

Many thanks also to Wiebke Möller, without whose arrangements and dedication many things may have emerged less pleasantly and effortlessly.

In addition I thank Bonnie, Bento, Anna and the rest of the pack. You make my life more worthy of living.

Moreover, I like to use this opportunity to thank some people for being such great friends. In particular these are Marian, Lili, Ludwig, Martin, and above all Marcus and Daniel.

Finally, I like to thank the three most important people in my life. On the one hand these are my parents Undine and Holger Schmidt. An appropriate appreciation of all you did for me would outshine this thesis easily, which is why I restrain myself to thank you for your financial and moral support, on which I could always rely and I hope that one day I will be able to pay back at least a fraction of it. On the other hand Sarah Harrison. Instead of writing all you would deserve, I merely thank you for being as you are: perfect.

Danksagung

Es liegt beinahe in der Natur eines solch umfangreichen Projektes wie einer Doktorarbeit, dass man vielen Menschen zu Dank verpflichtet ist, ohne die dieses entweder weit weniger erfolgreich oder sogar überhaupt nicht in die Tat umgesetzt worden wäre. Auch ist zu befürchten, dass einige Personen, die zumindest ein geschriebenes Dankeswort verdient hätten, ungenannt bleiben. Bei diesen Personen bitte ich bereits jetzt um Entschuldigung und hoffe, dass sie sich dennoch angesprochen fühlen.

Ich bedanke mich bei meinem Betreuer Prof. Dr. Andreas Ruschhaupt, der mich nicht nur in ein überaus interessantes Thema eingeführt, sondern mich auch in all der Zeit bei meinen Fortschritten begleitet hat. Wann immer ich Fragen hatte oder in eine Sackgasse geraten war, konnte ich mir seiner Hilfe sicher sein.

Des Weiteren bedanke ich mich bei Prof. Dr. Reinhard Werner, sowohl für seine Betreuung und Hilfe in jeglicher Hinsicht, als auch mir die Gelegenheit zu geben in einer Arbeitsgruppe zu arbeiten, die insbesondere dank seiner Leitung nicht nur in wissenschaftlicher, sondern auch in menschlicher Hinsicht ihresgleichen sucht.

In diesem Sinne bedanke ich mich auch bei allen anderen Arbeitsgruppenmitgliedern, die eine Atmosphäre schaffen in der es ungemein Spaß bereitet zu arbeiten und insbesondere danke ich Prof. Dr. Tobias Osborne, auf dessen Hilfe ich mich verlassen konnte als es notwendig war.

Zu großem Dank bin ich zudem Prof. Dr. Gonzalo Muga verpflichtet, sowohl für die überaus interessante und fruchtbare Zusammenarbeit, die sich in sämtlichen Ergebnissen dieser Arbeit widerspiegelt, als auch seiner Gastfreundschaft und der großartigen Zeit, die ich in Bilbao verbringen durfte.

Dieser Dank erstreckt sich selbstverständlich auch auf seine Arbeitsgruppe, die es mir schwerfallen ließ Bilbao wieder zu verlassen. Mucias gracias.

Weiterhin danke ich Jörg Duhme, Torsten Franz, Florian Richter, Fabian Transchel und Sarah Harrison, die es auf sich genommen haben diese Arbeit zu lesen und mich auf kleinere und größere Probleme hinzuweisen. Eure Beiträge zu dieser Arbeit waren für mich von unschätzbarem Wert.

Großen Dank verdient zudem Wiebke Möller, ohne deren Organisation und Einsatz vieles vielleicht weniger erfreulich oder mühelos verlaufen wäre.

Weiter danke ich Bonnie, Bento, Anna und dem ganzen Rest der Bande. Ihr macht mein Leben lebenswerter.

Zudem möchte ich die Gelegenheit nutzen mich bei einigen Personen dafür zu bedanken, dass sie solch großartige Freunde sind. Insbesondere sind dies Marian, Lili, Ludwig, Martin und vor allem Marcus und Daniel.

Schließlich danke ich den drei wichtigsten Personen in meinem Leben. Zum einen meinen Eltern Undine und Holger Schmidt. Eine angemessene Würdigung all dessen was ihr für mich getan habt würde diese Arbeit spielend in den Schatten stellen, weshalb ich mich darauf beschränke mich für eure finanzielle und moralische Unterstützung zu bedanken, auf die ich mich immer verlassen konnte und hoffe, dass ich zumindest einen Bruchteil all dessen eines Tages werde zurückgeben können. Zum anderen Sarah Harrison. Anstatt all das zu schreiben, was du verdient hättest, bedanke ich mich lediglich dafür dass du so bist wie du bist: perfekt.

*In memory of Etris, for Sarah, Undine and Holger.
Without you my life would not be as perfect as it is.*

In Erinnerung an Etris, für Sarah, Undine und Holger.
Ohne Euch wäre mein Leben nicht so vollkommen wie es ist.

“Aristotle maintained that women have fewer teeth than men; although he was twice married, it never occurred to him to verify this statement by examining his wives’ mouths.”

Bertrand Russell, *The Impact of Science on Society*

Contents

1	Introduction	1
2	Theoretical Preliminaries	5
2.1	Interaction between a Two-Level Atom and Classical Monochromatic Light	5
2.2	Interaction between a Two-Level Atom and Quantized Light	11
2.3	Spontaneous Emission	13
2.4	The Quantum Jump Approach	18
3	A Quantum Stopper	25
3.1	Introduction	25
3.2	A Quantum Stopper in 1d	26
3.2.1	Classical Particles	26
3.2.2	Quantum Particles	43
3.3	A Quantum Stopper in 2d	63
3.3.1	Classical Particles	63
3.3.2	Quantum Particles	72
3.4	The Quantum Stopper used for Expansion and Compression in 2d . . .	87
3.4.1	Expansion and Compression of a Ring: One Classical Particle . .	87
3.4.2	Expansion and Compression of a Ring: Quantum Particles . . .	91
3.5	Summary and Conclusion	95
4	A Quantum Catcher	97
4.1	Introduction	97
4.2	Classical Particles	98
4.3	Quantum Particles	107
4.4	Summary and Conclusion	121
5	A Shortcut to Adiabaticity	123
5.1	Introduction	123
5.2	Inverse-Invariant Method	125
5.2.1	Invariants of the Hamiltonian	126
5.2.2	Inverse-Invariant Protocol	131
5.3	Applications: Cooling via Expansion of a Harmonic Trap	132
5.3.1	General Considerations	132
5.3.2	Inverse Engineering of Trajectories	136
5.3.3	Comparison to Adiabatic Following	139
5.3.4	Remarks and Experimental Implementation	140
5.3.5	The Effect of Noise	141
5.4	Applications: Transport of a Bose-Einstein Condensate	148
5.4.1	General Considerations	149

5.4.2	Inverse Engineering of Harmonic Transport	149
5.4.3	Anharmonic Transport	152
5.4.4	Effect of Perturbations	153
5.5	Optimal Control of Transport	156
5.6	Summary and Conclusion	169
6	Conclusion and Outlook	171
Appendix		175
A	Effective Potential for an Accelerated Laser	175
B	Numerical Evolution of the Schrödinger Equation with Time-Dependent Potential	179
B.1	Crank-Nicholson Method for Time-Dependent Boundary Conditions	180
B.2	Operator-Splitting for Time-Dependent Hamiltonians	186
C	Perturbation Theory for Time-Dependent Hamiltonians	189
D	Interswitching Time via “Conjugate Point” Method in Optimal Control Theory	193
E	Source Codes for Time-Evolution	197
E.1	Quantum Stopper 1d	197
E.1.1	Classical Particles	197
E.1.2	Quantum Particles: Crank-Nicholson	197
E.1.3	Quantum Particles: Operator-Splitting	203
E.2	Quantum Stopper 2d	204
E.2.1	Classical Particles	204
E.2.2	Quantum Particles: Operator-Splitting	212
E.3	Quantum Stopper 2d: Expansion and Compression	227
E.3.1	Classical Particles	227
E.3.2	Quantum Particles: Operator-Splitting	227
E.4	Quantum Catcher	245
E.4.1	Classical Particles	245
E.4.2	Quantum Particles: Quantum Jump Approach	253
List of Figures		269
List of Tables		277
List of Publications and Bibliography		279

1 Introduction

[Science] is not perfect. It can be misused. It is only a tool. But it is by far the best tool we have, self-correcting, ongoing, applicable to everything. It has two rules. First: there are no sacred truths; all assumptions must be critically examined; arguments from authority are worthless. Second: whatever is inconsistent with the facts must be discarded or revised. ... The obvious is sometimes false; the unexpected is sometimes true.

(Carl Sagan, Cosmos)

Motivation

The control and manipulation of cold atoms is of great interest for various reasons. It allows insights into fundamental physical phenomena and is an important part in the field of quantum information processing as well as an essential premise for atom laser generation. Furthermore, it has applications in metrology or interferometry. Cold atoms are relatively easy to produce and they offer, with respect to other particles, many possibilities for coherent manipulation with lasers, magnetic fields, or mechanical interactions. They may be trapped in artificial lattices, can be guided in effectively one-dimensional wires, or adopt interesting collective behavior; also, their mutual interactions can be changed, or suppressed. All this flexibility facilitates the creation of “control devices” in quantum optics like atom mirrors and diodes.

An essential tool for the control and manipulation of the atomic degrees of freedom in quantum optical experiments is the interaction with a laser. The basic mechanism hereby is the atomic absorption or emission of a photon. The large variety of possible implementations of this seemingly simple process offers applications in abundance.

Over the last decades it has become possible not only to slow down atoms to velocities of the order of centimeters and even millimeters per second, but also to trap them in suitable laser fields. In such traps these atoms can be stored and cooled down further, even to their motional ground state, thereby facilitating experiments to gain insight into the foundations of quantum mechanics. Furthermore, such schemes also lead to the first realizations of simple quantum simulators and are still among the most promising candidates on the way to actually developing a quantum computer of practical use. However, as marvelous as the progress in all these fields has been over the last decades, there is still a plethora of questions to be answered and goals to be achieved. Accomplishing the latter also crucially relies on the design of new schemes to manipulate atoms.

The present work is therefore concerned with the theoretical development of new laser-based techniques, designed to control the atomic motional states, namely to stop, to cool or to transport atoms. The chapters presenting results on these goals contain more detailed introductions into each of the corresponding subjects.

Outline of Thesis

In order to ensure the present work is self-contained, in **Chapter 2** we provide some necessary preliminaries to understand the mechanisms on which the subsequent theoretical proposals are based. These preliminaries contain well-known and basic theoretical results in quantum optics and a more detailed derivation of these can be found in nearly every textbook on this topic.

We propose the “**quantum stopper**” in **Chapter 3**. One technique to alter the atomic velocity is based on its reflection from a uniformly moving potential barrier, or mirror, which, for example, can be created by a detuned laser. Using a mirror with constant velocity is motivated by the fact that a classical particle is stopped if the mirror moves with half the particle velocity at the collision time. However, such schemes, which are already successfully used in experiments, are therefore best suited for atoms with a well-defined velocity. On the other hand, for whole ensembles with a velocity distribution, like atoms in a pulse, they lose their efficiency. We therefore propose a new scheme, making it possible to stop or at least largely reduce the atomic velocity even if the initial velocity is unknown. We show that a mirror moving along a square-root in time trajectory stops a classical particle irrespective of its initial velocity. Using this result still in a classical setting we then consider more realistic conditions and show the efficiency of the method. However, especially for cold atoms, a classical description, also used in most of the preceding studies of this effect, is not sufficient. Therefore we also examine the square-root in time trajectory in the quantum mechanical framework, and show that the method still leads to a similar velocity reduction. Finally, we extend this idea to a two-dimensional setting and study different mirror geometries as well as cooling cycles implemented by the expansion and compression of a ring.

The “**quantum catcher**” is devised in **Chapter 4**. Based on the efficiency of a square-root in time mirror trajectory to reduce the atomic velocity, we design a scheme to trap and simultaneously cool atoms. This scheme consists of an atom diode, i.e. a “one-way barrier” for atoms, followed by a mirror potential. Both the atom diode and the mirror potential move along a square-root in time trajectory and have fixed distance. Atoms passing the atom diode will be slowed due to reflection with the mirror potential and additionally be trapped, since they cannot pass the atom diode from the other direction. They therefore undergo repeated reflections, where the absolute value of the final velocity will always be strictly smaller than the initial velocity. Depending on the initial width of the ensemble in position space and the diode-mirror distance, we also obtain a reduction of the width in position space, which in total leads to a reduction of phase-space volume and cooling of the atomic ensemble.

In **Chapter 5** we propose “**shortcuts to adiabaticity**”. Many applications to control the atomic state rely on the tuning of the parameters of a time-dependent Hamiltonian. Frequently the objective is to transfer the state of the atom from some initial state to a final one, where the initial and final states are instantaneous eigenstates of the corresponding Hamiltonian at the respective times. This can in general be achieved by performing the process adiabatically, i.e. sufficiently slowly. From the adiabatic theorem it then follows that the state remains an eigenstate of the Hamiltonian at all

times. In order to reduce decoherence effects or to increase repetition rates on the other hand, faster processes are often desirable. These then lead to increasing deviations from the final eigenstate, since the adiabatic approximation becomes invalid. Therefore one often faces the problem of finding a compromise between the speed and fidelity of the process. The shortcut to adiabaticity we propose provides, in an idealized, albeit standard scheme, a perfect fidelity of the process in very short time and also proves to be stable with respect to perturbations, i.e. deviations from the idealized setup. The method is based on invariants of the Hamiltonian, which can be designed such that their eigenstates match the Hamiltonians at initial and final times. By fulfilling some auxiliary equations, we then ensure that during the process the state evolves along the invariants basis instead of the adiabatic one. Only after this we deduce the physical trajectories for the process, i.e. in a certain sense “inversely”. This leads in principle to a much faster process than the corresponding adiabatic one as well as those provided by other protocols so far.

In **Chapter 6** we summarize the results and discuss extensions for future work.

Finally, in the **Appendix** we will provide both supplementary material for the analytical studies and more detailed information of the numerical methods applied to obtain the results of this thesis. Furthermore, we additionally provide the source codes used to simulate the different proposed schemes.

2 Theoretical Preliminaries

It is also not possible to make someone accept the methods of physics, just as they are effectively used, if that person refuses a priori the possibility that one can observe objectively real facts, i.e., if that person does not want to accept, as a basis of science, *the completely normal and unconscious behaviour of men with respect to their usual environment as a world of things objectively present and of events being held objectively.*

(Günther Ludwig, A New Foundation of Physical Theories)

2.1 Interaction between a Two-Level Atom and Classical Monochromatic Light

Several proposals in this theses are based on the reflection of atoms from an effective potential induced by a detuned laser. In the following we will therefore briefly discuss the interaction between an atom and a laser, which is in large parts guided by the corresponding, but more detailed, discussion in [5] and can also be found in most other textbooks about quantum optics, i.a. [6, 7]. In many applications, and especially the ones we are proposing, it is a good approximation to consider the atom as a two-level system, since the laser frequency can be adjusted in such a way that it only couples two levels of the atomic spectrum¹. Furthermore, laser light can in good approximation be described classically [6], i.e. we only have to consider the interaction between a two-level quantum system and classical monochromatic light.

We start with the Schrödinger equation (SE) for one quantum particle without spin interacting with the electromagnetic field, which is given by

$$i\hbar \frac{\partial}{\partial t} \psi(\vec{r}, t) = \frac{1}{2m} \left(\frac{\hbar}{i} \nabla - e\vec{A}(\vec{r}, t) \right)^2 \psi(\vec{r}, t) + e\phi(\vec{r}, t) \psi(\vec{r}, t) \quad (2.1)$$

where $\vec{A}(\vec{r}, t)$ is a vector potential and $\phi(\vec{r}, t)$ a scalar potential with

$$\vec{E}(\vec{r}, t) = -\nabla\phi(\vec{r}, t) - \frac{\partial}{\partial t} \vec{A}(\vec{r}, t), \quad \vec{B}(\vec{r}, t) = \nabla \times \vec{A}(\vec{r}, t), \quad (2.2)$$

$\vec{E}(\vec{r}, t)$ and $\vec{B}(\vec{r}, t)$ are the electric and magnetic field respectively, e the electric unit charge and m the mass. Recall that this form of the Schrödinger equation is motivated

¹ In Chapter 4 we will consider a three-level system. However, still only two levels are coupled by a laser and the single transitions in the whole system can be described separately.

by considering the Schrödinger equation with a general potential $V(\vec{r},t)$, i.e.

$$i\hbar\frac{\partial}{\partial t}\psi(\vec{r},t) = \left[-\frac{\hbar^2}{2m}\Delta + V(\vec{r},t) \right] \psi(\vec{r},t), \quad (2.3)$$

and requiring invariance of this equation under a local gauge transformation of the form

$$\tilde{\psi}(\vec{r},t) = e^{\frac{i}{\hbar}e\Lambda(\vec{r},t)}\psi(\vec{r},t). \quad (2.4)$$

The principle of minimal coupling then leads to eq. (2.1), which is exactly that equation invariant under a transformation

$$\tilde{\phi}(\vec{r},t) = \phi(\vec{r},t) - \frac{\partial}{\partial t}\Lambda(\vec{r},t), \quad \tilde{\vec{A}}(\vec{r},t) = \vec{A}(\vec{r},t) + \nabla\Lambda(\vec{r},t), \quad (2.5)$$

which are precisely the transformations not altering $\vec{E}(\vec{r},t)$ and $\vec{B}(\vec{r},t)$.

We now proceed by considering an atom consisting of one proton and one electron, i.e. a hydrogen atom, interacting with an external electromagnetic field and choose the Coulomb gauge, i.e. $\nabla\vec{A}(\vec{r},t) = 0$ and $\phi(\vec{r},t) = 0$. In this gauge, the Hamiltonian H for the combined system of a proton and an electron interacting with an external electromagnetic field is given by

$$\begin{aligned} H &= \frac{\vec{p}_e^2}{2m} - \frac{e}{m_e}\vec{A}(\vec{r}_e,t)\vec{p}_e + \frac{e^2}{2m_e}\vec{A}^2(\vec{r}_e,t) \\ &+ \frac{\vec{p}_p^2}{2m} - \frac{e}{m_p}\vec{A}(\vec{r}_p,t)\vec{p}_p + \frac{e^2}{2m_p}\vec{A}^2(\vec{r}_p,t) \\ &- \frac{1}{4\pi\epsilon_0}\frac{e^2}{|\vec{r}_e - \vec{r}_p|}, \end{aligned} \quad (2.6)$$

where the indices e and p denote the components for the electron and proton respectively. We proceed by applying various approximations to this Hamiltonian such that the problem becomes tractable. However, first we go to the center of mass frame by introducing the new variables

$$\begin{aligned} \vec{P} &= \vec{p}_e + \vec{p}_p, \quad \vec{p} = \frac{m_p}{M}\vec{p}_e - \frac{m_e}{M}\vec{p}_p, \quad M = m_e + m_p, \quad \mu = \frac{m_em_p}{m_e + m_p} \\ \vec{r} &= \vec{r}_e - \vec{r}_p, \quad \vec{R} = \frac{m_p}{M}\vec{r} - \vec{r}_e = \frac{m_e}{M}\vec{r} + \vec{r}_p \end{aligned} \quad (2.7)$$

such that the Hamiltonian can be written as

$$\begin{aligned} H &= \frac{\vec{P}^2}{2M} + \frac{\vec{p}^2}{2\mu} - \frac{1}{4\pi\epsilon_0}\frac{e^2}{|\vec{r}|} \\ &- \frac{e}{m_e}\vec{A}\left(\vec{R} + \frac{m_p}{M}\vec{r},t\right)\left(\frac{m_e}{M}\vec{P} + \vec{p}\right) + \frac{e^2}{2m_e}\vec{A}^2\left(\vec{R} + \frac{m_p}{M}\vec{r},t\right) \\ &+ \frac{e}{m_p}\vec{A}\left(\vec{R} - \frac{m_e}{M}\vec{r},t\right)\left(\frac{m_p}{M}\vec{P} - \vec{p}\right) + \frac{e^2}{2m_p}\vec{A}^2\left(\vec{R} - \frac{m_e}{M}\vec{r},t\right). \end{aligned} \quad (2.8)$$

We now apply the so called dipol approximation, i.e. we assume that the electromagnetic field does only change slightly over an area of the size of an atom and therefore $\vec{A}(\vec{R} + \delta\vec{r}) \approx \vec{A}(\vec{R})$, where $\delta \in]-1, 1[$. The Hamiltonian therefore further simplifies to

$$\begin{aligned} H &= \frac{\vec{P}^2}{2M} + \frac{\vec{p}^2}{2\mu} - \frac{1}{4\pi\epsilon_0} \frac{e^2}{|\vec{r}|} - \frac{e}{\mu} \vec{A}(\vec{R}, t) \vec{p} + \frac{e^2}{2\mu} \vec{A}^2(\vec{R}, t) \\ &= \frac{\vec{P}^2}{2M} + \frac{1}{2\mu} \left(\vec{p} - e\vec{A}(\vec{R}, t) \right)^2 - \frac{1}{4\pi\epsilon_0} \frac{e^2}{|\vec{r}|}. \end{aligned} \quad (2.9)$$

Applying the gauge transformation

$$\tilde{\psi}(\vec{r}, \vec{R}, t) = e^{-\frac{i}{\hbar} e\Lambda(\vec{r}, \vec{R}, t)} \psi(\vec{r}, \vec{R}, t), \quad \Lambda(\vec{r}, \vec{R}, t) = \vec{r} \cdot \vec{A}(\vec{R}, t) \quad (2.10)$$

and using $\nabla_r \Lambda = \vec{A}(\vec{R}, t)$, $\Delta_r \Lambda = 0$ as well as $\frac{\partial}{\partial t} \Lambda = \vec{r} \cdot \frac{\partial}{\partial t} \vec{A}(\vec{R}, t) = -\vec{r} \cdot \vec{E}(\vec{R}, t)$, the Hamiltonian becomes

$$\tilde{H} = \frac{1}{2M} (\vec{P} + e\nabla_R \Lambda)^2 + \left(\frac{\vec{p}^2}{2\mu} - \frac{1}{4\pi\epsilon_0} \frac{e^2}{|\vec{r}|} \right) - e\vec{r} \cdot \vec{E}(\vec{R}, t). \quad (2.11)$$

Assuming $\nabla_R \Lambda \ll 1$ the Hamiltonian further reduces to

$$\tilde{H} = \frac{\vec{P}^2}{2M} + \left(\frac{\vec{p}^2}{2\mu} - \frac{1}{4\pi\epsilon_0} \frac{e^2}{|\vec{r}|} \right) - e\vec{r} \cdot \vec{E}(\vec{R}, t), \quad (2.12)$$

where the second term is the atoms Hamiltonian H_{atom} and the last term the interaction Hamiltonian H_{int} . For some energy eigenstate $\phi_j(\vec{r}) =: |j\rangle$ let us denote the energy eigenvalues of H_{atom} by $\hbar\omega_j$. The atoms Hamiltonian is then given by

$$H_{atom} = \sum_j \hbar\omega_j |j\rangle \langle j|.$$

Assuming we only have to consider two levels, we therefore have

$$H_{atom} = \hbar\omega_1 |1\rangle \langle 1| + \hbar\omega_2 |2\rangle \langle 2|. \quad (2.13)$$

Accordingly, in the energy representation and under the two-level approximation, the interaction Hamiltonian is given by

$$\begin{aligned} H_{int} &= -\{ |1\rangle \langle 1| e\vec{r} |1\rangle \langle 1| + |1\rangle \langle 1| e\vec{r} |2\rangle \langle 2| + |2\rangle \langle 2| e\vec{r} |1\rangle \langle 1| + |2\rangle \langle 2| e\vec{r} |2\rangle \langle 2| \} \vec{E}(\vec{R}, t) \\ &= -\vec{\mu}_D \vec{E}(\vec{R}, t) \end{aligned} \quad (2.14)$$

with the dipol operator $\vec{\mu}_D$ defined by the terms in brackets. Assuming that the states $|1\rangle$ and $|2\rangle$ have well defined parity, we have

$$\langle j| e\vec{r} |j\rangle = \int d^3r |\phi_j(\vec{r})|^2 e\vec{r} = 0, \quad (2.15)$$

since $|\phi_j(\vec{r})|^2$ is symmetric and $e\vec{r}$ antisymmetric. For the Hamiltonian in eq. (2.12) we therefore have

$$H_s = \frac{\vec{P}^2}{2M} + \hbar\omega_1|1\rangle\langle 1| + \hbar\omega_2|2\rangle\langle 2| - \vec{\mu}_D\vec{E}(\vec{R},t), \quad (2.16)$$

with

$$\vec{\mu}_D = |1\rangle\langle 1|e\vec{r}|2\rangle\langle 2| + |2\rangle\langle 2|e\vec{r}|1\rangle\langle 1| = \vec{\mu}_{12}|1\rangle\langle 2| + \vec{\mu}_{12}^*|2\rangle\langle 1|. \quad (2.17)$$

Here where we dropped the tilde to keep the notation clear and introduced the index s to emphasize that this Hamiltonian is given in the Schrödinger picture. The problem of this formulation is that this Hamiltonian is explicitly time-dependent. This can be overcome by going from the Schrödinger picture to the interaction picture and applying the so called rotating wave approximation, i.e. neglecting the fast oscillating time-dependent terms, since their contributions will cancel when averaged over a sufficiently large time interval. Recall that the interaction picture can be viewed as the intermediate picture between the Schrödinger picture, where the time-dependence is carried by the states and the Heisenberg picture, where the time-dependence is carried by the observables¹. Given a state $|\psi_s(t)\rangle$ and Hamiltonian $H_s(t) = H_0 + H_1(t)$ in the Schrödinger picture, we obtain the state $|\psi_i(t)\rangle$ in the interaction picture by

$$|\psi_i(t)\rangle = e^{\frac{i}{\hbar}H_0t} |\psi_s(t)\rangle \quad (2.18)$$

and, by considering the corresponding Schrödinger equation, the Hamiltonian in the interaction picture $H_i(t)$

$$H_i(t) = e^{\frac{i}{\hbar}H_0t} H_1(t) e^{-\frac{i}{\hbar}H_0t}. \quad (2.19)$$

The aim is now to obtain a time-independent interaction Hamiltonian.

We continue by restricting the following analysis to classical monochromatic light, e.g. laser light, that is

$$\vec{E}(\vec{R},t) = \text{Re} \left[\vec{E}_0(\vec{R}) e^{i\vec{k}_L\vec{R} - i\omega_L t} \right], \quad (2.20)$$

where $\vec{E}_0(\vec{R})$ denotes the amplitude, \vec{k}_L the wave vector and ω_L the laser frequency. Furthermore, since we are only interested in the energy difference of the two levels considered, w.l.o.g. we set $\omega_1 \equiv 0$, and we write the Hamiltonian (2.16) in a more convenient form

$$\begin{aligned} H_s &= H_0 - \hbar(\omega_L - \omega_2)|2\rangle\langle 2| + \frac{\vec{P}^2}{2M} - \vec{\mu}_D\vec{E}(\vec{R},t) \\ &= H_0 - \hbar\Delta|2\rangle\langle 2| + \frac{\vec{P}^2}{2M} - \vec{\mu}_D\vec{E}(\vec{R},t), \end{aligned} \quad (2.21)$$

¹ Strictly speaking the equivalence of the different picture only holds in the finite dimensional case.

with $H_0 = \hbar\omega_L|2\rangle\langle 2|$ and detuning $\Delta := \omega_L - \omega_2$. Using eqs. (2.19) and (2.20), the Hamiltonian (2.21) in the interaction picture is given by

$$H_i = e^{it\omega_L|2\rangle\langle 2|} \left\{ \frac{\vec{P}^2}{2M} - \hbar\Delta|2\rangle\langle 2| - \frac{\vec{\mu}_D \cdot \vec{E}_0(\vec{R}) e^{i\vec{k}_L \vec{R} - i\omega_L t} + \vec{E}_0^*(\vec{R}) e^{-i\vec{k}_L \vec{R} + i\omega_L t}}{2} \right\} e^{-it\omega_L|2\rangle\langle 2|}. \quad (2.22)$$

We can further simplify this expression by calculating

$$\begin{aligned} & e^{it\omega_L|2\rangle\langle 2|} |1\rangle\langle 2| e^{-it\omega_L|2\rangle\langle 2|} \\ &= \left[\mathbb{1} + \sum_{n=1}^{\infty} \frac{1}{n!} (it\omega_L)^n (|2\rangle\langle 2|)^n \right] |1\rangle\langle 2| \left[\mathbb{1} + \sum_{m=1}^{\infty} \frac{1}{m!} (-it\omega_L)^m (|2\rangle\langle 2|)^m \right] \\ &= \left[\mathbb{1} + \left(\sum_{n=1}^{\infty} \frac{1}{n!} (it\omega_L)^n \right) |2\rangle\langle 2| \right] |1\rangle\langle 2| \left[\mathbb{1} + \left(\sum_{m=1}^{\infty} \frac{1}{m!} (-it\omega_L)^m \right) |2\rangle\langle 2| \right] \\ &= \left[\mathbb{1} + (e^{it\omega_L} - 1)|2\rangle\langle 2| \right] |1\rangle\langle 2| \left[\mathbb{1} + (e^{-it\omega_L} - 1)|2\rangle\langle 2| \right] \\ &= |1\rangle\langle 2| + (e^{-it\omega_L} - 1)|1\rangle\langle 2| = e^{-it\omega_L} |1\rangle\langle 2| \end{aligned} \quad (2.23)$$

and similarly

$$e^{it\omega_L|2\rangle\langle 2|} |2\rangle\langle 1| e^{-it\omega_L|2\rangle\langle 2|} = e^{it\omega_L} |2\rangle\langle 1| \quad (2.24)$$

which leads to

$$\begin{aligned} H_i &= \frac{\vec{P}^2}{2M} - \hbar\Delta|2\rangle\langle 2| - \frac{\vec{\mu}_{12}|1\rangle\langle 2|}{2} \left\{ \vec{E}_0(\vec{R}) e^{i\vec{k}_L \vec{R} - 2i\omega_L t} + \vec{E}_0^*(\vec{R}) e^{-i\vec{k}_L \vec{R}} \right\} \\ &\quad - \frac{\vec{\mu}_{12}^*|2\rangle\langle 1|}{2} \left\{ \vec{E}_0(\vec{R}) e^{i\vec{k}_L \vec{R}} + \vec{E}_0^*(\vec{R}) e^{-i\vec{k}_L \vec{R} + 2i\omega_L t} \right\}. \end{aligned} \quad (2.25)$$

Finally, we apply the so called rotating wave approximation, i.e. we neglect the fast oscillating terms (which in this case are all the time-dependent terms). Defining the Rabi frequency $\Omega(\vec{R}) := \frac{\vec{\mu}_{12} \vec{E}_0^*(\vec{R})}{\hbar}$ we therefore obtain the Hamiltonian H_i in the rotating wave approximation

$$\begin{aligned} H_i &= \frac{\vec{P}^2}{2M} - \hbar\Delta|2\rangle\langle 2| - \frac{\hbar}{2} \left[|1\rangle\langle 2| \Omega(\vec{R}) e^{-i\vec{k}_L \vec{R}} + |2\rangle\langle 1| \Omega^*(\vec{R}) e^{i\vec{k}_L \vec{R}} \right] \\ &= \frac{\vec{P}^2}{2M} - \frac{\hbar}{2} \begin{pmatrix} 0 & \Omega(\vec{R}) e^{-i\vec{k}_L \vec{R}} \\ \Omega^*(\vec{R}) e^{i\vec{k}_L \vec{R}} & 2\Delta \end{pmatrix}. \end{aligned} \quad (2.26)$$

We now wish to derive the effective potential an atom in the ground state experiences due to the dipol interaction, since for a suitable detuning this realizes a repelling potential leading to a reflection of the atom, which is used in the proposals in Chapters 3 and 4. A common approach is to use a semiclassical description and the Bloch equations [7, 8]. However, here we will present another derivation of this effective potential using the two-level Schrödinger equation with interaction Hamiltonian given by eq. (2.26). Since we only wish to illustrate the general idea at this point, we are content with

a simplified and less strict derivation. A more thorough analysis can be found in [9]. Furthermore, the following analysis as well as the one in [9] apply to the case of a stationary laser considered so far, i.e. a Rabi frequency with time-independent position. This is also enough to demonstrate why the interaction in principle leads to such an effective potential for the atom. However, in the aforementioned chapters the laser will have a time-dependent position and since the effective potential is so important, we will give a more thorough derivation in the time-dependent case in the Appendix A. Componentwise the two-level Schrödinger equation with Hamiltonian (2.26) is given by

$$\begin{aligned} i\hbar\frac{\partial}{\partial t}\Psi^1 &= -\frac{\hbar^2}{2m}\nabla^2\Psi^1 - \frac{\hbar}{2}\Omega(\vec{R})e^{-i\vec{k}_L\vec{R}}\Psi^2 \\ i\hbar\frac{\partial}{\partial t}\Psi^2 &= -\frac{\hbar^2}{2m}\nabla^2\Psi^2 - \frac{\hbar}{2}\Omega^*(\vec{R})e^{i\vec{k}_L\vec{R}}\Psi^1 - \hbar\Delta\Psi^2 \end{aligned} \quad (2.27)$$

with the $\Psi^1 = \Psi^1(\vec{R},t)$ and $\Psi^2 = \Psi^2(\vec{R},t)$ corresponding to $|1\rangle$ and $|2\rangle$ respectively. These are given as a superposition of the stationary eigenvectors $\Phi^{1,E}(\vec{R})$ and $\Phi^{2,E}(\vec{R})$ corresponding to the energy eigenvalue E , i.e.

$$\begin{aligned} \Psi^1(\vec{R},t) &= \int dE e^{-i\frac{E}{\hbar}t}\Phi^{1,E}(\vec{R}) \\ \Psi^2(\vec{R},t) &= \int dE e^{-i\frac{E}{\hbar}t}\Phi^{2,E}(\vec{R}), \end{aligned} \quad (2.28)$$

where $\Phi^{1,E} = \Phi^{1,E}(\vec{R})$ and $\Phi^{2,E} = \Phi^{2,E}(\vec{R})$ are solutions of the stationary equations

$$\begin{aligned} E\Phi^{1,E} &= -\frac{\hbar^2}{2m}\nabla^2\Phi^{1,E} - \frac{\hbar}{2}\Omega(\vec{R})e^{-i\vec{k}_L\vec{R}}\Phi^{2,E} \\ E\Phi^{2,E} &= -\frac{\hbar^2}{2m}\nabla^2\Phi^{2,E} - \frac{\hbar}{2}\Omega^*(\vec{R})e^{i\vec{k}_L\vec{R}}\Phi^{1,E} - \hbar\Delta\Phi^{2,E}. \end{aligned} \quad (2.29)$$

We are interested in the situation where the atom is in the ground state and will derive an effective stationary Schrödinger equation for this state in the case that $\hbar\Delta$ is much larger than the energy eigenvalue and the kinetic term. First we rewrite the expression for $\Phi^{2,E}$ such that

$$\Phi^{2,E} = \frac{1}{E + \frac{\hbar^2}{2m}\nabla^2 + \hbar\Delta} \left(-\frac{\hbar}{2}\Omega^*(\vec{R})e^{i\vec{k}_L\vec{R}} \right) \Phi^{1,E}. \quad (2.30)$$

For large detuning this expression therefore reduces to

$$\Phi^{2,E} \approx -\frac{\Omega^*(\vec{R})e^{i\vec{k}_L\vec{R}}}{2\Delta}\Phi^{1,E}, \quad (2.31)$$

which implies that the probability for the atom to be in state $|2\rangle$ is much smaller than one, i.e. $|\Phi^{2,E}|^2 \ll 1$. Using this approximation for the stationary equation for the

ground state we obtain

$$\begin{aligned} E\Phi^{1,E} &= -\frac{\hbar^2}{2m}\nabla^2\Phi^{1,E} - \frac{\hbar}{2}\Omega(\vec{R})e^{-i\vec{k}_L\vec{R}}\left(-\frac{\Omega^*(\vec{R})e^{i\vec{k}_L\vec{R}}}{2\Delta}\Phi^{1,E}\right) \\ &= -\frac{\hbar^2}{2m}\nabla^2\Phi^{1,E} + \frac{\hbar}{4}\frac{|\Omega(\vec{R})|^2}{\Delta}\Phi^{1,E}, \end{aligned} \quad (2.32)$$

and therefore we have

$$i\hbar\frac{\partial}{\partial t}\Psi^1(\vec{R},t) = -\frac{\hbar^2}{2m}\nabla^2\Psi^1(\vec{R},t) + \frac{\hbar}{4}\frac{|\Omega(\vec{R})|^2}{\Delta}\Psi^1(\vec{R},t), \quad (2.33)$$

where $\frac{\hbar}{4}\frac{|\Omega(\vec{R})|^2}{\Delta}$ is the effective potential. Depending on the detuning this potential is attractive or repulsive. If $\omega_L > \omega_2$ (or generally $\omega_L > \omega_2 - \omega_1$) we have $\Delta > 0$, which is called “blue detuning”, and therefore the atom experiences a repulsive potential. If $\omega_L < \omega_2$ (or generally $\omega_L < \omega_2 - \omega_1$) we have $\Delta < 0$, which is called “red detuning”, and therefore the atom experiences an attractive potential. Although the detuning has to be large compared to the kinetic term, on the other hand it should not be too large compared to the Rabi frequency, since otherwise the potential becomes very small, i.e. only transitions with small detuning relative to the Rabi frequency are effected by the light. This effective potential allows applications in various ways, e.g. to create traps or optical lattices as well as potential barriers or mirrors for neutral atoms. In Chapters 3 and 4 we will use the latter effect for our proposals based on the reflection of atoms from an accelerated potential barrier.

2.2 Interaction between a Two-Level Atom and Quantized Light

In Chapter 4 we will propose a scheme to trap and cool atoms, which is based on effective potentials created by detuned lasers and spontaneous emission. The first part can be described in the framework reviewed in Section 2.1, but for the process of spontaneous emission we need a quantum mechanical description of the electromagnetic field and its interaction with a two-level atom. A derivation of the quantization of the electromagnetic field can be found in nearly every text book on quantum optics, i.a. [5, 6, 7], and will not be discussed here. Instead, we will use that the Hamiltonian for a single polarization s and wave vector \vec{k} is given by a quantized harmonic oscillator, and the complete Hamiltonian is therefore given as the sum over over all s and \vec{k} . In the following we will focus on the interaction between the quantized electromagnetic field and a two-level atom, which is guided by a more detailed discussion in [5].

We start with the Hamiltonian H describing a two-level atom interacting with the electromagnetic field in the Schrödinger picture, where we assume that the atom is at rest at $\vec{r} = 0$, i.e.

$$H_s = H_{atom} + H_{field} + H_{int}, \quad (2.34)$$

with

$$\begin{aligned}
H_{atom} &= \hbar\omega_2|2\rangle\langle 2| + \hbar\omega_1|1\rangle\langle 1| \\
H_{field} &= \sum_s \sum_{\vec{k}} \hbar\omega_{\vec{k}} \hat{a}_{\vec{k}s}^\dagger \hat{a}_{\vec{k}s} \\
H_{int} &= -|1\rangle\langle 2| \vec{\mu}_{12} \vec{E}(0) - |2\rangle\langle 1| \vec{\mu}_{12}^* \vec{E}(0),
\end{aligned} \tag{2.35}$$

the dipol operator $\vec{\mu}_{12}$ defined in eq. (2.17), the electric field operator generally given by

$$\vec{E}(\hat{r}) = \frac{1}{L^{\frac{3}{2}}} \sum_s \sum_{\vec{k}} \sqrt{\frac{\hbar\omega_{\vec{k}}}{2\epsilon_0}} \left\{ i\hat{a}_{\vec{k}s} \vec{\epsilon}_{\vec{k}s} e^{i\vec{k}\hat{r}} - i\hat{a}_{\vec{k}s}^\dagger \vec{\epsilon}_{\vec{k}s}^* e^{-i\vec{k}\hat{r}} \right\}, \tag{2.36}$$

where L as usual denotes the length of the box assumed for quantization. Therefore

$$\vec{E}(0) = \frac{1}{L^{\frac{3}{2}}} \sum_s \sum_{\vec{k}} \sqrt{\frac{\hbar\omega_{\vec{k}}}{2\epsilon_0}} i \left\{ \hat{a}_{\vec{k}s} \vec{\epsilon}_{\vec{k}s} - \hat{a}_{\vec{k}s}^\dagger \vec{\epsilon}_{\vec{k}s}^* \right\}, \tag{2.37}$$

where the creation and annihilation operators $\hat{a}_{\vec{k}s}^\dagger$ and $\hat{a}_{\vec{k}s}$ of the electromagnetic field obey the usual bosonic commutation relations

$$[\hat{a}_{\vec{k}s}^\dagger, \hat{a}_{\vec{k}'s'}^\dagger] = 0, [\hat{a}_{\vec{k}s}, \hat{a}_{\vec{k}'s'}] = 0, [\hat{a}_{\vec{k}s}, \hat{a}_{\vec{k}'s'}^\dagger] = \delta_{\vec{k},\vec{k}'} \delta_{s,s'}. \tag{2.38}$$

Since we are only interested in the energy difference of the two atomic levels, w.l.o.g. again we set $\omega_1 \equiv 0$. Furthermore, once more we change to the interaction picture to apply the rotating wave approximation, see Section 2.1. Defining $H_0 := H_{atom} + H_{field}$ and $H_1 = H_{int}$ we obtain for the Hamiltonian H_i in the interaction picture

$$\begin{aligned}
H_i &= e^{\frac{i}{\hbar}tH_0} H_s e^{-\frac{i}{\hbar}tH_0} = e^{\frac{i}{\hbar}tH_0} H_1 e^{-\frac{i}{\hbar}tH_0} \\
&= -(|1\rangle\langle 2| \vec{\mu}_{12} e^{-i\omega_2 t} + |2\rangle\langle 1| \vec{\mu}_{12}^* e^{i\omega_2 t}) \frac{1}{L^{\frac{3}{2}}} \sum_{s,\vec{k}} \sqrt{\frac{\hbar\omega_{\vec{k}}}{2\epsilon_0}} i \left\{ \hat{a}_{\vec{k}s} \vec{\epsilon}_{\vec{k}s} e^{-i\omega_{\vec{k}} t} - \hat{a}_{\vec{k}s}^\dagger \vec{\epsilon}_{\vec{k}s}^* e^{i\omega_{\vec{k}} t} \right\} \\
&= -i \sqrt{\frac{\hbar\omega_{\vec{k}}}{2\epsilon_0 L^3}} \left\{ |1\rangle\langle 2| \vec{\mu}_{12} \vec{\epsilon}_{\vec{k}s} \hat{a}_{\vec{k}s} e^{-i(\omega_2 + \omega_{\vec{k}})t} - |1\rangle\langle 2| \vec{\mu}_{12} \vec{\epsilon}_{\vec{k}s}^* \hat{a}_{\vec{k}s}^\dagger e^{i(\omega_{\vec{k}} - \omega_2)t} \right. \\
&\quad \left. + |2\rangle\langle 1| \vec{\mu}_{12}^* \vec{\epsilon}_{\vec{k}s} \hat{a}_{\vec{k}s} e^{i(\omega_2 - \omega_{\vec{k}})t} - |2\rangle\langle 1| \vec{\mu}_{12}^* \vec{\epsilon}_{\vec{k}s}^* \hat{a}_{\vec{k}s}^\dagger e^{i(\omega_{\vec{k}} + \omega_2)t} \right\},
\end{aligned} \tag{2.40}$$

where we used

$$\begin{aligned}
e^{\frac{i}{\hbar}tH_{field}} \hat{a}_{\vec{k}s} e^{-\frac{i}{\hbar}tH_{field}} &= \hat{a}_{\vec{k}s} e^{-it\omega_{\vec{k}}} \\
e^{\frac{i}{\hbar}tH_{field}} \hat{a}_{\vec{k}s}^\dagger e^{-\frac{i}{\hbar}tH_{field}} &= \hat{a}_{\vec{k}s}^\dagger e^{it\omega_{\vec{k}}},
\end{aligned}$$

which is straightforward to show using the series expansion of $e^{\pm \frac{i}{\hbar}tH_{field}}$ and the commutation relations for $\hat{a}_{\vec{k}s}^\dagger$ and $\hat{a}_{\vec{k}s}$ given by eq. (2.38). Applying the rotating wave

approximation to this Hamiltonian we finally obtain¹

$$\begin{aligned}
H_i &= i\sqrt{\frac{\hbar\omega_{\vec{k}}}{2\epsilon_0 L^3}} \left\{ |1\rangle\langle 2| \vec{\mu}_{12}^* \vec{\epsilon}_{\vec{k}s}^{\dagger} \hat{a}_{\vec{k}s}^{\dagger} e^{i(\omega_{\vec{k}} - \omega_2)t} - |2\rangle\langle 1| \vec{\mu}_{12}^* \vec{\epsilon}_{\vec{k}s}^{\dagger} \hat{a}_{\vec{k}s} e^{i(\omega_2 - \omega_{\vec{k}})t} \right\} \\
&= |1\rangle\langle 2| \hat{a}_{\vec{k}s}^{\dagger} e^{i\Delta_{\vec{k}} t} \left[i\sqrt{\frac{\hbar\omega_{\vec{k}}}{2\epsilon_0 L^3}} \vec{\mu}_{12}^* \vec{\epsilon}_{\vec{k}s}^{\dagger} \right] + |2\rangle\langle 1| \hat{a}_{\vec{k}s} e^{-i\Delta_{\vec{k}} t} \left[i\sqrt{\frac{\hbar\omega_{\vec{k}}}{2\epsilon_0 L^3}} \vec{\mu}_{12}^* \vec{\epsilon}_{\vec{k}s}^{\dagger} \right]^* \\
&= |1\rangle\langle 2| \hat{a}_{\vec{k}s}^{\dagger} e^{i\Delta_{\vec{k}} t} \hbar g_{\vec{k}s}^* + |2\rangle\langle 1| \hat{a}_{\vec{k}s} e^{-i\Delta_{\vec{k}} t} g_{\vec{k}s}
\end{aligned} \tag{2.41}$$

where we defined the detuning $\Delta_{\vec{k}} := \omega_{\vec{k}} - \omega_2$.

2.3 Spontaneous Emission

In this section we will briefly review the derivation of the master-equation describing spontaneous emission, since we will need it to simulate the trapping and cooling scheme² proposed in Chapter 4. The following discussion is guided by the more detailed description in [6]. For a more general introduction we refer the reader for example to [5, 6, 7, 13, 14, 15]. Furthermore, for a rigorous definition of quantum dynamical semigroups and the derivation of a large class of master-equations see the seminal paper [16].

We will consider the interaction of a two-level atom with the quantized light field, which acts as a bath. The evolution of the whole system consisting of the atom and the reservoir is of course unitary, but far too complex to be solved explicitly due to the degrees of freedom. However, what we are interested in is the time-evolution of the state of the atom, i.e. in the end we will discard the field part, which mathematically corresponds to taking the partial trace with respect to the field. Considering only the subsystem atom of course then leads to a dissipative evolution. Applying different approximations, e.g. the Born approximation and Markov approximation, one obtains a far more tractable equation describing the dynamics of the state of the atom. We will treat the problem in the interaction picture. We start with Hamiltonian H_i in the interaction picture for the system consisting of a two-level atom and the light field, which we derived in Section 2.2 and which is given by

$$\begin{aligned}
H_i(t) &= \hbar \sum_{\vec{k}s} \left[|1\rangle\langle 2| g_{\vec{k}s}^* \hat{a}_{\vec{k}s}^{\dagger} e^{i\Delta_{\vec{k}} t} + |2\rangle\langle 1| g_{\vec{k}s} \hat{a}_{\vec{k}s} e^{-i\Delta_{\vec{k}} t} \right] \\
&= \hbar \left[\sigma_- \hat{F}^{\dagger}(t) + \sigma_+ \hat{F}(t) \right],
\end{aligned} \tag{2.42}$$

where $\sigma_- = |1\rangle\langle 2|$ and $\sigma_+ = |2\rangle\langle 1|$ are the atomic raising and lowering operators, $\hat{F}(t) := \sum_{\vec{k}s} g_{\vec{k}s} \hat{a}_{\vec{k}s} e^{-i\Delta_{\vec{k}} t}$, $\hat{a}_{\vec{k}s}^{\dagger}$ and $\hat{a}_{\vec{k}s}$ are the creation and annihilation operators of

¹ Note that the terms neglected in this approximation correspond to the cases where either a photon is absorbed and a transition from $|2\rangle$ to $|1\rangle$ occurs or a photon is created and a transition from $|1\rangle$ to $|2\rangle$ occurs.

² For a general introduction to laser trapping and cooling we refer the reader to [10, 11]. Furthermore, an interesting study of the notion of temperature can be found in [12].

the electromagnetic field and

$$g_{\vec{k}s} = \frac{1}{\hbar} \sqrt{\frac{\hbar \omega_{\vec{k}}}{2\epsilon_0 L^3}} (-i) \vec{\mu}^* \vec{\epsilon}_{\vec{k}s}, \quad \Delta_{\vec{k}} = \omega_{\vec{k}} - \omega_2. \quad (2.43)$$

Here we set the frequency ω_1 corresponding to the state $|1\rangle$ w.l.o.g. to zero, ω_2 is the frequency corresponding to the excited state $|2\rangle$, $\vec{\mu}$ the dipole moment, $\vec{\epsilon}_{\vec{k}s}$ the polarisation vector, \vec{k} is the wave vector of the electromagnetic field and s the polarisation. Let $\rho(t)$ be the density operator of the whole system, i.e. of the atom and the field. The time-evolution in the interaction picture is given by the von Neumann equation

$$\frac{d}{dt}\rho(t) = -\frac{i}{\hbar}[H_i(t), \rho(t)]. \quad (2.44)$$

Formally integrating this equation with initial condition $\rho(0)$ we obtain the solution

$$\rho(t) = \rho(0) - \frac{i}{\hbar} \int_0^t dt_1 [H_i(t_1), \rho(t_1)],$$

and by repeating this for $\rho(t_1)$ we have

$$\rho(t) = \rho(0) - \frac{i}{\hbar} \int_0^t dt_1 [H_i(t_1), \rho(0)] + \left(-\frac{i}{\hbar}\right)^2 \int_0^t dt_1 \int_0^{t_1} dt_2 [H_i(t_1), [H_i(t_2), \rho(t_2)]].$$

The time-evolution can therefore be written as

$$\frac{d}{dt}\rho(t) = -\frac{i}{\hbar}[H_i(t), \rho(0)] + \left(-\frac{i}{\hbar}\right)^2 \int_0^t dt_1 [H_i(t), [H_i(t_1), \rho(t_1)]].$$

We are actually only interested in the time-evolution of the state of the atom $\rho_a(t)$ which is given as the partial trace over the field of the whole system, i.e. $\rho_a(t) = \text{Tr}_f[\rho(t)]$. The time-evolution of $\rho_a(t)$ is therefore given by

$$\frac{d}{dt}\rho_a(t) = -\frac{i}{\hbar}\text{Tr}_f[H_i(t), \rho(0)] + \left(-\frac{i}{\hbar}\right)^2 \int_0^t dt_1 \text{Tr}_f[H_i(t), [H_i(t_1), \rho(t_1)]]. \quad (2.45)$$

As a remark, note that the state of the atom is the same in the interaction and the Schrödinger picture, since

$$\rho_{a,s}(t) = \text{Tr}_f[e^{-\frac{i}{\hbar}H_0t} \rho_i(t) e^{\frac{i}{\hbar}H_0t}] = \text{Tr}_f[\rho_i(t)] = \rho_{a,i} \quad (2.46)$$

where we used the cyclicity of the trace. We will now proceed with applying different approximations to eq. (2.45). First we assume that initially, i.e. at time $t = 0$, the atom and the field¹ are uncorrelated, such that

$$\rho(0) = \rho_a(0) \otimes \rho_f(0) \quad (2.47)$$

¹ In other words the system and the reservoir.

where $\rho_f(0)$ is the initial state of the field. Furthermore, we assume that the reservoir is large in the sense that it (almost) does not change¹ and use the approximation that the state of the system at some later time t is given by the tensor product of the state of the atom at that time and the state of the field plus terms of the order of the interaction Hamiltonian H_i , i.e.

$$\rho(t) = \rho_a(t) \otimes \rho_f + \mathcal{O}(H_i). \quad (2.48)$$

Using eq. (2.48) in eq. (2.45) and considering only terms up to second order in H_i , which is called the Born approximation, leads to

$$\begin{aligned} \frac{d}{dt}\rho_a(t) &\approx -\frac{i}{\hbar}\text{Tr}_f[H_i(t),\rho_a(0) \otimes \rho_f] \\ &+ \left(-\frac{i}{\hbar}\right)^2 \int_0^t dt_1 \text{Tr}_f[H_i(t),[H_i(t_1),\rho_a(t_1) \otimes \rho_f]]. \end{aligned} \quad (2.49)$$

In the final step we set $\rho_a(t_1) \rightarrow \rho_a(t)$, which can be understood in two different ways. First we can consider the series expansion of $\rho_a(t)$, where for the first order we have $\frac{d}{dt}\rho_a(t) \sim \mathcal{O}(H_i)$. Since the integral is already of second order in H_i , we neglected this term and higher order contributions, because we only consider terms up to order $\mathcal{O}(H_i^2)$. Second we can use the Markov approximation². However, in both cases we obtain for eq. (2.49)

$$\begin{aligned} \frac{d}{dt}\rho_a(t) &\approx -\frac{i}{\hbar}\text{Tr}_f[H_i(t),\rho_a(0) \otimes \rho_f] \\ &+ \left(-\frac{i}{\hbar}\right)^2 \int_0^t dt_1 \text{Tr}_f[H_i(t),[H_i(t_1),\rho_a(t) \otimes \rho_f]], \end{aligned} \quad (2.50)$$

which is the master-equation in the Born-Markov approximation. Using eq. (2.42) we will now evaluate the remaining first and second order terms in eq. (2.50) further. We have

$$\begin{aligned} \text{Tr}_f[H_i(t),\rho_a(0) \otimes \rho_f] &= \text{Tr}_f[\hbar(\sigma_+\rho_a(0)) \otimes (\hat{\Gamma}(t)\rho_f) + \hbar(\sigma_-\rho_a(0)) \otimes (\hat{\Gamma}^\dagger(t)\rho_f) \\ &\quad - \hbar(\rho_a(0)\sigma_+) \otimes (\rho_f\hat{\Gamma}(t)) + \hbar(\rho_a(0)\sigma_-) \otimes (\rho_f\hat{\Gamma}^\dagger(t))] \\ &= \hbar\sigma_+\rho_a(0)\text{Tr}_f[\hat{\Gamma}(t)\rho_f] + \hbar\sigma_-\rho_a(0)\text{Tr}_f[\hat{\Gamma}^\dagger(t)\rho_f] \\ &\quad - \hbar\sigma_+\rho_a(0)\text{Tr}_f[\rho_f\hat{\Gamma}(t)] - \hbar\sigma_-\rho_a(0)\text{Tr}_f[\rho_f\hat{\Gamma}^\dagger(t)] \\ &= \hbar[\sigma_+\text{Tr}_f[\hat{\Gamma}(t)\rho_f] + \sigma_-\text{Tr}_f[\hat{\Gamma}^\dagger(t)\rho_f],\rho_a(0)] \\ &= \hbar[\sigma_+\langle\hat{\Gamma}(t)\rangle + \sigma_-\langle\hat{\Gamma}^\dagger(t)\rangle,\rho_a(0)] \end{aligned} \quad (2.51)$$

¹ This assumption can also be interpreted as photons being absorbed nearly instantly.

² In other words we assume a short memory of the system.

with $\langle \hat{\Gamma}(t) \rangle = \text{Tr}_f[\hat{\Gamma}(t)\rho_f]$. After a similar but lengthy calculation we obtain for the second order term

$$\begin{aligned} & \text{Tr}_f[H_i(t), [H_i(t_1), \rho_a(t) \otimes \rho_f]] \quad (2.52) \\ &= \hbar^2 \{ -2\sigma_+\rho_a(t)\sigma_+ \langle \hat{\Gamma}(t_1)\hat{\Gamma}(t) \rangle - 2\sigma_-\rho_a(t)\sigma_- \langle \hat{\Gamma}^\dagger(t_1)\hat{\Gamma}^\dagger(t) \rangle \\ &+ (\rho_a(t)\sigma_+\sigma_- - \sigma_-\rho_a(t)\sigma_+) \langle \hat{\Gamma}(t_1)\hat{\Gamma}^\dagger(t) \rangle + (\sigma_+\sigma_-\rho_a(t) - \sigma_-\rho_a(t)\sigma_+) \langle \hat{\Gamma}(t)\hat{\Gamma}^\dagger(t_1) \rangle \\ &+ (\sigma_-\sigma_+\rho_a(t) - \sigma_+\rho_a(t)\sigma_-) \langle \hat{\Gamma}^\dagger(t)\hat{\Gamma}(t_1) \rangle + (\rho_a(t)\sigma_-\sigma_+ - \sigma_+\rho_a(t)\sigma_-) \langle \hat{\Gamma}^\dagger(t_1)\hat{\Gamma}(t) \rangle \} \end{aligned}$$

with $\langle \hat{\Gamma}(t_1)\hat{\Gamma}(t) \rangle = \text{Tr}_f[\hat{\Gamma}(t_1)\hat{\Gamma}(t)\rho_f]$. Using these results in eq. (2.50) we obtain the master-equation for a two-level atom interacting with the light field

$$\begin{aligned} \frac{d}{dt}\rho_a(t) &= -i[\sigma_+\langle \hat{\Gamma}(t) \rangle + \sigma_-\langle \hat{\Gamma}^\dagger(t) \rangle, \rho_a(0)] \\ &- \left\{ -2\sigma_+\rho_a(t)\sigma_+ \int_0^t dt' \langle \hat{\Gamma}(t')\hat{\Gamma}(t) \rangle \right. \\ &\quad - 2\sigma_-\rho_a(t)\sigma_- \int_0^t dt' \langle \hat{\Gamma}^\dagger(t')\hat{\Gamma}^\dagger(t) \rangle \\ &\quad + (\rho_a(t)\sigma_+\sigma_- - \sigma_-\rho_a(t)\sigma_+) \int_0^t dt' \langle \hat{\Gamma}(t')\hat{\Gamma}^\dagger(t) \rangle \\ &\quad + (\sigma_+\sigma_-\rho_a(t) - \sigma_-\rho_a(t)\sigma_+) \int_0^t dt' \langle \hat{\Gamma}(t)\hat{\Gamma}^\dagger(t') \rangle \\ &\quad + (\sigma_-\sigma_+\rho_a(t) - \sigma_+\rho_a(t)\sigma_-) \int_0^t dt' \langle \hat{\Gamma}^\dagger(t)\hat{\Gamma}(t') \rangle \\ &\quad \left. + (\rho_a(t)\sigma_-\sigma_+ - \sigma_+\rho_a(t)\sigma_-) \int_0^t dt' \langle \hat{\Gamma}^\dagger(t')\hat{\Gamma}(t) \rangle \right\}. \quad (2.53) \end{aligned}$$

In the following we will determine the master-equation in the case that the field is just the vacuum, i.e. $\rho_f = |0\rangle\langle 0|$, which we will need in the scheme proposed in Chapter 4. Using $\hat{\Gamma}(t) = \sum_{\vec{k}s} g_{\vec{k}s} \hat{a}_{\vec{k}s} e^{-i\Delta_{\vec{k}}t}$ we have

$$\langle \hat{\Gamma}(t) \rangle = \text{Tr}_f[\hat{\Gamma}(t)\rho_f] = \text{Tr}_f\left[\sum_{\vec{k}s} g_{\vec{k}s} \hat{a}_{\vec{k}s} e^{-i\Delta_{\vec{k}}t} |0\rangle\langle 0|\right] = \sum_{\vec{k}s} g_{\vec{k}s} e^{-i\Delta_{\vec{k}}t} \langle 0|\hat{a}_{\vec{k}s}|0\rangle = 0. \quad (2.54)$$

Similarly we obtain

$$\langle \hat{\Gamma}^\dagger(t) \rangle = 0, \quad \langle \hat{\Gamma}(t)\hat{\Gamma}(t') \rangle = 0, \quad \langle \hat{\Gamma}^\dagger(t)\hat{\Gamma}^\dagger(t') \rangle = 0, \quad \langle \hat{\Gamma}^\dagger(t)\hat{\Gamma}(t') \rangle = 0 \quad (2.55)$$

and

$$\langle \hat{\Gamma}(t)\hat{\Gamma}^\dagger(t') \rangle = \sum_{\vec{k}s} \sum_{\vec{k}'s'} g_{\vec{k}s} e^{-i\Delta_{\vec{k}}t} g_{\vec{k}'s'}^* e^{i\Delta_{\vec{k}'}t'} \underbrace{\langle 0|\hat{a}_{\vec{k}s}\hat{a}_{\vec{k}'s'}^\dagger|0\rangle}_{\delta_{\vec{k}\vec{k}'}\delta_{ss'}} = \sum_{\vec{k}s} |g_{\vec{k}s}|^2 e^{-i\Delta_{\vec{k}}(t-t')}. \quad (2.56)$$

For eq. (2.53) we therefore have

$$\begin{aligned} \frac{d}{dt}\rho_a(t) &= -\left\{(\rho_a(t)\sigma_+\sigma_- - \sigma_-\rho_a(t)\sigma_+) \int_0^t dt' \sum_{\vec{k}s} |g_{\vec{k}s}|^2 e^{-i\Delta_{\vec{k}}(t-t')} \right. \\ &\quad \left. + (\sigma_+\sigma_-\rho_a(t) - \sigma_-\rho_a(t)\sigma_+) \int_0^t dt' \sum_{\vec{k}s} |g_{\vec{k}s}|^2 e^{i\Delta_{\vec{k}}(t-t')} \right\}. \end{aligned} \quad (2.57)$$

Using eq. (2.43) and corresponding definitions the integrals in eq. (2.57) can be evaluated approximately. We have

$$\begin{aligned} \int_0^t dt' \sum_{\vec{k}s} |g_{\vec{k}s}|^2 e^{-i\Delta_{\vec{k}}(t-t')} &= \int_0^t dt' \frac{1}{L^3} \sum_{\vec{k}s} \frac{1}{\hbar} \frac{\omega_{\vec{k}}}{2\epsilon_0} |\vec{\mu}_{12}^* \vec{\epsilon}_{\vec{k}s}|^2 e^{-i\Delta_{\vec{k}}(t-t')} \\ &= \int_0^t dt' \left(\frac{1}{L} \sum_{n_x=-\infty}^{\infty} \right) \left(\frac{1}{L} \sum_{n_y=-\infty}^{\infty} \right) \left(\frac{1}{L} \sum_{n_z=-\infty}^{\infty} \right) \sum_s \frac{\omega_{\vec{k}}}{2\hbar\epsilon_0} |\vec{\mu}_{12}^* \vec{\epsilon}_{\vec{k}s}|^2 e^{-i\Delta_{\vec{k}}(t-t')}, \end{aligned}$$

where $k_{x,y,z} = \frac{2\pi}{L}n_{x,y,z}$ and using $\Delta k_{x,y,z} = \frac{2\pi}{L}$ we therefore have

$$\begin{aligned} &\int_0^t dt' \sum_{\vec{k}s} |g_{\vec{k}s}|^2 e^{-i\Delta_{\vec{k}}(t-t')} \\ &\approx \frac{1}{(2\pi)^3} \int_0^t dt' \int_{-\infty}^{\infty} dk_x \int_{-\infty}^{\infty} dk_y \int_{-\infty}^{\infty} dk_z \sum_s \frac{\omega_{\vec{k}}}{2\hbar\epsilon_0} |\vec{\mu}_{12}^* \vec{\epsilon}_{\vec{k}s}|^2 e^{-i\Delta_{\vec{k}}(t-t')} \\ &= \frac{1}{(2\pi)^3} \int_0^t dt' \int_{-\infty}^{\infty} d^3k \frac{\omega_{\vec{k}}}{2\hbar\epsilon_0} \left(\sum_s |\vec{\mu}_{12}^* \vec{\epsilon}_{\vec{k}s}|^2 \right) e^{-i\Delta_{\vec{k}}(t-t')}. \end{aligned} \quad (2.58)$$

Using cylindrical coordinates and the relation $\omega_{|k|} = c|k|$, the integral over k can be written as

$$\int d^3k = \frac{1}{c^3} \int_0^{\infty} d\omega \int_0^{\pi} d\theta \int_0^{2\pi} d\phi \omega^2 \sin\theta. \quad (2.59)$$

Furthermore, using $\vec{\epsilon}_{\vec{k}1} \times \vec{\epsilon}_{\vec{k}2} = \frac{\vec{k}}{|\vec{k}|} = \vec{e}_{\vec{k}}$ and $\vec{k} \cdot \vec{\epsilon}_{\vec{k}s} = 0$ we have

$$\begin{aligned} \sum_{s=1}^2 |\vec{\mu}_{12}^* \vec{\epsilon}_{\vec{k}s}|^2 &= \sum_{s=1}^2 (\vec{\mu}_{12}^* \vec{\epsilon}_{\vec{k}s}) (\vec{\epsilon}_{\vec{k}s}^* \vec{\mu}_{12}) = \vec{\mu}_{12}^* (\vec{\epsilon}_{\vec{k}1} \langle \vec{\epsilon}_{\vec{k}1}^* | \vec{\mu}_{12} \rangle) + \vec{\mu}_{12}^* (\vec{\epsilon}_{\vec{k}2} \langle \vec{\epsilon}_{\vec{k}2}^* | \vec{\mu}_{12} \rangle) \\ &= \vec{\mu}_{12}^* \underbrace{(|\vec{\epsilon}_{\vec{k}1}^* \rangle \langle \vec{\epsilon}_{\vec{k}1}^*| + |\vec{\epsilon}_{\vec{k}2}^* \rangle \langle \vec{\epsilon}_{\vec{k}2}^*|)}_{1 - |\vec{e}_{\vec{k}} \rangle \langle \vec{e}_{\vec{k}}|} \vec{\mu}_{12} = |\vec{\mu}_{12}|^2 - \vec{\mu}_{12}^* \frac{\vec{k}}{|\vec{k}|} \frac{\vec{k}^*}{|\vec{k}|} \vec{\mu}_{12}. \end{aligned} \quad (2.60)$$

We now choose $\vec{\mu}_{12}$ in “z-direction”, i.e. $\vec{\mu}_{12}^* \frac{\vec{k}}{|\vec{k}|} = \vec{\mu}_{12}^* \hat{z} \frac{\vec{k}}{|\vec{k}|} = \vec{\mu}_{12}^* \cos\theta$. Then

$$\sum_{s=1}^2 |\vec{\mu}_{12}^* \vec{\epsilon}_{\vec{k}s}|^2 = |\vec{\mu}_{12}|^2 \sin^2\theta \quad (2.61)$$

and it follows for eq. (2.58)

$$\begin{aligned} & \int_0^t dt' \sum_{\vec{k}_s} |g_{\vec{k}_s}|^2 e^{-i\Delta_{\vec{k}}(t-t')} \\ & \approx \frac{1}{(2\pi)^3} \int_0^t dt' \frac{1}{c^3} \int_0^\infty d\omega \int_0^\pi d\theta \int_0^{2\pi} d\phi \omega^2 \sin\theta \frac{\omega}{2\hbar\epsilon_0} (|\vec{\mu}_{12}|^2 \sin^2\theta) e^{-i(\omega-\omega_2)(t-t')}. \end{aligned} \quad (2.62)$$

Evaluating the integrals over θ and ϕ and setting $\Delta := \omega - \omega_2$ as well as $\tau := t - t'$ we obtain

$$\begin{aligned} & \int_0^t dt' \sum_{\vec{k}_s} |g_{\vec{k}_s}|^2 e^{-i\Delta_{\vec{k}}(t-t')} \approx \frac{1}{6\pi\hbar\epsilon_0 c^3} |\vec{\mu}_{12}|^2 \int_0^t d\tau \int_{-\omega_2}^\infty d\Delta (\omega_2 + \Delta)^3 e^{-i\Delta\tau} \\ & = \frac{\omega_2^3}{6\pi\hbar\epsilon_0 c^3} |\vec{\mu}_{12}|^2 \int_0^{t\omega_2} d\tilde{\tau} \int_{-1}^\infty d\tilde{\Delta} (1 + \tilde{\Delta})^3 e^{-i\tilde{\Delta}\tilde{\tau}}. \end{aligned} \quad (2.63)$$

Since typically $\omega_2 \approx 10^{15}/\text{s}$ and $t \approx 10^{-12}\text{s}$ we have $\omega_2 t \gg 1$ and therefore

$$\begin{aligned} & \int_0^{t\omega_2} d\tilde{\tau} \int_{-1}^\infty d\tilde{\Delta} (1 + \tilde{\Delta})^3 e^{-i\tilde{\Delta}\tilde{\tau}} \approx \int_0^\infty d\tilde{\tau} \int_{-1}^\infty d\tilde{\Delta} (1 + \tilde{\Delta})^3 e^{-i\tilde{\Delta}\tilde{\tau}} \\ & = \int_{-1}^\infty d\tilde{\Delta} (1 + \tilde{\Delta})^3 \underbrace{\int_0^\infty d\tilde{\tau} e^{-i\tilde{\Delta}\tilde{\tau}}}_{\pi\delta(\tilde{\Delta}) - \frac{1}{i}\mathcal{P}\frac{1}{\tilde{\Delta}}} = \pi - \frac{1}{i} \int_{-1}^\infty d\tilde{\Delta} \mathcal{P}\frac{1}{\tilde{\Delta}} (1 + \tilde{\Delta})^3. \end{aligned} \quad (2.64)$$

The last term is the so called ‘‘line-shift’’. Neglecting this contribution we obtain

$$\int_0^t dt' \sum_{\vec{k}_s} |g_{\vec{k}_s}|^2 e^{-i\Delta_{\vec{k}}(t-t')} = \frac{\omega_2^3 |\vec{\mu}_{12}|^2}{6\pi\hbar\epsilon_0 c^3} =: \frac{\gamma}{2} \quad (2.65)$$

where $\gamma \in \mathbb{R}$ is called the Einstein coefficient. Using these results in eq. (2.57) we therefore finally obtain

$$\begin{aligned} \frac{d}{dt}\rho_a(t) & = \frac{\gamma}{2} \left\{ -\rho_a(t)\sigma_+\sigma_- + 2\sigma_-\rho_a(t)\sigma_+ - \sigma_+\sigma_-\rho_a(t) \right\} \\ & = \frac{\gamma}{2} \left\{ -\rho_a(t)|2\rangle\langle 2| + 2|1\rangle\langle 2|\rho_a(t)|2\rangle\langle 1| - |2\rangle\langle 2|\rho_a(t) \right\} \end{aligned} \quad (2.66)$$

with γ defined in eq. (2.65).

2.4 The Quantum Jump Approach

In this section we will introduce a method called quantum jump approach, Monte-Carlo wavefunction approach or quantum trajectory approach [13, 17, 18] and which can be used to numerically solve master-equations. We will apply this method to obtain the results presented in Chapter 4, where we have to solve the master-equation describing a three-level atom interacting with a laser including spontaneous emission. In the following we will therefore first describe the general ansatz of this method and then apply it to our specific problem.

Although we consider a three-level atom in Chapter 4, the laser only couples two of these levels as does the transition due to spontaneous emission only occur between two of them. Therefore we can use the result from the previous section, where we derived the master-equation describing spontaneous emission for a two-level atom in the vacuum in the Born-Markov approximation, which is given by eq. (2.66). This master-equation has to be extended by taking the additional coupling to a laser into account, i.e. the complete master-equation for the density operator of a two-level atom interacting with a laser including spontaneous emission is given by

$$\frac{d}{dt}\rho_a(t) = -\frac{i}{\hbar} [H_L, \rho_a(t)]_- - \frac{\gamma}{2} \{ \rho_a(t) |2\rangle\langle 2| + |2\rangle\langle 2| \rho_a(t) \} + \gamma |1\rangle\langle 2| \rho_a(t) |2\rangle\langle 1|. \quad (2.67)$$

We will present the algorithm based on the quantum jump approach to solve this equation after introducing the general concept. A generic master-equation describing the time evolution of the atomic state can be written as [13]

$$\frac{d}{dt}\rho_a(t) = \Lambda(\rho_a(t)) = \Lambda\rho_a(t) \quad (2.68)$$

with Λ being a (linear) superoperator and furthermore

$$\frac{d}{dt}\rho_a(t) = \Lambda\rho_a(t) = (\Lambda_0 + \alpha J(t))\rho_a(t), \quad (2.69)$$

with some initial Λ_0 . We now make the Ansatz

$$\rho_a(t) = e^{t\Lambda_0} \tilde{\rho}_a(t) \quad (2.70)$$

such that

$$\frac{d}{dt}\rho_a(t) = \Lambda_0\rho_a(t) + e^{t\Lambda_0} \frac{d}{dt} \tilde{\rho}_a(t) \stackrel{!}{=} \Lambda_0\rho_a(t) + \alpha J(t) e^{t\Lambda_0} \tilde{\rho}_a(t). \quad (2.71)$$

Therefore it follows that

$$\frac{d}{dt} \tilde{\rho}_a(t) \stackrel{!}{=} \alpha e^{-t\Lambda_0} J(t) e^{t\Lambda_0} \tilde{\rho}_a(t). \quad (2.72)$$

Formally integrating this differential equation we obtain

$$\tilde{\rho}_a(t) = \tilde{\rho}_a(0) + \alpha \int_0^t dt_1 \alpha e^{-t_1\Lambda_0} J(t_1) e^{t_1\Lambda_0} \tilde{\rho}_a(t_1).$$

Multiplying this equation by $e^{t\Lambda_0}$ we obtain for $\rho_a(t)$

$$\rho_a(t) = e^{t\Lambda_0} \rho_a(0) + \alpha \int_0^t dt_1 e^{(t-t_1)\Lambda_0} J(t_1) \rho_a(t_1). \quad (2.73)$$

Repeating this process for $\rho_a(t_i)$, $i \in \mathbb{N}_+$, we have

$$\begin{aligned}
\rho_a(t) &= e^{t\Lambda_0} \rho_a(0) + \alpha \int_0^t dt_1 e^{(t-t_1)\Lambda_0} J(t_1) e^{t_1\Lambda_0} \rho_a(0) \\
&+ \alpha^2 \int_0^t dt_1 e^{(t-t_1)\Lambda_0} J(t_1) \int_0^{t_1} dt_2 e^{(t_1-t_2)\Lambda_0} J(t_2) \rho_a(t_2) \\
&= e^{t\Lambda_0} \rho_a(0) + \alpha \int_0^t dt_1 e^{(t-t_1)\Lambda_0} J(t_1) e^{(t_1-0)\Lambda_0} \rho_a(0) \\
&+ \alpha^2 \int_0^t dt_2 \int_0^{t_2} dt_1 e^{(t-t_2)\Lambda_0} J(t_2) e^{(t_2-t_1)\Lambda_0} J(t_1) e^{(t_1-0)\Lambda_0} \rho_a(0) \\
&+ \mathcal{O}(\alpha^3).
\end{aligned}$$

By induction this leads to

$$\begin{aligned}
\rho_a(t) &= \sum_{m=0}^{\infty} \alpha^m \int_0^t dt_m \dots \int_0^{t_2} dt_1 \\
&\left[e^{(t-t_m)\Lambda_0} J(t_m) e^{(t_m-t_{m-1})\Lambda_0} J(t_{m-1}) \dots J(t_1) e^{(t_1-0)\Lambda_0} \right] \rho_a(0)
\end{aligned}$$

which is formally a Dyson series. Setting¹

$$\tilde{\rho}_m(t, t_1, \dots, t_m) := e^{(t-t_m)\Lambda_0} J(t_m) \dots J(t_1) e^{(t_1-0)\Lambda_0} \rho_a(0) \quad (2.74)$$

it follows that

$$\rho_a(t) = \sum_{m=0}^{\infty} \alpha^m \int_0^t dt_m \dots \int_0^{t_2} dt_1 \tilde{\rho}_m(t, t_1, \dots, t_m). \quad (2.75)$$

We call $\tilde{\rho}_m(t, t_1, \dots, t_m)$ a ‘‘trajectory’’ and the events $J(t_i)$ occurring at times t_i between free time-evolution ‘‘jumps’’. We now have to make the connection to the master-equation given by eq. (2.67) and wish to determine the atomic state at time t which is given by eq. (2.75). We therefore set

$$J\rho_a(t) := \gamma |1\rangle\langle 2| \rho_a(t) |2\rangle\langle 1| = \gamma \sigma_- \rho_a(t) \sigma_+ \quad (2.76)$$

which describes a jump from $|2\rangle$ to $|1\rangle$. Then

$$\begin{aligned}
\Lambda_0 \rho_a(t) &= -\frac{i}{\hbar} [H_L, \rho_a(t)]_- - \frac{\gamma}{2} (\rho_a(t) |2\rangle\langle 2| + |2\rangle\langle 2| \rho_a(t)) \\
&= -\frac{i}{\hbar} [H_L, \rho_a(t)]_- - \frac{\gamma}{2} \{\rho_a(t), |2\rangle\langle 2|\}_+.
\end{aligned} \quad (2.77)$$

Let $\rho_a(t)$ be initially a pure state, i.e.

$$\rho_a(0) = |\Psi(0)\rangle\langle \Psi(0)|. \quad (2.78)$$

1 As a remark, in [13] we have $\tilde{\rho}_m(t, t_1, \dots, t_m) = \tilde{\rho}_c(t)$.

We will now treat the time-evolution piecewise by considering alternately the free time-evolutions and the subsequent jumps. We begin with the conditional state $\rho_c(t)$ given by

$$\rho_c(t) = e^{t\Lambda_0} \rho_c(0) = e^{t\Lambda_0} \rho_a(0), \quad (2.79)$$

i.e. this state describes the time-evolution until a jump occurs, and therefore

$$\frac{d}{dt} \rho_c(t) = \Lambda_0 \rho_c(t). \quad (2.80)$$

Using the Ansatz that $\rho_c(t)$ is also given by a pure state, i.e.

$$\rho_c(t) = |\Psi_c(t)\rangle \langle \Psi_c(t)|, \quad (2.81)$$

for eq. (2.80) it follows that

$$\begin{aligned} & \left(\frac{d}{dt} |\Psi_c(t)\rangle \right) \langle \Psi_c(t)| + |\Psi_c(t)\rangle \left(\frac{d}{dt} \langle \Psi_c(t)| \right) \\ &= -\frac{i}{\hbar} H_L |\Psi_c(t)\rangle \langle \Psi_c(t)| + \frac{i}{\hbar} |\Psi_c(t)\rangle \langle \Psi_c(t)| H_L \\ & \quad - \frac{\gamma}{2} \left(|\Psi_c(t)\rangle \langle \Psi_c(t)| 2 \langle 2| + |2\rangle \langle 2| \Psi_c(t)\rangle \langle \Psi_c(t)| \right) \\ &= \left[-\frac{i}{\hbar} H_L - \frac{\gamma}{2} |2\rangle \langle 2| \right] |\Psi_c(t)\rangle \langle \Psi_c(t)| + |\Psi_c(t)\rangle \langle \Psi_c(t)| \left[\frac{i}{\hbar} H_L - \frac{\gamma}{2} |2\rangle \langle 2| \right], \end{aligned} \quad (2.82)$$

i.e. the state remains pure. This is equivalent to

$$i\hbar \frac{d}{dt} |\Psi_c(t)\rangle = \left[H_L - i\frac{\hbar}{2} \gamma |2\rangle \langle 2| \right] |\Psi_c(t)\rangle. \quad (2.83)$$

For some initial state $|\Psi_c(0)\rangle$, the state $|\Psi_c(t)\rangle$ is therefore given by

$$|\Psi_c(t)\rangle = e^{-\frac{i}{\hbar} t H_c} |\Psi_c(0)\rangle \quad (2.84)$$

where H_c is the conditional Hamiltonian given by

$$H_c = H_L - i\frac{\hbar}{2} \gamma |2\rangle \langle 2|. \quad (2.85)$$

This Hamiltonian is apparently not hermitian and therefore the time-evolution is not unitary, instead the norm decreases with time¹. Furthermore, consider

$$J\rho_c(t) = \gamma |1\rangle \langle 2| \Psi_c(t)\rangle \langle \Psi_c(t)| 2 \langle 1| = |\tilde{\Psi}_c\rangle \langle \tilde{\Psi}_c| \quad (2.86)$$

where we defined

$$|\tilde{\Psi}_c\rangle = \sqrt{\gamma} |1\rangle \langle 2| \Psi_c(t)\rangle = \tilde{J} \Psi_c(t), \quad (2.87)$$

¹ In other words the unitary evolution operator is altered to a semigroup of contractions generated by H_c , i.e. operators $V_t = e^{-\frac{i}{\hbar} t H_c}$ with $\|V_t\| \leq 1$.

i.e. the state remains pure too. Summarizing, starting with a pure state $\rho_a(0) = |\Psi_a(0)\rangle\langle\Psi_a(0)| = |\Psi_c(0)\rangle\langle\Psi_c(0)|$ we have

$$e^{tA_0}|\Psi_c(0)\rangle\langle\Psi_c(0)| = \left\{ e^{-\frac{i}{\hbar}tH_c} |\Psi_c(0)\rangle \right\} \left\{ \langle\Psi_c(0)| e^{\frac{i}{\hbar}tH_c^\dagger} \right\}, \quad (2.88)$$

with the conditional Hamiltonian given by eq. (2.85) and

$$J|\Psi_c(0)\rangle\langle\Psi_c(0)| = \left\{ \tilde{J} |\Psi_c(0)\rangle \right\} \left\{ \langle\Psi_c(0)| \tilde{J}^\dagger \right\}, \quad (2.89)$$

with \tilde{J} defined in eq. (2.86). Therefore it finally follows for eq. (2.75) that

$$\rho_a(t) = \sum_{m=0}^{\infty} \int_0^t dt_m \dots \int_0^{t_2} dt_1 \left\{ e^{-\frac{i}{\hbar}(t-t_m)H_c} \tilde{J} e^{-\frac{i}{\hbar}(t_m-t_{m-1})H_c} \dots \tilde{J} e^{-\frac{i}{\hbar}t_1 H_c} |\Psi_c(0)\rangle \right\} \left\{ \langle\Psi_c(0)| e^{\frac{i}{\hbar}t_1 H_c^\dagger} \tilde{J}^\dagger e^{\frac{i}{\hbar}(t_2-t_1)H_c} \dots \tilde{J}^\dagger e^{\frac{i}{\hbar}(t-t_m)H_c^\dagger} \right\}. \quad (2.90)$$

We can now numerically solve this equation for the density operator with the following algorithm¹ [19]

Quantum Jump Algorithm

Step 1: *Initialization*

Set $t_0 = 0$ and chose an initial state $|\Psi_c(0)\rangle = |\Psi_a(0)\rangle$ with $\|\Psi_c(0)\| = 1$.

Step 2: *Randomness*

Choose a uniformly distributed random number $r \in [0,1[$.

Step 3: *Time-Evolution*

Evolve $|\Psi_c(t)\rangle$ in time via solving the ‘‘Schrödinger equation’’

$$i\hbar \frac{d}{dt} |\Psi_c(t)\rangle = H_c |\Psi_c(t)\rangle,$$

with H_c given by eq. (2.85), until t_1 which is determined by

$$r \stackrel{!}{=} 1 - \|\Psi_c(t_1)\|^2 = \underbrace{\int_{t_0}^{t_1} dt' \langle\Psi_c(t')|\tilde{J}^\dagger \tilde{J}|\Psi_c(t')\rangle}_{\text{probability for jump in the interval } [t_0, t_1]}.$$

Step 4: *Spontaneous Emission and Renormalization*

A photon is emitted spontaneously, i.e. a jump occurs and the next part of the free time-evolution begins with the renormalized state given by

$$|\Psi_c(t_1)\rangle \rightarrow \frac{\tilde{J}|\Psi_c(t_1)\rangle}{\|\tilde{J}|\Psi_c(t_1)\rangle\|}.$$

¹ There are other versions of this algorithm, but the one given below was used in the numerical simulations performed to derive the results in Chapter 4.

Quantum Jump Algorithm

Step 5: *Repeat procedure*
Go back to *Step 2* with t_1 instead of t_0 .

Step 6: *Terminate*
Stop when $t = t_{final}$ and renormalize again to obtain the final state, i.e.

$$|\Psi_c(t_{final})\rangle \rightarrow \frac{|\Psi_c(t_{final})\rangle}{\| |\Psi_c(t_{final})\rangle \|}.$$

Step 7: *Averaging*
Sum over a sufficiently large number N of these renormalized final states $|\Psi_{c,n}(t_{final})\rangle$, $n = 1, 2, \dots, N$. This then constitutes an approximate solution of the master-equation (2.67) given by eq. (2.90), i.e. we have

$$\rho_a(t) \approx \frac{1}{N} \sum_{n=1}^N |\Psi_{c,n}(t_{final})\rangle \langle \Psi_{c,n}(t_{final})|.$$

3 A Quantum Stopper

Truth in science can be defined as the working hypothesis best suited to open the way to the next better one.

(Konrad Z. Lorenz)

3.1 Introduction

Particles in a beam or pulse can be slowed down by reflection from a potential wall (or, as we will often call it, a “mirror”) that moves in the same direction. An early example demonstrating this is the production of a beam of ultracold neutrons colliding with a moving Ni-surface [20]. Moving mirrors for cold atoms have also been implemented with a time-modulated, blue-detuned evanescent light wave propagating along the surface of a glass prism [21, 22, 23]. More recently, Helium atoms in a beam have been slowed down using a Si-crystal on a spinning rotor [24, 25]. Also, Rubidium atoms have been stopped with a moving magnetic mirror on a conveyor belt [26], which provides a promising mechanism to generate a continuous, intense and slow beam of atoms. Furthermore, a state-dependent potential for Rubidium created by a laser beam has, for example, been implemented in [27]. There is clearly a great potential for practical applications of such processes and much interest in their fundamental properties and optimization [24, 28]. In most cases the analysis is made with classical trajectories, but quantum motion effects may become important for ultracold atoms, as shown in a recent study on matter-wave/moving-mirror interaction [29]. One further limitation of standard settings so far is that for a fixed mirror velocity only pulses of particles with a specific and well defined initial velocity are stopped. The following analysis focuses on atoms in a pulse¹ and we will consider the more general case where the initial velocities of these atoms are arbitrary, possibly broadly distributed, or unknown. Stopping a pulse in these conditions is a much more challenging objective, and the central subject of this chapter.

This chapter is organized as follows. In Section 3.2 we will examine the problem of stopping a pulse of particles in one dimension in the classical and in the quantum case. Since in the quantum mechanical description we use that such a mirror potential can be created via a suitably detuned laser, we refer the reader to Section 2.1 and Appendix A, where we show how the interaction between a two-level atom in the ground state and a detuned laser can be described by an effective potential. Motivated by these results we will treat the problem in Section 3.3 in two dimensions, firstly to provide an even more realistic description and secondly to explore effects not appearing in the

¹ This is the fixed frame of reference in the remainder of this chapter. Any subsequent comparisons, e.g. claims of superiority, are to be understood with respect to this context.

one dimensional situation. Finally in Section 3.4 we will study if this efficient way of stopping particles in a pulse can also be used to implement cooling cycles. This work was completed in collaboration with J. G. Muga and A. Ruschhaupt.

3.2 A Quantum Stopper in 1d

In this section we will examine the problem of stopping particles in a pulse in one dimension. In 3.2.1 we will first consider one particle with unknown velocity in an idealized and classical setup and derive a trajectory with which to stop such a particle. Afterwards we will apply this solution to the stopping of classical particles in a pulse. In 3.2.2 we will then study the problem in the quantum mechanical framework. There we will give both analytical and numerical results, showing that the method works in the quantum case as well. Furthermore we will show that, loosely speaking, it is optimal compared to any linear-in-time mirror trajectory in the sense that only for the trajectory derived below, the average energy for every mode tends to zero in the limit of infinite time. The results in Section 3.2.1, and partially those in 3.2.2 were published in [1].

3.2.1 Classical Particles

One Classical Particle and One Moving Mirror under Ideal Conditions

The general question we want to answer in this section can loosely be stated as

*Can we stop a classical particle of **unknown** velocity with a moving hard wall?*

We will show that the answer to this question is in fact yes, and that the trajectory of such a wall is very simple.

We start with an idealized situation by assuming a classical point-particle emitted at $x_s = 0$, $t_0 = 0$, moving with unknown velocity $v_s \geq 0$ along x . A heavy hard wall (compared to the mass of the particle) moves in front of the particle with trajectory $x_m(t)$, where by “heavy” we always mean that the reflection is elastic, i.e. there is no momentum transfer from the particle to the wall, and by “hard” that no particle can penetrate the wall. If the particle with velocity v_s collides with the wall at time t_c and the wall is moving with velocity $v_m(t_c)$ at t_c , then the final velocity v_f of the particle after a perfect reflection is given by

$$v_f = -v_s + 2v_m(t_c). \quad (3.1)$$

This is straightforward to see using the reference frame in which the mirror is at rest at time t_c . The initial and final velocity \tilde{v}_s , \tilde{v}_f in this reference frame are simply given by $\tilde{v}_s = v_s - v_m(t_c)$ and $\tilde{v}_f = v_f - v_m(t_c)$. Furthermore, we have the relation $\tilde{v}_f = -\tilde{v}_s$. Returning to the laboratory frame one obtains eq. (3.1).

To fulfill the goal that the particle is at rest in the laboratory frame after the collision, the mirror velocity should be $v_m(t_c) = v_s/2$ at the time of the collision. Since the trajectory of the particle with velocity $v_s > 0$ is $x(t) = v_s t$ and the trajectory of the mirror is $x_m(t)$, the time t_c of the collision is given as a solution of $x_m(t_c) = v_s t_c$. The

condition for stopping the particle is now

$$\frac{dx_m}{dt}(t_c) = v_m(t_c) = \frac{v_s}{2}. \quad (3.2)$$

This condition is actually used in experiments, where the mirror velocity is usually held constant and is, depending on the situation, chosen in the most efficient way. However, usually one is interested in slowing an ensemble of atoms, where not all atoms have the same velocity and instead one has to deal with a velocity distribution. A common compromise and the optimal solution for a mirror with constant velocity is to use half the mean velocity of the ensemble as the mirror velocity. However, this poses the problem that the more the particle velocity deviates from this value, the less efficient the slowing becomes.

The question of interest therefore becomes, if it is possible to stop a particle independent of its initial velocity. This is closely related¹ to stopping an ensemble of non-interacting particles with different velocities. We will study this more general problem after giving the solution to the idealized one particle problem.

So far we only considered a mirror with constant velocity, but to fulfill the condition for stopping it is only necessary that the mirror moves with half the particle velocity when the collision occurs, i.e. at the collision time t_c . We now use the simple fact, that at time t_c the particle and the mirror have to have the same position, i.e. $v_s = x_m(t_c)/t_c$. Using this in eq. (3.2) we therefore obtain the ordinary differential equation (ODE)

$$\frac{dx_m}{dt}(t_c) = \frac{x_m(t_c)}{2t_c}. \quad (3.3)$$

The trajectory for the mirror we are looking for is found as the solution of this ordinary differential equation with the initial condition $x_m(0) = 0$, i.e. we have:

A mirror potential moving in front of a particle, which starts at position $x_s = 0$ and moves with constant, but arbitrary velocity $v_s > 0$, stops this particle independent of its initial velocity, if it moves along a trajectory

$$x_m(t) = \alpha\sqrt{t}, \quad 0 < \alpha \in \mathbb{R}, \quad (3.4)$$

which is obtained by solving the ODE given by eq. (3.3) with initial condition $x_m(0) = 0$.

The parameter α is in principle arbitrary, but its value will determine the location and time of the particle-mirror collision, which is quite important in a practical implementation with limited space and time. The situation for two particles with different initial velocities is depicted in Fig. 3.1. Every ray from the origin, describing the trajectory of a particle with initial velocity v_s , is transformed into a horizontal line, i.e. it has final velocity zero.

Note that the velocity of the wall $dx_m(t)/dt$ would be infinite at $t = 0$ according to eq.

¹ To describe the situation for an ensemble of non-interacting particles we additionally have to consider a position distribution.

(3.4). In practice the trajectory given by eq. (3.4) may be approximated by one with finite velocity, e.g. truncating or shifting the short time segment of the trajectory, see Section 3.2.2 for an example. This would only affect very fast particles so one could design the truncation depending on the maximal velocity in such a way, that the mirror starts moving along a square-root in time trajectory before the fastest particle could arrive and thus has negligible effects in practice.

Instead of α we will deal for now with more intuitive and physically meaningful parameters¹. We assume a final time t_f , which may be a maximal time we are ready to consider in our experiment. At this time, the wall has moved a distance d (see Fig. 3.1), so we have $\alpha = d/\sqrt{t_f}$. Another important quantity is $v_b := d/t_f$, the boundary velocity for no collision until t_f , i.e., a particle with an initial velocity $v_s < v_b$ will not hit the mirror before t_f .

One Classical Particle and One Moving Mirror under Realistic Conditions

The considerations above apply only to the one-particle case, but actually we want to stop an ensemble of particles, which not only has a velocity distribution, but also a position distribution. We will therefore now allow a more general scenario where the initial position of the particle at $t = 0$ is not necessarily zero but $x(0) = x_s \leq 0$, as for particles in a pulse². We are interested in the particle's final position x_f and velocity v_f at t_f . It is useful to introduce dimensionless variables to simplify the notation in the following, namely

$$\chi = \frac{x}{d}, \nu = \frac{v}{v_b}, \tau = \frac{t}{t_f}. \quad (3.5)$$

It is now straightforward to calculate the final velocity and position of the particle, $\nu_f(\chi_s, \nu_s)$ and $\chi_f(\chi_s, \nu_s)$, depending on the initial values. The collision time is easily calculated via the relation $\chi_s + \nu_s \tau_c = \sqrt{\tau_c}$, again simply expressing the fact that mirror and particle have the same position at t_c . This can now be used to first calculate $\nu_f(\chi_s, \nu_s)$ via the relation (3.1) in dimensionless variables, and then to calculate $\chi_f(\chi_s, \nu_s)$ using $\chi_s + \nu_s \tau_c = \chi_f - \nu_f \tau_c$.

1 However, later we will also use α again, since it can be more convenient depending on the situation.
 2 For a hard wall of course it is not useful to consider $x(0) = x_s \geq 0$, because this would lead to a positive acceleration, but one could imagine a diodic device instead, similar to the one in Chapter 4, which would overtake the particle at first and then slow it when the particle catches up again. Furthermore, we could consider particles starting in front of the mirror, but with a shifted position and a velocity such that they would have started behind the mirror for an earlier time. This situation can be described via a mirror trajectory $\alpha\sqrt{t} + t_0$, $t_0 > 0$, which is interesting in its own right and will be considered below.

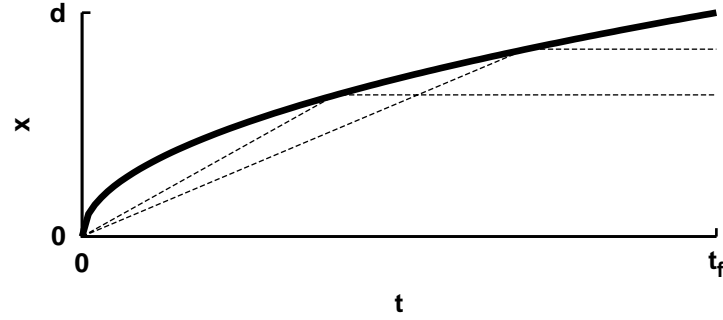


Figure 3.1: Scheme of the stopping of classical particles: a hard wall moving with trajectory $x_m(t) = d\sqrt{t/t_f}$ (solid line); examples of two particle trajectories with different initial velocities (dashed lines).

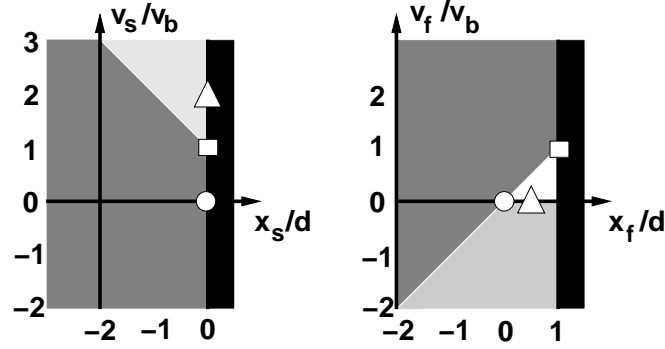


Figure 3.2: Scheme of the transformation between initial parameters and final parameters, the wall is indicated by the black box, the dark grey region is for free motion, and the light grey region for motion with collision. The symbols provide examples connecting final and initial parameters: $x_s/d = \chi_s = 0, v_s/v_b = \nu_s = 0 \rightarrow x_f/d = \chi_f = 0, v_f/v_b = \nu_f = 0$ (free motion, circles); $\chi_s = 0, \nu_s = 1 \rightarrow \chi_f = 1, \nu_f = 1$ (free motion, boxes); $\chi_s = 0, \nu_s = 2 \rightarrow \chi_f = 1/2, \nu_f = 0$ (collision, triangles).

For a particle starting at position $\chi_s \leq 0$ with velocity $\nu_s > 0$, its final position and velocity at time $\tau = 1$ are given by:

$$\nu_f(\chi_s, \nu_s) = \begin{cases} \frac{1}{\eta(\chi_s, \nu_s)} - \nu_s & : \nu_s > 1 - \chi_s \\ \nu_s & : \text{otherwise} \end{cases} \quad (3.6)$$

$$\chi_f(\chi_s, \nu_s) = \begin{cases} \chi_s + \frac{1}{\eta(\chi_s, \nu_s)} - \nu_s + 2\nu_s\eta^2(\chi_s, \nu_s) - \eta(\chi_s, \nu_s) & : \nu_s > 1 - \chi_s \\ \chi_s + \nu_s & : \text{otherwise} \end{cases} \quad (3.7)$$

with

$$\eta(\chi_s, \nu_s) = \frac{1}{2\nu_s} \left(1 + \sqrt{1 - 4\chi_s\nu_s} \right).$$

¹If $\nu_s \leq 1 - \chi_s$ the particle keeps its initial velocity, i.e. it moves too slowly to collide with the moving wall before $\tau = 1$, see also Fig. 3.2. If a collision occurs ($\nu_s > 1 - \chi_s \geq 0$) then

$$\nu_f = \frac{1}{\eta(\chi_s, \nu_s)} - \nu_s = \underbrace{\frac{\nu_s}{1 + \sqrt{1 - 4\chi_s\nu_s}}}_{>0} \underbrace{\left(1 - \sqrt{1 - 4\chi_s\nu_s}\right)}_{\leq 0} \leq 0. \quad (3.8)$$

This means that the particle is always moving backwards after a collision, independently² of its initial parameters.

In a similar way we can also determine the inverse transformation to obtain the initial position and velocity from the final parameters for $\chi_f \leq 1$.

The initial position and velocity of a particle with final position χ_f and velocity ν_f at time $\tau = 1$ are given by

$$\nu_s(\chi_f, \nu_f) = \begin{cases} \lambda(\chi_f, \nu_f) - \nu_f & : \chi_f > \nu_f \text{ and } \nu_f \leq 0 \\ \nu_f & : \text{otherwise} \end{cases} \quad (3.9)$$

$$\chi_s(\chi_f, \nu_f) = \begin{cases} \chi_f - \nu_f + \frac{2}{\lambda^2(\chi_f, \nu_f)} \left(\nu_f - \frac{\lambda(\chi_f, \nu_f)}{2} \right) & : \chi_f > \nu_f \text{ and } \nu_f \leq 0 \\ \chi_f - \nu_f & : \text{otherwise} \end{cases} \quad (3.10)$$

with

$$\lambda(\chi_f, \nu_f) = \frac{1}{2(\chi_f - \nu_f)} \left(1 + \sqrt{1 - 4\nu_f(-\nu_f + \chi_f)} \right).$$

Note that final values χ_f and ν_f fulfilling $\chi_f > \nu_f > 0$ are not possible (white region in Fig. 3.2) since the two inequalities are in contradiction: from eq. (3.8), a positive final velocity means that no collision has occurred such that, using eq. (3.7) and $\chi_s \leq 0$, we have $\nu_f = \nu_s$ and $\chi_f = \chi_s + \nu_f \leq \nu_f$.

The function $v_f(x_s, v_s) = v_b \nu_f(x_s/d, v_s/v_b) = v_b \nu_f(\chi_s, \nu_s)$ is important as it describes the extent to which the moving mirror fails to stop the particles when their position and velocity deviate from the ideal conditions $\chi_s = 0$ and $\nu_s \geq 1$. This function is shown in Fig. 3.3, where the thick black line separates the regions with or without a collision. In the region where a collision occurs the absolute value of the final velocity increases for increasing initial distance $d_s = -\chi_s$, as is also the case for increasing initial velocity if $\chi_s < 0$ ³. That this behaviour of the final velocity is true in general is straightforward to prove. We consider the case $\nu_s > 1 - \chi_s$ (and $\chi_s \leq 0$), i.e. a collision has occurred

1 We chose the + sign for the square-root in $\eta(\chi_s, \nu_s)$ to ensure that the times are positive.

2 That means for the parameter ranges considered. For a particle starting behind the mirror the situation is obviously different.

3 In the case that $\chi_s = 0$ one of course recovers the ideal situation in which all particles, as long as a collision occurs, are stopped.

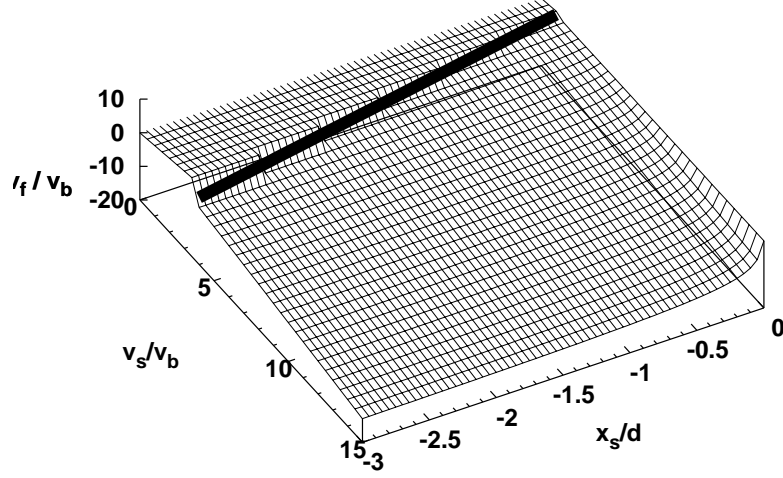


Figure 3.3: The final velocity $\chi_f(\chi_s, \nu_s) = v_f(x_s, v_s)/v_b(x_s, v_s)$ depending on the initial position and velocity. The line at $\nu_s = 1 - \chi_s$ separates the regions with or without a collision before $\tau = 1$.

before $\tau = 1$, which implies that the final velocity is negative, i. e. $\nu_f \leq 0$, see eq. (3.8). Furthermore we have

$$\frac{\partial \nu_f}{\partial \nu_s} = -1 - \frac{1}{2\chi_s} \left(\frac{1}{4\chi_s^2} - \frac{\nu_s}{\chi_s} \right)^{-\frac{1}{2}} = -1 + \frac{1}{\sqrt{1 - 4\nu_s\chi_s}} < 0, \quad (3.11)$$

and

$$\begin{aligned} \frac{\partial \nu_f}{\partial \chi_s} &= \frac{-\frac{1}{2\chi_s^3} + \frac{\nu_s}{\chi_s^2}}{2\sqrt{\frac{1}{4\chi_s^2} - \frac{\nu_s}{\chi_s}}} - \frac{1}{2\chi_s^2} = \frac{1}{2\chi_s^2} \left(\frac{-\frac{1}{2\chi_s} + \nu_s}{\sqrt{\frac{1}{4\chi_s^2} - \frac{\nu_s}{\chi_s}}} - 1 \right) \\ &= \frac{1}{2\chi_s^2} \left(\frac{\nu_s - \frac{1}{2\chi_s} - \sqrt{-\frac{\nu_s}{\chi_s} + \frac{1}{4\chi_s^2}}}{\sqrt{-\frac{\nu_s}{\chi_s} + \frac{1}{4\chi_s^2}}} \right) = \frac{1}{2\chi_s^2} \left(\frac{\nu_s - \frac{1}{2\chi_s} - \sqrt{(\nu_s - \frac{1}{2\chi_s})^2 - \nu_s^2}}{\sqrt{-\frac{\nu_s}{\chi_s} + \frac{1}{4\chi_s^2}}} \right) \\ &> 0, \end{aligned} \quad (3.12)$$

because $-\chi_s > 0$ and $\nu_s > 0$. From this follows that

The absolute value of the final velocity ν_f increases with increasing initial distance $d_s = -\chi_s$ and velocity ν_s .

This result suggests to us a possible strategy to select the parameters d and t_f and optimize the stopping: assume that the initial parameters x_s and v_s are fixed (they may correspond to estimates of the least favorable values expected or permitted, such as the farthest distance from the origin allowed by the initial geometry of the launching

conditions and a lower bound for the speed). First we choose d and t_f such that

$$v_b = \frac{d}{t_f} \ll v_s, \quad (3.13)$$

Increasing the distance d , while keeping v_b constant, i.e. increasing t_f accordingly, for the final velocity we have

$$v_f(x_s, v_s) = v_b \nu_f \left(\frac{x_s}{d}, \frac{v_s}{v_b} \right) \xrightarrow{d \rightarrow \infty} 0 \quad (v_b \text{ fixed}). \quad (3.14)$$

This can loosely be stated as

For sufficiently large d , thereby also increasing t_f such that $v_b = \frac{d}{t_f}$ remains constant, the final velocity goes to zero according to eq. (3.14), even with imperfect conditions.

The condition $v_b(1 - x_s/d) < v_s$ should also be satisfied for the chosen d , such that the particle collides with the wall. That this is indeed the case can easily be seen via

$$v_b \left(1 - \frac{x_s}{d} \right) \xrightarrow{d \rightarrow \infty} v_b \ll v_s \quad (v_b \text{ fixed}), \quad (3.15)$$

which is fulfilled due to our initial choice of v_b in eq. (3.13).

An Ensemble of Classical Particles and One Moving Mirror

We shall now discuss the more general case in which the initial position and the velocity of the particle are characterized by a probability density $p_s(x_s, v_s)$, which is equivalent¹ to the situation of an ensemble of non-interacting classical particles. The final probability density for position and velocity of the particle is given by

$$p_f(x_f, v_f) = p_s[x_s(x_f, x_f), v_s(v_f, v_f)]. \quad (3.16)$$

In particular we shall consider examples with

$$p_s(x, v) = \frac{1}{N} \exp \left[-\frac{(v - v_0)^2}{2\Delta v^2} - \frac{(x - x_0)^2}{2\Delta x^2} \right] \quad (3.17)$$

for $x < 0$, and $p_s(x, v) = 0$ for $x \geq 0$ (N being a normalization constant). The initial probability density p_s for the parameters $x_0/d = -0.04$, $\Delta x/d = 0.008$, $v_0/v_b = 5.0$ and $\Delta v/v_b = 2.0$ is shown in Fig. 3.4a (solid graph), as well as the final probability density (striped graph). One observes a narrowing of the velocity component, which is accompanied by a broadening of the position component². The position and velocity

¹ At least if we assume as before that the collisions do not alter the mirror trajectory.

² Which is necessarily the case, since the phase-space volume is conserved.

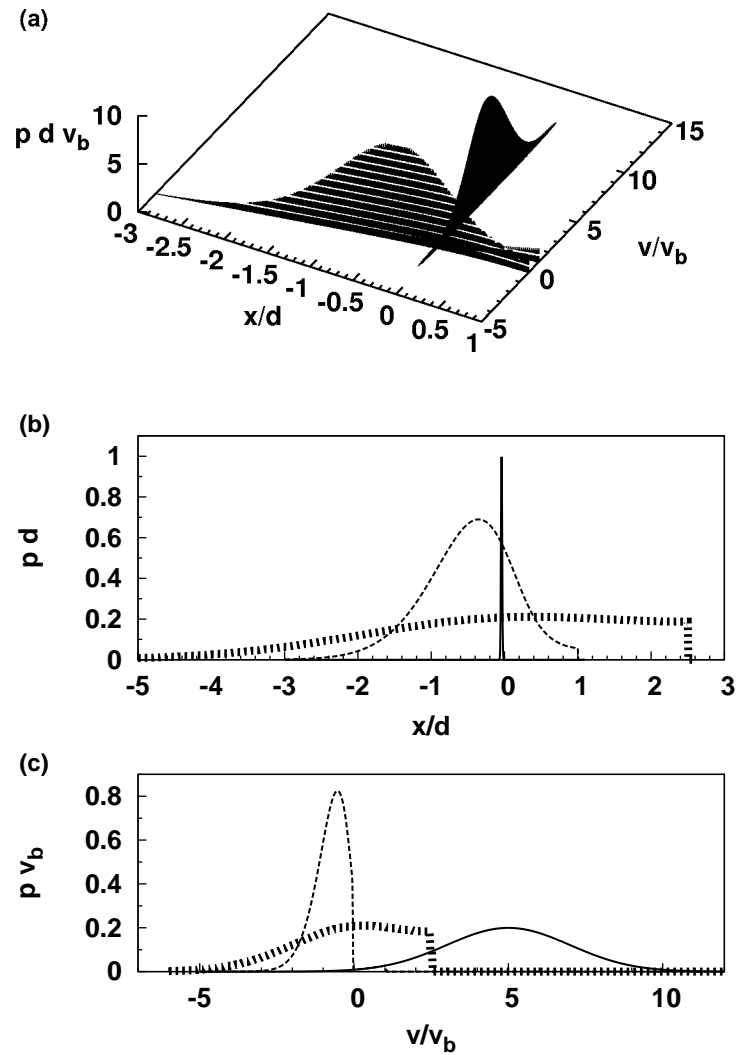


Figure 3.4: Classical particles, $x_0/d = -0.04$, $\Delta x/d = 0.008$, $v_0/v_b = 5.0$ and $\Delta v/v_b = 2.0$; the p in the vertical axis is shorthand for the different probability densities, multiplied by d or v_b to obtain a dimensionless quantity. (a) Initial joint probability density of position and velocity p_s (solid graph) and final probability density p_f (striped graph); (b) Position distributions: initial ($p_{x,s}$, solid line, scaled by a factor of $1/50$), final ($p_{x,f}$, dashed line), and final for a mirror with constant velocity ($\bar{p}_{x,f}$, thick dotted line); (c) Velocity distributions: initial ($p_{v,s}$, solid line), final ($p_{v,f}$, dashed line), and final for constant-velocity mirror $\bar{p}_{v,f}$ (thick dotted line).

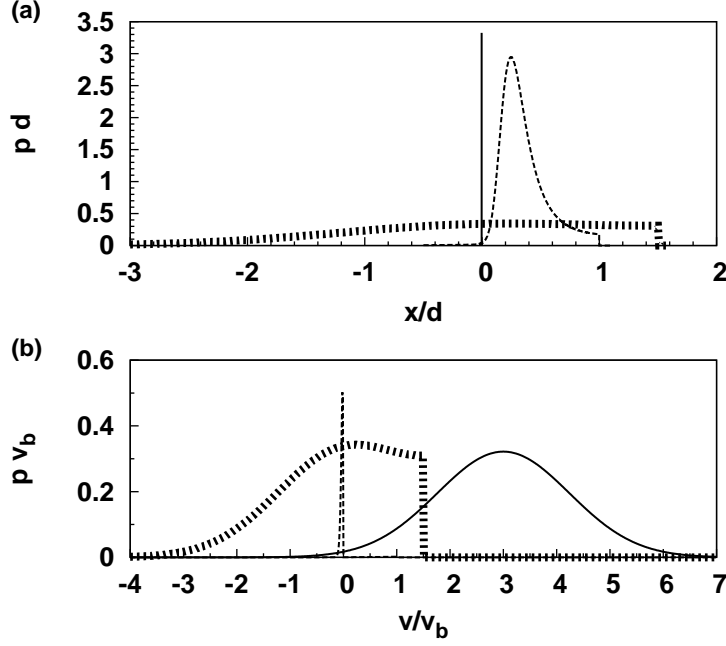


Figure 3.5: Classical particles, $x_0/d = -0.003$, $\Delta x/d = 0.0003$, $v_0/v_b = 3.0$ and $\Delta v/v_b = 1.24$; as in the previous figure, the p in the vertical axis represents the different probability densities, multiplied by d or v_b to obtain a dimensionless quantity. (a) Position distributions: initial ($p_{x,s}$, solid line, scaled by a factor of $1/400$), final ($p_{x,f}$, dashed line) and final for constant-velocity mirror ($\bar{p}_{x,f}$, thick dotted line); (b) Velocity distributions: initial ($p_{v,s}$, solid line), final ($p_{v,f}$, dashed line, scaled by a factor of $1/40$), and final for a constant-velocity mirror ($\bar{p}_{v,f}$, thick dotted line).

marginals

$$p_{x,s/f}(x) = \int dv p_{s/f}(x,v), \quad (3.18)$$

$$p_{v,s/f}(v) = \int dx p_{s/f}(x,v), \quad (3.19)$$

for this example are shown in Fig. 3.4b and c.

Fig. 3.4c illustrates the slowing of the particles and shows the narrowing of the final velocity distribution (dashed line) compared to the initial one (solid line). Moreover, a small fraction of particles have not hit the wall: they correspond to the final distribution in the interval $0 < v/v_b < 1$.

Additionally the results are compared with those of a wall with constant velocity $\frac{v_0}{2}$, see $\bar{p}_{x,f}$ resp. $\bar{p}_{v,f}$ in Fig. 3.4b and c. Note that $\bar{p}_{x,f} = 0$ for $x \geq t_f \frac{v_0}{2}$ because there are never particles on the right-hand side of the wall. Both the final position and velocity distribution for a constant wall velocity are clearly broader than the final distributions for a wall trajectory $\sim \sqrt{t}$. Furthermore, only particles with initial velocity $v_s > \frac{v_0}{2}$ (and t_f large enough) are decelerated by the accelerated wall, whereas particles with velocity $v_s < \frac{v_0}{2}$ never reach the mirror with constant velocity. Therefore we have for

the parameter ranges considered

A mirror moving along a trajectory $\sim \sqrt{t}$ slows particles in a pulse much more efficiently than a mirror moving with constant velocity.

For particles in a beam instead of a pulse the situation is of course different, because then the initial distance increases monotonically and the particles will be slowed less and less for a square-root in time trajectory, whereas for a mirror moving with constant velocity the slowing is always the same. In some sense the situations are complementary, but in contrast to a mirror with constant velocity, for a square-root in time trajectory we have the degree of freedom α and can explore this to suppress the effect of imperfect conditions, as was shown in eq. (3.14) and resumed in the subsequent result.

One further example is shown in Fig. 3.5, where, compared to the previous example, an even larger velocity reduction can be observed. The width of the position distribution increases accordingly, because, as was already noted, the phase-space volume is conserved.

One Classical Particle and One Mirror: A Different Trajectory

In the previous considerations we started with the ideal case of a particle having the same initial position as the mirror and showed that a square-root in time trajectory stops such a particle independently of its initial velocity. We then considered the more realistic situation that the particle has a finite distance to the mirror and showed that a mirror with such a square-root trajectory still slows the particle efficiently for not too large distances and velocities. However, we excluded the case that the particle starts behind the mirror, i.e. that for a mirror starting at $x_m(0) = 0$, the particle has an initial position $x_s > 0$. Since we are considering a hard or impenetrable wall¹, this is a necessary condition for slowing the particle, because otherwise the collision with the mirror would lead to a positive acceleration of the particle instead. However, we can consider an initial position and velocity of the particle such that the particle would have been behind the mirror, if it had started at an earlier time. Such a situation is schematically depicted in Fig. 3.6, where the square-root denotes the mirror trajectory and the straight line the particle trajectory starting at some time $t_0 > 0$ with initial position $x_s > 0$ and constant initial velocity $v_s > 0$. The dashed line shows that the particle would have started behind the mirror for $t_0 = 0$ in this situation. Before we explain why considering this situation is interesting in its own right, we will describe the situation in a more suitable coordinate system with coordinates (x', t') where $x' = x$ and $t' = t - t_0$, i.e. we simply consider a time translation, such that the particle starts at time $t'_0 = 0$. In the following we will denote these coordinates by x and t again. The mirror then has a trajectory $\alpha\sqrt{t + t_0}$, so actually we are considering a different situation compared to the trajectory used in this section so far.

The particle would have started behind the mirror if the condition $\frac{x_s}{t_0} > v_s \Leftrightarrow x_s - v_s t_0 > 0$ is fulfilled. This situation is of interest, since the velocity after a collision is always

¹ One could of course envision using an atom diode instead of a mirror, an idea which was used to create a different scheme for trapping and cooling an ensemble of particles via a square-root in time trajectory, see Chapter 4. Such an atom diode could overtake the particle at first without interacting with it, only to be caught up by the particle at some later time, but now acting as a barrier, such that it slows the particle.

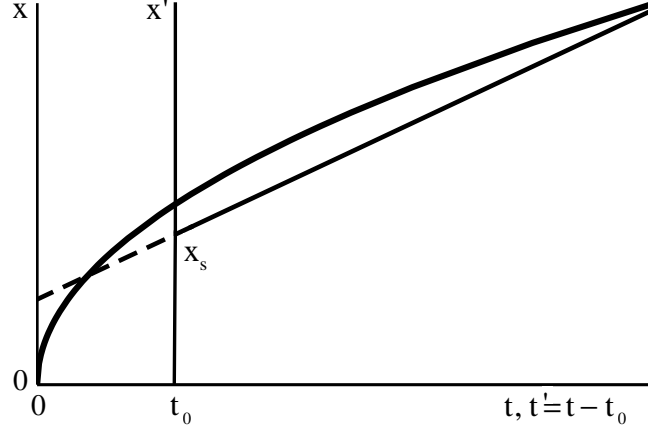


Figure 3.6: Scheme of a particle which would have started behind the mirror at time $t = 0$. Changing coordinates such that the particle starts at time t' , this situation can equivalently be described by an altered mirror trajectory $\alpha\sqrt{t' + t_0}$ and is therefore different from the one considered so far.

positive, but thereby still smaller than the initial velocity. That the absolute value of the final velocity is smaller than the initial one is clear from eq. (3.1) and that it is positive is also straightforward to show. First we need the collision time t_c again, which can be determined via $x_s + v_s t_c = \alpha\sqrt{t_c + t_0}$ and one obtains

$$t_c = -t_0 + \frac{\alpha^2}{4v_s^2} \left(1 + \sqrt{1 + \frac{4(-x_s + v_s t_0)v_s}{\alpha^2}} \right)^2. \quad (3.20)$$

For the final velocity v_f one therefore obtains

$$v_f = -v_s + \frac{\alpha}{\sqrt{t_c + t_0}} = -v_s + \frac{2v_s}{\left(1 + \sqrt{1 + \frac{4(-x_s + v_s t_0)v_s}{\alpha^2}} \right)}. \quad (3.21)$$

If $x_s - v_s t_0 > 0 \Leftrightarrow -x_s + v_s t_0 < 0$ we have for the denominator

$$1 + \sqrt{1 + \frac{4(-x_s + v_s t_0)v_s}{\alpha^2}} < 2 \quad (3.22)$$

and therefore v_f is positive.

The consequence is that multiple collisions occur, because the mirror is decelerated and the particle always catches up at some time. Furthermore, it is straightforward to see that in the limit of $t \rightarrow \infty$ the final velocity goes to zero, because according to the previous discussion the particle's trajectory is sandwiched between a horizontal line and the mirror's trajectory, but the mirror velocity also goes to zero in the limit of infinite time, i.e. $\lim_{t \rightarrow \infty} v_m(t) = \lim_{t \rightarrow \infty} \frac{\alpha}{2\sqrt{t+t_0}} = 0$. Therefore the particle's velocity goes to

zero too.

Although we will not necessarily consider the case $x_s - v_s t_0 > 0$, in the following we will also use this altered trajectory for some of our numerical studies of the efficiency of a square-root in time trajectory.

One Classical Particle and Two Mirrors

We close this section with a brief discussion of a classical particle confined between two mirror potentials which move in opposite directions along a square-root in time trajectory. This situation is interesting in its own right, but it also explains (at least heuristically) some effects in Section 3.3 where we will pursue the idea of a square-root in time expansion in 2d.

The mirrors will be symmetric to the origin and both will move along the previously discussed trajectory given by $x_m(t) = \alpha\sqrt{t + t_0}$ with $0 < \alpha$, $t_0 \in \mathbb{R}$.

An interesting and important difference when considering two mirrors moving apart is, that in principle multiple collisions can occur for all initial velocities $v_s \neq 0$ as we will see below¹. Since we discussed the stopping with one mirror, we will focus on this new aspect and use some of the results in the 2d case too.

That multiple collisions can occur in general is straightforward to see. If the particle is not stopped perfectly during the first collision, which would only be the case if it had the same initial position as the mirror, then the final velocity is smaller than zero² and constant. Both mirrors on the other hand are constantly decelerated, such that the particle necessarily reaches the second mirror if the final time is large enough. For simplicity we now consider the situation for a particle with initial velocity $v_s > 0$ and initial position $x_s = 0$. The final velocity after the first collision v_{f1} is just given by

$$v_{f1}(\alpha, v_s, t_0) = -v_s + \frac{\alpha}{\sqrt{t_{c1} + t_0}} \quad (3.23)$$

with first collision time $t_{c1} = t_{c1}(\alpha, v_s, t_0)$

$$t_{c1}(\alpha, v_s, t_0) = \frac{\alpha^2}{2v_s^2} \left(1 + \sqrt{1 + \frac{4v_s^2 t_0}{\alpha^2}} \right), \quad (3.24)$$

see also eq. (3.7). In the following we will neglect the arguments of most functions, or at least those dependences we do not need to consider, to simplify the notation. For a second collision to occur we necessarily have

$$\begin{aligned} x_{f1}(t_{c1}) + v_{f1}(t_f - t_{c1}) &\leq -\alpha\sqrt{t_f + t_0} \\ \Leftrightarrow \alpha\sqrt{t_{c1} + t_0} + v_{f1}(t_f - t_{c1}) &\leq -\alpha\sqrt{t_f + t_0} \end{aligned} \quad (3.25)$$

¹ For one mirror a certain position and velocity regime was necessary to ensure this.

² That this is always true in this setup, although we use the altered trajectory, will be shown below.

In a similar way one derives expressions for subsequent collisions. It is worth studying these inequalities a bit further. For larger t_0 the first collision time t_{c1} and the absolute value of v_{f1} increase. To see this we first note that although the mirrors now move along the trajectory $\alpha\sqrt{t+t_0}$, the first final velocity is always negative in this setting¹, because

$$\begin{aligned} v_{f1} &= -v_s + 2v_m(t_{c1}) = -v_s + \frac{\alpha}{\sqrt{t_{c1} + t_0}} = -v_s + \frac{\alpha}{\sqrt{\frac{\alpha^2}{2v_s^2} \left(1 + \sqrt{1 + \frac{4v_s^2 t_0}{\alpha^2}}\right) + t_0}} \\ &= -v_s + \frac{\sqrt{2}v_s}{\sqrt{1 + \sqrt{1 + \frac{4v_s^2 t_0}{\alpha^2}} + \frac{2v_s^2 t_0}{\alpha^2}}} = \left(\frac{\sqrt{2}}{\sqrt{1 + \sqrt{1 + s} + \frac{s}{2}}} - 1 \right) v_s \\ &\stackrel{s > 0}{<} 0 \end{aligned} \quad (3.26)$$

with $s := \frac{4v_s^2 t_0}{\alpha^2}$. Now it just remains to show that v_{f1} is monotonically decreasing with respect to t_0 , which is also straightforward. We have

$$\frac{\partial}{\partial t_0} v_{f1}(t_0) = -\frac{\alpha}{2} \frac{1}{(t_{c1}(t_0) + t_0)^{\frac{3}{2}}} \left(\frac{1}{(1 + \frac{4v_s^2 t_0}{\alpha^2})^{1/2}} + 1 \right) < 0, \quad (3.27)$$

because $t_{c1}(t_0) + t_0 > 0$ and $\frac{4v_s^2 t_0}{\alpha^2} > 0$.

If only one collision occurs larger t_0 are disadvantageous, which is not surprising at all, but since multiple collisions are possible, this might not be true in general. To see why, we focus on the first and second collision, although the following analysis could also be applied to further collisions and more complicated situations.

We consider two particles a_1 and a_2 with the same initial position velocity, but colliding with mirrors with different initial times $0 < t_{01} < t_{02}$. Since particle a_2 will be faster after the first collision than particle a_1 , for a fixed final time t_f this might lead to a second collision only for a_2 , such that the particle will actually be slower after the whole process. If this can be the case depends on two things:

1. The second collision time for a_2 has to be smaller than the one for a_1 , i.e. we have to determine if for $t_{02} > t_{01}$ it is possible that $t_{c2}(t_{02}) < t_{c2}(t_{01})$. This is not obvious, since the faster particle a_2 also has to travel a longer distance.
2. Even if this is possible, it is also not obvious if the second collision reduces the velocity of a_2 so much, that it is smaller than the first final velocity of a_1 , i.e. we have to determine if for $t_{02} > t_{01}$ and $t_{c2}(t_{02}) < t_{c2}(t_{01})$ it is possible that $v_{f2}(t_{02}) < v_{f1}(t_{01})$.

We begin with the first question and therefore will derive the explicit form of the second collision time t_{c2} depending on the initial time t_0 . At the second collision the following equality must hold

$$\alpha\sqrt{t_{c1}(t_0) + t_0} + v_{f1}(t_{c2}(t_0) - t_{c1}(t_0)) = -\alpha\sqrt{t_{c2}(t_0) + t_0}.$$

¹ This is also clear when considering under which condition one obtains a positive final velocity for one mirror with this trajectory, i.e. $x_s - v_s t_0 > 0$. Here we have $x_s = 0$ and $v_s > 0$ and therefore the condition is never fulfilled.

We therefore have

$$(t_{c2}(t_0) + t_0) + \frac{\alpha}{v_{f1}} \sqrt{t_{c2}(t_0) + t_0} = (t_{c1}(t_0) + t_0) - \frac{\alpha}{v_{f1}} \sqrt{t_{c1}(t_0) + t_0}.$$

Using the condition $t_{c2} > 0$ we obtain

$$\begin{aligned} t_{c2}(\alpha, v_s, t_0) &= -t_0 + \left(-\frac{\alpha}{2v_{f1}} + \sqrt{\frac{\alpha^2}{4v_{f1}^2} + t_{c1} + t_0 - \frac{\alpha}{v_{f1}} \sqrt{t_{c1} + t_0}} \right)^2 \\ \Leftrightarrow t_{c2}(\alpha, v_s, t_0) &= t_{c1} - \frac{2\alpha}{v_{f1}} \sqrt{t_{c1} + t_0} + \frac{\alpha^2}{v_{f1}^2} \end{aligned} \quad (3.28)$$

where v_{f1} and t_{c1} are given by eqs. (3.23) and (3.24) respectively. Important is that t_{c2} does not depend monotonically on the initial time $t_0 \in [0, \infty]$, but instead it has in general a minimum for some $t_0 \in]0, \infty[$. This can also be understood from the following simple considerations. For $t_0 \rightarrow 0$ we have the ideal case in which the particle is perfectly stopped and therefore t_{c2} goes to infinity. This apparently also happens for $t_0 \rightarrow \infty$ because no collision occurs for t_f finite. As an example t_{c2} is plotted against t_0 and v_s for $\alpha = 1$ in Fig. 3.7. We therefore can conclude that there are initial times $t_{02} > t_{01}$ for

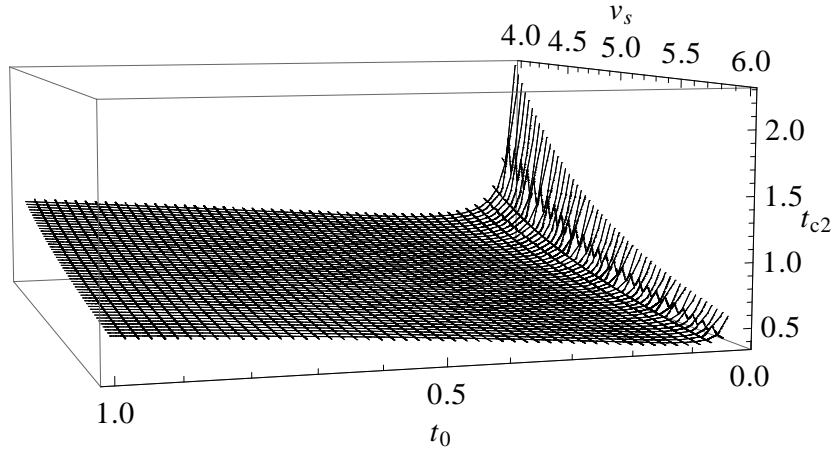


Figure 3.7: The second collision time t_{c2} depending on the initial time t_0 and v_s for a particle moving between two mirror potentials. We set the parameter $\alpha = 1$.

which $t_{c2}(t_{02}) < t_{c2}(t_{01})$, but it remains to determine if in such a situation the velocity reduction at $t_{c2}(t_{02})$ is large enough such that $v_{f2}(t_{02}) < v_{f1}(t_{01})$. However, first we only wish to determine if $v_{f2}(t_{02}) < v_{f1}(t_{01})$ is at least in principle possible and neglect for now the influence of the final time t_f .

As before we assume $x_s = 0$ and therefore we have $v_{f1} < 0$ and $v_{f2} > 0$, which implies $|v_{f2}(t_{02})| = v_{f2}(t_{02})$ and $|v_{f1}(t_{01})| = -v_{f1}(t_{01})$. Thus we simply have to find

values v_s , t_{01} and t_{02} such that

$$\stackrel{\text{eq.(3.23)}}{\Leftrightarrow} \frac{|v_{f2}(t_{02})| < |v_{f1}(t_{01})| \Leftrightarrow v_{f2}(t_{02}) < -v_{f1}(t_{01})}{\frac{1}{\sqrt{t_{c1}(t_{02}) + t_{02}} + \frac{1}{\sqrt{t_{c2}(t_{02}) + t_{02}}} - \frac{1}{\sqrt{t_{c1}(t_{01}) + t_{01}}} > 0. \quad (3.29)$$

is fulfilled. W.l.o.g. we set $\alpha = 1$. For example choosing $v_s = 5$, $t_{01} = 1$ and $t_{02} = 2t_{01} = 2$ and using eqs. (3.23) and (3.28) we obtain

$$\frac{1}{\sqrt{t_{c1}(2) + 2}} + \frac{1}{\sqrt{t_{c2}(2) + 2}} - \frac{1}{\sqrt{t_{c1}(1) + 1}} \approx 0.33 > 0.$$

Furthermore, in Fig. 3.8 the strictly positive part of $|v_{f1}(t_{01})| - |v_{f2}(t_{02})| = -v_{f1}(t_{01}) - v_{f2}(t_{02})$, with $t_{02} = t_{01} + \epsilon$ is plotted over ϵ and v_s for $\alpha = 1$ and $t_0 = 1$. It shows that for an initial velocity $v_s \in [4,6]$, $|v_{f2}(t_{02})| = |v_{f2}(1 + \epsilon)|$ is indeed smaller for all $\epsilon \in [0,3]$. However, in the previous analysis we did not consider if $v_{f2}(t_{02}) < v_{f1}(t_{01})$ can

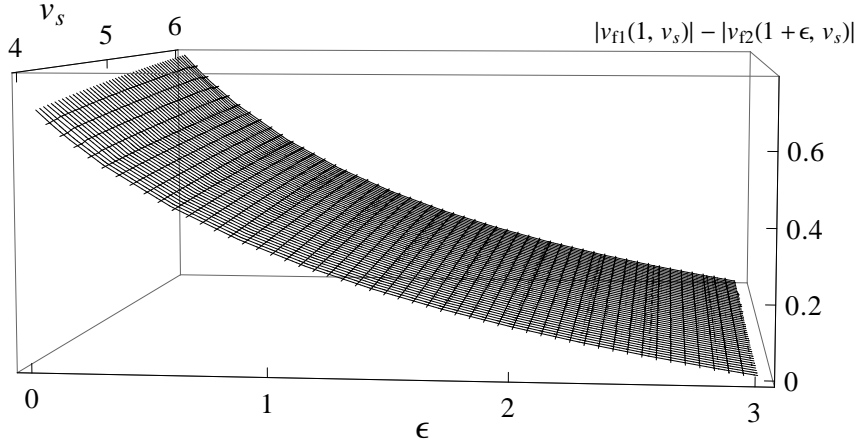


Figure 3.8: Plot of the strictly positive part of the difference between the first and second final velocity $|v_{f1}(1, v_s)| - |v_{f2}(1 + \epsilon, v_s)|$ depending on ϵ and v_s for a particle moving between two mirror potentials. We set the parameter $\alpha = 1$.

be fulfilled for $t_{c2}(t_{02}) < t_{c2}(t_{01})$. In other words it is important to take t_f into account and although in principle one finds smaller velocities after the second collision for larger initial times, it is still not clear if these second collisions leading to smaller velocities actually occur. The answer to this remaining question is positive, i.e. larger t_0 can indeed be useful in the sense that for a given final time t_f a particle is slower after the process, because it undergoes more reflections and the additional velocity reduction compensates for the less efficient stopping during the first collision. This is shown in Fig. 3.9, where we chose units such that $\alpha = 1$, $t_f = 1$ and plotted the absolute value of the final velocity v_f now only depending on t_0 and v_s . Moving along lines of constant initial velocities v_s there exist regions where $|v_f|$ decreases for increasing t_0 , which are given by the rims of the plateaus in Fig. 3.9. However, the comparison might still be unfair, because the final time t_f we used in Fig. 3.9 did not take the different t_0 into account. Therefore the

final distances $d_f = \sqrt{t_f + t_0}$ the mirror moved differ, whereas using the same maximal distance d_{fmax} would be more appropriate. In Fig. 3.10 we therefore plotted v_f for a constant final distance. Still we observe plateaus which show that for some v_s , $|v_f|$ decreases for increasing t_0 . In both cases this effect is due to additional collisions and therefore we conclude that seemingly worse initial conditions, i.e. larger t_0 , can actually be useful due to multiple collisions depending on the chosen or accessible parameters.

The considerations above only apply to the one-particle case and are only meant to demonstrate that multiple collisions could be useful. In the case of an ensemble it is not clear whether multiple collisions are useful too, even in the classical case, due to the dependence on v_s . Here useful would mean that a larger t_0 lead to a smaller mean velocity and variance. However, in Section 3.3.2 we will see an example where even in the quantum case in two dimensions larger initial times turn out to be useful in this sense.

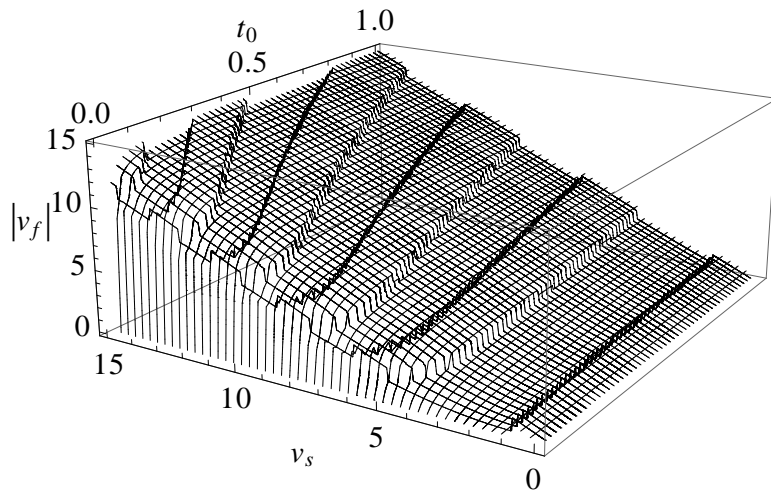


Figure 3.9: The absolute value of the final velocity $|v_f|$ depending on v_s and t_0 for a particle moving between two mirror potentials moving apart in opposite directions along a trajectory $\sqrt{t + t_0}$. For the final time we always set $t_f = 1$, such that the mirrors final distance increases with increasing t_0 , i.e. $d_f = \sqrt{1 + t_0}$.

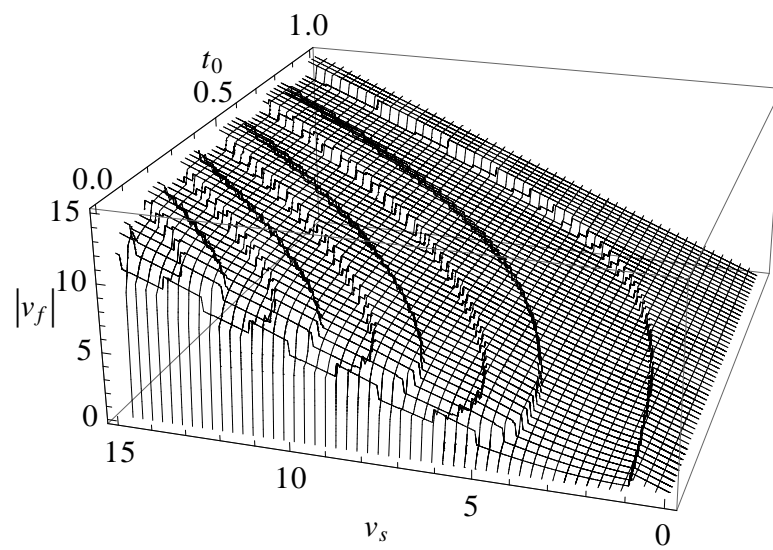


Figure 3.10: The absolute value of the final velocity $|v_f|$ depending on v_s and t_0 for a particle moving between two mirror potentials moving apart in opposite directions along a trajectory $\sqrt{t+t_0}$. For the final time we set $t_f = 1 - t_0$, such that the mirrors final distance is always $d_f = 1$.

3.2.2 Quantum Particles

So far we have investigated the problem of stopping a particle with unknown velocity in the classical framework, where we could calculate particle trajectories and give explicit transformations between initial and final positions and velocities also in the case where particle and mirror do not have the same initial position. However, a classical treatment alone is not sufficient, since for small velocities quantum mechanical effects cannot be neglected. It is not a priori clear if the proposed scheme still works in this case, e.g. interference could cause a breakdown of the effect. In the following we will therefore consider the problem in the quantum mechanical framework. First we will investigate the problem numerically and compare it with the classical results. Afterwards we will be concerned with the analytical treatment of the problem. We will derive the analytical solution of this problem with an infinitely high potential and the corresponding scattering solutions [30] to construct the complete solution for all times, and compare analytical and numerical results. Finally, we will show that in the quantum case the square-root in time trajectory is also optimal at least compared to any trajectory with an additional linear in time term.

Numerical Treatment

We start with the one-dimensional Schrödinger equation for the particle and the moving mirror potential. It is given by

$$i\hbar \frac{\partial}{\partial t} \psi(x, t) = -\frac{\hbar^2}{2m} \frac{\partial^2}{\partial x^2} \psi(x, t) + V(x - x_m(t)) \psi(x, t), \quad (3.30)$$

where $V(x)$ is the potential of the wall with trajectory

$$x_m(t) = d\sqrt{t/t_f}. \quad (3.31)$$

The mass in the example below is that of ^{85}Rb ($m = 14.19226 \cdot 10^{-26}$ kg). Due to our assumptions the probability densities in the classical case do not depend on the mass of the particle, but in the quantum case they do. The initial wavefunction is a Gaussian¹,

$$\psi_0(x) = \frac{1}{N} \exp \left\{ -\frac{\mu}{2(1+2i\Delta v^2\mu\delta)} [iv_0(\delta v_0 - 2x) + 2\Delta v^2\mu((x - \beta)^2 + 2\delta v_0\beta)] \right\}, \quad (3.32)$$

where $\delta = \sqrt{4\Delta x^2 - 1/(\Delta v^2\mu^2)}/(2\Delta v)$, and $\beta = x_0 - \delta v_0$, $\mu = m/\hbar$. The form of Heisenberg's uncertainty relation is $\Delta x \Delta v \geq 1/(2\mu)$. In the simulations we shall use both an infinitely high wall, i.e.,

$$V_i(x - x_m(t)) = \begin{cases} \infty & : x \geq x_m(t) \\ 0 & : x < x_m(t) \end{cases}, \quad (3.33)$$

¹ Here and in all the following numerical simulations we always ensure that the average distance of the corresponding initial position distribution to the initial mirror position is at least five variances, such that we can neglect its contribution at the initial mirror position. In other words we ensure that the particles start far enough away from the mirror.

where the numerical results are obtained via a time-dependent version of the Crank-Nicholson method (see Appendix B.1), and a Gaussian potential, i.e.

$$V_G(x - x_m(t)) = V_0 \exp[-(x - x_m(t))^2 / (2\Delta x_V^2)], \quad (3.34)$$

where the numerical results were obtained via time-evolution based on a time-dependent operator-splitting (see Appendix B.2) and Fast Fourier Transform (FFT). For cold atoms such a potential could be implemented with a detuned laser (see Section 2.1 and Appendix A). We shall indeed concentrate on cold atoms for examining the effect of the accelerated mirror in the quantum case since quantum motion effects may be more important at low temperatures. The first example corresponds to the parameters in Table 3.1. Note that these parameters correspond to the classical example shown in Fig. 3.4. We have $x_0/d = 0.04 \ll 1$. The height of the Gaussian potential is set to $V_0/\hbar = 3.75 \times 10^6/\text{s}$ and we set $\Delta x_V = 0.4 \mu\text{m}$. Both parameters must be chosen such that the particle is reflected with high probability. The corresponding initial and final quantum probability densities for the two potentials given by eqs. (3.33) and (3.34) are shown in Fig. 3.11. The final position distributions are clearly broader than the initial one, whereas the final velocity distributions average and width are largely reduced. The difference between the final distributions for an infinitely high potential and a Gaussian one are due to the latter ones finite width, such that a reflection can already occur at smaller distances. In contrast to the classical simulations one observes interference fringes in the final distributions, but for both potentials a square-root in time trajectory clearly leads to the anticipated velocity reduction. We therefore conclude

Even in an appropriate quantum mechanical description, a mirror potential moving along a square-root in time trajectory provides a way to largely reduce the velocity of atoms in a pulse .

So far the initial velocity of the wall $dx_m(t)/dt$ is infinite at $t = 0$. This is apparently not realizable in practice but, as the particles have finite velocities, we can modify the small time part of the mirror trajectory without affecting the results, for example by choosing

$$x'_m(t) = \begin{cases} d\sqrt{t_0/t_f} & : t \leq t_0 \\ d\sqrt{t/t_f} & : t > t_0 \end{cases} \quad (3.35)$$

Initial State Parameters:		
$x_0 = -2 \mu\text{m}$	$\Delta x = 0.4 \mu\text{m}$	
$v_0 = 3.125 \text{ cm/s}$	$\Delta v = 1.25 \text{ cm/s}$	$m = 14.19226 \cdot 10^{-26} \text{ kg}$
Mirror Parameters:		
$V_0/\hbar = 3.75 \times 10^6/\text{s}$	$\Delta x_V = 0.4 \mu\text{m}$	
Other Parameters:		
$v_b = 0.625 \text{ cm/s} \ll v_0$	$d = 50 \mu\text{m}$	$t_f = 8 \text{ ms}$

Table 3.1: Set of parameters in the quantum case corresponding to the results shown in Fig. 3.11.

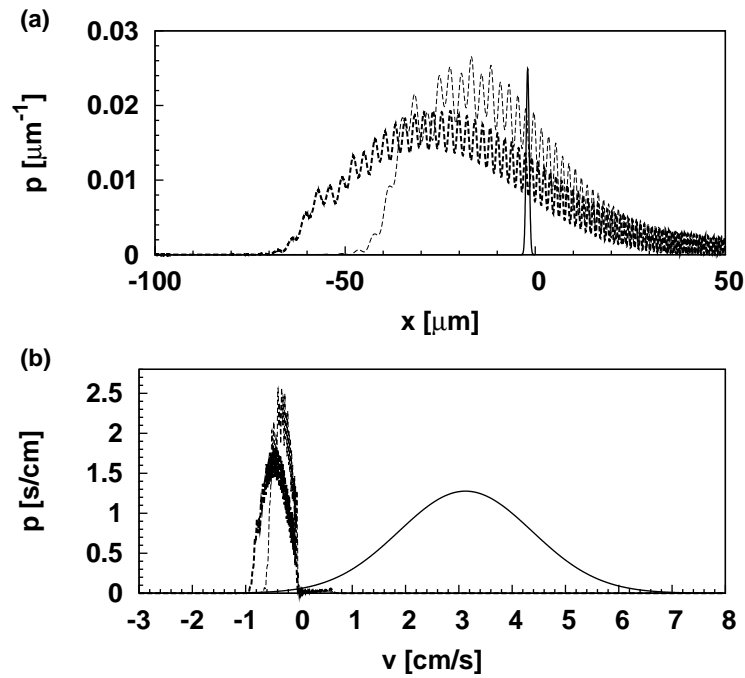


Figure 3.11: Quantum particle, see Table 3.1 for parameters; (a) Position distributions: $p_{x,s}(t=0)$, solid line, scaled by a factor of $1/40$, $p_{x,f}$ with an ideal wall ($t=t_f$, thick dashed line), $p_{x,f}$ with a Gaussian wall ($t=t_f$, thin dashed line); (b) Velocity distributions: $p_{v,s}(t=0)$, solid line, scaled by a factor of 4, $p_{v,f}$ with an ideal wall ($t=t_f$, thick dashed line) and $p_{v,f}$ with a Gaussian wall ($t=t_f$, thin dashed line).

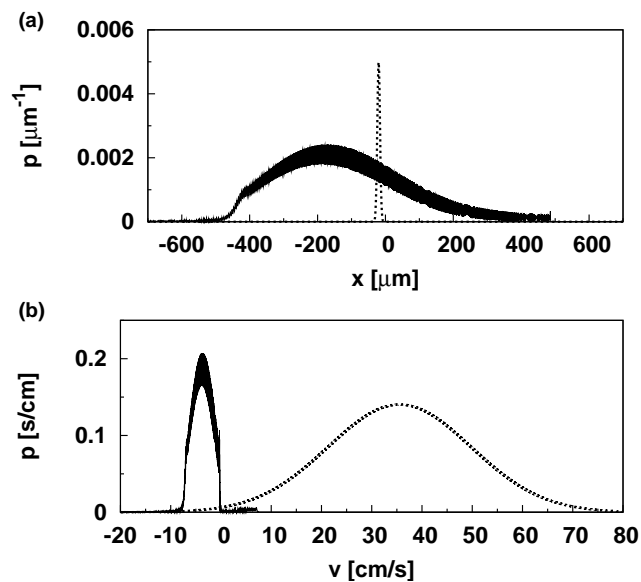


Figure 3.12: Quantum particle, see Table 3.2 for parameters; (a) Position distributions: $p_{x,s}(t=0)$, dotted line, scaled by a factor of $1/100$, $p_{x,f}$ with a Gaussian wall ($t=t_f$, $t_0=0.01t_f$, solid line); (b) Velocity distributions: $p_{v,s}(t=0)$, dotted line, scaled by a factor of 100, $p_{v,f}$ with a Gaussian wall ($t=t_f$, $t_0=0.01t_f$, solid line).

where t_0 has to be chosen sufficiently small. A classical estimate is $t_0 \ll t' = \frac{d^2}{t_f(v_0 + \Delta v)^2}$, where t' is the time to reach the mirror for a particle with initial velocity $v_0 + \Delta v$ and initial position $x = 0$.

Another example using a Gaussian wall following the trajectory given by eq. (3.35) can be seen in Fig. 3.12, where we have chosen the mass of ${}^6\text{Li}$ ($m = 9.99 \times 10^{-27}$ kg). The whole set of parameters can be found in Table 3.2. We have $v_b < v_0$ and $x_0/d = 0.04 \ll 1$. The height of the Gaussian potential is set to $V_0/\hbar = 2.56 \cdot 10^7/\text{s}$ and its width to $\Delta x_V = 4 \mu\text{m}$. In Fig. 3.12, the initial distributions are given by the dotted lines and the final distributions are given by the solid lines. As before a significant velocity reduction can be observed. Note that the resulting final distributions are also nearly indistinguishable from those one would obtain with a Gaussian wall moving with an idealized trajectory given by eq. (3.31).

Analytical Treatment

So far we treated the problem in the quantum case purely numerically, showing that atoms in a pulse, which are reflected by a mirror potential moving along a square-root in time trajectory, experience a large velocity reduction. We will now derive the analytical solution of the Schrödinger equation (3.30) for an infinitely high potential wall with time-dependent position $x = d\sqrt{t/t_f} = \alpha\sqrt{t}$, i.e. we have the time-dependent boundary condition $\Psi(\alpha\sqrt{t}, t) = 0$ for all t . On the topic of partial differential equations with time-dependent or moving boundary conditions see for example [31]-[36]. The problem is that this partial differential equation (PDE) cannot be solved by separation of variables in a direct way. In a first step we therefore transform the equation such that it describes the situation in the reference frame of the mirror. This in turn will lead to a time-independent boundary condition. By a suitable change of variables the new coordinate variable becomes time-independent and the equation becomes separable. To clarify, we want to solve the Schrödinger equation

$$\left[-\frac{\hbar^2}{2m} \frac{\partial^2}{\partial x^2} + V(x,t) \right] \Psi(x,t) = i\hbar \frac{\partial}{\partial t} \Psi(x,t) \quad (3.36)$$

Initial State Parameters:		
$x_0 = -20 \mu\text{m}$	$\Delta x = 4 \mu\text{m}$	
$v_0 = 35.25 \text{ cm/s}$	$\Delta v = 14.21 \text{ cm/s}$	$m = 9.99 \times 10^{-27} \text{ kg}$
Mirror Parameters:		
$V_0/\hbar = 2.56 \cdot 10^7/\text{s}$	$\Delta x_V = 4 \mu\text{m}$	
Other Parameters:		
$v_b = 7.10 \text{ cm/s} \ll v_0$	$d = 500 \mu\text{m}$	$t_f = 7.03 \text{ ms}$
$t_0 = 0.01 \text{ s}$	$t' \approx 0.02 t_f < t_f$	

Table 3.2: Set of parameters in the quantum case corresponding to the results shown in Fig. 3.12.

where

$$V(x,t) = \begin{cases} 0 & x < \alpha\sqrt{t} \\ \infty & x \geq \alpha\sqrt{t} \end{cases}. \quad (3.37)$$

However, this is not a well-defined problem yet, since we have to clarify the meaning of the boundary condition we wish to consider. Precisely, we want to solve the time-dependent Schrödinger equation

$$-\frac{\hbar^2}{2m} \frac{\partial^2}{\partial x^2} \Psi(x,t) = i\hbar \frac{\partial}{\partial t} \Psi(x,t) \quad (3.38)$$

with time-dependent boundary condition $\Psi(\alpha\sqrt{t}, t) = 0$. We now make a change of variables. We introduce a scaled time $\tilde{t} = \frac{t}{\hbar}$, where we drop the tilde in subsequent calculations. Furthermore $x \rightarrow y = \frac{x}{\alpha\sqrt{t}}$ and let $\Phi(y,t) = \Psi(y\alpha\sqrt{t}, t)$. Then $\Phi(1,t) = 0$ and

$$\begin{aligned} \frac{\partial}{\partial t} \Psi(x,t) &= \frac{\partial y}{\partial t} \frac{\partial}{\partial y} \Phi(y,t) + \frac{\partial}{\partial t} \Phi(y,t) = -\frac{1}{2t} y \Phi'(y,t) + \dot{\Phi} \\ \frac{\partial}{\partial x} \Psi(x,t) &= \frac{\partial y}{\partial x} \frac{\partial}{\partial y} \Phi(y,t) = \frac{1}{\alpha\sqrt{t}} \Phi'(y,t) \\ \frac{\partial^2}{\partial x^2} \Psi(x,t) &= \frac{1}{\alpha^2 t} \Phi''(y,t), \end{aligned} \quad (3.39)$$

where primes and dots as usual represent derivatives with respect to y and t respectively. This leads to the equation

$$-\frac{1}{2m\alpha^2 t} \Phi''(y,t) + \frac{i}{2t} y \Phi'(y,t) = i\dot{\Phi}(y,t). \quad (3.40)$$

Assuming $\Phi(y,t) = g(y)f(t)$ we have

$$-\frac{1}{2m\alpha^2} f(t)g''(y) + \frac{i}{2} y f(t)g'(y) = itg(y)\dot{f}(t) \quad (3.41)$$

and therefore

$$-\frac{1}{2m\alpha^2} \frac{g''(y)}{g(y)} + \frac{i}{2} y \frac{g'(y)}{g(y)} = \lambda = it \frac{\dot{f}(t)}{f(t)} \quad (3.42)$$

with $\lambda \in \mathbb{C}$. For $f(t) = f_\lambda(t)$ it follows that

$$f_\lambda(t) = k_\lambda t^{-i\lambda}, \quad (3.43)$$

$k_\lambda \in \mathbb{C}$ and $g(y) = g_\lambda(y)$ is a solution of the equation

$$-\frac{1}{2m\alpha^2} g_\lambda''(y) + \frac{i}{2} y g_\lambda'(y) = \lambda g_\lambda(y). \quad (3.44)$$

Proposition 1. *Setting $a = i\lambda$, $b = \frac{1}{2}$, $u = \frac{im\alpha^2}{2} y^2$ and $g(y) = w\left(\frac{im\alpha^2}{2} y^2\right)$, eq. (3.44)*

is equivalent to

$$u \frac{d^2}{du^2} w(u) + (b - u) \frac{d}{du} w(u) - aw(u) = 0. \quad (3.45)$$

A differential equation of the type (3.45) is called a Kummer equation.

Proof. Verifying the equivalence of eq. (3.44) and eq. (3.45) is straightforward. Making the substitution $u = \frac{im\alpha^2}{2}y^2$ (which is not invertible), and $g(y) = w\left(\frac{im\alpha^2}{2}y^2\right)$ we obtain

$$\begin{aligned} \frac{d}{du} &= \frac{1}{im\alpha^2 y} \frac{d}{dy} \\ \frac{d^2}{du^2} &= \frac{dy}{du} \frac{dy^2}{dy} \frac{d}{dy} + \left(\frac{dy}{du}\right)^2 \frac{d^2}{dy^2} = \frac{1}{m^2\alpha^4 y^3} \frac{d}{dy} - \frac{1}{m^2\alpha^4 y^2} \frac{d^2}{dy^2} \end{aligned} \quad (3.46)$$

and for eq. (3.45) it follows

$$\begin{aligned} &\frac{im\alpha^2}{2}y^2 \left[\frac{1}{m^2\alpha^4 y^3} \frac{d}{dy} - \frac{1}{m^2\alpha^4 y^2} \frac{d^2}{dy^2} \right] w\left(\frac{im\alpha^2}{2}y^2\right) \\ &+ \left[\frac{1}{2} - \frac{im\alpha^2}{2}y^2 \right] \frac{1}{im\alpha^2 y} \frac{d}{dy} w\left(\frac{im\alpha^2}{2}y^2\right) - i\lambda w\left(\frac{im\alpha^2}{2}y^2\right) = 0 \\ \Leftrightarrow &\frac{i}{2m\alpha^2 y} \frac{d}{dy} g(y) - \frac{i}{2m\alpha^2} \frac{d^2}{dy^2} g(y) + \frac{1}{2im\alpha^2 y} \frac{d}{dy} g(y) - \frac{1}{2}y \frac{d}{dy} g(y) - i\lambda g(y) = 0 \\ \Leftrightarrow &-\frac{1}{2m\alpha^2} \frac{d^2}{dy^2} g(y) + \frac{i}{2}y \frac{d}{dy} g(y) - \lambda g(y) = 0 \end{aligned}$$

which proves the proposition. \square

Two linear independent solutions of eq. (3.45) are given by $F(a, b, u)$ and $u^{1-b} F(1 + a - b, 2 - b, u)$, where $F(a, b, u)$ denotes a confluent hypergeometric function¹, see [37, 38]. According to Proposition 1 the solution of eq. (3.44) is therefore given by

$$\begin{aligned} g_\lambda(y) &= \tilde{c}_\lambda \left[-\sqrt{2m\alpha} y F\left(i\lambda, \frac{1}{2}, \frac{im\alpha^2}{2}\right) \cdot F\left(\frac{1}{2} + i\lambda, \frac{3}{2}, \frac{im\alpha^2}{2}y^2\right) \right. \\ &\quad \left. + \sqrt{2m\alpha} F\left(\frac{1}{2} + i\lambda, \frac{3}{2}, \frac{im\alpha^2}{2}\right) \cdot F\left(i\lambda, \frac{1}{2}, \frac{im\alpha^2}{2}y^2\right) \right] \end{aligned} \quad (3.47)$$

where we have used the boundary condition $g_\lambda(1) = 0$ to determine the first integration constant and $\tilde{c}_\lambda \in \mathbb{C}$ is the remaining one. We therefore have

¹ In the literature other notations for confluent hypergeometric functions are common too, e.g. ${}_1F_1(a, b, u)$ or $M(a, b, u)$.

The solution of the time-dependent Schrödinger equation (3.38) is given by

$$\begin{aligned}\Psi_\lambda(x,t) &= \Phi_\lambda\left(\frac{x}{\alpha\sqrt{t}},t\right) = g_\lambda\left(\frac{x}{\alpha\sqrt{t}}\right) f_\lambda(t) \\ &= c_\lambda t^{-i\lambda} \left[-\sqrt{2m} \frac{x}{\sqrt{t}} F\left(i\lambda, \frac{1}{2}, \frac{im\alpha^2}{2}\right) \cdot F\left(\frac{1}{2} + i\lambda, \frac{3}{2}, \frac{im}{2} \frac{x^2}{t}\right) \right. \\ &\quad \left. + \sqrt{2m} \alpha F\left(\frac{1}{2} + i\lambda, \frac{3}{2}, \frac{im\alpha^2}{2}\right) \cdot F\left(i\lambda, \frac{1}{2}, \frac{im}{2} \frac{x^2}{t}\right) \right] \end{aligned} \quad (3.48)$$

with $c_\lambda = k_\lambda \tilde{c}_\lambda \in \mathbb{C}$.

Note that the operator $-\frac{1}{2m\alpha^2} \frac{d^2}{dy^2} + \frac{i}{2} y \frac{d}{dy}$ in eq. (3.44) is not hermitian. We used the preceding ansatz because it is straightforward to show the connection to the Kummer equation which has well known solutions. Now we will derive the solution (3.48) in another way, because it leads to a stationary equation with a hermitian operator, which provides a more physical interpretation of the eigenvalues. Furthermore, it allows us to solve the problem for a broader class of trajectories $l(t)$, where the square-root in time is a special case. This was investigated in [36] and we will use the general results later in Section 3.2.2 when studying the optimality of the square-root in time trajectory in the quantum case.

Again we transform to variables with constant boundary condition, i.e. $x \rightarrow y = \frac{x}{\alpha\sqrt{t}}$. In addition we introduce a position and time-dependent phase $\phi(y,t)$ by setting

$$\Psi(y\alpha\sqrt{t},t) = \Phi(y,t) = e^{\phi(y,t)} \chi(y,t). \quad (3.49)$$

Now using eq. (3.39) and

$$\begin{aligned}\frac{d}{dt} \left(e^{\phi(y,t)} \chi(y,t) \right) &= -\frac{1}{2t} y \phi'(y,t) e^{\phi(y,t)} \chi(y,t) - \frac{1}{2t} y e^{\phi(y,t)} \chi'(y,t) \\ &\quad + \dot{\phi}(y,t) e^{\phi(y,t)} \chi(y,t) + e^{\phi(y,t)} \dot{\chi}(y,t) \\ \frac{d}{dy} \left(e^{\phi(y,t)} \chi(y,t) \right) &= \phi'(y,t) e^{\phi(y,t)} \chi(y,t) + e^{\phi(y,t)} \chi'(y,t) \\ \frac{d^2}{dy^2} \left(e^{\phi(y,t)} \chi(y,t) \right) &= \phi''(y,t) e^{\phi(y,t)} \chi(y,t) + (\phi'(y,t))^2 e^{\phi(y,t)} \chi(y,t) \\ &\quad + \phi'(y,t) e^{\phi(y,t)} \chi'(y,t) + e^{\phi(y,t)} \chi''(y,t), \end{aligned} \quad (3.50)$$

where a prime as usual denotes a derivative with respect to y and a dot a derivative with respect to time. For eq. (3.38) it follows that

$$\begin{aligned} &-\frac{1}{2m\alpha^2 t} \chi'' - \frac{1}{2m\alpha^2 t} \phi'' \chi - \frac{1}{2m\alpha^2 t} (\phi')^2 \chi - \frac{1}{m\alpha^2 t} \phi' \chi' + \frac{i}{2t} y \phi' \chi + \frac{i}{2t} y \chi' - i \dot{\phi} \chi = i \dot{\chi} \\ \Leftrightarrow &-\frac{1}{2m} \chi'' + \left[-\frac{1}{m} \phi' + \frac{i\alpha^2}{2} y \right] \chi' + \left[-\frac{1}{2m} \phi'' - \frac{1}{2m} (\phi')^2 + \frac{i\alpha^2}{2} y \phi' - i\alpha^2 t \dot{\phi} \right] \chi = i\alpha^2 t \dot{\chi}. \end{aligned} \quad (3.51)$$

To keep the notation clear we have dropped all arguments of the functions. For separability, the coefficient of χ' in eq. (3.51) should at most be a function of y and

not depend on t^1 . However, we will not use this degree of freedom and assume that the coefficient vanishes. Therefore

$$-\frac{1}{m}\phi' + \frac{i\alpha^2}{2}y = 0 \Rightarrow \phi = \frac{im\alpha^2}{4}y^2 + c(t) \quad (3.52)$$

and we choose $c(t) = -\frac{1}{2}\ln(\alpha\sqrt{t})$. With eq. (3.52) it follows for eq. (3.51)

$$\begin{aligned} & -\frac{1}{2m}\chi'' + \left[-\frac{1}{2m}\frac{im\alpha^2}{2} - \frac{1}{2m}\left(\frac{im\alpha^2}{2}y\right)^2 + \frac{i\alpha^2}{2}y\left(\frac{im\alpha^2}{2}y\right) - i\alpha^2t\left(-\frac{1}{4t}\right) \right] \chi = i\alpha^2t\dot{\chi} \\ \Leftrightarrow & -\frac{1}{2m}\chi'' - \frac{m\alpha^4}{8}y^2\chi = i\alpha^2t\dot{\chi}. \end{aligned} \quad (3.53)$$

Deviding by α^2 and making the ansatz $\chi(y,t) = \tilde{g}(y) \cdot \tilde{f}(t)$, it follows that

$$-\frac{1}{2m\alpha^2}\frac{\tilde{g}''}{\tilde{g}} - \frac{m\alpha^2}{8}y^2 = \tilde{\lambda} = it\frac{\dot{\tilde{f}}}{\tilde{f}}$$

with $\tilde{\lambda} \in \mathbb{C}$. Therefore $\tilde{f}(t) = \tilde{f}_{\tilde{\lambda}}(t)$ is similarly given by

$$\tilde{f}(t) = \tilde{k}_{\tilde{\lambda}} t^{-i\tilde{\lambda}}, \quad (3.54)$$

$\tilde{k}_{\tilde{\lambda}} \in \mathbb{C}$ and $\tilde{g}(y) = \tilde{g}_{\tilde{\lambda}}(y)$ is a solution of

$$-\frac{1}{2m\alpha^2}\tilde{g}'' - \frac{m\alpha^2}{8}y^2\tilde{g} = \tilde{\lambda}\tilde{g}. \quad (3.55)$$

Combining these results we obtain

The solution of the time-dependent Schrödinger equation (3.38) is given by

$$\Psi_{\lambda}(x,t) = \Phi_{\lambda}(y,t) = e^{\frac{im\alpha^2}{4}y^2} \cdot (\alpha\sqrt{t})^{-\frac{1}{2}} \cdot \tilde{g}_{\tilde{\lambda}}(y) \cdot \tilde{f}_{\tilde{\lambda}}(t) \quad (3.56)$$

with $\tilde{f}_{\tilde{\lambda}}(t) = \tilde{k}_{\tilde{\lambda}} t^{-i\tilde{\lambda}}$, $\tilde{k}_{\tilde{\lambda}} \in \mathbb{C}$, and $\tilde{g}_{\tilde{\lambda}}(y)$ is a solution of eq. (3.55).

We note that the results given by eqs. (3.56) and (3.48) must of course be equal. It is straightforward to prove this by considering the connection between eqs. (3.44) and (3.55) and to show how $\tilde{f}_{\tilde{\lambda}}(t)$ and $f_{\lambda}(t)$ as well as $\tilde{g}_{\tilde{\lambda}}(y)$ and $g_{\lambda}(y)$ are related. To do this we will use²

Proposition 2. *An ODE of the form*

$$g''(y) + a(y)g'(y) + b(y)g(y) = 0 \quad (3.57)$$

1 The coefficient of χ has to have a certain form too and this would lead to additional constraints, but the following ansatz for the function ϕ turns out to be enough to ensure separability and serves our purposes in subsequent calculations. However, this does not mean that one could not use a slightly more general ansatz for ϕ .

2 Although derived independently, we assume that the following result is a standard one used in the theory of ODE.

can be transformed into an ODE of the form

$$\tilde{g}''(y) + \eta(y)\tilde{g}(y) = 0, \quad (3.58)$$

where

$$\eta(y) = b(y) - \frac{1}{4}a^2(y) - \frac{1}{2}a'(y), \quad (3.59)$$

via the transformation

$$g(y) = \tilde{g}(y)e^{-\frac{1}{2}\int_0^y a(s) ds + \text{const}}. \quad (3.60)$$

Proof. Substituting the ansatz $g(y) = \tilde{g}(y)e^{\kappa(y)}$ in eq. (3.57) we obtain

$$\begin{aligned} & \tilde{g}''(y) + 2\kappa'(y)\tilde{g}'(y) + (\kappa'(y))^2\tilde{g}(y) + \kappa''(y)\tilde{g}(y) + a(y)\tilde{g}'(y) \\ & + a(y)\kappa'(y)\tilde{g}(y) + b(y)\tilde{g}(y) = 0 \\ \Leftrightarrow & \tilde{g}''(y) + (2\kappa'(y) + a(y))\tilde{g}'(y) + [(\kappa'(y))^2 + \kappa''(y) + a(y)\kappa'(y) + b(y)]\tilde{g}(y) = 0. \end{aligned}$$

Since we want the coefficient of $\tilde{g}'(y)$ to vanish we have

$$\kappa'(y) = -\frac{1}{2}a(y) \Rightarrow \kappa(y) = -\frac{1}{2}\int_0^y a(s) ds + \text{const} \quad (3.61)$$

from which follows eq. (3.60). Furthermore we obtain

$$\begin{aligned} & \tilde{g}''(y) + [(\kappa'(y))^2 + \kappa''(y) + a(y)\kappa'(y) + b(y)]\tilde{g}(y) = 0 \\ \Leftrightarrow & \tilde{g}''(y) + \left[\left(-\frac{1}{2}a(y)\right)^2 - \frac{1}{2}a'(y) - \frac{1}{2}a^2(y) + b(y) \right] \tilde{g}(y) = 0 \\ \Leftrightarrow & \tilde{g}''(y) + \left[b(y) - \frac{1}{4}a^2(y) - \frac{1}{2}a'(y) \right] \tilde{g}(y) = 0 \\ = & \tilde{g}''(y) + \eta(y)\tilde{g}(y) \end{aligned} \quad (3.62)$$

which proves the proposition. \square

Proposition 3. *The solutions of the Schrödinger equation (3.38) given by eqs. (3.56) and (3.48) are indeed equal, i.e. we have*

$$g_\lambda(y) f_\lambda(t) = e^{\frac{i m \alpha^2}{4} y^2} (\alpha \sqrt{t})^{-\frac{1}{2}} \tilde{f}_\lambda(t) \tilde{g}_\lambda(y). \quad (3.63)$$

Proof. Let $g(y) = g_\lambda(y)$ be a solution of eq. (3.44). Using Proposition 2 with $a(y) = -i m \alpha^2 y$, $b(y) = 2 m \alpha^2$ and setting $\text{const} = -1/2 \ln(\alpha)$, we have

$$g(y) = \tilde{g}(y) e^{\frac{i m \alpha^2}{4} y^2 - \frac{1}{2} \ln(\alpha)} = \tilde{g}(y) e^{\frac{i m \alpha^2}{4} y^2} \alpha^{-\frac{1}{2}}, \quad (3.64)$$

and

$$\begin{aligned}
& \tilde{g}''(y) + \left(2m\alpha^2\lambda + \frac{m^2\alpha^4}{4}y^2 + \frac{i m\alpha^2}{2} \right) \tilde{g}(y) = 0 \\
\Leftrightarrow & -\frac{1}{2m\alpha^2}\tilde{g}''(y) - \frac{m\alpha^2}{8}y^2\tilde{g}(y) - \left(\lambda + \frac{i}{4} \right) \tilde{g}(y) = 0 \\
\Leftrightarrow & -\frac{1}{2m\alpha^2}\tilde{g}''(y) - \frac{m\alpha^2}{8}y^2\tilde{g}(y) - \tilde{\lambda}\tilde{g}(y) = 0,
\end{aligned}$$

i.e. $\tilde{g}(y) = \tilde{g}_{\tilde{\lambda}}(y)$ is a solution of eq. (3.55) with $\tilde{\lambda} = \lambda + \frac{i}{4}$. Therefore

$$\begin{aligned}
g_\lambda(y) \cdot f_\lambda(t) &= e^{\frac{i m\alpha^2}{4}y^2} \alpha^{-\frac{1}{2}} \tilde{g}_{\tilde{\lambda}}(y) t^{-i\lambda} \\
&= e^{\frac{i m\alpha^2}{4}y^2} \alpha^{-\frac{1}{2}} \tilde{g}_{\tilde{\lambda}}(y) t^{-\frac{1}{4}} t^{-i(\lambda + \frac{i}{4})} \\
&= e^{\frac{i m\alpha^2}{4}y^2} (\alpha\sqrt{t})^{-\frac{1}{2}} \tilde{g}_{\tilde{\lambda}}(y) \tilde{f}_{\tilde{\lambda}}(t),
\end{aligned} \tag{3.65}$$

which shows that eqs. (3.56) and (3.48) are indeed equal and

$$\begin{aligned}
f_\lambda(t) &= t^{-\frac{1}{4}} \tilde{f}_{\tilde{\lambda}}(t) \\
g_\lambda(y) &= \alpha^{-\frac{1}{2}} e^{\frac{i m\alpha^2}{4}y^2} \tilde{g}_{\tilde{\lambda}}(y).
\end{aligned} \tag{3.66}$$

□

Note that unlike the operator in eq. (3.44), $-\frac{1}{2m\alpha^2}\frac{d^2}{dy^2} - \frac{m\alpha^2}{8}y^2$ in eq. (3.55) is hermitian. Therefore eq. (3.55) has a physical interpretation. It describes the interaction of the particle in the reference frame of the mirror with an effective potential. This effective potential is a repulsive harmonic potential with the boundary condition $\tilde{g}_{\tilde{\lambda}}(1) = 0$, which is depicted in Fig. 3.13.

We now return to our goal of constructing the complete solution $\Psi(x,t)$ of eq. (3.38) via superposition of the $\Psi_\lambda(x,t)$ for a chosen initial distribution, e.g. a Gaussian, and compare our analytical results with the numerical results obtained in the ideal case of an infinitely high potential. To achieve this we have to determine the remaining constant c_λ in eq. (3.48) and this can be achieved by deriving the scattering solutions [30] of eq. (3.48). To be more precise, we want to show the following:

Proposition 4. *Setting $c_\lambda := \frac{1}{\sqrt{2\pi}} \frac{1}{d_\lambda \alpha^{2i\lambda}}$ for the solution of the Schrödinger equation (3.38) given by eq. (3.48) it follows that*

$$\begin{aligned}
\Psi_\lambda(x,t) = g_\lambda\left(\frac{x}{\alpha\sqrt{t}}\right) f_\lambda(t) &\xrightarrow{t \rightarrow 0} \frac{1}{\sqrt{2\pi}} (-x)^{-2i\lambda} \\
&= \frac{1}{\sqrt{2\pi}} e^{-2i\lambda \ln(-x)} \\
&= \frac{1}{\sqrt{2\pi}} e^{ikz}
\end{aligned} \tag{3.67}$$

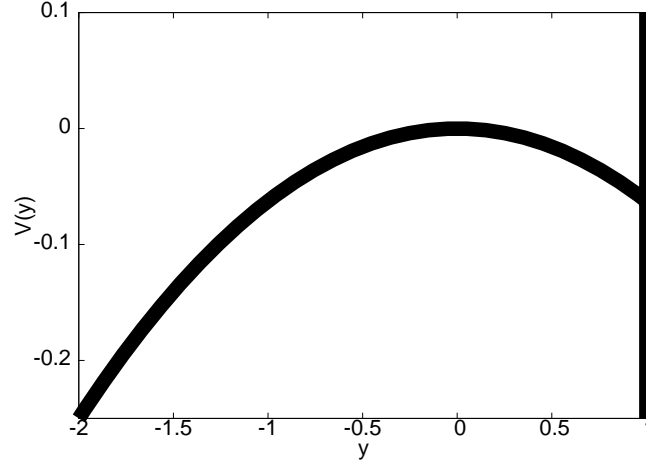


Figure 3.13: Black curve: The potential $V(y)$ the particles interact with in the mirror reference frame, where we chose the parameters $m = 1/2$, $\alpha = 1$, so that $V(y) = -\frac{1}{16}y^2$. The black vertical line indicates the boundary condition at $y = 1 \Leftrightarrow x = \alpha\sqrt{t}$.

with $x < 0$ and d_λ given by

$$\begin{aligned} d_\lambda &= \sqrt{2m} \alpha F\left(i\lambda, \frac{1}{2}, \frac{im\alpha^2}{2}\right) \frac{\Gamma(\frac{3}{2})}{\Gamma(1-i\lambda)} e^{\pm \frac{i\pi}{2}} e^{\mp \pi\lambda} \left(\frac{im\alpha^2}{2}\right)^{-(\frac{1}{2}+i\lambda)} \\ &+ \sqrt{2m} \alpha F\left(\frac{1}{2} + i\lambda, \frac{3}{2}, \frac{im\alpha^2}{2}\right) \frac{\Gamma(\frac{1}{2})}{\Gamma(\frac{1}{2}-i\lambda)} e^{\mp \pi\lambda} \left(\frac{im\alpha^2}{2}\right)^{-i\lambda}, \end{aligned} \quad (3.68)$$

and where $F(a,b,u)$ denotes a confluent hypergeometric function as before and $\Gamma(z)$ the gamma function [37].

Note that although λ is not necessarily real, we simply wish to determine if such a scattering solution given by eq. (3.67) exists, where we choose $\lambda \in \mathbb{R}$. To prove Proposition 4 we require the following theorem, see [37].

Theorem 1. For a, b fixed and u sufficiently large, the confluent hypergeometric function has the form

$$\begin{aligned} F(a,b,u) &= \frac{\Gamma(b)}{\Gamma(b-a)} e^{\pm i\pi a} u^{-a} \left[\sum_{n=0}^{R-1} \frac{(a)_n (1+a-b)_n}{n!} (-u)^{-n} + O(|u|^{-R}) \right] \\ &+ \frac{\Gamma(b)}{\Gamma(a)} e^u u^{a-b} \left[\sum_{n=0}^{S-1} \frac{(b-a)_n (1-a)_n}{n!} (u)^{-n} + O(|u|^{-S}) \right] \end{aligned} \quad (3.69)$$

with $+$ for $-\frac{\pi}{2} < \arg(u) < \frac{3}{2}\pi$ and $-$ for $-\frac{3}{2}\pi < \arg(u) < -\frac{\pi}{2}$.

Using Theorem 1 we will now prove Proposition 4.

Proof. We start with proving that for the stationary solution given by eq. (3.47) we have

$$\begin{aligned} g_\lambda \left(\frac{x}{\alpha\sqrt{t}} \right) &\xrightarrow{t \rightarrow 0} d_\lambda \alpha^{2i\lambda} t^{i\lambda} (-x)^{-2i\lambda} \\ &\Leftrightarrow d_\lambda y^{-2i\lambda}, \end{aligned} \quad (3.70)$$

where d_λ is given by eq. (3.68)¹.

Now using Theorem 1, where for the solution of eq. (3.36) we have $a = i\lambda$, $b = \frac{1}{2}$, and $u = \frac{im\alpha^2}{2}y^2$, $y \in [-1, \infty]$, we obtain

$$\begin{aligned} yF(1+a-b, 1+b, u) &= yF\left(\frac{1}{2} + i\lambda, \frac{3}{2}, \frac{im\alpha^2}{2}y^2\right) \\ &= \underbrace{y \frac{\Gamma(\frac{3}{2})}{\Gamma(1-i\lambda)} e^{\pm i\pi(\frac{1}{2}+i\lambda)} \left(\frac{im\alpha^2}{2}\right)^{-\frac{1}{2}+i\lambda} y^{-1-2i\lambda} \left[\sum \dots (-y^2)^{-n} \dots\right]}_{=:I} \\ &+ \underbrace{y \frac{\Gamma(\frac{3}{2})}{\Gamma(\frac{1}{2}+i\lambda)} e^{\frac{im\alpha^2}{2}y^2} \left(\frac{im\alpha^2}{2}\right)^{-1+i\lambda} y^{2(-1+i\lambda)} \left[\sum \dots (y^2)^{-n} \dots\right]}_{=:II} \end{aligned}$$

and

$$\begin{aligned} F(a, b, u) &= F\left(i\lambda, \frac{1}{2}, \frac{im\alpha^2}{2}y^2\right) \\ &= \underbrace{\frac{\Gamma(\frac{1}{2})}{\Gamma(\frac{1}{2}-i\lambda)} e^{\pm i\pi(i\lambda)} \left(\frac{im\alpha^2}{2}\right)^{-i\lambda} y^{-2i\lambda} \left[\sum \dots (-y^2)^{-n} \dots\right]}_{=:III} \\ &+ \underbrace{\frac{\Gamma(\frac{1}{2})}{\Gamma(i\lambda)} e^{\frac{im\alpha^2}{2}y^2} \left(\frac{im\alpha^2}{2}\right)^{-\frac{1}{2}+i\lambda} y^{-1+2i\lambda} \left[\sum \dots (y^2)^{-n} \dots\right]}_{=:IV}. \end{aligned}$$

Since $y \in [-1, \infty]$, it follows that $II, IV \rightarrow 0$ for $y \rightarrow \infty$. For I and III only the summand for $n = 0$ remains when $y \rightarrow \infty$. Therefore for the stationary solution we

¹ Note that for convenience we defined y here to be $-\frac{x}{\alpha\sqrt{t}}$. For the subsequent calculations this only changes the domain of y and the minus sign in the first term in eq. (3.47) becomes part of y .

have

$$g_\lambda(-y) \xrightarrow{y \rightarrow \infty} \underbrace{\left[\text{const}_1 \frac{\Gamma(\frac{3}{2})}{\Gamma(1-i\lambda)} e^{\pm \frac{i\pi}{2}} e^{\mp \pi \lambda} \left(\frac{im\alpha^2}{2} \right)^{-(\frac{1}{2}+i\lambda)} \right]}_{d_{1\lambda}} y^{-2i\lambda} + \underbrace{\left[\text{const}_2 \frac{\Gamma(\frac{1}{2})}{\Gamma(\frac{1}{2}-i\lambda)} e^{\mp \pi \lambda} \left(\frac{im\alpha^2}{2} \right)^{-i\lambda} \right]}_{d_{2\lambda}} y^{-2i\lambda}$$

with $\text{const}_1 = \sqrt{2m} \alpha F\left(i\lambda, \frac{1}{2}, \frac{im\alpha^2}{2}\right)$ and $\text{const}_2 = \sqrt{2m} \alpha F\left(\frac{1}{2} + i\lambda, \frac{3}{2}, \frac{im\alpha^2}{2}\right)$. It follows that

$$g_\lambda(-y) \xrightarrow{y \rightarrow \infty} d_\lambda y^{-2i\lambda} \quad (3.71)$$

with

$$\begin{aligned} d_\lambda &= (d_{1\lambda} + d_{2\lambda}) \\ &= \left[\sqrt{2m} \alpha F\left(i\lambda, \frac{1}{2}, \frac{im\alpha^2}{2}\right) \frac{\Gamma(\frac{3}{2})}{\Gamma(1-i\lambda)} e^{\pm \frac{i\pi}{2}} e^{\mp \pi \lambda} \left(\frac{im\alpha^2}{2} \right)^{-(\frac{1}{2}+i\lambda)} \right. \\ &\quad \left. + \sqrt{2m} \alpha F\left(\frac{1}{2} + i\lambda, \frac{3}{2}, \frac{im\alpha^2}{2}\right) \frac{\Gamma(\frac{1}{2})}{\Gamma(\frac{1}{2}-i\lambda)} e^{\mp \pi \lambda} \left(\frac{im\alpha^2}{2} \right)^{-i\lambda} \right]. \end{aligned} \quad (3.72)$$

Proposition 4 is now an immediate consequence of setting $c_\lambda = \frac{1}{\sqrt{2\pi} d_\lambda \alpha^{2i\lambda}}$ in the solution given by eq. (3.48). \square

The complete solution of the time-dependent Schrödinger equation (3.38) is given by

$$\begin{aligned} \Psi(x,t) &= \int d\lambda \rho(\lambda) \Psi_\lambda(x,t) \\ &= \int d\lambda \rho(\lambda) \frac{1}{\sqrt{2\pi} d_\lambda \alpha^{2i\lambda}} t^{-i\lambda} g_\lambda\left(\frac{x}{\alpha\sqrt{t}}\right), \end{aligned} \quad (3.73)$$

where $g_\lambda\left(\frac{x}{\alpha\sqrt{t}}\right)$ is given by

$$\begin{aligned} g_\lambda\left(\frac{x}{\alpha\sqrt{t}}\right) &= \left[-\sqrt{2m}\alpha \frac{x}{\alpha\sqrt{t}} F\left(i\lambda, \frac{1}{2}, \frac{im\alpha^2}{2}\right) \cdot F\left(\frac{1}{2} + i\lambda, \frac{3}{2}, \frac{im\alpha^2}{2} \frac{x^2}{\alpha^2 t}\right) \right. \\ &\quad \left. + \sqrt{2m}\alpha F\left(\frac{1}{2} + i\lambda, \frac{3}{2}, \frac{im\alpha^2}{2}\right) \cdot F\left(i\lambda, \frac{1}{2}, \frac{im\alpha^2}{2} \frac{x^2}{\alpha^2 t}\right) \right], \end{aligned} \quad (3.74)$$

d_λ is given by eq. (3.68) and $\rho(\lambda)$ is some initial distribution.

In our numerical simulations we used a Gaussian for the initial position distribution. To compare these results to the analytical results we have to determine the corresponding $\rho(\lambda)$, because the scattering solution given by eq. (3.67) depends on the variable z .

Using the previous results for eq. (3.73) it follows that

$$\Psi\left(-e^{-\frac{z}{2}}, 0\right) =: F(z) = \frac{1}{\sqrt{2\pi}} \int_{-\infty}^{\infty} d\lambda \rho(\lambda) e^{ikz}$$

with $z \in]-\infty, \infty[$. $\rho(\lambda)$ is then given by

$$\begin{aligned} \rho(\lambda) &= \frac{1}{\sqrt{2\pi}} \int_{-\infty}^{\infty} dz F(z) e^{-i\lambda z} \\ &= \frac{1}{\sqrt{2\pi}} \int_{-\infty}^{\infty} dz \Psi\left(-e^{-\frac{z}{2}}, 0\right) e^{-i\lambda z} \end{aligned} \quad (3.75)$$

with $\lambda \in]-\infty, \infty[$.

In our numerical simulations $\Psi(x, 0)$ is given by eq. (3.32). A plot of the corresponding $\rho(\lambda)$ for the parameters in Table 3.1 is shown in Fig. 3.14. Given the general

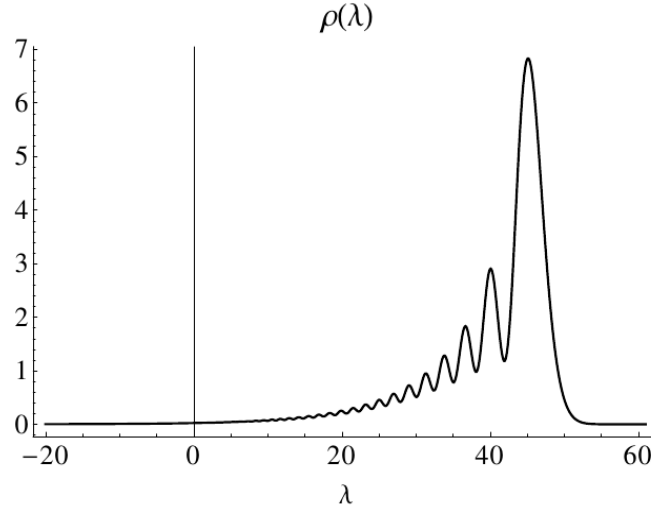


Figure 3.14: Initial distribution $\rho(\lambda)$ for the parameters in Table 3.1.

solution (3.73) one can of course calculate the exact solution in momentum space via

$$\Phi_\lambda(k, t) = \frac{1}{2\pi} \int_{-\infty}^{\alpha\sqrt{t}} dx \Psi_\lambda(x, t) e^{-ikx} \quad (3.76)$$

which is given by

$$\begin{aligned} \Phi(k, t) &= \frac{1}{2\pi} \int_{-\infty}^{\alpha\sqrt{t}} dx e^{-ikx} \Psi(x, t) = \frac{1}{2\pi} \int_{-\infty}^{\alpha\sqrt{t}} dx e^{-ikx} \int d\lambda \rho(\lambda) \Psi_\lambda(x, t) \\ &= \frac{1}{2\pi} \int d\lambda \rho(\lambda) \int_{-\infty}^{\alpha\sqrt{t}} dx e^{-ikx} \Psi_\lambda(x, t) \\ &= \frac{1}{2\pi} \int_{-\infty}^{\infty} d\lambda \rho(\lambda) \int_{-\infty}^{\alpha\sqrt{t}} dx \frac{1}{\sqrt{2\pi\tilde{c}_\lambda\alpha^{2i\lambda}}} t^{-i\lambda} g_\lambda\left(\frac{x}{\alpha\sqrt{t}}\right) e^{-ikx} \end{aligned}$$

$$\begin{aligned}
&= \frac{1}{2\pi} \int_{-\infty}^{\infty} d\lambda \rho(\lambda) \frac{1}{\sqrt{2\pi} \tilde{c}_\lambda \alpha^{2i\lambda-1}} t^{-i\lambda+\frac{1}{2}} \int_{-\infty}^1 dy g_\lambda(y) e^{-ik\alpha\sqrt{t}y} \\
&= \int_{-\infty}^{\infty} d\lambda \rho(\lambda) \Phi_\lambda(k,t).
\end{aligned} \tag{3.77}$$

In Fig. 3.15 the position and velocity distributions derived with the analytical solution are shown¹ and are indistinguishable from the corresponding numerical results shown in Fig. 3.11. Furthermore, in Figs. 3.16, 3.17 and 3.18 we show $\rho(\lambda)$ and the position and velocity distributions for a different set of parameters and varying mass. In all cases one observes a significant velocity reduction. Moreover, comparing these results shows that the width of the oscillations in position space is antiproportional to m .

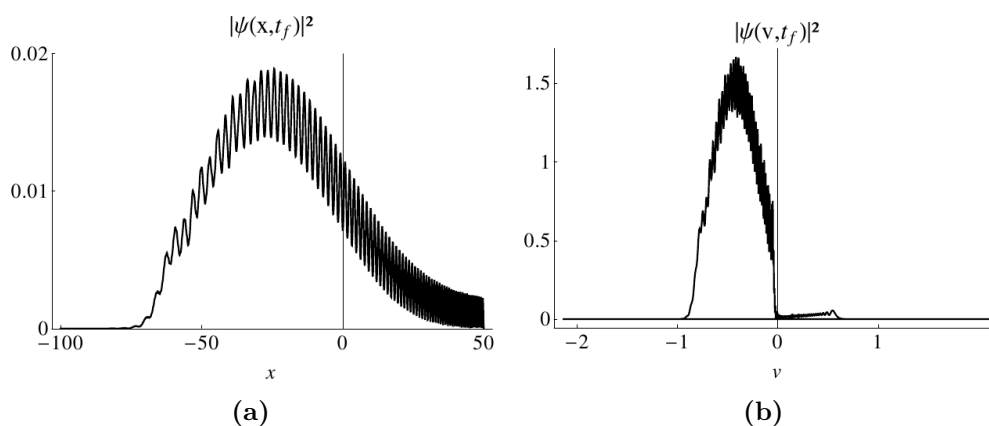


Figure 3.15: (a) Final position distribution $|\Psi(x, t_f)|^2$ and (b) final velocity distribution $|\Psi(v, t_f)|^2$ for the parameters in Table (3.1) derived with the analytical solution (3.73). For the initial distributions see Fig. 3.11.

Instead of determining the exact solution in momentum space via eq. (3.77), we can apply a useful approximation in extending the limit of integration in eq. (3.76) in x from $\alpha\sqrt{t}$ to ∞ . One can then evaluate the integral

$$\frac{1}{\sqrt{2\pi}} \int_{-\infty}^{\infty} dy g_\lambda \left(\frac{x}{\alpha\sqrt{t}} \right) e^{-ikx}$$

explicitly, because the Fourier transformations of the corresponding confluent hypergeo-

¹ Do not confuse the vertical line in these and the following figures with the mirror position.

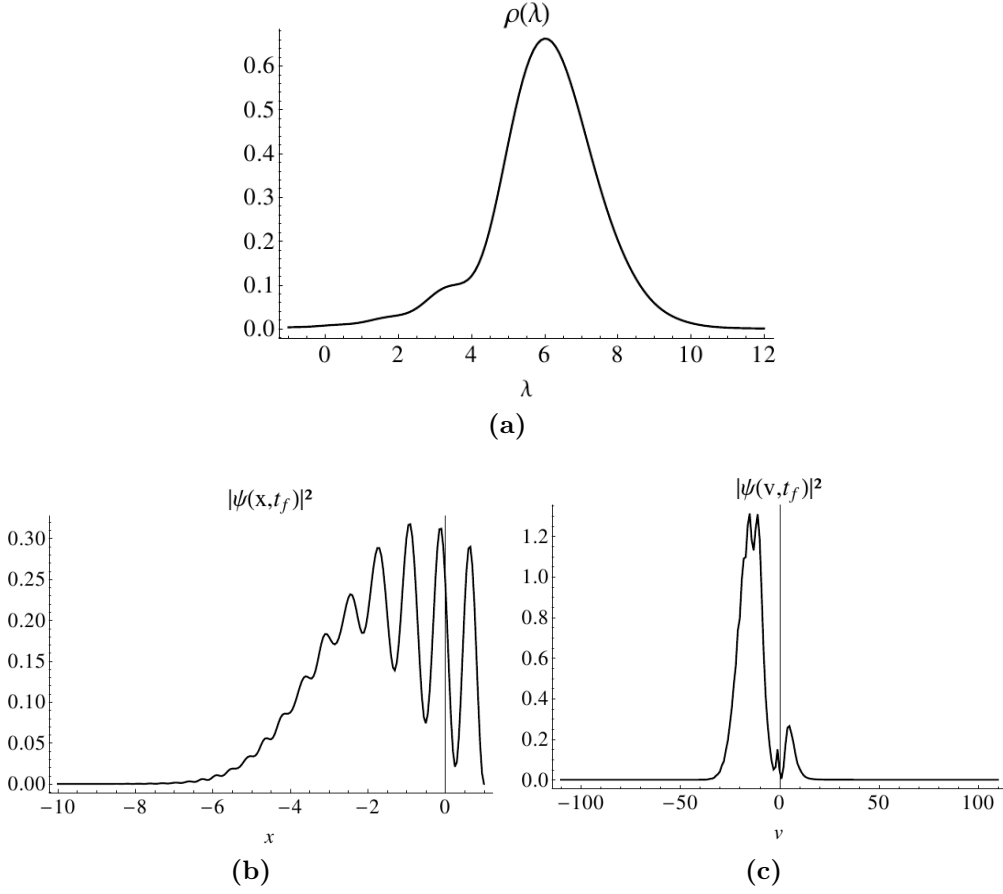


Figure 3.16: (a) Initial distribution $\rho(\lambda)$, (b) final position distribution $|\Psi(x, t_f)|^2$ and (c) final velocity distribution $|\Psi(v, t_f)|^2$ (c) for mass $m=2.5$, where we chose units such that $\hbar = 1$.

metric functions are known. This leads to an approximate solution

$$\begin{aligned}
\Phi_{app}(k, t) &= \frac{1}{2\pi} \int_{-\infty}^{\infty} d\lambda \rho(\lambda) \frac{1}{\tilde{c}_\lambda \alpha^{2i\lambda}} t^{-i\lambda} FT \left\{ g_\lambda \left(\frac{x}{\alpha\sqrt{t}} \right) \right\} \\
&= \frac{1}{2\pi} \int_{-\infty}^{\infty} d\lambda \rho(\lambda) \frac{1}{\tilde{c}_\lambda \alpha^{2i\lambda}} t^{-i\lambda} \frac{\sqrt{\pi} 2^{-i\lambda} \left(-\frac{im}{t} \right)^{-i\lambda}}{\sqrt{m} \Gamma\left(\frac{1}{2} + i\lambda\right) \Gamma(i\lambda)} \frac{|k|^{-1+2i\lambda}}{k} e^{-\frac{ik^2 t}{2m}} \\
&\cdot \left\{ 2m\alpha k \Gamma\left(\frac{1}{2} + i\lambda\right) F\left(\frac{1}{2}, \frac{3}{2}, \frac{im\alpha^2}{2}\right) \right. \\
&- \left. \sqrt{2}\sqrt{t} \left(-\frac{im}{t} \right)^{\frac{1}{2}+i\lambda} \left(\frac{it}{m} \right)^{i\lambda} |k| \Gamma(i\lambda) F\left(i\lambda, \frac{1}{2}, \frac{im\alpha^2}{2}\right) \right\} \\
&= \frac{1}{2\pi} \sqrt{\frac{\pi}{m}} \int_{-\infty}^{\infty} d\lambda \rho(\lambda) \frac{(-2im)^{-i\lambda}}{\tilde{c}_\lambda \alpha^{2i\lambda}} \frac{|k|^{2i\lambda}}{k} e^{-\frac{ik^2 t}{2m}} \\
&\cdot \left\{ \pm 2m\alpha [\Gamma(i\lambda)]^{-1} F\left(\frac{1}{2}, \frac{3}{2}, \frac{i\alpha^2 m}{2}\right) \right. \\
&- \left. (-2im)^{\frac{1}{2}} \left[\Gamma\left(\frac{1}{2} + i\lambda\right) \right]^{-1} F\left(i\lambda, \frac{1}{2}, \frac{i\alpha^2 m}{2}\right) \right\} \tag{3.78}
\end{aligned}$$

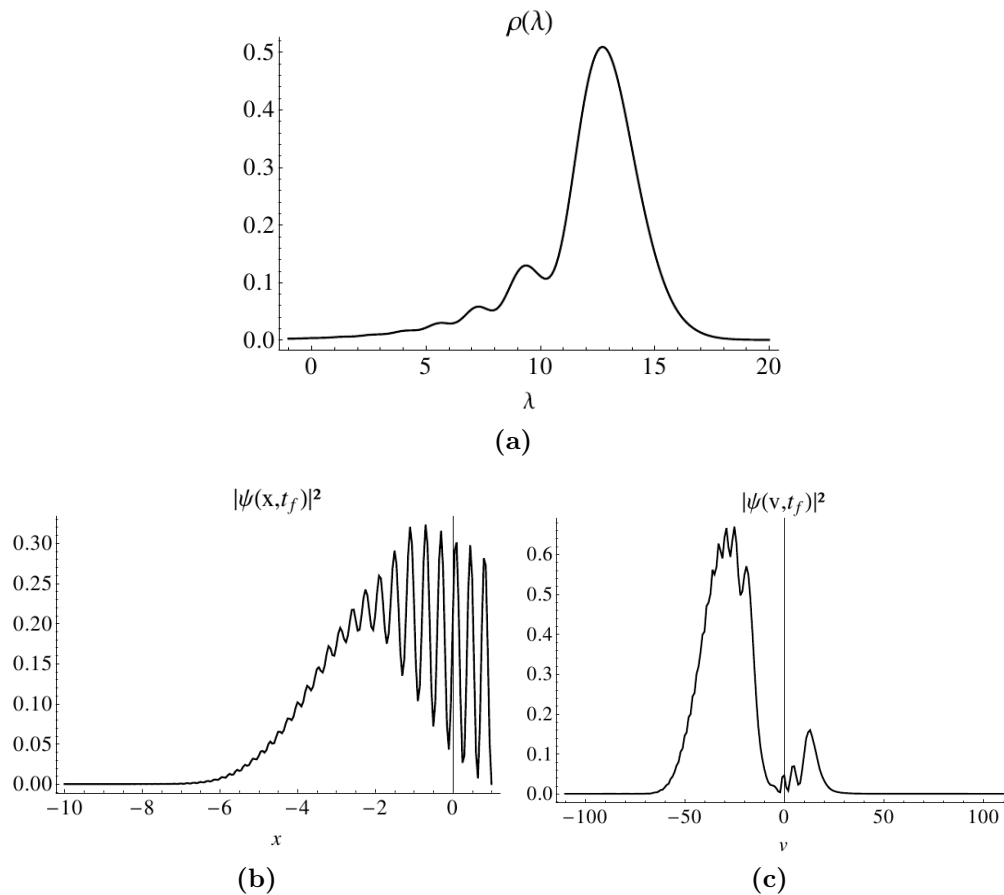


Figure 3.17: (a) Initial distribution $\rho(\lambda)$, (b) final position distribution $|\Psi(x, t_f)|^2$ and (c) final velocity distribution $|\Psi(v, t_f)|^2$ for mass $m=5$, where we chose units such that $\hbar = 1$.

where $+$ for positive k and $-$ for negative k . This approximation works very well for $k < 0$. Moreover, for large times, i.e. when every particle is reflected from the wall, we are mainly interested in the solution for $k < 0$ anyway, since the particle velocity has to be negative after the collision. The exact solution and the corresponding approximation for the parameters in Table 3.1 are compared in Fig. 3.19. This approximation is useful, because it gives a significant speed-up in calculating the solution in momentum space.

Optimality of the Square-Root in Time for Quantum Particles

In Section 3.2.2 we calculated the analytical solution of the Schrödinger equation (3.38) with the time-dependent boundary condition $\Psi(\alpha\sqrt{t}, t) = 0$. As already mentioned, by using the ansatz in eq. (3.49) the problem can be treated more generally for a moving wall with trajectory $l(t)$, i.e. with time-dependent boundary condition $\Psi(l(t), t) = 0$. As was shown in [36], the equation can be separated for $l(t) = \sqrt{at^2 + bt + c}$. Using the ansatz given by eq. (3.49), the general “one-mode” solution of the time-dependent Schrödinger equation (3.38) with time-dependent boundary condition $\Psi(l(t), t) = 0$ is

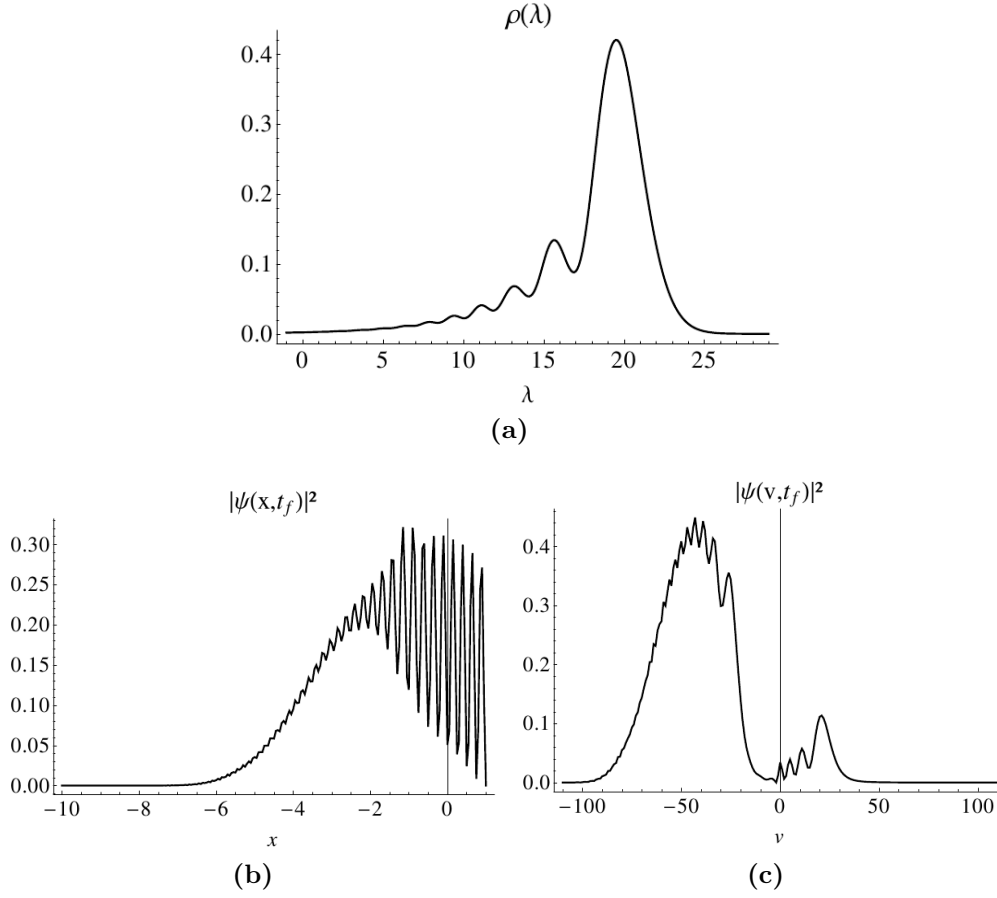


Figure 3.18: (a) Initial distribution $\rho(\lambda)$, (b) final position distribution $|\Psi(x, t_f)|^2$ and (c) final velocity distribution $|\Psi(v, t_f)|^2$ for mass $m=7.5$, where we chose units such that $\hbar = 1$.

given by

$$\Psi_\lambda(x, t) = e^{\frac{i}{2} \dot{l} \frac{y^2}{2}} \cdot l(t)^{-\frac{1}{2}} \cdot g_\lambda(y) \cdot f_\lambda(t) \quad (3.79)$$

with $y = \frac{x}{l(t)}$, $l(t) = \sqrt{at^2 + bt + c}$, $f_\lambda(t) = e^{-i\lambda\tau(t)}$, $\tau = \int_0^t \frac{1}{l(s)^2} ds$ and $g_\lambda(y)$ the solution of the ODE

$$-\frac{d^2}{dy^2} g_\lambda + \frac{r}{4} y^2 g_\lambda = \lambda g_\lambda \quad (3.80)$$

with $r = ac - \frac{b^2}{4}$. To keep the notation clear, here and in subsequent calculations we dropped the previously used tilde denoting the solution for a square-root in time trajectory derived with this ansatz.

We use this result to show that at least among these $l(t)$ the square-root in time trajectory $\sqrt{bt + c}$ is the optimal solution, where we will specify in the following what

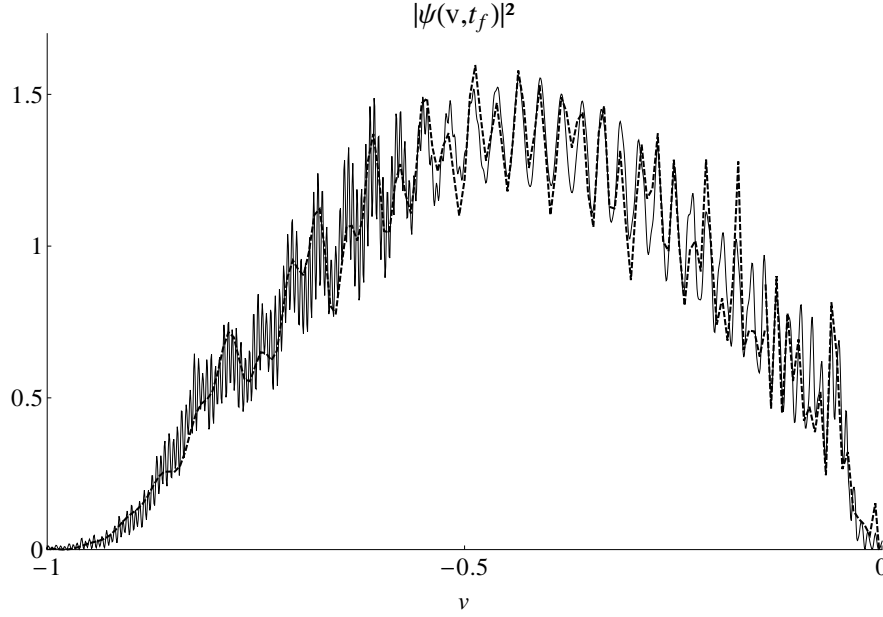


Figure 3.19: (Thin black line) The exact final velocity distribution for the parameters in Table (3.1). (Thick black dashed line) The final velocity distribution calculated with (3.78) for the same parameters.

we mean by optimal. The quantity we will consider is the energy expectation value $E_\lambda(t)$ and we will show that the square-root in time trajectory is optimal in the sense that for every mode $E_\lambda(t)$ goes to zero for $t \rightarrow \infty$ if and only if $a = 0^1$, i.e.

Proposition 5. *For a mirror potential moving along a trajectory $l(t) = \sqrt{at^2 + bt + c}$ and $\forall \lambda$, the energy expectation value $E_\lambda(t)$ obeys*

$$\lim_{t \rightarrow \infty} E_\lambda(t) = 0 \quad \text{if and only if} \quad a = 0. \quad (3.81)$$

Proof. The energy expectation value $E_\lambda(t)$ is given by

$$E_\lambda(t) = \langle \Psi_\lambda | \hat{H} | \Psi_\lambda \rangle = \frac{1}{N_\Psi} \int dx \Psi_\lambda^\dagger i \frac{\partial}{\partial t} \Psi_\lambda. \quad (3.82)$$

with $N_\Psi = \int dx |\Psi_\lambda|^2$. Using eq. (3.79) it follows that

$$\begin{aligned} \frac{\partial}{\partial t} \Psi_\lambda &= \frac{\partial}{\partial t} \left[g_\lambda(y) \cdot f_\lambda(t) \cdot e^{\frac{i}{2} i l \frac{y^2}{2}} \cdot l^{-\frac{1}{2}} \right] \\ &= \dot{g}_\lambda(y) \cdot f_\lambda(t) \cdot e^{\frac{i}{2} i l \frac{y^2}{2}} \cdot l^{-\frac{1}{2}} + \frac{-i\lambda}{l^2} \cdot g_\lambda(y) \cdot e^{\frac{i}{2} i l \frac{y^2}{2}} \cdot l^{-\frac{1}{2}} \\ &+ \frac{i}{2} \frac{y^2}{2} l^2 \left(\frac{\partial l}{\partial t} \right) \cdot g_\lambda(y) \cdot f_\lambda(t) \cdot e^{\frac{i}{2} i l \frac{y^2}{2}} \cdot l^{-\frac{1}{2}} \\ &+ \left(-\frac{1}{2} (2at + b) l^{-\frac{3}{2}} \right) \cdot g_\lambda(y) \cdot f_\lambda(t) \cdot e^{\frac{i}{2} i l \frac{y^2}{2}} \end{aligned}$$

¹ Although the following result was derived independently, a similar one in a more general setting was already stated in [39].

where $l = l(t)$ and

$$\dot{g}_\lambda(y) = \frac{\partial y}{\partial t} \frac{\partial}{\partial y} g_\lambda(y) = -(2at + b) \frac{y}{l} \frac{\partial}{\partial y} g_\lambda(y).$$

Using $|f_\lambda(t)|^2 = 1$ and $|e^{\frac{i}{2} l \frac{y^2}{2}}|^2 = 1$ it follows that

$$\begin{aligned} \Psi_\lambda^\dagger \cdot i \frac{\partial}{\partial t} \Psi_\lambda &= -i g_\lambda^*(y) (2at + b) \frac{y}{l^2} \frac{\partial}{\partial y} g_\lambda(y) + \frac{\lambda}{l^2} \frac{|g_\lambda(y)|^2}{l} \\ &\quad - \frac{1}{4} y^2 l^2 \left(\frac{\partial}{\partial t} \frac{i}{l} \right) \frac{|g_\lambda(y)|^2}{l} - \frac{i}{2} (2at + b) \frac{1}{l} \frac{|g_\lambda(y)|^2}{l}. \end{aligned} \quad (3.83)$$

Since $|\Psi_\lambda|^2 = \frac{|g_\lambda(y)|^2}{l}$, substituting $y = \frac{x}{l}$, $dy = \frac{dx}{l}$ we have

$$N_\Psi = \int dx |\Psi_\lambda|^2 = \int dy |g_\lambda(y)|^2 = N_g \quad (3.84)$$

and

$$\begin{aligned} E_\lambda(t) &= \frac{1}{N_g} \int dy \left[-\frac{i}{l} g_\lambda^*(y) (2at + b) y \frac{\partial}{\partial y} g_\lambda(y) + \frac{\lambda}{l^2} |g_\lambda(y)|^2 \right. \\ &\quad \left. - \frac{1}{4} y^2 l^2 \left(\frac{\partial}{\partial t} \frac{i}{l} \right) |g_\lambda(y)|^2 - \frac{i}{2l} (2at + b) |g_\lambda(y)|^2 \right]. \end{aligned} \quad (3.85)$$

Furthermore, recall that g_λ can always be chosen to be real, since $\left(-\frac{d^2}{dy^2} + \frac{r}{4}y^2\right)$ is a hermitian operator (as was mentioned earlier for the special case $l(t) = \alpha\sqrt{t}$). Therefore it follows for the first term in eq. (3.85) (apart from y -independent factors) that

$$\begin{aligned} \int_{-\infty}^1 g_\lambda(y) y \frac{\partial}{\partial y} g_\lambda(y) &= \left[|g_\lambda(y)|^2 y \right]_{-\infty}^1 - \int_{-\infty}^1 dy \left[g_\lambda(y) + y \frac{\partial}{\partial y} g_\lambda(y) \right] g_\lambda(y) \\ \Rightarrow \int_{-\infty}^1 g_\lambda(y) y \frac{\partial}{\partial y} g_\lambda(y) &= \frac{1}{2} \left[|g_\lambda(y)|^2 y \right]_{-\infty}^1 - \frac{1}{2} \int_{-\infty}^1 |g_\lambda(y)|^2 dy. \end{aligned} \quad (3.86)$$

Now, $\left[|g_\lambda(y)|^2 y \right]_{-\infty}^1 = 0$ due to the boundary condition and $|g_\lambda(y)|^2 y \rightarrow 0$ for $y \rightarrow -\infty$. Furthermore, taking the y -independent factors into account, the second term cancels because of the last term in eq. (3.85). The energy expectation value therefore reduces to

$$E_\lambda(t) = \frac{\lambda}{l^2} - \frac{1}{4} l^2 \left(\frac{\partial}{\partial t} \frac{i}{l} \right) \langle y^2 \rangle_\lambda = \frac{1}{l^2} \left(\lambda - \frac{1}{4} l^4 \left(\frac{\partial}{\partial t} \frac{i}{l} \right) \langle y^2 \rangle_\lambda \right) \quad (3.87)$$

with constant variance $\langle y^2 \rangle_\lambda = \frac{1}{N_g} \int dy y^2 |g_\lambda(y)|^2$. Furthermore we have

$$l^3 \ddot{l} = -(2at + b)^2 + 4a \underbrace{(at^2 + bt + c)}_{=l^2} = 4ac - b^2 = \text{const} =: d_1$$

and therefore

$$l^2 \dot{l}^2 = \frac{(2at + b)^2}{4} = al^2 - \frac{d_1}{4}$$

such that

$$\frac{1}{4} l^4 \left(\frac{\partial \dot{l}}{\partial t} \right) = \frac{l^3 \ddot{l}}{4} - \frac{l^2 \dot{l}^2}{4} = \frac{d_1}{4} + \frac{d_1}{16} - \frac{al^2}{4} = d - \frac{al^2}{4} \quad (3.88)$$

with $d = \frac{d_1}{4} + \frac{d_1}{16}$. Using eq. (3.88) in eq. (3.87) it finally follows that

$$E_\lambda(t) = \frac{1}{l^2} \left(\lambda - \left(d - \frac{al^2}{4} \right) \langle y^2 \rangle_\lambda \right) = \frac{1}{l^2} \left(\lambda - d \langle y^2 \rangle_\lambda \right) + \frac{al^2}{4} \langle y^2 \rangle_\lambda. \quad (3.89)$$

We now take the limit $t \rightarrow \infty$ which proves the proposition. \square

With optimality understood in the sense defined above, we therefore obtain

For a moving mirror potential the square-root in time solution is optimal in the set of trajectories $l(t) = \sqrt{at^2 + bt + c}$, with $a, b, c \in \mathbb{R}$.

3.3 A Quantum Stopper in 2d

In Section 3.2 we considered the problem of stopping a particle or an ensemble of non-interacting particles in one dimension. This for example describes the situation in a waveguide [40, 41] and also in two and three dimensions for a moving flat wall and for the particle velocity component parallel to the mirror trajectory, such that it is also sufficient for ensembles with a narrow momentum distribution around zero in the directions perpendicular to the mirror trajectory. But there are at least two reasons to consider the problem in higher dimensions. Firstly, in the case that the initial velocity distribution is such that one cannot treat the problem as an effectively one-dimensional one, this allows for different mirror geometries, which also affect the velocity components perpendicular to the mirror trajectory. This might lead to an overall gain compared to a flat wall, especially if the velocity reduction for the component parallel to the mirror trajectory remains nearly the same. Later we will see that this is indeed the case for a mirror whose surface is given by a quadratic polynomial. Secondly the treatment in higher dimensions allows for geometries better suited to pursue the question if the square-root in time trajectory might be useful to implement cooling cycles, e.g. by expanding and compressing a ring shaped mirror (see also [42]). In the following we will therefore consider the problem of stopping particles with a mirror moving along a square-root in time trajectory in two dimensions.

3.3.1 Classical Particles

General Considerations

We use similar assumptions as in the one-dimensional case, e.g. the mirror is given by a heavy hard wall, that is the reflection of a particle is elastic and perfect, see

also Section 3.2. In the following we will consider a mirror that both moves and has a time-dependent surface. We start with deriving the formulae for the final position \vec{x}_f and velocity \vec{v}_f of a particle given the initial ones and some final time t_f and vice versa.

The mirror surface shall be connected and we parametrize it such that at a given time t every surface point of the potential acting as a mirror will be specified by a vector

$$(x_1 + x_{m1}(t), x_2 + x_{m2}(t))^T = (f(x_2, t) + x_{m1}(t), x_2 + x_{m2}(t))^T \quad (3.90)$$

where $f(x_2, t)$ will be determined by the mirror geometry considered and $x_{m1}(t)$, $x_{m2}(t)$ are the changes of mirror position. At the collision time t_c the following equality must hold

$$(f(x_2, t) + x_{m1}(t), x_2 + x_{m2}(t))^T = (x_{s1} + v_{s1}t_c, x_{s2} + v_{s2}t_c)^T = \vec{x}_s + \vec{v}_s t_c \quad (3.91)$$

where \vec{x}_s , \vec{v}_s as usual describe the initial position and velocity respectively. Component-wise this leads to

$$\begin{aligned} f(x_2, t_c) &= x_{s1} + v_{s1}t_c - x_{m1}(t_c) \\ x_2 &= x_{s2} + v_{s2}t_c - x_{m2}(t_c) \end{aligned} \quad (3.92)$$

Therefore it follows that the collision time for a mirror potential with time-dependent position and surface depending on the initial velocity, position and the final time can be obtained by solving

$$f(x_{s2} + v_{s2}t_c - x_{m2}(t_c), t_c) \stackrel{!}{=} x_{s1} + v_{s1}t_c - x_{m1}(t_c), \quad (3.93)$$

that is we have $t_c = t_c(\vec{x}_s, \vec{v}_s, t_f)$.

Furthermore, we have to determine the transformations between the initial and final velocities. As in the 1d case this can most easily be done by going to the mirror's instantaneous restframe. We will treat the tangential and normal component separately. For a given time t the transformations are simply given by

$$\vec{v}_{st} - \vec{v}_{mt}(t) = \vec{v}_{st}, \quad \vec{v}_{sn} - \vec{v}_{mn}(t) = \vec{v}_{sn}, \quad \vec{v}_{ft} - \vec{v}_{mt}(t) = \vec{v}_{ft}, \quad \vec{v}_{fn} - \vec{v}_{mn}(t) = \vec{v}_{fn}$$

where the subscripts n and t denote the normal and tangential component respectively and $\vec{v}_{s,f,t,n}$ the particle velocities in the mirror restframe. In this frame we have the simple connections

$$\vec{v}_{ft} = \vec{v}_{st}, \quad \vec{v}_{fn} = -\vec{v}_{sn} \quad (3.94)$$

which just express the fact that a collision in the mirror reference frame does not alter the tangential velocity component and the normal component simply reverses direction. Using this we find for the final velocity in the moving mirror frame

$$\begin{aligned} \vec{v}_f &= \vec{v}_{ft} + \vec{v}_{fn} = \vec{v}_{ft} + \vec{v}_{mt}(t_c) + \vec{v}_{fn} + \vec{v}_{mn}(t_c) = \vec{v}_{st} + \vec{v}_{mt}(t_c) - \vec{v}_{sn} + \vec{v}_{mn}(t_c) \\ &= \vec{v}_{st} - \vec{v}_{mt}(t_c) + \vec{v}_{mt}(t_c) - \vec{v}_{sn} + \vec{v}_{mn}(t_c) + \vec{v}_{mn}(t_c) \\ &= \vec{v}_{st} + \vec{v}_{sn} - 2\vec{v}_{sn} + 2\vec{v}_{mn}(t_c) = \vec{v}_s - 2(\vec{v}_{sn} - \vec{v}_{mn}(t_c)). \end{aligned} \quad (3.95)$$

We therefore have

The final particle velocity and position after a collision are given by

$$\vec{v}_f = \vec{v}_s - 2\vec{n}(\vec{v}_s - \vec{v}_m(t_c))\vec{n} \quad (3.96)$$

and

$$\vec{x}_f = \vec{x}_s + \vec{v}_s t_c + \vec{v}_f(t_f - t_c). \quad (3.97)$$

where $\vec{n} = \frac{1}{\sqrt{1+f'(x_{c2}, t_c)^2}}(-1, f'(x_{c2}, t_c))^T$ is a normal vector at the collision point
 $\vec{x}_c = (x_{c1}, x_{c2})^T$ with $x_{c1,2} = x_{s1,2} + v_{s1,2}t_c$.

After a similar calculation one obtains for the inverse transformations

The initial particle velocity and position before a collision are given by

$$\vec{v}_s = \vec{v}_f - 2\vec{n}(\vec{v}_f - \vec{v}_m(t_c))\vec{n} \quad (3.98)$$

and

$$\vec{x}_s = \vec{x}_f - \vec{v}_f(t_f - t_c) - \vec{v}_s t_c. \quad (3.99)$$

where $\vec{n} = \frac{1}{\sqrt{1+f'(x_{c2}, t_c)^2}}(-1, f'(x_{c2}, t_c))^T$ is a normal vector at the collision point
 $\vec{x}_c = (x_{c1}, x_{c2})^T$ with $x_{c1,2} = x_{f1,2} - v_{f1,2}(t_f - t_c)$.

The collision time depending on the final velocity and position can similarly be obtained by solving

$$f(x_{f2} - v_{f2}t_f + v_{f2}t_c - x_{m2}(t_c), t_c) \stackrel{!}{=} x_{f1} - v_{f1}t_f + v_{f1}t_c - x_{m1}(t_c), \quad (3.100)$$

that is we have $t_c = t_c(\vec{x}_f, \vec{v}_f, t_f)$.

In the following section we will present an example of stopping an ensemble of classical particles in two dimensions.

Stopping with a Polynomial Mirror

We consider a mirror with static surface which is given by a quadratic polynomial and which moves along a square-root in time trajectory, i.e. we consider

$$(-\kappa x_2^2 + \alpha\sqrt{t}, x_2)^T, \quad \kappa, \alpha \in \mathbb{R}_+$$

The situation is schematically depicted in Fig. 3.20. This geometry was chosen because of its simplicity (but thereby not being trivial) and symmetry, which is a reasonable requirement to achieve our goal of an additional velocity reduction of the component perpendicular to the mirror's direction of movement. The collision time t_c is given as a solution of the equation

$$\kappa(x_{s2} + v_{s2}t_c)^2 + x_{s1} + v_{s1}t_c - \alpha\sqrt{t_c} = \kappa x_{c2}^2 + x_{c1} - \alpha\sqrt{t_c} = 0, \quad (3.101)$$

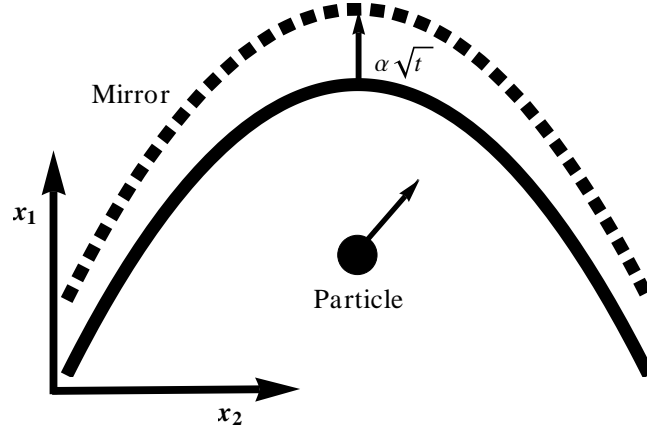


Figure 3.20: Schematic picture of the situation considered in this section. Particles start at some initial position \vec{x}_s with some initial velocity \vec{v}_s and collide with a mirror whose static shape is given by a quadratic polynomial and which moves along a square-root in time trajectory.

where as before we set $x_{c1} = x_{s1} + v_{s1}t_c$, $x_{c2} = x_{s2} + v_{s2}t_c$. The final velocity and position are given by eqs. (3.96) and (3.97) respectively, where

$$\vec{n} = -\frac{1}{\sqrt{1 + 4\kappa^2 x_{c2}^2}}(1, 2\kappa x_{c2})^T. \quad (3.102)$$

In the following we present numerical results where we considered initial distributions

$$p_s(x_1, x_2, v_1, v_2) = \frac{1}{N} \exp \left[-\frac{(v_1 - v_{s1})^2}{2\Delta v_1^2} - \frac{(v_2 - v_{s2})^2}{2\Delta v_2^2} - \frac{(x_1 - x_{s1})^2}{2\Delta x_1^2} - \frac{(x_2 - x_{s2})^2}{2\Delta x_2^2} \right] \quad (3.103)$$

for $x_2 < -\kappa x_2^2$, and $p_s(x_1, x_2, v_1, v_2) = 0$ otherwise (N being a normalization constant).

For the subsequent examples we used the parameters in Table 3.3. In Fig. 3.21

Parameters Initial Distribution:			
$x_{s1} = -0.0042$	$x_{s2} = 0$	$\Delta x_1 = 0.0047430$	$\Delta x_2 = 0.0047430$
$v_{s1} = 5$	$v_{s2} = 0$	$\Delta v_1 = 1.2$	$\Delta v_2 = 0.47430$
Other Parameters:			
$t_f = 1$	$\alpha = 1$	$\kappa = 1, 1.5, \dots, 5$	

Table 3.3: Dimensionless parameters for the simulations with a polynomial mirror in the classical case.

κ	$\langle v_1 \rangle$	$\langle v_2 \rangle$	Δv_1	Δv_2
0	-0.492	0	0.193	0.471
1	-0.505	0	0.187	0.209
1.5	-0.504	0	0.192	0.121
2	-0.498	0	0.197	0.167
2.5	-0.491	0	0.204	0.268
3	-0.491	0	0.203	0.332
3.5	-0.496	0	0.198	0.340
4	-0.523	0	0.201	0.322
4.5	-0.546	0	0.202	0.303
5	-0.560	0	0.205	0.286

Table 3.4: Expectation values and standard deviations of the final velocity distributions for a polynomial mirror and the parameters in Table 3.3 in the classical case.

the final position and velocity marginals

$$\begin{aligned}
 p_f(x_1, x_2) &= \int dv_1 dv_2 p_f(x_1, x_2, v_1, v_2), \\
 p_f(v_1, v_2) &= \int dx_1 dx_2 p_f(x_1, x_2, v_1, v_2),
 \end{aligned}
 \tag{3.104}$$

for $\kappa = 1.5$ are compared to the initial ones¹. One not only observes a narrow velocity distribution around zero for the v_1 component, but also a reduced width for the v_2 component. In Fig. 3.22 the velocity marginals

$$\begin{aligned}
 p_f(v_1) &= \int dv_2 p_f(v_1, v_2), \\
 p_f(v_2) &= \int dv_1 p_f(v_1, v_2),
 \end{aligned}
 \tag{3.105}$$

for all κ in Table 3.3 are shown. The results for the v_1 component are hardly effected by the change of curvature in the parameter range considered and are especially nearly the same for $\kappa = 0$ (flat wall), whereas the v_2 component changes significantly compared to the flat wall and one observes a velocity reduction also for this component. To see this even more clearly, the results for $\kappa = 0$, for $\kappa = 1$, and $\kappa = 3.5$ are compared to the initial distributions in Fig. 3.23, which for the v_2 component is of course equal to the one for a flat wall. Furthermore, the corresponding expectation values can be found in Table 3.4. The final distributions hardly differ for the v_1 component, whereas for the v_2 component the final distributions differ significantly and compared to $\kappa = 0$ an additional slowing can be observed. Compared to the initial distributions, in contrast to a flat wall, for the mirror with curvature $\kappa > 0$ we therefore observe a significant slowing of the particles both for the v_1 and v_2 component, which shows that overall it

¹ The slightly coarse surface of the final position distribution is simply due to the discretization, i.e. the finite number of plot points, and is not to be confused, for example, with local maxima or minima.

has a superior performance compared to a flat wall. On the other hand one can also see that larger curvature does not necessarily lead to a larger velocity reduction. We obtained the best result for $\kappa = 1.5$, but we did not seek to optimize this numerically.

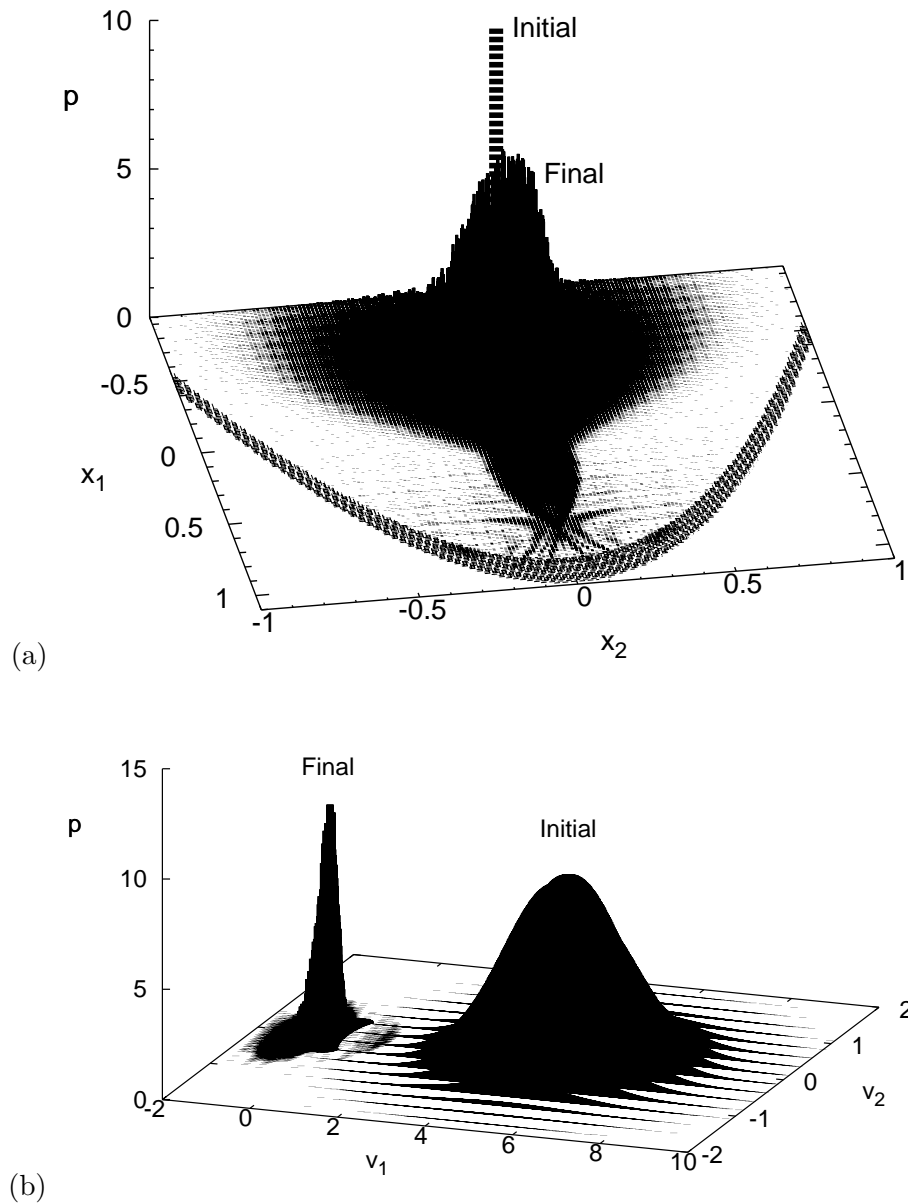


Figure 3.21: Classical Case. The surface of the mirror potential is given by a quadratic polynomial.
 (a) The (dashed) initial and (solid) final position probability distributions $p_{s,f}(x_1, x_2)$, where the initial distribution is given by eq. (3.103) with the parameters in Table 3.3 and $\kappa = 1.5$. Additionally the final mirror position is plotted.
 (b) The corresponding initial and final velocity probability distributions $p_{s,f}(v_1, v_2)$. The initial distribution was scaled by a factor 30.

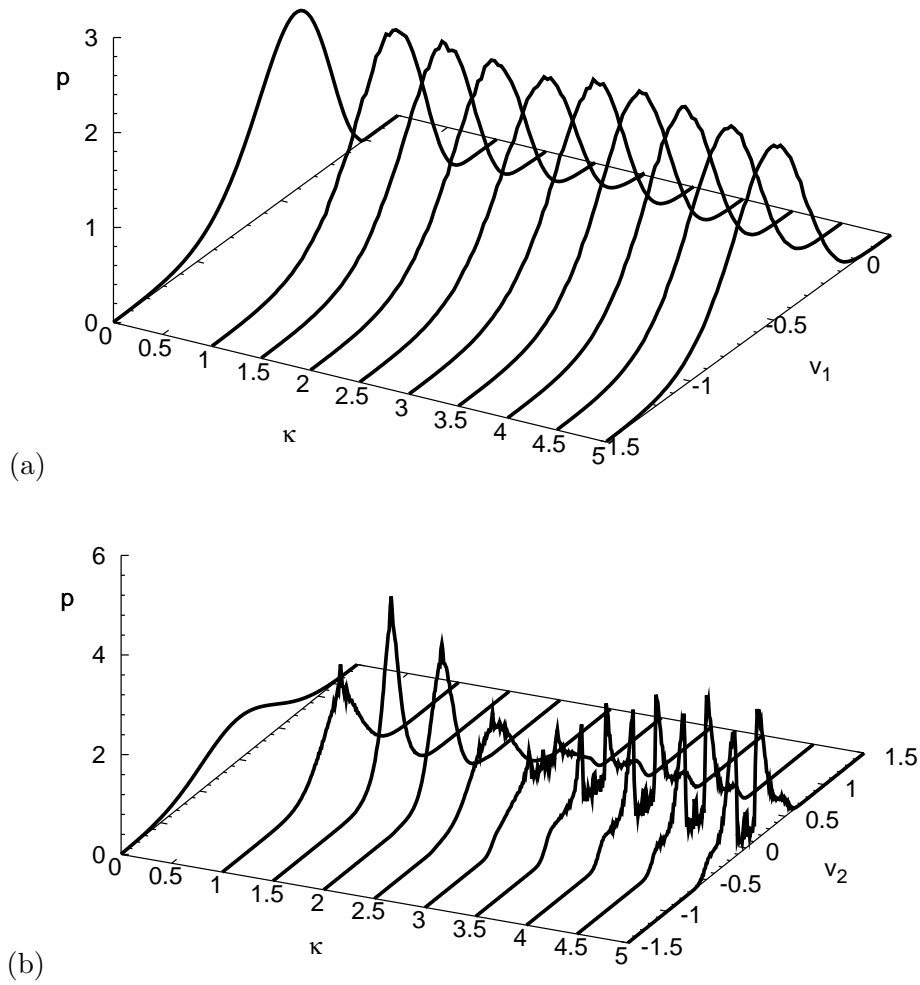


Figure 3.22: Classical Case. The surface of the mirror potential is given by a quadratic polynomial.

(a) The final velocity marginals $p_f(v_1)$ for the parameters in Table 3.3.

(b) The final velocity marginals $p_f(v_2)$ for the parameters in Table (3.3).

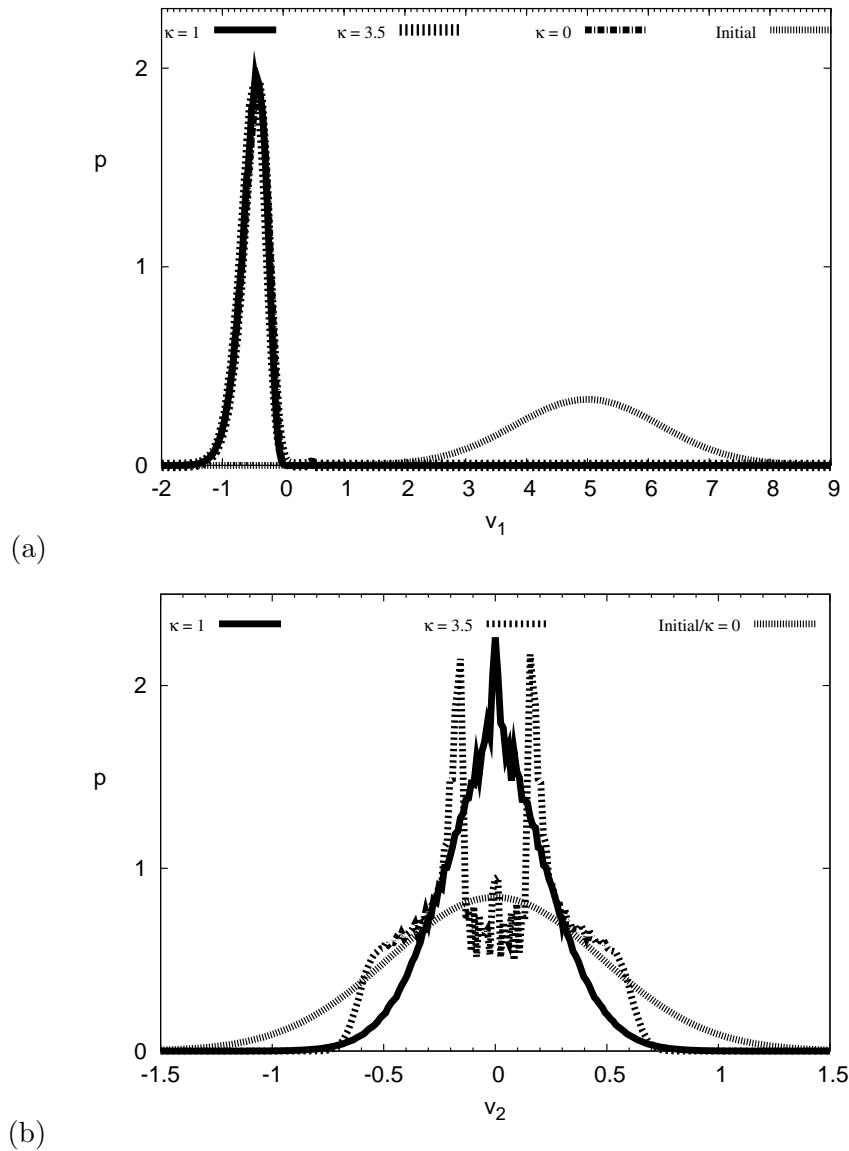


Figure 3.23: Classical Case. The surface of the mirror potential is given by a quadratic polynomial.

(a) The velocity marginals $p_f(v_1)$ for the parameters in Table 3.3 for $\kappa = 0$ (flat wall), $\kappa = 1$ and $\kappa = 3.5$ compared to the initial distribution.

(b) The velocity marginals $p_f(v_2)$ for the parameters in Table 3.3 for $\kappa = 0$ (flat wall), $\kappa = 1$ and $\kappa = 3.5$ compared to the initial distribution.

3.3.2 Quantum Particles

General Considerations

In Section 3.3.1 we investigated the stopping of particles in two dimensions in the classical framework and as an example considered a mirror whose surface is given by a quadratic polynomial. We now proceed by investigating a similar situation in the quantum mechanical framework, but instead of a perfectly reflecting and impenetrable potential modelled via a boundary condition for the classical particles, we will consider an actually realizable potential, i.e. a Gaussian in the examples below. Therefore, the subsequent results are foremost meant to demonstrate that the square-root in time trajectory leads to a significant velocity reduction for both components even under these more realistic conditions. The classical results are only there to illustrate that the idea works in an idealized setup and we will at most seek a qualitative comparison between these and the quantum mechanical ones. The reason is that, apart from the obvious difference due to the different frameworks, using these potentials leads to differences which even arise in a purely classical description. To see this consider a classical particle with a certain initial position. Given a specific mirror geometry and trajectory, in the case of an infinitely high potential its initial velocity then determines the collision point. In the case of a more realistic Gaussian potential this holds too, but due to the potentials finite spread and height different velocities lead to an additional change in the collision point. To be more precise, due to the finite spread and height a faster particle has to move further to be repelled by the potential, because it requires a higher potential energy for this to happen¹.

We start with the two-dimensional Schrödinger equation for the particle and the moving mirror potential. It is given by

$$i\hbar \frac{\partial}{\partial t} \psi(x_1, x_2, t) = -\frac{\hbar^2}{2m} \left(\frac{\partial^2}{\partial x_1^2} + \frac{\partial^2}{\partial x_2^2} \right) \psi(x_1, x_2, t) + V(x_1, x_2, t) \psi(x_1, x_2, t), \quad (3.106)$$

where the potential $V(x_1, x_2, t)$ will be specified in the examples below. In all the examples considered in subsequent sections, the initial state is a Gaussian, but not necessarily a minimal uncertainty one,

$$\begin{aligned} & \psi_0(x_1, x_2) \quad (3.107) \\ &= \frac{1}{N_1} \exp \left\{ -\frac{\mu}{2(1+2i\Delta v_1^2 \mu \delta_1)} [i v_{s1} (\delta_1 v_{s1} - 2x_1) + 2\Delta v_1^2 \mu ((x_1 - \beta_1)^2 + 2\delta_1 v_{s1} \beta_1)] \right\} \\ &\times \frac{1}{N_2} \exp \left\{ -\frac{\mu}{2(1+2i\Delta v_2^2 \mu \delta_2)} [i v_{s2} (\delta_2 v_{s2} - 2x_2) + 2\Delta v_2^2 \mu ((x_2 - \beta_2)^2 + 2\delta_2 v_{s2} \beta_2)] \right\}, \end{aligned}$$

where $\delta_1 = \sqrt{4\Delta x_1^2 - 1/(\Delta v_1^2 \mu^2)}/(2\Delta v_1)$, $\delta_2 = \sqrt{4\Delta x_2^2 - 1/(\Delta v_2^2 \mu^2)}/(2\Delta v_2)$, $\beta_1 = x_{s1} - \delta_1 v_{s1}$, $\beta_2 = x_{s2} - \delta_2 v_{s2}$, and $\mu = m/\hbar$. The form of Heisenberg's uncertainty

¹ This difference already occurred in the one-dimensional case, which we briefly pointed out when discussing the differences between the results for an infinitely high potential and a Gaussian in the quantum case. However, in the one-dimensional case we could compare the results in both frameworks for an infinitely high potential, whereas here we are content with considering a Gaussian potential in the quantum case.

relation is $\Delta x_1 \Delta v_1 \geq 1/(2\mu)$ and $\Delta x_2 \Delta v_2 \geq 1/(2\mu)$.

Stopping with a Polynomial Mirror

In this section we again consider a mirror whose surface is given by a quadratic polynomial, but, in contrast to the classical case, instead of an infinitely high potential we consider a Gaussian. To be more precise the x_1 component of the potential has a Gaussian profile, i.e. the potential is given by

$$V_G(x_1, x_2, t) = V_0 \exp[-(x_1 + \kappa x_2^2 - \alpha \sqrt{t})^2 / (2\Delta x_{12V}^2)], \quad \kappa \in \mathbb{R}_+. \quad (3.108)$$

Although we are not aiming for a comparison between the classical and the quantum mechanical results due to the reasons discussed in the beginning of this section, we used similar parameters for the initial wavefunction (3.107) and the potential (3.108), which can be found in Table 3.5. The only difference between the parameters in Table 3.3 and Table 3.5 is the average initial position x_{s1} . We chose a different value in the quantum case to take the finite spread of the potential at least partially into account, because x_{s1} is the distance to the initial position of the potential maximum, but, depending on the velocity, it might be reflected at a smaller distance.

Considering a classical estimate for the kinetic energy using the average initial velocity v_{s1} , the average initial position x_{s1} chosen for the simulations in the quantum case corresponds approximately to the average initial position x_{s1} chosen in the classical case for an infinitely high potential. We only have to adjust the x_1 -distance, because the x_1 component has a Gaussian profile, whereas the thereby altered average initial position x_{s2} then automatically corresponds to the average initial x_{s2} in the classical case for the average initial velocity v_{s2} . To see this just consider the full width half maximum of the potential (3.108) at time $t = 0$, i.e. $|x_1 - \kappa x_2^2| \leq \Delta x_{12v}$. For x_1 it follows that $\kappa x_2^2 - \Delta x_{12v} \leq x_1 \leq \kappa x_2^2 + \Delta x_{12v}$, i.e. in the x_1 direction we have a Gaussian for every x_2 , which are “glued” together along a parabola.

In Fig. 3.24 the initial and final probability distributions for position and velocity for the parameters in Table 3.5 and $\kappa = 1.5$ are shown. As in the classical case one obtains a narrow velocity distribution around zero for the v_1 component and also observes a narrowing of the distribution for the v_2 component. This can be seen more clearly in

Initial State Parameters:			
$x_{s1} = -0.023715$	$x_{s2} = 0$	$\Delta x_1 = 0.00474299$	$\Delta x_2 = 0.00474299$
$v_{s1} = 5$	$v_{s2} = 0$	$\Delta v_1 = 1.2$	$\Delta v_2 = 0.474299$
$m = 296.033$			
Mirror Parameters:			
$V_0 = 3 \cdot 10^4$	$\Delta x_{12v} = 0.01$	$\kappa = 1, 1.5 \dots 5$	
Other Parameters:			
$t_f = 1$	$\alpha = 1$		

Table 3.5: Dimensionless parameters for the simulations with a polynomial mirror in the quantum case.

Initial State Parameters:			
$x_{s1} = -6.3 \mu\text{m}$	$x_{s2} = 0$	$\Delta x_1 = 0.7 \mu\text{m}$	$\Delta x_2 = 0.7 \mu\text{m}$
$v_{s1} = 10.6 \text{ cm/s}$	$v_{s2} = 0$	$\Delta v_1 = 2.5 \text{ cm/s}$	$\Delta v_2 = 1 \text{ cm/s}$
$m_{Li} = 9.99 \cdot 10^{-27} \text{ kg}$			
Mirror Parameters:			
$V_0/\hbar = 3.75 \cdot 10^6/\text{s}$		$\Delta x_{12v} = 1.4 \mu\text{m}$	
Other Parameters:			
$t_f = 7 \text{ ms}$		$d_f = 14.8 \mu\text{m}$	

Table 3.6: Example of dimensioned parameters corresponding to the dimensionless ones in Table 3.5 for Lithium.

Fig. 3.25, where the velocity marginals for all κ in Table 3.5 are shown. In addition we provide an exemplary set of dimensioned parameters in Table 3.6. Note that these are just one possible choice, where we used the mass of Lithium. Similar values can for example be obtained for Rubidium. The expectation values and variances we obtain for the different κ can be found in Table 3.7. Again the result for the v_1 component is hardly effected by the change of curvature in the parameter range considered and is nearly the same as for a flat wall ($\kappa = 0$), whereas the v_2 component changes significantly compared to the flat wall and one observes a large velocity reduction also for this component. To see this more clearly, the results for a flat wall, for $\kappa = 1$ and $\kappa = 3.5$ are again compared to the initial distributions in Fig. 3.26 and we observe both for the v_1 and v_2 component a significant slowing of the particles. Furthermore, we have an overall superior performance for a mirror with a curvature $\kappa > 0$, see again Table 3.7. On the other hand one can also see that larger curvature does not necessarily lead to superior stopping. We obtained the best result for $\kappa = 1.5$, but we did not seek to optimize this by numerical search.

Finally, although being aware that the situations are at most qualitatively compa-

κ	$\langle v_1 \rangle$	$\langle v_2 \rangle$	Δv_1	Δv_2
0	-0.444	0	0.160	0.471
1	-0.469	0	0.156	0.193
1.5	-0.467	0	0.160	0.102
2	-0.458	0	0.166	0.142
2.5	-0.442	0	0.175	0.246
3	-0.441	0	0.168	0.307
3.5	-0.458	0	0.164	0.314
4	-0.481	0	0.167	0.296
4.5	-0.501	0	0.171	0.278
5	-0.517	0	0.175	0.264

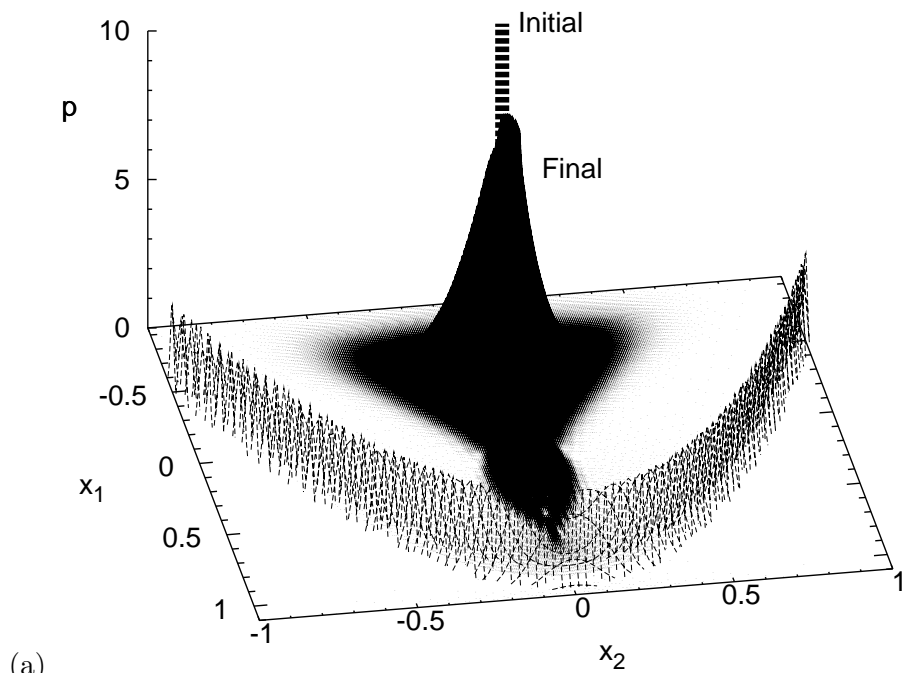
Table 3.7: Expectation values and standard deviations of the final velocity distributions for a polynomial mirror and the parameters in Table 3.5 in the quantum case.

rable due to the reasons discussed in the beginning, we wish to determine if the results in the quantum case at least become more similar to the classical ones if we increase the mass¹. This is done in Fig. 3.27, where the results in the quantum case again for the parameters in Table 3.5 and $\kappa = 3.5$ as well as the results for a mass $m = 600$ are compared to the corresponding classical results. They show that for an increasing mass the results in the quantum case indeed become more similar to the classical ones.

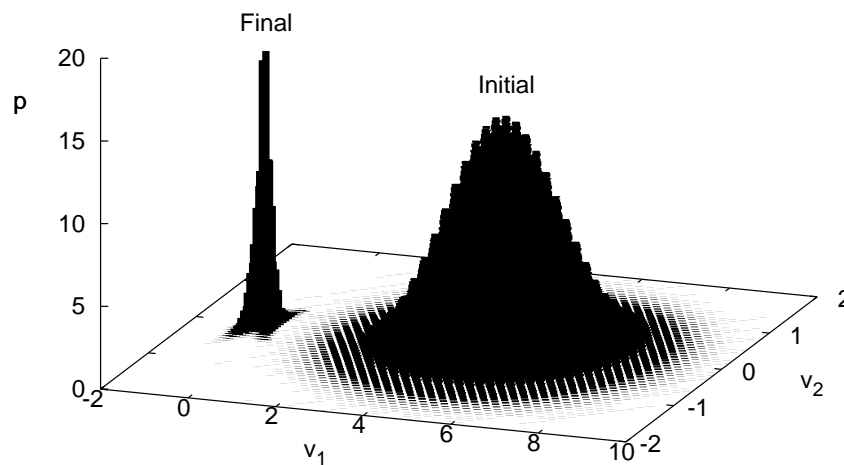
As mentioned above the dimensioned parameters in Table 3.6 corresponding to the results shown in Figs. 3.24-3.27 are only meant to serve as an example and similar values can be obtained for example for Rubidium. Furthermore, by adjusting the dimensioned parameters t_f and d_f ² larger initial distances as well as velocities can be compensated such that one obtains the same final distributions. Also by using different dimensionless parameters, e.g. smaller initial distances, the final velocity distribution can in principle be made arbitrarily narrow. Choosing large enough t_f and d_f in turn, one could obtain the same initial state parameters in Table 3.6 for such an in principle arbitrarily narrow final velocity distribution, that is one is only limited by the conditions in the laboratory.

1 Heuristically this corresponds to a classical limit.

2 This corresponds to a change of the parameter α .



(a)



(b)

Figure 3.24: Quantum Case. The mirror potential is given by eq. (3.108).

(a) The (dashed) initial and (solid) final position probability distributions $p_{s,f}(x_1, x_2)$ for an initial wavefunction (3.107) with the parameters in Table 3.5 and $\kappa = 1.5$. Additionally the potential is plotted at $t_f = 1$.

(b) The initial and final velocity probability distributions $p_{s,f}(v_1, v_2)$ for an initial wavefunction (3.107) with the parameters in Table 3.5 and $\kappa = 1.5$. The initial distribution was scaled by a factor 50.

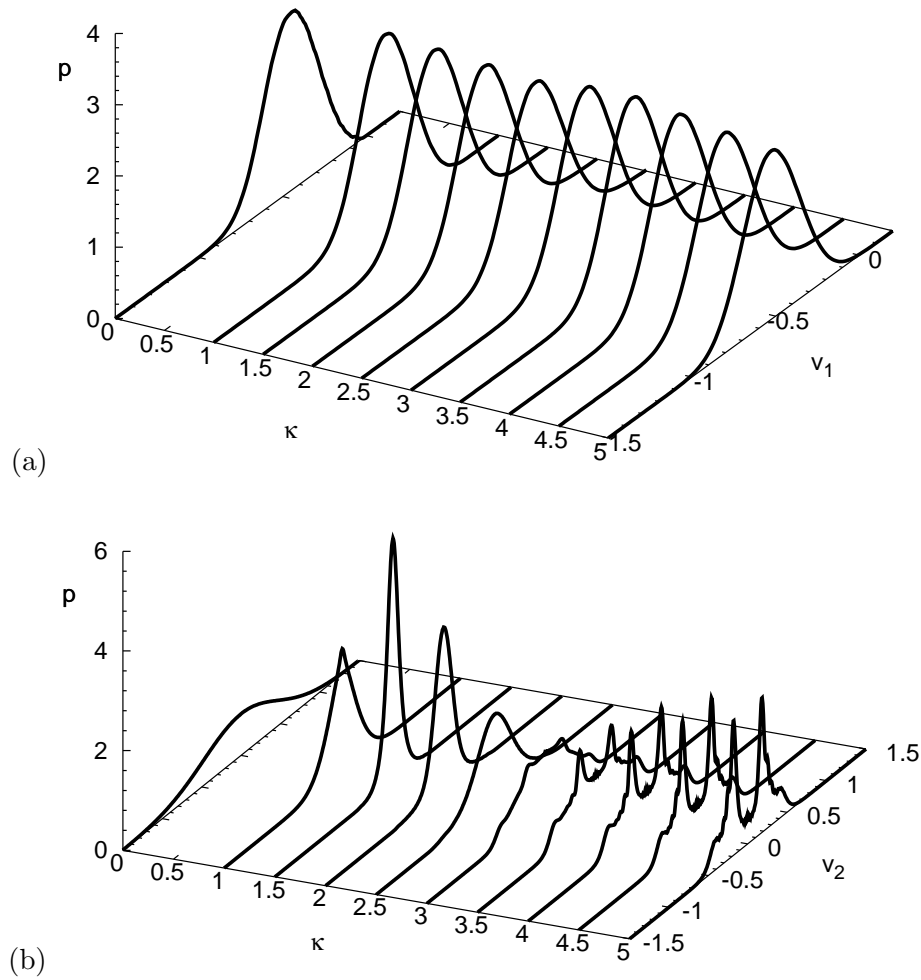


Figure 3.25: Quantum Case. The mirror potential is given by eq. (3.108).
 (a) The final velocity marginals $p_f(v_1)$ for the parameters in Table 3.5.
 (b) The final velocity marginals $p_f(v_2)$ for the parameters in Table 3.5.

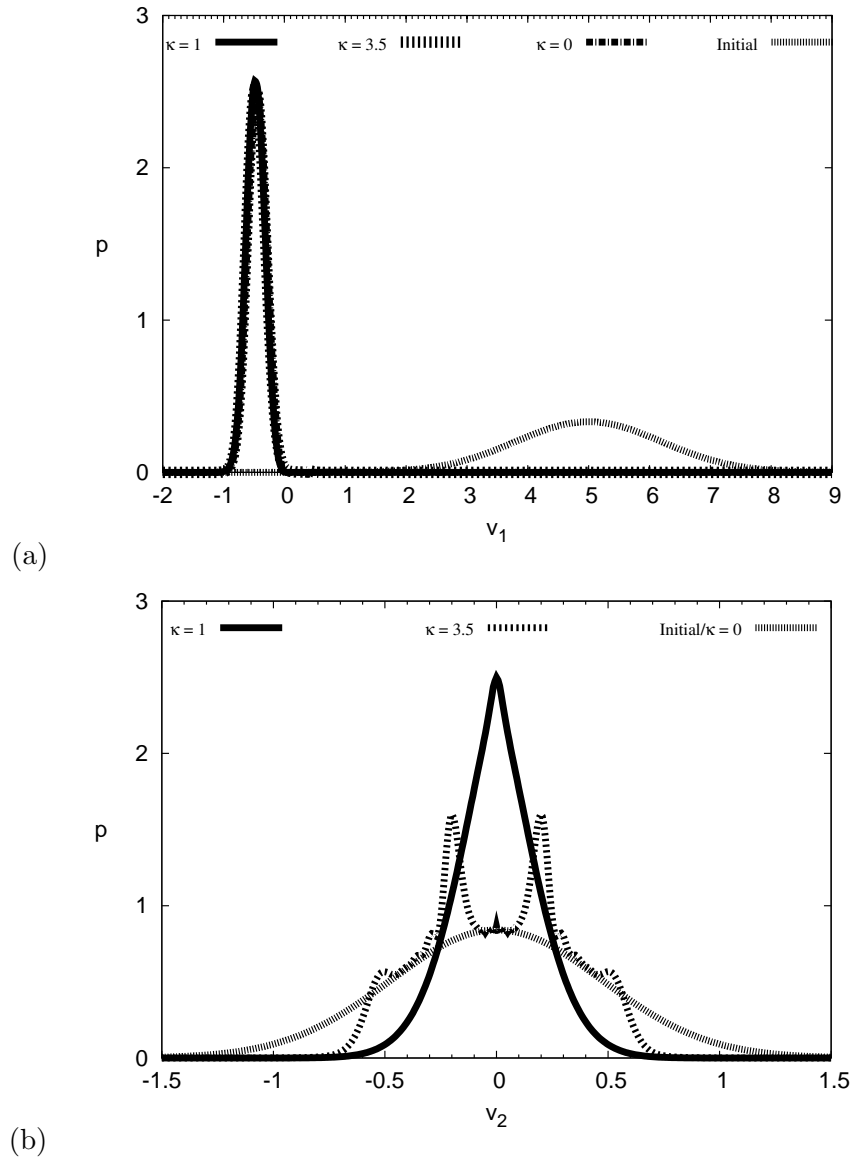


Figure 3.26: Quantum Case. The mirror potential is given by eq. (3.108).
 (a) The velocity marginals $p_f(v_1)$ for the parameters in Table 3.5 for flat wall ($\kappa = 0$), $\kappa = 1$ and $\kappa = 3.5$ compared to the initial distribution.
 (b) The velocity marginals $p_f(v_2)$ for the parameters in Table 3.5 for flat wall ($\kappa = 0$), $\kappa = 1$ and $\kappa = 3.5$ compared to the initial distribution.

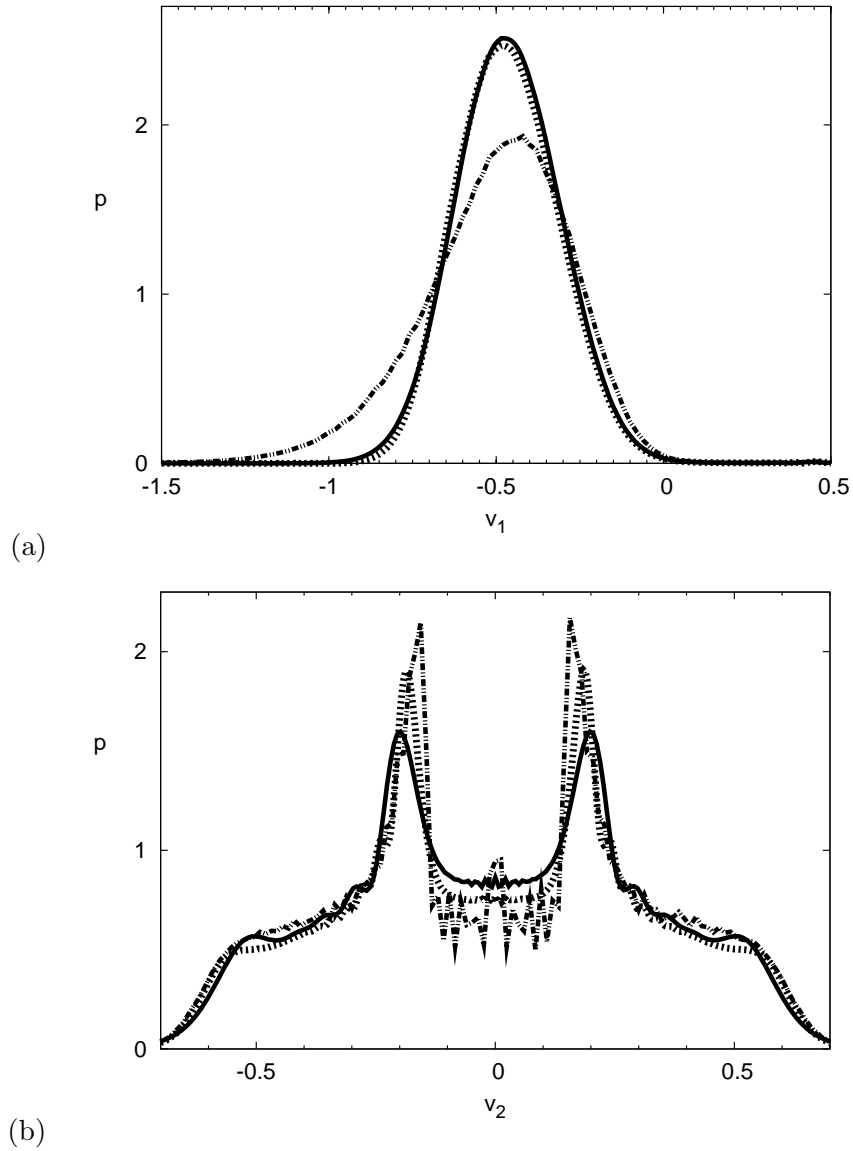


Figure 3.27: The velocity marginals $p_f(v_1)$ and $p_f(v_2)$ in the quantum case for the parameters in Table 3.5 and $\kappa = 3.5$ (solid line) as well as for $m = 600$ (thick dashed line) compared to the corresponding classical results (dotted dashed line). (a) The velocity marginals $p_f(v_1)$. (b) The velocity marginals for $p_f(v_2)$.

Stopping with a Ring

As a further example in the quantum case we now consider a mirror potential given by an expanding ring¹, see Fig. 3.28. Such a ring could be implemented by creating a

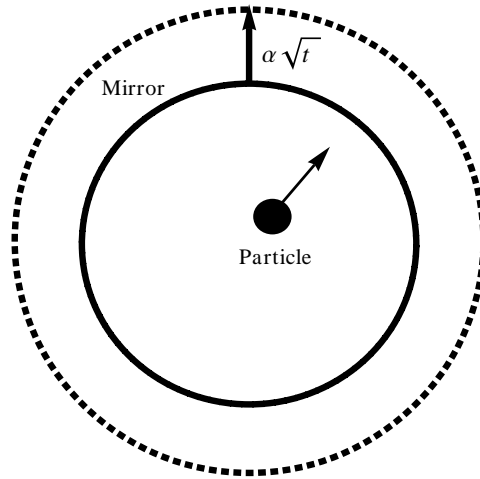


Figure 3.28: Schematic picture of the situation considered in this section. Particles start at some initial position \vec{x}_s with some initial velocity \vec{v}_s and collide with a ring shaped mirror whose radius increases with a square-root in time.

dark spot inside a laser beam [45]-[47] and is therefore more than just convenient from a mathematical point of view. This geometry is interesting for at least two reasons. Firstly, in the classical case with one particle initially in the ring center this problem reduces to the one-dimensional case, but in the quantum case this is apparently not true. Still, this geometry is in some sense the natural two-dimensional extension and as it was important in the one-dimensional case to determine what influence a change of the average initial distance from the mirror has, it might be interesting to see what effect a shift of the average initial position from the origin has for an expanding ring, i.e. what happens if the symmetry of the problem is broken. Secondly, it is the most obvious and promising choice to implement cooling cycles by expansion and compression, see next section.

The ring will expand along the trajectory $\alpha\sqrt{t+t_0}$ with some initial time $t_0 \in \mathbb{R}_+$ and as in the case of a polynomial mirror, instead of an infinitely high potential we consider again a Gaussian mirror potential, where the Gaussian profile is given along the radius, i.e. the potential is

$$V_G(x_1, x_2, t) = V_0 \exp[-(\sqrt{x_1^2 + x_2^2} - \alpha\sqrt{t+t_0})^2 / (2\Delta x_{12V}^2)]. \quad (3.109)$$

¹ For an interesting study of the reflections of a classical particle inside an expanding ring as well as an ellipsoid see [43, 44] and for a different study of the general case of classical and quantum particles inside an expanding force field [39].

For the initial wavefunction (3.107) and the potential (3.109) we used the parameters in Table 3.8. In Fig. 3.29 the initial and final probability distributions for position and velocity for $t_0 = 0.004$ are shown, where one again observes a significant slowing of the particles. Furthermore, in Fig. 3.30 the velocity marginals for all t_0 in Table 3.8 are shown. The “wandering” of the peaks can at least heuristically be understood by multiple reflections and the corresponding classical considerations in Section 3.2.1. For the chosen examples one can also follow the time evolution directly and observe the reflections of the wavefunction. It turns out that a second one becomes more likely for larger t_0 , i.e. a larger part of the wavefunction is reflected. This also explains heuristically the shape of the final distributions for different t_0 in Fig. 3.31. For $t_0 = 0.003$ essentially only one reflection occurred and we observe a narrow distribution with a peak at negative velocities. For $t_0 = 0.005$ the peak at negative velocities is shifted to the left because the velocity reduction becomes worse, but on the other hand we observe that a larger part of the wavefunction was reflected a second time, which is expressed by a second peak in the range of positive velocities. This peak is located at smaller velocities, since every reflection leads to an additional velocity reduction. Finally, for $t_0 = 0.01$ the situation is qualitatively the same, but now the wavefunction was completely reflected a second time. The corresponding expectation values and standard deviations of the absolute value of the final velocity show that there actually can be an overall gain due to larger t_0 , see Table 3.9 and also Section 3.2.1 for a classical example.

Finally we considered shifts (or offsets) of the average initial positions x_{s1} and x_{s2} from the origin only in x_1 -direction or only in x_2 -direction respectively, as well as both in x_1 - and x_2 -direction for $t_0 = 0.005$. The corresponding marginals for v_1 and v_2

Initial State Parameters:			
$x_{s1} = 0$	$x_{s2} = 0$	$\Delta x_1 = 0.0047430$	$\Delta x_2 = 0.0047430$
$v_{s1} = 5$	$v_{s2} = 5$	$\Delta v_1 = 1.2$	$\Delta v_2 = 1.2$
$m = 296.033$			
Mirror Parameters:			
$V_0 = 3 \cdot 10^4$	$x_{12v} = 0.01$	$t_0 = 0.003, 0.004, \dots, 0.01$	
Other Parameters:			
$t_f = 1$	$\alpha = 1$		

Table 3.8: Dimensionless parameters for the simulations with a ring in the quantum setting.

t_0	$\langle v_1 \rangle$	$\langle v_2 \rangle$	Δv_1	Δv_2
0.003	0.255	0.255	0.179	0.179
0.005	0.394	0.394	0.281	0.281
0.01	0.386	0.386	0.252	0.252

Table 3.9: Expectation values and standard deviations of the absolute value of the final velocities for a ring and the parameters in Table 3.8 and $t_0 = 0.003$, $t_0 = 0.005$ and $t_0 = 0.01$ in the quantum case.

are shown in Figs. 3.32, 3.33 and 3.34. In Fig. 3.32 one observes that increasing the shift x_{s1} in the direction of the considered velocity component v_1 reduces the slowing of the particles, because with increasing x_{s1} the peak for negative velocities is shifted to more negative velocities. Due to the symmetry this of course also holds for v_2 when increasing x_{s2} . The opposite happens for the velocity component perpendicular to the shift from the origin v_2 , i.e. we observe a velocity reduction for the perpendicular component, see Fig 3.33. Due to the symmetry this again also holds for v_1 when increasing x_{s2} . These results might be counterintuitive at first and do not have a one-dimensional analogue, because there a shift that brings the particle initially closer to the mirror reduces the velocity further. This also happens in the classical case. An elementary but lengthy calculation shows that, w.l.o.g, the final velocity component $v_{f1}(x_{s1}, x_{s2})$ after the first collision is monotonically decreasing with respect to x_{s1} and monotonically increasing with respect to x_{s2} for $v_{s1}, v_{s2} > 0$, because the latter implies $v_{f1} < 0$ and we have

$$\left(\frac{\partial}{\partial x_{s1}} v_{f1}(x_{s1}, x_{s2}) \right) \Big|_{v_{s1}, v_{s2} > 0} < 0 \quad \text{and} \quad \left(\frac{\partial}{\partial x_{s2}} v_{f1}(x_{s1}, x_{s2}) \right) \Big|_{v_{s1}, v_{s2} > 0} > 0.$$

This implies that a shift in the direction of movement increases the absolute value of v_{f1} and a perpendicular shift reduces the absolute value of v_{f1} . The same is of course true for v_{f2} . In Fig. 3.34 the results for an equal shift both in x_1 - and in x_2 -direction are shown. These results confirm the expectation, since the shift just results in a shift along the radius. Therefore the situation corresponds approximately to an ensemble with the origin as its average initial position, but interacting with a potential with smaller t_0 . However, note that these situations are of course not equal, firstly because we do not consider an initial radius r_0 and a trajectory $\alpha\sqrt{t}$, but a trajectory $\alpha\sqrt{t + t_0}$ instead and secondly we not only consider a position distribution along the direction of movement, but also perpendicular to it.

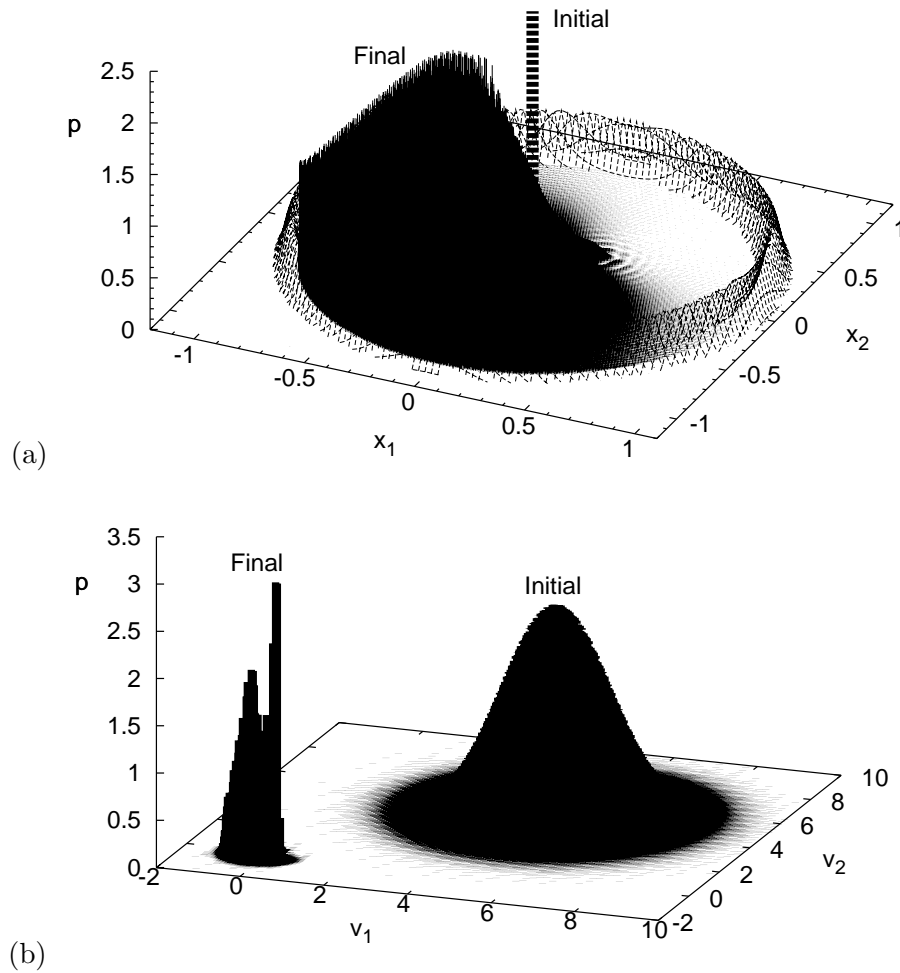


Figure 3.29: Quantum Case. The mirror potential is given by eq. (3.109).

(a) The (dashed) initial and (solid) final position probability distribution $p_{s,f}(x_1, x_2)$ for an initial wavefunction (3.107) with the parameters in Table 3.8 and $t_0 = 0.004$.

Additionally the potential is plotted for $t_f = 1$.

(b) The initial and final velocity probability distributions $p_{s,f}(v_1, v_2)$ for an initial wavefunction (3.107) with the parameters in Table 3.8 and $t_0 = 0.004$. The initial distribution was scaled by a factor 20.

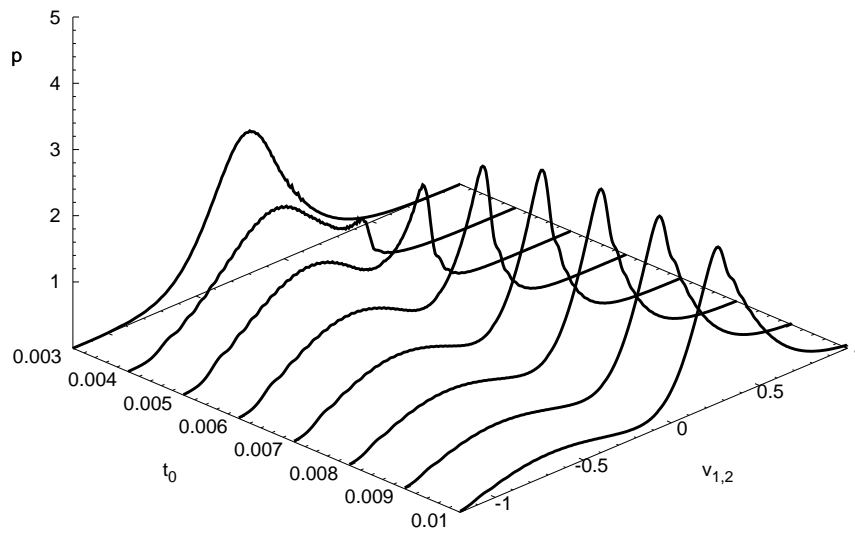


Figure 3.30: Quantum Case. The mirror potential is given by eq. (3.109). The final velocity marginals $p_f(v_1)$ and $p_f(v_2)$, which are equal due to the symmetry of the situation, for the parameters in Table 3.8.

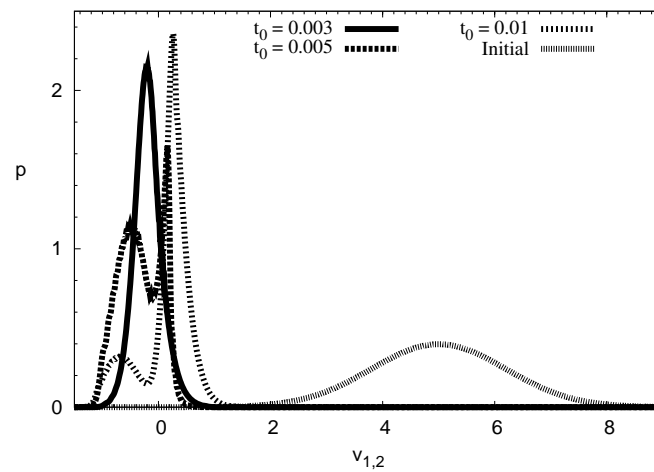


Figure 3.31: Quantum Case. The mirror potential is given by eq. (3.109). The velocity marginals $p_f(v_1)$ and $p_f(v_2)$, which are equal due to the symmetry of the situation, for the parameters in Table 3.8 and for $t_0 = 0.003$, $t_0 = 0.005$ as well as $t_0 = 0.01$ compared to the initial distribution.

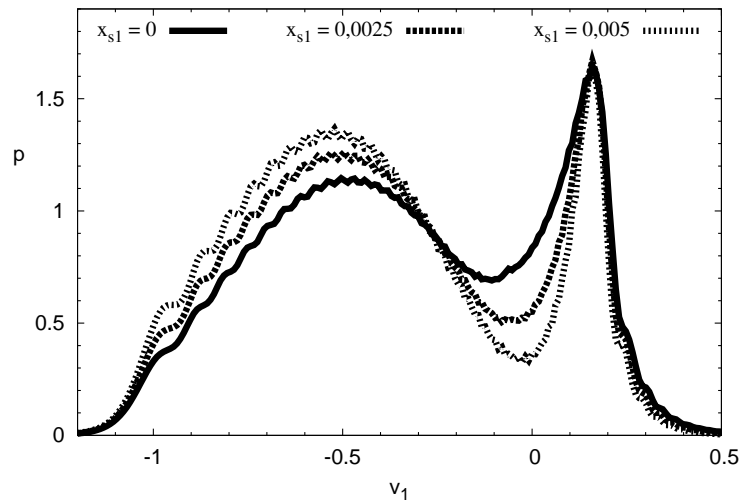


Figure 3.32: Quantum Case. The mirror potential is given by eq. (3.109). The velocity marginals $p_f(v_1)$ for the parameters in Table 3.5 for $t_0 = 0.005$ and $x_{s1} = 0.0025$ as well as $x_{s1} = 0.005$. Due to the symmetry the results for $p_f(v_2)$ with $x_{s2} = 0.0025$ as well as $x_{s2} = 0.005$ instead are the same.

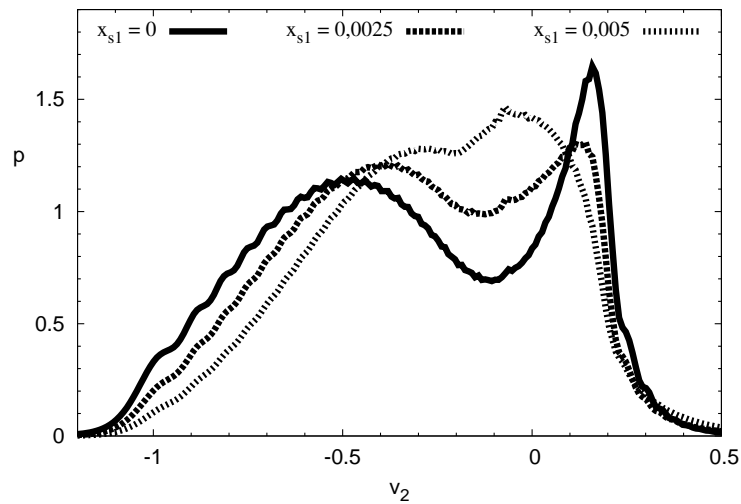


Figure 3.33: Quantum Case. The mirror potential is given by eq. (3.109). The velocity marginals $p_f(v_2)$ for the parameters in Table 3.5 for $t_0 = 0.005$ and $x_{s1} = 0.0025$ as well as $x_{s1} = 0.005$. Due to the symmetry the results for $p_f(v_1)$ with $x_{s2} = 0.0025$ as well as $x_{s2} = 0.005$ instead are the same.

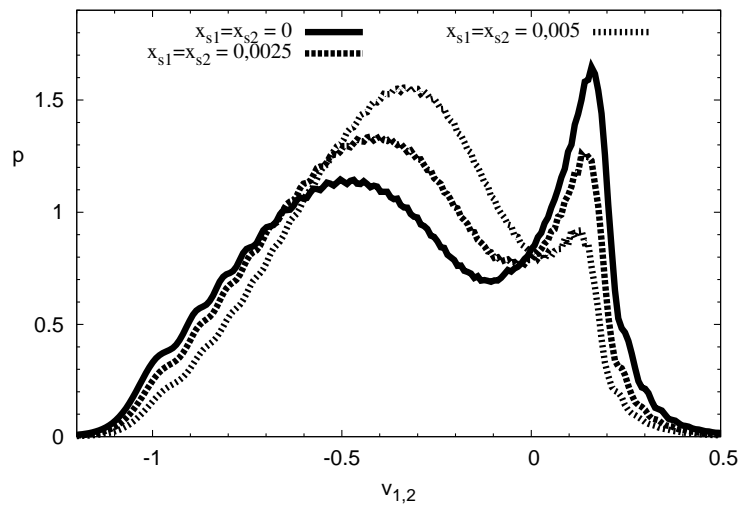


Figure 3.34: Quantum Case. The mirror potential is given by eq. (3.109). The velocity marginals $p_f(v_1)$ and $p_f(v_2)$, which are the same due to the symmetry of the situation, for the parameters in Table 3.5 for $t_0 = 0.005$ and $x_{s1} = x_{s2} = 0.0025$ as well as $x_{s1} = x_{s2} = 0.005$.

3.4 The Quantum Stopper used for Expansion and Compression in 2d

As discussed in the corresponding section the expanding ring was chosen as a promising geometry to implement cooling cycles. Therefore in this section we will extend this idea and discuss a ring which first expands along a square-root in time trajectory and is then compressed along a linear in time trajectory to its initial radius. The situation is depicted in Fig. 3.35. Again we will first examine the problem in the classical case, but only for one particle and the numerical examples will even be effectively one-dimensional problems due to the chosen symmetry. It is clear that, not to mention the fact that the frameworks will lead to differences, even in a purely classical description the one-particle case would not be sufficient to deduce statements about an ensemble of particles. Therefore discussing this idealized and reduced setup just serves the purpose of being a first simple test case. Furthermore, it is also clear that such an expansion and compression does not alter the phase-space volume, because there is no irreversible step in the process¹. Still, as the potential we are considering is time-dependent, we might achieve a velocity reduction at final time for the particle or the whole ensemble². Finally, instead of additionally studying a classical ensemble as an intermediate step, after the one-particle case we will immediately treat the quantum mechanical problem.

3.4.1 Expansion and Compression of a Ring: One Classical Particle

The expanding ring in the classical case is given by

$$\left(\pm \sqrt{r(t)^2 - x_2^2}, x_2 \right)^T \quad t \in [0, t_{exp}],$$

with $r(t) = \alpha \sqrt{t + t_0}$, $\alpha \in \mathbb{R}_+$ and some expansion time $t_{exp} \in \mathbb{R}_+$. After the expansion we will consider a linear compression with velocity $\beta > 0$, i.e. after t_{exp} we have

$$\left(\pm \sqrt{r(t)^2 - x_2^2}, x_2 \right)^T, \quad t \in]t_{exp}, t_f],$$

with $r(t) = \alpha \sqrt{t_{exp} + t_0} - \beta(t - t_{exp})$, $\alpha \in \mathbb{R}_+$ and some final time $t_{exp} < t_f \in \mathbb{R}_+$, which is chosen such that the compression continues until the ring returns to its initial radius $\alpha \sqrt{t_0}$. Therefore we have a final time

$$t_f = t_{exp} + \frac{\alpha}{\beta} (\sqrt{t_{exp} + t_0} - \sqrt{t_0}). \quad (3.110)$$

The goal is to determine whether we can achieve a velocity reduction, despite the particle being confined in the same volume.

Both for the expansion and for the compression we have to take multiple collisions into

¹ For a proof that a phase-space compression cannot be achieved with time-dependent potentials or other time-dependent terms in the Hamiltonian see [48].

² In other words although the phase-space volume does not change, it might be shifted to a region with smaller velocities.

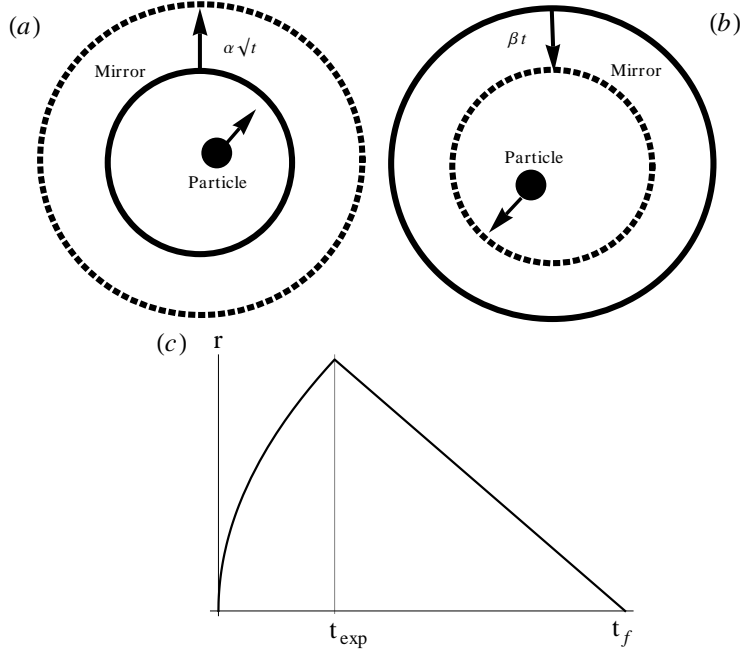


Figure 3.35: Schematic pictures of the situation considered in this section. Particles start at some initial position \vec{x}_s with some initial velocity \vec{v}_s and collide with a ring shaped mirror whose radius (a) first increases with a square-root in time and (b) after some expansion time decreases linearly with velocity β . (c) Additionally the time evolution of the radius is schematically depicted. First an expansion occurs along a square-root in time until some expansion time t_{exp} which is then followed by a linear compression until some final time t_f .

account. The collision times t_{cn} , with $n = 1, \dots, k$ are given as a solution of

$$\alpha^2(t_{cn} + t_0) - (x_{s1} + v_{s1}(t_{cn} - t_{cn-1}))^2 - (x_{s2} + v_{s2}(t_{cn} - t_{cn-1}))^2 \stackrel{!}{=} 0, \quad (3.111)$$

where we set $t_{c0} = t_{init} = 0$ and $t_k \leq t_{exp}$. The final velocity and position are given by eq. (3.96) and eq. (3.97) respectively, where

$$\vec{n} = \frac{1}{\sqrt{1 + \frac{x_{c2}^2}{\alpha^2(t_{cn} + t_0) - x_{c2}^2}}} \left(\text{sign}(x_{c1}), \frac{x_{c2}}{\sqrt{\alpha^2(t_{cn} + t_0) - x_{c2}^2}} \right)^T. \quad (3.112)$$

Here $x_{c1,2} = x_{f1,2} + v_{f1,2}(t_{cn} - t_{cn-1})$ are the new collision points calculated with the updated position and velocity and where the first collision points are simply given by $x_{c1,2} = x_{s1,2} + v_{s1,2}t_{c1}$.

In a similar way the collision times during the compression t_{cm} , with $m = n + 1, \dots, l$, are given as a solution of

$$\begin{aligned} & (\alpha\sqrt{t_{exp} + t_0} - \beta(t_{cm+1} - t_{exp}))^2 - (x_{s1} + v_{s1}(t_{cm+1} - t_{cm}))^2 \\ & - (x_{s2} + v_{s2}(t_{cm+1} - t_{cm}))^2 \stackrel{!}{=} 0 \end{aligned} \quad (3.113)$$

where we set $t_{cn+1} = t_{exp}$ and $t_l \leq t_f$. The new initial values $x_{s1,2}$, $v_{s1,2}$ are the final position and velocity at the expansion time t_{exp} . The final velocity and position are also given by eq. (3.96) and eq. (3.97) respectively, where

$$\vec{n} = \frac{1}{\sqrt{1 + \frac{x_{c2}^2}{(\alpha\sqrt{t_{exp}+t_0} - \beta(t_{cm+1}-t_f))^2 - x_{c2}^2}}} \cdot \left(\text{sign}(x_{c1}), \frac{x_{c2}}{\sqrt{(\alpha\sqrt{t_{exp}+t_0} - \beta(t_{cm+1}-t_f))^2 - x_{c2}^2}} \right)^T \quad (3.114)$$

In Fig. 3.36 the numerical results for the parameters in Table 3.10 are shown. The upper picture shows the ratio of the absolute value of the final velocity $\vec{v}_{f,comp}$ after the compression and the absolute value of the initial velocity \vec{v}_s depending on v_{s1} as well as v_{s2} for $\beta = 0.001$. For a successful velocity reduction the ratio has to be smaller than 1, i.e. $|\vec{v}_{f,comp}|/|\vec{v}_s| < 1$, which is fulfilled for all velocities considered. A drop of the ratio $|\vec{v}_{f,comp}|/|\vec{v}_s|$ corresponds to less collisions during the compression for these parameters, where the number of collisions then increases again for increasing velocity, which is expressed by the slope of the plateau. In the lower picture additionally β is varied for the same initial parameters and the final velocity increases in general for increasing β . The zig zack behaviour of the plot for varying $|\vec{v}_s|$ and β is also due to a changing number of collisions. However, for the parameter ranges considered we observe a velocity reduction after the compression at least in the case of one classical particle.

Initial Particle Parameters:			
$x_{s1} = 0$	$x_{s2} = 0$	$v_{s1} = 3, 3.04 \dots 7$	$v_{s2} = 3, 3.04 \dots 7$
Other Parameters:			
$t_0 = 0.1$	$t_{exp} = 1$	$t_f = 104 \dots 1040$	
$\alpha = 1$	$\beta = 0.001 \dots 0.01$		

Table 3.10: Dimensionless parameters for the simulations of a ring used to reduce the velocity of one classical particle via expansion and compression.

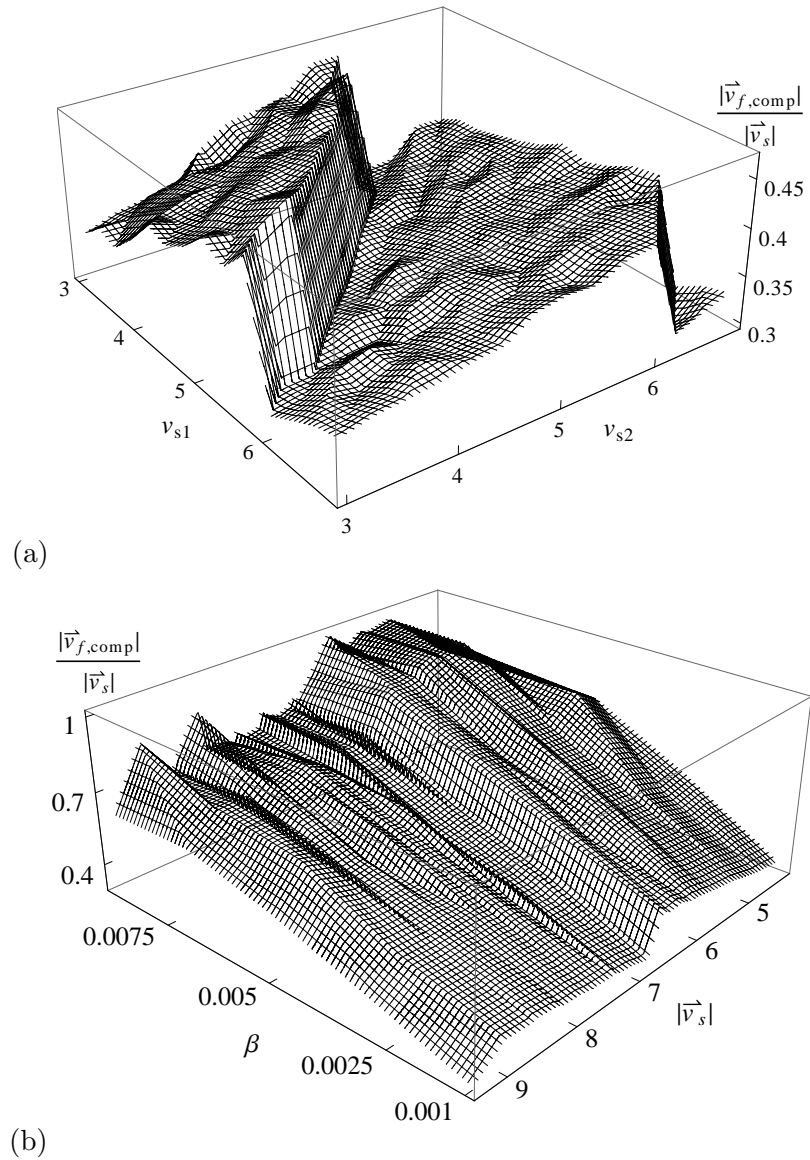


Figure 3.36: Expansion and compression of a ring for one classical particle. The results are independent of the relative angle.

(a) The dependence of the ratio of the final velocity $|\vec{v}_{f,comp}|$ after the compression and the absolute value of the initial velocity $|\vec{v}_s|$ on the components of the initial velocity for $\beta = 0.001$.

(b) The dependence of the ratio of the final velocity $|\vec{v}_{f,comp}|$ after the compression and the absolute value of the initial velocity $|\vec{v}_s|$ on the initial velocity and β .

3.4.2 Expansion and Compression of a Ring: Quantum Particles

In this section we consider the expansion and compression of a ring in the quantum case. The mirror potential, which has again a Gaussian profile along the radius, expands along a square-root in time trajectory and is compressed along a linear in time trajectory, i.e. it is given by

$$V_G(x_1, x_2, t) = \begin{cases} V_0 e^{-(\sqrt{x_1^2+x_2^2}-\alpha\sqrt{t+t_0})^2/(2\Delta x_{12V}^2)} & 0 \leq t \leq t_{exp} \\ V_0 e^{-(\sqrt{x_1^2+x_2^2}-\alpha\sqrt{t_{exp}+t_0}+\beta(t-t_{exp}))^2/(2\Delta x_{12V}^2)} & t_{exp} < t \leq t_f \end{cases} \quad (3.115)$$

For the initial wavefunction (3.107) and the potential given by eq. (3.115) we used the parameters in Table 3.11.

In Fig. 3.37 the final position and velocity distributions for $\beta = 0.1$ are shown. The position and velocity distributions after the expansion as well as the initial velocity distribution are the same as in Fig. 3.29. In contrast to the classical case we do not observe a remaining velocity reduction after the compression, instead the situation becomes seemingly worse compared to the initial distribution. Similar results were obtained for all β in Table 3.11.

In the following we will discuss why this expansion and compression scheme, at least for the parameter ranges considered, does not lead to a velocity reduction. This is caused by one of two different possible problems. The reason for a linear compression using small β , i.e. compressing slowly, is of course that we wish this part of the process to be adiabatic, such that the state remains unchanged for these parameters. The first problem now is if this condition is actually matched or if our choice of β leads to a non-adiabatic compression. If the process is adiabatic the second possible explanation for the scheme's failing to cool is that compressing the ring increases the distance between the energy eigenvalues, where the energy in this situation is only kinetic energy. Therefore an increase in the spacing between the energy eigenvalues also increases the velocities.

For a further and more rigorous analysis of this problem we will restrict our reasoning to a ring with infinitely high walls instead of a Gaussian. It is straightforward to show that the energy eigenvalues for a ring with radius R are given by $E_n = \frac{\hbar^2 z_{n,u}^2}{2m} \frac{1}{R^2}$,

Initial State Parameters:			
$x_{s1} = 0$	$x_{s2} = 0$	$\Delta x_1 = 0.0047430$	$\Delta x_2 = 0.0047430$
$v_{s1} = 5$	$v_{s2} = 5$	$\Delta v_1 = 1.2$	$\Delta v_2 = 1.2$
Mirror Parameters:			
$V_0 = 3 \cdot 10^4$	$x_{12v} = 0.01$	$t_0 = 0.004$	
Other Parameters:			
$\alpha = 1$	$t_{exp} = 1$	$\beta = 0.001, 0.01, 0.1$	$t_f = 10.4, 104, 1040$

Table 3.11: Dimensionless parameters for the simulations of a ring used to cool via expansion and compression in the quantum case.

where $z_{n,u}^2$ denotes the u th zero of the Besselfunction $J_n\left(\sqrt{\frac{2mE}{\hbar^2}}r\right)$ solving the corresponding radial equation for this problem at position $r = R$. The calculations are elementary and can be found in various textbooks and publications, see for example [49], important for the subsequent analysis is only that the energy eigenvalues are proportional to $\frac{1}{R^2}$. Furthermore, if the compression is adiabatic, the state $|\Psi(t)\rangle$ is given as a superposition of eigenstates $|\Phi_n(t)\rangle$ with time-dependent phases, which we do not have to know explicitly for our analysis and therefore we will not consider them explicitly. To be more precise in the adiabatic approximation we have

$$|\Psi(t)\rangle \approx \sum_n c_n e^{-i\gamma_n(t)} |\Phi_n(t)\rangle \quad (3.116)$$

with $\gamma_n(t) : \mathbb{R} \rightarrow \mathbb{R}$. For the energy expectation value and higher moments at time t it therefore follows that

$$\begin{aligned} \langle \Psi(t) | \hat{H}^q(t) | \Psi(t) \rangle &\approx \sum_m c_m^* e^{i\gamma_m(t)} \langle \Phi_m(t) | \sum_n c_n e^{-i\gamma_n(t)} \hat{H}^q(t) | \Phi_n(t) \rangle \\ &= \sum_{m,n} c_m^* c_n e^{i(\gamma_m(t) - \gamma_n(t))} E_n^q(t) \underbrace{\langle \Phi_m(t) | \Phi_n(t) \rangle}_{\delta_{m,n}} \\ &= \sum_n |c_n|^2 E_n^q(t) = \sum_n |c_n|^2 \left(\frac{\hbar^2 z_{n,u}^2}{2m} \right)^q \frac{1}{R(t)^{2q}} \\ &= \frac{1}{R^{2q}(t)} \sum_n |c_n|^2 \left(\frac{\hbar^2 z_{n,u}^2}{2m} \right)^q \\ &= \frac{R^{2q}(0)}{R^{2q}(t)} \langle \Psi(0) | \hat{H}^q(0) | \Psi(0) \rangle \end{aligned} \quad (3.117)$$

where $q \in \mathbb{N}$. For the first moment, i.e. the energy expectation value, which we denote by $E(t) = \langle H(t) \rangle$, we therefore have

$$E(t) = \langle H(t) \rangle \sim \frac{1}{R^2(t)}. \quad (3.118)$$

In Fig. 3.38 the energy expectation value during the compression corresponding to the previous numerical example is plotted over $\frac{1}{R^2(t)}$. We find a linear dependence for the chosen β and conclude therefore that the compression is indeed adiabatic and that the increase in velocity we observed is due to the increase in spacing between the eigenvalues for smaller radii. This shows, at least for the parameter ranges considered, that in the quantum case a square-root in time expansion followed by a linear compression cannot be used for cooling.

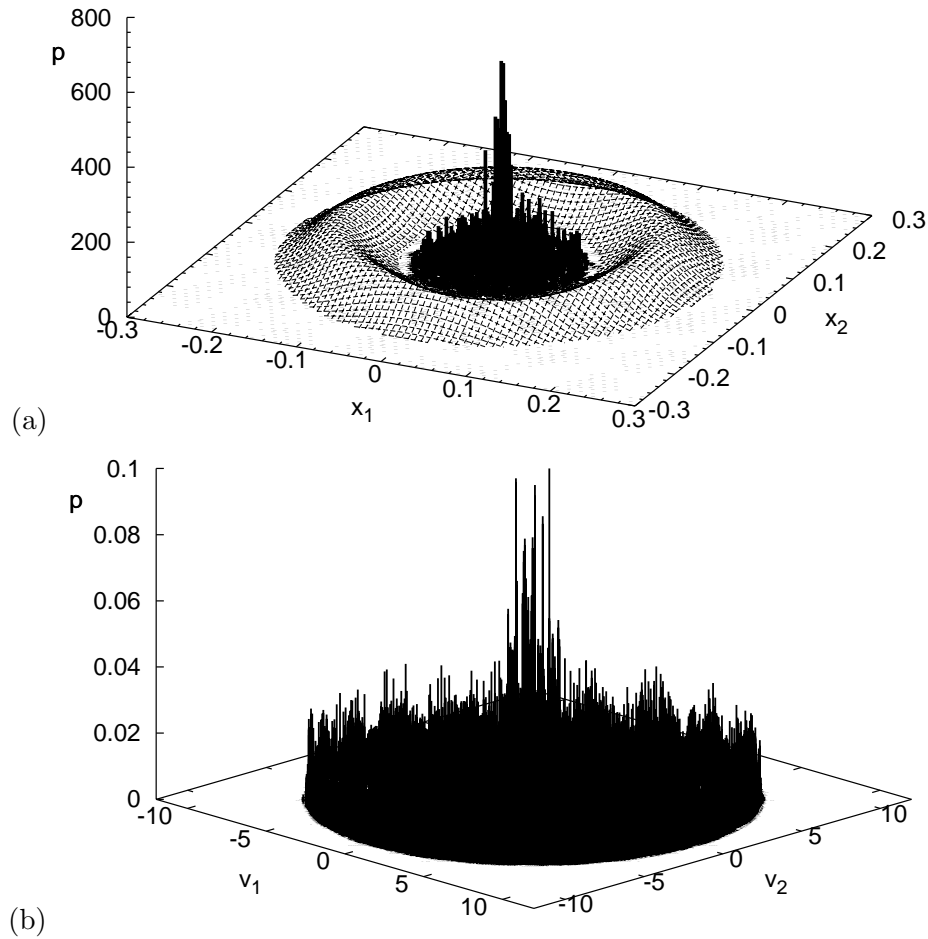


Figure 3.37: Quantum Case. The mirror potential is given by eq. (3.115).

(a) The final position probability distribution $p_f(x_1, x_2)$ after a square-root in time expansion and a linear in time compression for an initial wavefunction (3.107) for the parameters in Table 3.8 and $t_0 = 0.004$. Additionally the potential is plotted for $t_f = 10.4$.

(b) The final velocity probability distributions $p_{s,f}(v_1, v_2)$ after a square-root in time expansion and a linear compression for an initial wavefunction (3.107) for the parameters in Table 3.8 and $t_0 = 0.004$.

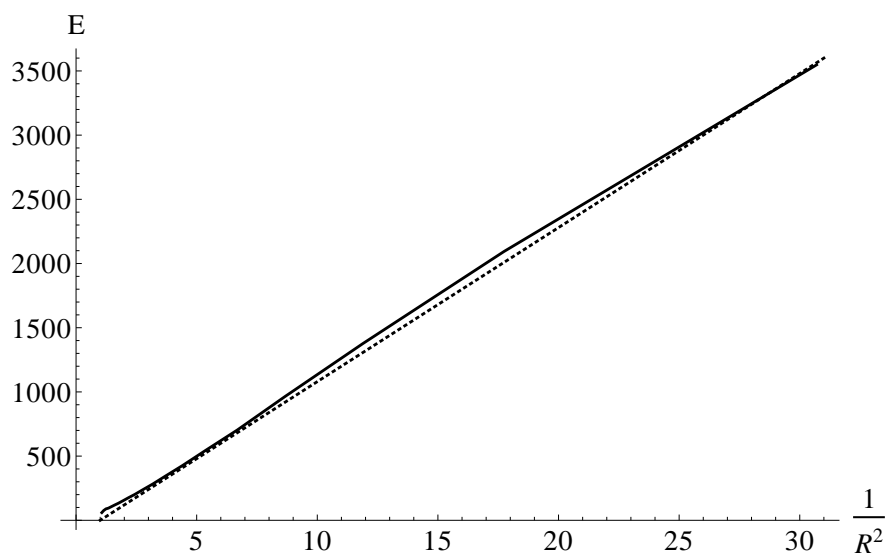


Figure 3.38: Quantum Case. (Solid line) The energy expectation value E during the compression of the ring with velocity $\beta = 0.1$ over the inverse of the squared radius. (Dashed line) As a reference a straight line was added.

3.5 Summary and Conclusion

We began this chapter with the surprising finding that in a one-dimensional setting, a hard wall whose trajectory is proportional to the square-root in time stops all classical particles located at the origin at time $t = 0$ irrespective of their velocity. If the particle is initially not at the origin or if it is too slow, it is not perfectly stopped in a finite time. Explicit expressions are given for the final velocity which show how to mitigate, and even suppress in the limit of large final times and distances, the effect of non-ideal initial conditions. Using numerical simulations we have illustrated the efficiency of the method and discussed its bounds. We have shown that the accelerated wall trajectory stops atoms in a pulse better than a wall moving with constant velocity (e.g. given by half of the mean velocity of the particles). Furthermore, we briefly discussed the effect of two mirrors moving apart from each other in the classical case and focused especially on the influence of multiple collisions. The stopping effect of the accelerated wall has also been investigated for quantum wave packets and we found that the method works in this case as well. Furthermore, we derived the analytical solution in the quantum case and were able to reproduce our numerical results. Additionally, we showed that the width of the interference fringes in position space is antiproportional to the mass of the particles. Finally, we showed that a square-root in time trajectory is optimal at least compared to any trajectory with an additional linear in time term in the quantum case as well. For cold atoms there are at least two types of applications that may be considered: one is the production of an atom laser from cold atomic pulses that have to be cooled down further, as in [26]. A second application is to improve adiabatic cooling techniques by accelerating the expansion of the trap. In this case a second wall has to be added as in [42] leading to multiple collisions and more complex dynamics.

We continued by examining the square-root in time trajectory for stopping particles in two dimensions both in the classical and the quantum case. We considered different mirror geometries and it turns out that in all cases the stopping works extremely well in both settings. Furthermore, a mirror whose surface is given by a quadratic polynomial on the one hand stops only slightly less efficient in the direction of movement than a flat wall, but on the other hand also leads to a significant velocity reduction for the component perpendicular of the direction of movement and therefore leads to an overall gain compared to a flat wall. In the quantum case we also considered an expanding ring which might for example be realized by creating a dark spot inside a laser beam. This geometry leads to a result which does not have an equivalent in the one dimensional case, i.e the dependence on the initial position of the particles inside the ring. We gave an example in which an initial position closer to the mirror leads to a larger final velocity in the same direction, whereas the perpendicular component was reduced. Moreover, we presented an example where, using the trajectory $\alpha\sqrt{t+t_0}$ for the mirror expansion, also in the quantum case a larger initial time t_0 leads both to smaller average velocities and variances of the final distribution. In other words larger t_0 can be useful depending on the given final time t_f .

Finally, we pursued the idea of using the square-root in time trajectory to implement cooling cycles by expansion and compression of a ring. To determine if this idea could at least work in principle we considered the highly simplified case of one classical particle and found that we achieve a velocity reduction even after compressing the ring to its initial radius. However, in the quantum case no velocity reduction could be observed

after the compression. Since we showed that the compression in our simulations was adiabatic, we inferred that the main reason for the failure is the increase of the energy eigenvalues due to the contraction of the ring the particles are confined in. We therefore conclude that, at least for the parameter ranges considered, the square-root in time cannot be used to implement cooling cycles via expansion and compression.

4 A Quantum Catcher

In so far as a scientific statement speaks about reality, it must be falsifiable; and in so far as it is not falsifiable, it does not speak about reality.

(Karl R. Popper, The Logic of Scientific Discovery)

4.1 Introduction

In Chapter 3 we considered an ensemble of particles being reflected by an accelerated potential and showed that a potential moving along a trajectory proportional to a square-root in time stops particles independently of their initial velocity. Again we refer the reader to Section 2.1 and Appendix A, where we show how the interaction between a two-level atom in the ground state and a far detuned laser can be described by an effective potential. Motivated by the results showing the efficiency of such a trajectory for stopping atoms in a pulse, we also pursued the idea to implement cooling cycles via expansion and compression of a ring. However, it emerged that this, at least in the parameter ranges considered, does not work in the quantum case, i.e. we did not obtain a velocity reduction at the end of the process. In this chapter we will propose a setup with which we can trap atoms and additionally actually achieve cooling and a compression in phase space. For this we introduce an irreversible step by combining an atom diode, here consisting of a state selective mirror potential followed by a pump laser (see [50]-[56]), with a mirror, which have a fixed distance and move along a square-root in time trajectory¹. Atoms in a pulse moving in the same direction will pass the state selective mirror potential at first unaffected, get excited by the pump laser between the two mirror potentials and decay to a metastable state in which the atoms are now reflected from both potentials. The atoms are trapped and their velocity will be reduced due to subsequent reflections, see Fig. 4.1.

This chapter is organized as follows. In Section 4.2 we will start with describing the basic idea in the idealized classical case for one pointlike particle. Afterwards we will briefly consider the more general classical situation for an ensemble of pointlike particles and give a numerical result showing a phase-space compression. In Section 4.3 we will treat the problem in the quantum mechanical framework. We will propose a setup for an experimental realization and show results deduced by numerically solving the corresponding master-equation via the quantum jump approach, see Section 2.4. This work was completed in collaboration with J. G. Muga and A. Ruschhaupt.

¹ In [57] a different proposal introducing an irreversible step by using a “one-way wall” of light can be found. However, note that although certain basic ideas are similar, the schemes are clearly distinct.

4.2 Classical Particles

For the sake of simplicity we consider at first one pointlike particle moving from left to right, i.e. the particle has constant initial velocity $v_{i,1} > 0$ and at $t_0 = 0$ initial position $x_i(0) = x_{i,1} < 0$. To the right of the particle shall be two mirrors that move in the same direction as the particle with velocity $v_{m,l}(t) = v_{m,r}(t) = \frac{\alpha}{2\sqrt{t}}$. Furthermore, the particle shall pass the first or “left” mirror unaffected the first time, so that the first collision occurs with the second or “right” mirror, i.e. the left mirror shall act as a diode. The mirror and particle trajectories are depicted schematically in Fig. 4.1. To be more precise at $t_0 = 0$ the right mirror shall be at $x_{m,r}(0) = x_{m,r} = 0$ and the left mirror at $x_{m,l}(0) = x_{m,l} < 0$, with $x_{i,1} < x_{m,l}$, which guarantees that the first collision occurs with the right mirror, since the mirror velocities are monotonically decreasing. In the following we will derive the expressions for the final velocities, positions and collision times for such a particle after subsequent collisions. As a reminder, for a particle in one dimension which has initial position x_i and moves with constant initial velocity v_i , the particle velocity v_f after a collision with a perfectly reflecting mirror potential is given by

$$v_f = -v_i + 2v_m(t_c) \quad (4.1)$$

where t_c is the collision time, v_i the initial particle velocity and $v_m(t)$ the mirror velocity at time t , as discussed in Section 3.2¹.

It is now straightforward to calculate the final velocity and position depending on the initial conditions. According to eq. (4.1) the final velocity after the first collision $v_{f,1}$ with a mirror moving along a square-root in time trajectory is given by

$$v_{f,1} = -v_{i,1} + \frac{\alpha}{\sqrt{t_{c,1}}} \quad (4.2)$$

and the final position is simply given by

$$x_{f,1} = x_{i,1} + v_{i,1}t_{c,1} \quad (4.3)$$

where

$$\sqrt{t_{c,1}} = \frac{\alpha}{2v_{i,1}} \left(1 + \sqrt{1 - \frac{4x_{i,1}v_{i,1}}{\alpha^2}} \right) \quad (4.4)$$

is the time of the first collision, see again also Section 3.2. We update the initial conditions using the previous final ones after the last collision. Therefore in the following we set $v_{i,n} := v_{f,n-1}$ and $x_{i,n} := x_{f,n-1}$ at time $t_{c,n-1}$, i.e. either the position of the right or left mirror at that time. The subsequent collision times can then be deduced from the

¹ We repeat this to stress that this is true in general, independent of the particle’s or mirror’s direction of movement, which we will use in subsequent calculations.

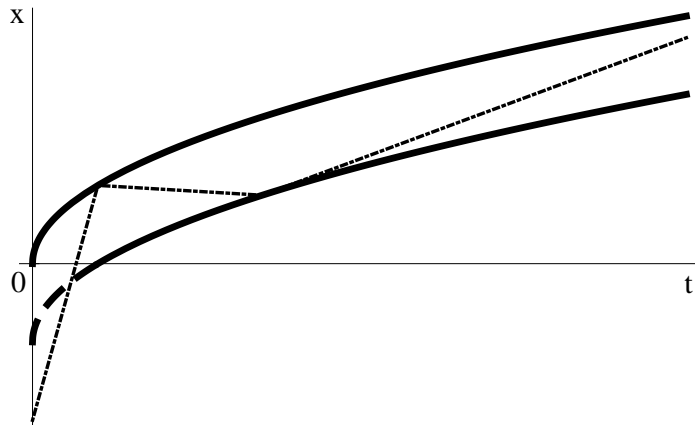


Figure 4.1: The figure schematically shows the setup considered in this chapter. The two mirrors both move along a trajectory $\alpha\sqrt{t}$, where the first mirror (thick dashed/solid line) lets the particle pass if it comes from the left, i.e. it acts as an atom diode, such that the particle is first reflected from the second mirror (thick solid line). The particle's trajectory is $\sim t$ (straight dotted-dashed lines) and the particle undergoes subsequent collisions while being trapped between both mirrors, thereby being effectively slowed, which is indicated by the decreasing slope.

equations

$$\begin{aligned}\alpha\sqrt{t_{c,n}} + x_{m,l} &= \alpha\sqrt{t_{c,n-1}} + v_{i,n}(t_{c,n} - t_{c,n-1}), & n \geq 2 \text{ even} \\ \alpha\sqrt{t_{c,n}} &= \alpha\sqrt{t_{c,n-1}} + x_{m,l} + v_{i,n}(t_{c,n} - t_{c,n-1}), & n \geq 3 \text{ odd}\end{aligned}$$

which express that the position of the particle and the respective mirror have to be equal. Solving these equations we obtain for the n th collision time $t_{c,n}$

$$\sqrt{t_{c,n}} = \frac{\alpha}{2v_{i,n}} \left(1 + (-1)^{n-1} \cdot \sqrt{1 + \frac{4(-\tilde{x}_{i,n} + (-1)^n x_{m,l} + t_{c,n-1} v_{i,n}) v_{i,n}}{\alpha^2}} \right) \quad (4.5)$$

where $2 \leq n \in \mathbb{N}$. The sign of the square root is chosen such that the collision time is positive and with new initial velocity

$$v_{i,n} = -v_{i,n-1} + \frac{\alpha}{\sqrt{t_{c,n-1}}} \quad (4.6)$$

as well as relative new initial position

$$\tilde{x}_{i,n} = \alpha\sqrt{t_{c,n-1}} = \begin{cases} x_{i,n} & n \geq 2 \text{ even} \\ x_{i,n} - x_{m,l} & n \geq 3 \text{ odd} \end{cases} \quad (4.7)$$

which we introduced to write the collision time in a more compact way.

Due to the first collision occurring with the right mirror, the particle will be slowed down and move in the opposite direction afterwards, which was shown in Section 3.2. Next it will collide with the left mirror, this collision resulting in a speed up of the particle and again a reversal of the direction it moves in. This process is repeated, the particle being reflected alternately between the mirrors. It is straightforward to show that the particle becomes effectively slowed if only the first collision occurs with the right mirror. To be more precise we have the following important proposition:

Proposition 6. *The absolute value of the particle's velocity $v_{i,n+1}$ after n reflections alternating from the right and left mirror is always strictly smaller than the absolute value of the initial velocity $|v_{i,1}|$, that is*

$$|v_{i,n+1}| < |v_{i,1}| \quad \forall n \in \mathbb{N}_+. \quad (4.8)$$

Proof. We start by considering the subsequent final velocities after each collision, which are given by:

$$v_{i,2} = -v_{i,1} + 2v_{m,r}(t_{c,1}), \quad v_{i,3} = -v_{i,2} + 2v_{m,l}(t_{c,2}), \quad v_{i,4} = -v_{i,3} + 2v_{m,r}(t_{c,3}), \dots$$

with $t_{c,1} < t_{c,2} < t_{c,3} < \dots$. By recursion, the n th particle velocity $v_{i,n+1}$ is therefore given by

$$v_{i,n+1} = v_{i,1} - 2 \sum_{j=1}^{\frac{n}{2}} \underbrace{(v_{m,r}(t_{c,2j-1}) - v_{m,l}(t_{c,2j}))}_{>0 \text{ for } t_{c,2j-1} < t_{c,2j}}$$

if n is even and

$$v_{i,n+1} = -v_{i,1} + 2 \sum_{j=1}^{\frac{n-1}{2}} \underbrace{(v_{m,r}(t_{c,2j-1}) - v_{m,l}(t_{c,2j}))}_{>0 \text{ for } t_{c,2j-1} < t_{c,2j}} + 2v_{m,r}(t_{c,n}),$$

if n is odd, and where the sum is defined as zero for $n = 1$. This can be written in a more compact way by using $v_{m,r}(t) = v_{m,l}(t) =: v_m(t)$, i.e.

$$v_{i,n+1} = (-1)^n v_{i,1} + 2 \sum_{k=1}^n (-1)^{k+n} v_m(t_{c,k}). \quad (4.9)$$

Using that $v_{i,1} > 0$, $v_{i,j+1} > 0$ for even j , and $v_{i,j+1} < 0$ for odd j , for the absolute value of the n th particle velocity given by eq. (4.9) we obtain

$$|v_{i,n+1}| = |v_{i,1}| - 2 \sum_{k=1}^n (-1)^{k+1} v_m(t_{c,k}) = |v_{i,1}| - 2 \sum_{k=1}^n s(k) \quad (4.10)$$

where we defined the sequence $s(k) := (-1)^{k+1} v_m(t_{c,k})$. This sequence $s(k)$ is alternating, $v_m(t)$ is monotone and goes to zero for $\lim_{k \rightarrow \infty}$, i.e. the sum in eq. (4.10) converges due to the Leibniz criterion where the limit is obviously positive. \square

Proposition 6 is especially important for a classical ensemble. It ensures that after the process all particles have a smaller absolute velocity independently of the number of collisions as long as at least one occurs. Furthermore, this result is also independent of the mirror distances and therefore, given a certain position distribution, one can always achieve an arbitrary reduction of its width by making the mirror distances sufficiently small and still guarantee that the particles are slowed down too.

From a practical point of view the following proposition is useful.

Proposition 7. *The particle's velocity after the second collision $|v_{i,3}|$, i.e. the velocity after the first collision with the right mirror, is an upper bound on all the velocities after a reflection, that is we have*

$$|v_{i,3}| > |v_{i,n+1}| \quad \forall n \in \mathbb{N}_+, n \neq 2. \quad (4.11)$$

Proof. The proof is straightforward, we have

$$\begin{aligned} & |v_{i,1}| > |v_{i,1}| - 2 \underbrace{(v_m(t_{c,1}) - v_m(t_{c,2}))}_{>0} \\ & > |v_{i,1}| - 2 \underbrace{(v_m(t_{c,1}) - v_m(t_{c,2}))}_{>0} - 2 \underbrace{(v_m(t_{c,3}) - v_m(t_{c,4}))}_{>0} \\ & \stackrel{l \geq 2}{>} |v_{i,1}| - 2 \left(\sum_{k=1}^l v_m(t_{c,2k-1}) - \sum_{k=1}^l v_m(t_{c,2k}) \right) \\ & > |v_{i,1}| - 2 \left(\sum_{k=1}^l v_m(t_{c,2k-1}) - \sum_{k=1}^{l-1} v_m(t_{c,2k}) \right) \\ & > |v_{i,1}| - 2 \left(\sum_{k=1}^{l-1} v_m(t_{c,2k-1}) - \sum_{k=1}^{l-2} v_m(t_{c,2k}) \right) \quad (\text{because } v_m(t_{c,2l-1}) - v_m(t_{c,2l-2}) < 0) \\ & > |v_{i,1}| - 2 \underbrace{(v_m(t_{c,1}) - v_m(t_{c,2}))}_{>0} - 2v_m(t_{c,3}) > |v_{i,1}| - 2v_m(t_{c,1}). \end{aligned}$$

Using eq. (4.10) we therefore obtain

$$|v_{i,1}| > |v_{i,3}| > |v_{i,5}| > \dots > |v_{i,4}| > |v_{i,2}|$$

which proves the proposition. \square

It is worth noting that in the inequalities in the proof above we rearranged the partial sums in the step from line two to line three. This means that our proof is only true for finite l , because the series $\sum_{k=1}^n |(-1)^{k+1} v_m(t_{c,k})| = \sum_{k=1}^n v_m(t_{c,k})$ does not converge. This follows from the integral criterion because the indefinite integral $\int_0^\infty \frac{\alpha}{\sqrt{t}} dt$ does not exist and therefore the series $\sum_{k=1}^n (-1)^{k+1} v_m(t_{c,k})$ does not converge absolutely. However, from a physicist's point of view, this is of no real importance, since the limit corresponds to an infinite time t . Also, the rearrangement was only used for clarity, but it is not necessary, and so the results above actually also hold for infinite l .

Proposition 7 is useful because now one can estimate suitable parameters depending on the “worst case” velocity. In the following we will examine how to choose the initial particle position $x_{i,1}$ and the initial position of the left mirror $x_{m,1}$ to ensure that $|v_{i,3}|$ becomes small¹. According to eq. (4.10) the absolute value of the particle’s velocity after the second collision is simply given by

$$|v_{i,3}| = |v_{i,1}| - 2v_m(t_{c,1}) + 2v_m(t_{c,2}). \quad (4.12)$$

We therefore want to ensure that

$$-2[v_m(t_{c,1}) - v_m(t_{c,2})] \stackrel{!}{\ll} 0 \Leftrightarrow v_m(t_{c,1}) - v_m(t_{c,2}) \stackrel{!}{\gg} 0. \quad (4.13)$$

Note that $-2[v_m(t_{c,1}) - v_m(t_{c,2})]$ is bounded from below by $-v_{i,1}$, i.e. we always have $-2[v_m(t_{c,1}) - v_m(t_{c,2})] \geq -v_{i,1}$. Using eq. (4.2) we therefore want to ensure that

$$\sqrt{t_{c,1}} \stackrel{!}{\ll} \sqrt{t_{c,2}} \Leftrightarrow \frac{\sqrt{t_{c,2}}}{\sqrt{t_{c,1}}} \stackrel{!}{\gg} 1.$$

For reasons which will become clear below, we will write this expression slightly more explicitly as

$$\frac{\sqrt{t_{c,2}}}{\sqrt{t_{c,1}}} = \frac{\alpha}{2(\alpha - \sqrt{t_{c,1}}v_{i,1})} - \frac{1}{2} \sqrt{\frac{(\alpha - 2\sqrt{t_{c,1}}v_{i,1})^2}{(\alpha - \sqrt{t_{c,1}}v_{i,1})^2} + \frac{4x_{m,l}}{\alpha^2\sqrt{t_{c,1}}(\alpha - \sqrt{t_{c,1}}v_{i,1})}} \quad (4.14)$$

where we simply used eq. (4.5) for $\sqrt{t_{c,2}}$, then eq. (4.1) for $v_{i,2}$ and applied some elementary algebraic manipulations. Introducing the dimensionless variable

$$\beta := \frac{\sqrt{t_{c,1}}v_{i,1}}{\alpha} = \frac{1}{2} \left(1 + \sqrt{1 - \frac{4x_{i,1}v_{i,1}}{\alpha^2}} \right) \quad (4.15)$$

and using $-x_{m,l} = |x_{m,l}|$ we have

$$\frac{\sqrt{t_{c,2}}}{\sqrt{t_{c,1}}} = -\frac{1}{2(\beta - 1)} + \frac{1}{2} \sqrt{\frac{(2\beta - 1)^2}{(\beta - 1)^2} + \frac{4|x_{m,l}|v_{i,1}}{\alpha^2\beta(\beta - 1)}}. \quad (4.16)$$

Since

$$x_{i,1} + v_{i,1}t_{c,1} = -|x_{i,1}| + v_{i,1}t_{c,1} = \alpha\sqrt{t_{c,1}}$$

and $x_{i,1} < 0$ as well as $\sqrt{t_{c,1}} > 0$ we have

$$v_{i,1}\sqrt{t_{c,1}} - \alpha = \frac{|x_{i,1}|}{\sqrt{t_{c,1}}} > 0 \Rightarrow \beta = \frac{\sqrt{t_{c,1}}v_{i,1}}{\alpha} = 1 + \frac{|x_{i,1}|}{\alpha\sqrt{t_{c,1}}} > 1. \quad (4.17)$$

The aim is now to show that eq. (4.16) is monotonically decreasing with β , which

¹ Considering the initial velocity in addition or even instead is not of interest, because the velocity is not a parameter one would or could adapt in an experiment.

implies that $v_{i,3}$ is too. As we will explain later this then immediately shows how to choose $x_{i,1}$ for fixed $v_{i,1}$, which will be the case from now on. We therefore want to show that

$$\frac{\partial \sqrt{t_{c,2}}}{\partial \beta \sqrt{t_{c,1}}} = \frac{1}{2(\beta-1)^2} + \frac{\frac{4(2\beta-1)}{(\beta-1)^2} - \frac{2(2\beta-1)^2}{(\beta-1)^3} - \frac{4v_{i,1}|x_{m,l}|}{\alpha^2\beta^2(\beta-1)} - \frac{4v_{i,1}|x_{m,l}|}{\alpha^2\beta(\beta-1)^2}}{4\sqrt{\frac{(2\beta-1)^2}{(\beta-1)^2} + \frac{4|x_{m,l}|v_{i,1}}{\alpha^2\beta(\beta-1)}}} < 0 \quad (4.18)$$

which is equivalent to

$$2(2\beta-1) - \frac{(2\beta-1)^2}{(\beta-1)} - \frac{2v_{i,1}|x_{m,l}|(2\beta-1)}{\alpha^2\beta^2} < -\sqrt{\frac{(2\beta-1)^2}{(\beta-1)^2} + \frac{4|x_{m,l}|v_{i,1}}{\alpha^2\beta(\beta-1)}}.$$

Using that $2(2\beta-1) - \frac{(2\beta-1)^2}{(\beta-1)} = -\frac{(2\beta-1)}{(\beta-1)}$, inverting signs and, since all the single terms are positive, squaring both sides the inequality simplifies to

$$\begin{aligned} & \frac{4v_{i,1}^2|x_{m,l}|^2(2\beta-1)^2}{\alpha^4\beta^4} + \frac{4v_{i,1}|x_{m,l}|(2\beta-1)^2}{\alpha^2\beta^2(\beta-1)} > \frac{4v_{i,1}|x_{m,l}|}{\alpha^2\beta(\beta-1)} \\ \Leftrightarrow & \frac{v_{i,1}|x_{m,l}|(2\beta-1)^2}{\alpha^4\beta^4} + \frac{4\beta^2-5\beta+1}{\alpha^2\beta^2(\beta-1)} > 0. \end{aligned} \quad (4.19)$$

The first summand is clearly positive as is the denominator of the second summand. The numerator has zeros at $\beta = 0.25$ and $\beta = 1$. Since it is a parabola and $\beta > 1$, the numerator has to be strictly positive too and therefore the inequality holds for all β . From this follows that to obtain small $v_{i,3}$ one has to choose small β , i.e. close to one. According to eq. (4.15), for fixed $v_{i,1}$ this can be achieved by choosing small $|x_{i,1}|$ under the constraint $x_{i,1} < x_{m,l}$, i.e. we have

For $|v_{i,3}|$ to be small, the absolute value of the initial particle distance $|x_{i,1}|$ should be chosen as small as possible under the constraint $|x_{i,1}| > |x_{m,l}|$, i.e. the particle should start outside the region between the mirrors.

Small β can also be obtained by increasing α^1 . However, we then cannot apply the analysis above, since we must consider the additional dependence on α in eq. (4.16). It emerges that eq. (4.16) does not depend monotonically on α , which is illustrated by the example in Fig. 4.2, where we show a plot of the ratio $v_{i,3}/v_{i,1}$ depending on $x_{i,1}$ and α for $x_{m,l} = -1$ and $v_{i,1} = 5$. The figure shows that the smallest “worst case” velocity is indeed obtained for a particle starting as close as possible to the mirror. For increasing α on the other hand one obtains an optimal value depending on $x_{i,1}$, $v_{i,1}$ and $x_{m,l}$. This optimal value has to be determined for a chosen set of parameters, since in general there does not exist a closed form for it given arbitrary initial parameters².

¹ Recall that α can be expressed in more physical quantities, i.e. the time t_f of the process and the distance d_f the mirrors move during this time, i.e. $d_f = \alpha\sqrt{t_f}$, such that α on the other hand is given as the ratio of these quantities, i.e. $\alpha = d/\sqrt{t_f}$.
² In other words, the equation to determine the zeros of the partial derivative of $v_{i,3}$ with respect to α is locally, but not globally, solvable.

Although it is of interest to control the “worst case” velocity, it should not be

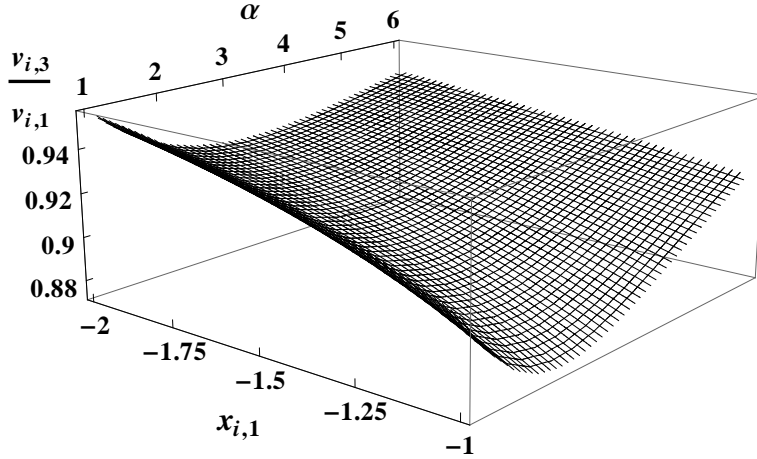


Figure 4.2: Classical Case: One particle. The dependence of the ratio of the “worst case” velocity $v_{i,3}$ and the initial velocity $v_{i,1}$ on the initial particle distance $x_{i,1}$ and α for a fixed mirror distance $x_{m,l} = -1$ and $v_{i,1} = 5$.

the prior concern in an application, because obtaining this velocity after the process leads only to a relatively small velocity reduction. Since we are actually interested in an ensemble of particles, in general different final velocities will occur depending on the initial position and velocity of the particles in the ensemble. We cannot control the process such that for all particles the same number of collisions occurs and therefore cannot stop the process such that all particles did undergo for example only one collision, which would be the optimal case. A different strategy therefore seems more advisable. Since each pair of collisions with the right and the left mirror effectively reduces the speed of the particles, one should use as large as possible final times. This has the additional effect, that the changes in the absolute value of the velocities decreases and therefore “smoothes” or “narrows” the distribution of the final velocities.

We close the one-particle discussion with an example of the final particle velocity v_f after the process for a final time $t_f = 1$. The example can be found in Fig. 4.3, where the dependence of $|v_f|$ in dimensionless parameters on the initial velocity $v_{i,1}$ and distance $x_{i,1}$ is shown, and where we additionally ensured that the last collision occurs with the right mirror¹. In this example we set $\alpha = 1$ and considered a fixed mirror distance $x_{m,l} = -0.01$. As long as the particle is initially fast enough to be reflected from the right mirror we always observe a velocity reduction, which increases with decreasing initial distance, i.e. to obtain the largest final velocity reduction, we automatically

¹ This seems to be in contrast to our remark earlier concerning the goal of treating an ensemble of particles and therefore the loss of control on the number of collisions. The constraint was chosen to obtain a clearer presentation of the results and for the final time chosen the velocity changes due to the last collisions are small, i.e. the constraint hardly changes the results in this case.

ensure the smallest “worst case” velocity too.

Ultimately we are not interested in the one-particle case but in the final phase-

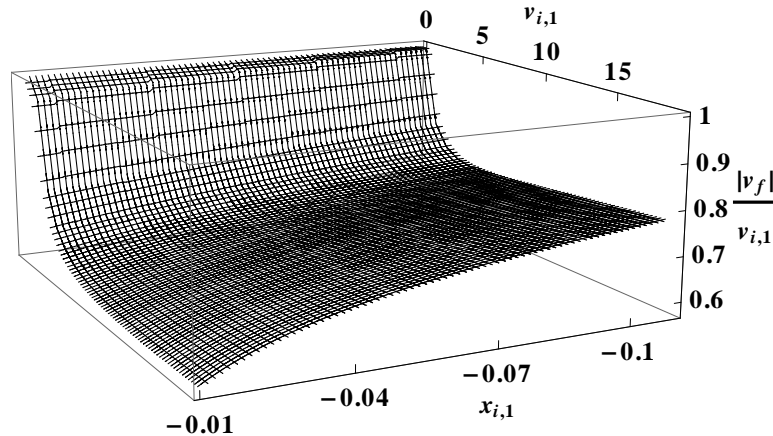


Figure 4.3: Classical Case: One particle. The dependence of the absolute final velocity $|v_f|$ on the initial particle velocity $v_{i,1}$ and distance $x_{i,1}$ for a fixed mirror distance $x_{m,l} = -0.01$ and $t_f = 1$. Note that we ensured that the last collision always occurs with the right mirror.

space density of particles in a pulse. For this we use a Gaussian distribution which, at time $t_0 = 0$, is given by

$$\rho_0(x,v) = \frac{1}{N} \exp\left(-\frac{(x - x_{i,1})^2}{2\Delta x_{i,1}^2} - \frac{(v - v_{i,1})^2}{2\Delta v_{i,1}^2}\right).$$

We will simply give one numerical example which shall serve to illustrate that in the classical case a phase-space compression is actually achieved. A quantitative and far more thorough analysis will be given in the next section, where we will treat the problem quantum mechanically. The example is shown in Fig. 4.4 where we used the parameters in Table 4.1. We clearly observe a reduction of the phase-space volume, which is emphasized by the narrowness of the position component. This confirms the previous analysis. The results in this section allow, at least in principle in this idealized setup, an nearly arbitrary compression in space, because we can reduce the distance between the mirrors to any value desired. In addition we can thereby be sure, according to Proposition 6, that for each particle the absolute value of the final velocity is always smaller than the absolute value of the initial one. In the next section we will determine if this method still works in the quantum mechanical framework and under more realistic conditions including realizable potentials.

Parameters Initial Distribution:			
$x_{i,1} = -0.0029$	$v_{i,1} = 4.49$	$\Delta x_{i,1} = 0.00058$	$\Delta v_{i,1} = 1.10$
Other Parameters:			
$x_{m,l} = -0.00015$	$\alpha = 1$	$t_f = 1$	

Table 4.1: Dimensionless parameters for the simulations of a particle confined between two accelerated mirrors in the classical case.

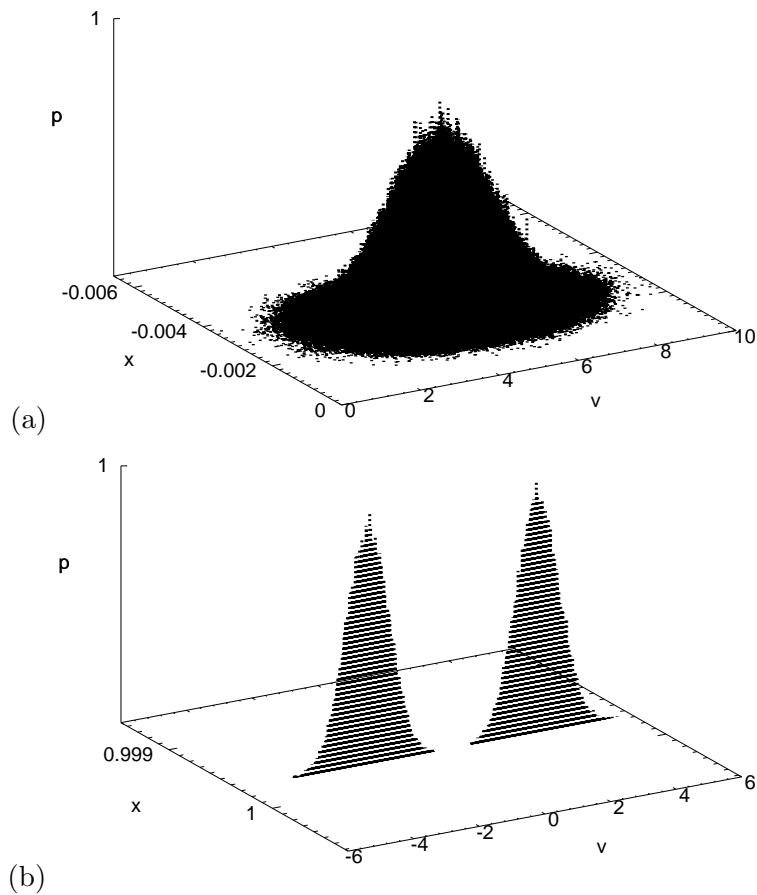


Figure 4.4: Classical Case: The initial and final phase-space density of particles in a pulse becoming confined between two accelerated mirror potentials and undergoing subsequent collisions for the parameters in Table 4.1.

(a) Initial phase space density. (b) Final phase space density.

4.3 Quantum Particles

In the previous section we described the idea of trapping and slowing particles in a pulse between two accelerated mirrors in an idealized classical setting. We did this to determine whether this idea works at least in principle. In this section we will proceed by treating the problem quantum mechanically. We begin with presenting a setup with which one is able to actually realize the proposed scheme in the quantum case and show results derived via solving the corresponding master-equation afterwards.

We consider a state selective mirror potential on the left, a mirror potential on the right and a pumping laser in the region between these mirrors. All three shall move with $v_{m,l}(t) = v_{m,r}(t) = v_p(t) = \frac{\alpha}{2\sqrt{t}}$ and $v_{m,l}(t)$ as before, where $v_{m,r}(t)$, $v_p(t)$ denote the velocities of the left mirror, the right mirror and the pumping laser respectively, see Fig. 4.5 for the scheme. The state selective mirror on the left and the pumping laser together serve as a simplified atom diode¹. The atoms will be considered as three-level systems with ground state $|1\rangle = (1,0,0)^T$, a metastable state $|2\rangle = (0,1,0)^T$, and a fastly decaying excited state $|3\rangle = (0,0,1)^T$, see again Fig. 4.5. An atom initially in the ground state $|1\rangle$ coming from the left will pass the left potential W_l unaffected and therefore it is guaranteed that the atom will at first be reflected from the right potential W_r . The pumping laser now excites the atom to the state $|3\rangle$, either before or after being reflected from the right potential W_r , which fastly decays to the metastable state $|2\rangle$. In this state the atom will be reflected from the left potential W_l too, which gives exactly the scheme used in the classical description, leading, as we will see, to trapping and cooling of the atoms in a pulse. In the following we will now model this scheme.

The corresponding Hamiltonian without decay is given by

$$H = \frac{p_x^2}{2m} + \frac{\hbar}{2} \begin{pmatrix} W_r(x,t) & 0 & \Omega_p(x,t) \\ 0 & W_l(x,t) + W_r(x,t) & 0 \\ \Omega_p(x,t) & 0 & 0 \end{pmatrix} \quad (4.20)$$

where $\Omega_p(x,t) = \hat{\Omega}_p \Pi_p(x,t)$, $W_l(x,t) = \hat{W}_l \Pi_l(x,t)$, $W_r(x,t) = \hat{W}_r \Pi_r(x,t)$ and

$$\Pi_o(x,t) = e^{-\frac{(x-x_o-\alpha\sqrt{t})^2}{2\Delta x_o^2}}$$

with $o = p, l, r$ respectively. Here we have applied usual approximations, including dipole and rotating wave approximations, semiclassical laser fields and neglecting atom-atom interactions. For more details on these approximations as well as the interaction between an atom and a laser, see Sections 2.1 and 2.2. Apart from the decay which we will take into account below, this Hamiltonian describes the situation we discussed in the beginning. We do not expect an absorption followed by stimulated emission to pose a real problem, because we assume a fast decay and even if a stimulated emission takes place a second excitation is likely to occur afterwards. Additionally the right mirror potential acts as such also for the atom in the ground state, such that the neces-

¹ See for example [50] for the theoretical proposal and [27] for its experimental implementation as well as [58] for a different experimentally realized cooling scheme using such an atom diode.

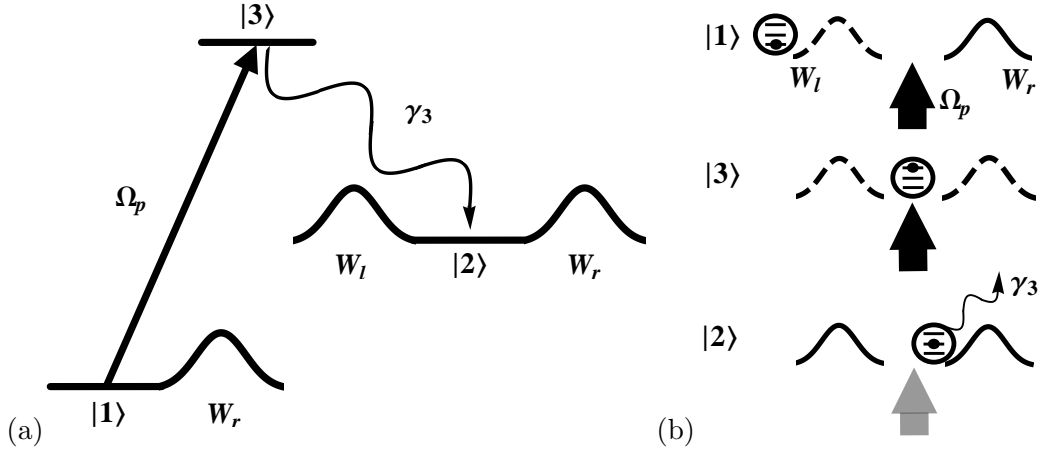


Figure 4.5: (a) Schematic picture of the level scheme considered and the corresponding state-dependent potentials the atom experiences in the respective states. We have a groundstate $|1\rangle$, which is coupled to a fastly decaying excited state $|3\rangle$ via the pumping laser with frequency Ω_p . The state $|3\rangle$ then decays with high rate γ_3 (inverse life-time) to the metastable state $|2\rangle$. (b) Schematic picture of the atom, described as a three-level system, interacting with the three lasers. At the beginning the atom is in the ground-state $|1\rangle$, passing the left potential W_l unaffected (dashed Gaussian), but not the right one W_r (solid Gaussian). In the region between the mirrors it gets excited by the pump laser (solid arrow) to the state $|3\rangle$ and decays afterwards to the metastable state $|2\rangle$. In this state it will now also be reflected by W_l (now solid), but it will not interact with the pump laser anymore (now grey arrow). Therefore the atom is trapped between both mirrors and undergoes repeated reflections.

sary excitation and the fast decay can also occur after the reflection from the right mirror.

Using the results in Sections 2.3 and 2.4, it is straightforward to determine the master-equation for the density operator describing the time-evolution of the three-level atom with spontaneous emission with rate γ_3 . Here the Hamiltonian H_L in eq. (2.67) is the Hamiltonian H describing the interaction with the different lasers given by eq. (4.20). Furthermore, in our scheme the transition due to spontaneous emission occurs from $|3\rangle$ to $|2\rangle$. The master-equation we have to solve is therefore given by

$$\frac{\partial}{\partial t}\rho = -\frac{i}{\hbar}[\rho, H]_- - \frac{\gamma_3}{2} \{ |3\rangle\langle 3|, \rho \}_+ + \gamma_3 |2\rangle\langle 3| \rho |3\rangle\langle 2|. \quad (4.21)$$

In our simulations of the time-evolution of $\rho(t)$ we start with a pure state $\rho(t_0) = |\Psi_{t_0}\rangle\langle\Psi_{t_0}|$ at $t_0 = 0$, namely a Gaussian (but not necessarily with minimal uncertainty)

$$\Psi_0(x) = \frac{1}{\sqrt{2\pi}} \int dk \Phi_0(k) e^{ikx} \quad (4.22)$$

with

$$\Phi_0(k) = \frac{1}{(2\pi)^{\frac{1}{4}}\sqrt{\Delta k}}(1,0,0)^T \times \exp\left[-\frac{(k-k_0)^2}{4\Delta k^2} - i(k-k_0)\left(x_0 - \frac{\hbar}{m}\Delta t k_0\right) - i\frac{\hbar}{m}\Delta t \frac{k^2}{2}\right] \quad (4.23)$$

where $k_0 = \frac{m}{\hbar}v_0$ and $\Delta k = \frac{m}{\hbar}\Delta v$. Using the quantum jump approach (see Section 2.4), we can determine the solution of eq. (4.21) via averaging over sufficiently many solutions of the three-level Schrödinger equation

$$i\hbar\frac{\partial}{\partial t}\vec{\Psi}(x,t) = H_c\vec{\Psi}(x,t) \quad (4.24)$$

with $\vec{\Psi}(x,t) = (\Psi^1(x,t), \Psi^2(x,t), \Psi^3(x,t))^T$, $\Psi^j(x,t) = \langle j|\Psi(x,t)\rangle$, and the conditional Hamiltonian

$$H_c = H - i\frac{\hbar}{2}\gamma_3|3\rangle\langle 3| \quad (4.25)$$

where H is given by eq. (4.20).

By assuming $\gamma_3 \gg 1$ we can achieve a computational simplification, because then we can approximate the three-level problem by a two-level problem, see [56] for a similar application and [9] for a more rigorous derivation of this approximation in the stationary case as well as Appendix A for the time-dependent case. Here we will present a simplified argument in the time-dependent case to motivate this approximation.

The following approximation applies to the states $\Psi^1(x,t)$ and $\Psi^3(x,t)$ and therefore we will not consider $\Psi^2(x,t)$ for now. The states $\Psi^1(x,t)$ and $\Psi^3(x,t)$ obey the equations

$$i\hbar\frac{\partial}{\partial t}\Psi^1(x,t) = -\frac{\hbar^2}{2m}\frac{\partial^2}{\partial x^2}\Psi^1(x,t) + W_r(x,t)\Psi^1(x,t) + \frac{\hbar}{2}\Omega_p(x,t)\Psi^3(x,t) \quad (4.26)$$

and

$$i\hbar\frac{\partial}{\partial t}\Psi^3(x,t) = -\frac{\hbar^2}{2m}\frac{\partial^2}{\partial x^2}\Psi^3(x,t) + \frac{\hbar}{2}\Omega_p(x,t)\Psi^1(x,t) - i\frac{\hbar}{2}\gamma_3\Psi^3(x,t). \quad (4.27)$$

Rearranging eq. (4.27) we have

$$\frac{\hbar}{2}\Omega_p(x,t)\Psi^1(x,t) = \left[i\hbar\frac{\partial}{\partial t} + \frac{\hbar^2}{2m}\frac{\partial^2}{\partial x^2} + i\frac{\hbar}{2}\gamma_3 \right] \Psi^3(x,t)$$

and therefore

$$-i\frac{\Omega_p(x,t)}{\gamma_3}\Psi^1(x,t) = \left[\frac{2}{\gamma_3}\frac{\partial}{\partial t} - i\frac{\hbar}{m\gamma_3}\frac{\partial^2}{\partial x^2} + 1 \right] \Psi^3(x,t). \quad (4.28)$$

Loosely speaking, for $\gamma_3 \gg 1$ the term in brackets on the right hand side of eq. (4.28) is approximately one, i.e.

$$\left[\frac{2}{\gamma_3}\frac{\partial}{\partial t} - i\frac{\hbar}{m\gamma_3}\frac{\partial^2}{\partial x^2} + 1 \right] \approx 1. \quad (4.29)$$

Therefore we make the Ansatz

$$\Psi^3(x,t) = -i \frac{\Omega_p(x,t)}{\gamma_3} \Psi^1(x,t) + \mathcal{O}\left(\frac{|\Omega_p(x,t)|^2}{\gamma_3^2}\right) \quad (4.30)$$

with $\frac{\gamma_3}{\Omega_{pm}} \gg 1$ and $\Omega_{pm} = \max_{x,t} |\Omega_p(x,t)|$. From eq. (4.28) it follows that

$$\begin{aligned} -i \frac{\Omega_p(x,t)}{\gamma_3} \Psi^1(x,t) &= \frac{1}{\gamma_3} \left[2 \frac{\partial}{\partial t} - i \frac{\hbar}{m} \frac{\partial^2}{\partial x^2} \right] \left(-i \frac{\Omega_p(x,t)}{\gamma_3} \Psi^1(x,t) + \mathcal{O}\left(\frac{|\Omega_p(x,t)|^2}{\gamma_3^2}\right) \right) \\ &- i \frac{\Omega_p(x,t)}{\gamma_3} \Psi^1(x,t) + \mathcal{O}\left(\frac{|\Omega_p(x,t)|^2}{\gamma_3^2}\right), \end{aligned} \quad (4.31)$$

i.e. we have equality up to order $\mathcal{O}\left(\frac{|\Omega_p(x,t)|^2}{\gamma_3^2}\right)$. Neglecting terms of this order for $\frac{\gamma_3}{\Omega_{pm}} \gg 1$ we therefore have that the third component obeys the approximation

$$\Psi^3(x,t) \approx -i \frac{\Omega_p(x,t)}{\gamma_3} \Psi^1(x,t) \quad (4.32)$$

and the first and second component approximately satisfy the two-level Schrödinger equation

$$i\hbar \frac{\partial}{\partial t} \Psi^{1,2}(x,t) = H_{approx} \Psi^{1,2}(x,t) \quad (4.33)$$

where $\Psi^{1,2}(x,t) = (\Psi^1(x,t), \Psi^2(x,t))^T$. The approximate Hamiltonian H_{approx} is given by

$$H_{approx} = \frac{p_x^2}{2m} + \frac{\hbar}{2} \begin{pmatrix} -iW_p(x,t) & 0 \\ 0 & W_l(x,t) + W_r(x,t) \end{pmatrix} \quad (4.34)$$

with $W_p(x,t) = \frac{|\Omega_p(x,t)|^2}{\gamma_3}$. We applied this two-dimensional approximation to the three-dimensional Schrödinger equation (4.24) to solve the master-equation (4.21) via the quantum jump approach. In the following we will give a few examples of the results we obtained. We start with three examples for which we change the parameters in such a way that one would expect an increasing phase-space compression, which is confirmed by the results. In addition we will give one further example for a different set of parameters.

In Fig. 4.6 the initial and final position distributions are shown for the parameters in Table 4.2 (note that the final one was shifted to fit into the same graph), and in Fig. 4.7 the corresponding initial and final velocity distributions are shown. These results were obtained by averaging over 200 jumps. Although we observe an increase of the width, because we now have both negative and positive parts, we still observe a reduction of velocity. Additionally we find that the probability of observing an atom between the mirror potentials is close to one, i.e. the atom is trapped, and we therefore obtain a large reduction of the width of the position distribution. The corresponding expectation values and variances can be found in Table 4.3. For the products of the variances we obtain $\Delta x_i \Delta v_i \approx 1.34 \Delta x_f \Delta v_f$. Taking these as a measure of the phase-space volume

we therefore observe a reduction of phase-space volume by a factor 1.34.

In Fig 4.8 the final velocity distribution for the same parameters as before is compared to the distribution obtained by averaging over 100 jumps instead, i.e. half the number of jumps. The results hardly differ, which shows that the number of jumps used to obtain these results should be sufficient.

For the next example we reduced the initial average distances for the state and the mirrors, see the parameters in Table 4.4. The corresponding initial and final position distributions are shown in Fig. 4.9 (note that the final one was again shifted to fit into the same graph), and in Fig. 4.10 the corresponding initial and final velocity distributions are depicted. These results were also obtained by averaging over 200 jumps. Although as before we observe an increase of the width in velocity space, overall we again observe a velocity reduction. We also find that the probability of observing an atom between the mirror potentials is again close to one, i.e. the atom is trapped, and obtain an even larger reduction of the width of the position distribution. The corresponding expectation values and variances can be found in Table 4.5. For the products of the variances we obtain $\Delta x_i \Delta v_i \approx 2.78 \Delta x_f \Delta v_f$. Taking these as a measure of the phase-space volume as before, we therefore observe a reduction of phase-space volume by a factor 2.78. In Fig. 4.11 the final velocity distribution for the same parameters as before is compared to the distribution obtained by averaging over 100 jumps instead, i.e. half the number of jumps. Furthermore, it is also compared to the distribution obtained for only 50 jumps but twice the number of steps in space. The results hardly differ, which shows that the number of jumps and steps used to obtain these results should be sufficient too.

For the last example with varying initial average distance, we reduced this even

Initial State Parameters:			
$x_i = -0.045$	$v_i = 20$	$\Delta x_i = 0.005$	$\Delta v_i = 3$
$m = 1000$			
Mirror Parameters:			
$x_{m,l} = -0.01$	$x_p = -0.005$	$x_{m,r} = 0$	
$\Delta x_{m,l} = 0.001$	$\Delta x_p = 0.001$	$\Delta x_{m,r} = 0.001$	
Other Parameters:			
$\alpha = 1$	$t_f = 1$	$d = 1$	

Table 4.2: Dimensionless parameters for the simulations of the quantum catcher shown in Figs. 4.6, 4.7 and 4.8.

$\langle x_i \rangle = -0.045$	$\Delta x_i = 0.005$	$\langle v_i \rangle = 20$	$\Delta v_i = 3$
$\langle x_f \rangle = 0.995$	$\Delta x_f = 0.0014$	$\langle v_f \rangle = 0.45$	$\Delta v_f = 8$
		$\langle v_f \rangle = 10.6$	$\Delta v_f = 3.2$

Table 4.3: Initial and final expectation values and variances corresponding to the results for the quantum catcher shown in Figs. 4.6, 4.7 and 4.8.

Initial State Parameters:			
$x_i = -0.04$	$v_i = 20$	$\Delta x_i = 0.005$	$\Delta v_i = 3$
$m = 1000$			
Mirror Parameters:			
$x_{m,l} = -0.005$	$x_p = -0.0025$	$x_{m,r} = 0$	
$\Delta x_{m,l} = 0.0005$	$\Delta x_p = 0.0005$	$\Delta x_{m,r} = 0.0005$	
Other Parameters:			
$\alpha = 1$	$t_f = 1$	$d = 1$	

Table 4.4: Dimensionless parameters for the simulations of the quantum catcher shown in Figs. 4.9, 4.10 and 4.11.

$\langle x_i \rangle = -0.04$	$\Delta x_i = 0.005$	$\langle v_i \rangle = 20$	$\Delta v_i = 3$
$\langle x_f \rangle = 0.997$	$\Delta x_f = 0.0006$	$\langle v_f \rangle = 1.93$	$\Delta v_f = 9$
		$\langle v_f \rangle = 11.5$	$\Delta v_f = 4.1$

Table 4.5: Initial and final expectation values and variances corresponding to the results for the quantum catcher shown in Figs. 4.9, 4.10 and 4.11.

further both for the state and the mirrors, see the parameters in Table 4.4. The corresponding initial and final position distributions can be found in Fig. 4.12 and in Fig. 4.13 the corresponding initial and final velocity distributions. These results were obtained by averaging over 100 jumps. According to the previous reasoning one would expect an even larger reduction of the phase-space volume and indeed this happens as can be deduced from the expectation values and variances in Table 4.7. We obtain $\Delta x_i \Delta v_i \approx 4.17 \Delta x_f \Delta v_f$ and therefore observe a reduction of phase-space volume by a factor 4.17. Finally in Fig. 4.14 we again compared the final velocity distributions for a different number of jumps and also observed hardly any difference in the results.

Finally we give one example for a different set of parameters, which can be found in Table 4.8, to show that the previous examples are not an exception due to a specific choice of parameters. In Fig. 4.15 the corresponding initial and final position distri-

Initial State Parameters:			
$x_i = -0.038$	$v_i = 20$	$\Delta x_i = 0.005$	$\Delta v_i = 3$
$m = 1000$			
Mirror Parameters:			
$x_{m,l} = -0.0025$	$x_p = -0.00125$	$x_{m,r} = 0$	
$\Delta x_{m,l} = 0.00025$	$\Delta x_p = 0.00025$	$\Delta x_{m,r} = 0.00025$	
Other Parameters:			
$\alpha = 1$	$t_f = 1$	$d = 1$	

Table 4.6: Dimensionless parameters for the simulations of the quantum catcher shown in Figs. 4.12, 4.13 and 4.14.

$\langle x_i \rangle$	=	-0.038	Δx_i	=	0.005	$\langle v_i \rangle$	=	20	Δv_i	=	3
$\langle x_f \rangle$	=	0.99987	Δx_f	=	0.0003	$\langle v_f \rangle$	=	3.78	Δv_f	=	12
						$\langle v_f \rangle$	=	15.7	$\Delta v_f $	=	8

Table 4.7: Initial and final expectation values and variances corresponding to the results for the quantum catcher shown in Figs. 4.12, 4.13 and 4.14.

butions are shown and in Fig. 4.16 the initial and final velocity distributions. These results were again obtained by averaging over 100 jumps and the expectation values and variances can be found in Table 4.9. We obtain $\Delta x_i \Delta v_i \approx 2.67 \Delta x_f \Delta v_f$ and therefore observe a reduction of phase-space volume by a factor 2.67. Furthermore, in Fig. 4.17 we again compared the final velocity distributions for 100 jumps and 50 jumps and observe hardly any difference between them.

Although we clearly observe a phase-space compression in the examples above, the reduction of phase-space volume is not exceptionally large. The main reason for this is the feasibility of the simulations. To obtain the last result in the sequence of examples with decreasing initial average distances, e.g. the necessary discretization in space lead to the maximal allocation of working memory available and although the simulations are massively parallelized, see Appendices B and E, obtaining one result takes an amount of time in the order of days. The results presented therefore do not show an optimal phase-space compression achievable with the proposed method. Instead we conjecture that further reduction of, say the initial distance, accompanied by a smaller mirror distance, would lead to a significantly larger phase-space reduction. Also other parameter changes, like the width of the distributions, could lead to relatively larger phase-space

Initial State Parameters:			
$x_i = -0.06$	$v_i = 10$	$\Delta x_i = 0.01$	$\Delta v_i = 2$
$m = 1000$			
Mirror Parameters:			
$x_{m,l} = -0.01$	$x_p = -0.005$	$x_{m,r} = 0$	
$\Delta x_{m,l} = 0.001$	$\Delta x_p = 0.001$	$\Delta x_{m,r} = 0.001$	
Other Parameters:			
$\alpha = 1$	$t_f = 1$	$d = 1$	

Table 4.8: Dimensionless parameters for the simulations of the quantum catcher shown in Figs. 4.15, 4.16 and 4.17.

$\langle x_i \rangle$	=	-0.06	Δx_i	=	0.01	$\langle v_i \rangle$	=	10	Δv_i	=	2
$\langle x_f \rangle$	=	0.995	Δx_f	=	0.0011	$\langle v_f \rangle$	=	0.37	Δv_f	=	6.8
						$\langle v_f \rangle$	=	5.2	$\Delta v_f $	=	2.1

Table 4.9: Initial and final expectation values and variances corresponding to the results for the quantum catcher shown in Figs. 4.15, 4.16 and 4.17.

compressions. Therefore the results shown should not be misinterpreted as showing the optimal efficiency of the method, instead they are obtained for a compromise between supposedly optimal parameters and numerical feasibility.

We close this chapter with an example of dimensioned parameters in Table 4.10, which correspond to the parameters in Table 4.4 and the results shown in Figs. 4.9, 4.10 and 4.11. Note that as before this is only one possible set of dimensioned parameters. Adjusting d and t_f accordingly we obtain the same results for different initial velocities and positions.

Initial State Parameters:			
$x_i = -34.9 \mu\text{m}$	$v_i = 24.2 \text{ cm/s}$	$\Delta x_i = 4.36 \mu\text{m}$	$\Delta v_i = 3.63 \text{ cm/s}$
$m = 9.99 \cdot 10^{-27} \text{ kg}$			
Mirror Parameters:			
$x_{m,l} = -4.36 \mu\text{m}$	$x_p = -2.18 \mu\text{m}$	$x_{m,r} = 0$	
$\Delta x_{m,l} = 0.436 \mu\text{m}$	$\Delta x_p = 0.436 \mu\text{m}$	$\Delta x_{m,r} = 0.436 \mu\text{m}$	
Other Parameters:			
$t_f = 72 \text{ ms}$		$d = 872 \mu\text{m}$	

Table 4.10: Example of dimensioned parameters for the results shown in Figs. 4.9, 4.10 and 4.11 and corresponding to the dimensionless parameters in Table 4.4.

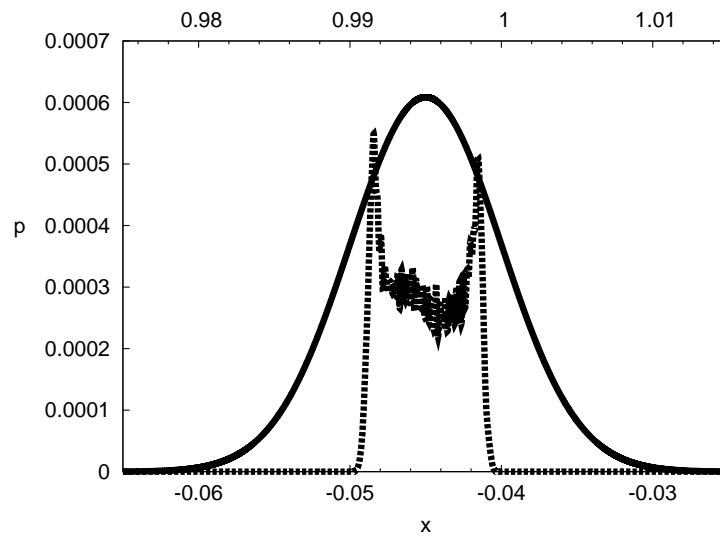


Figure 4.6: Quantum case: The initial position distribution (solid line) and final position distribution (dashed line) for an initial state (4.22) and the parameters in Table 4.2. The final distribution was shifted to fit it into the same graph. The actual position is given on the top axis.

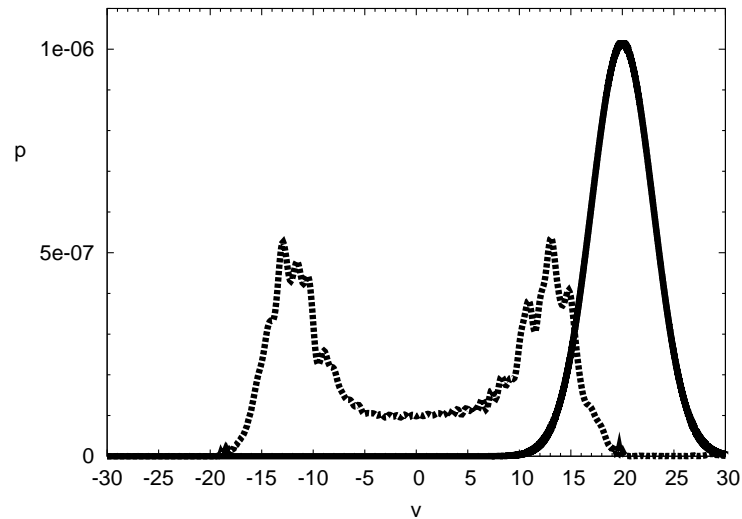


Figure 4.7: Quantum case: The initial velocity distribution (solid line) and final velocity distribution (dashed line) for an initial state (4.22) and the parameters in Table 4.2.

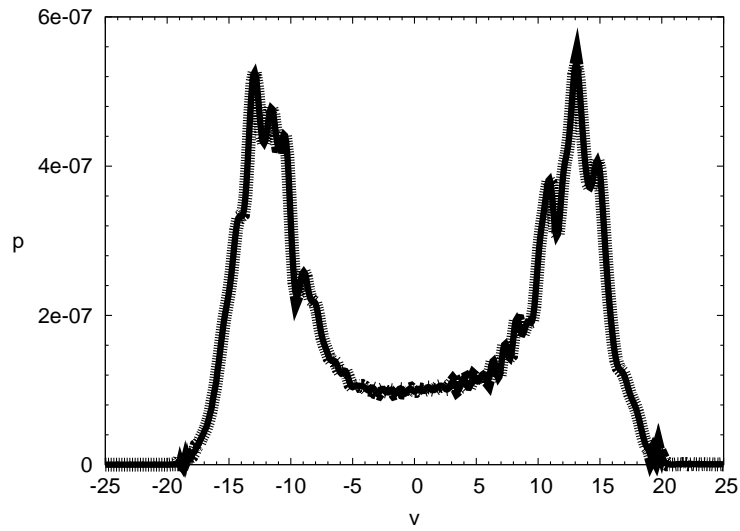


Figure 4.8: Quantum case: The final velocity distribution for 200 jumps (solid line) compared to those for 100 jumps (thick dashed line) for an initial state (4.22) and the parameters in Table 4.2.

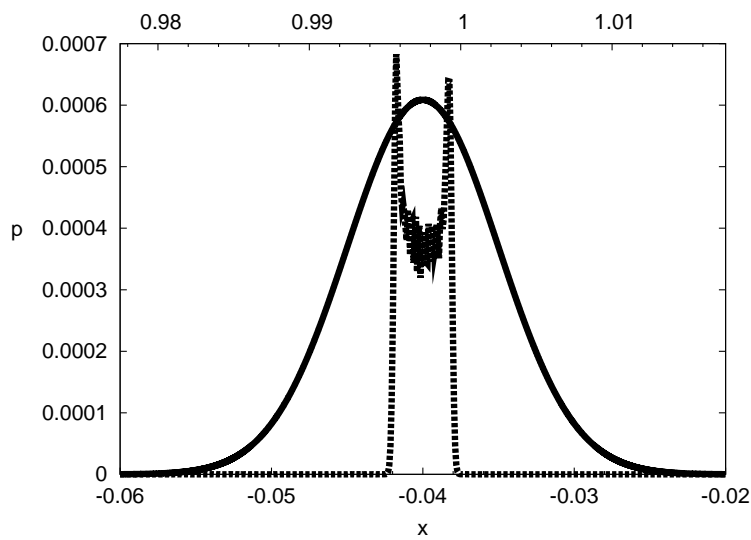


Figure 4.9: Quantum case: The initial position distribution (solid line) and final position distribution (dashed line) for an initial state (4.22) and the parameters in Table 4.4. The final distribution was shifted to fit it into the same graph. The actual position is given on the top axis.

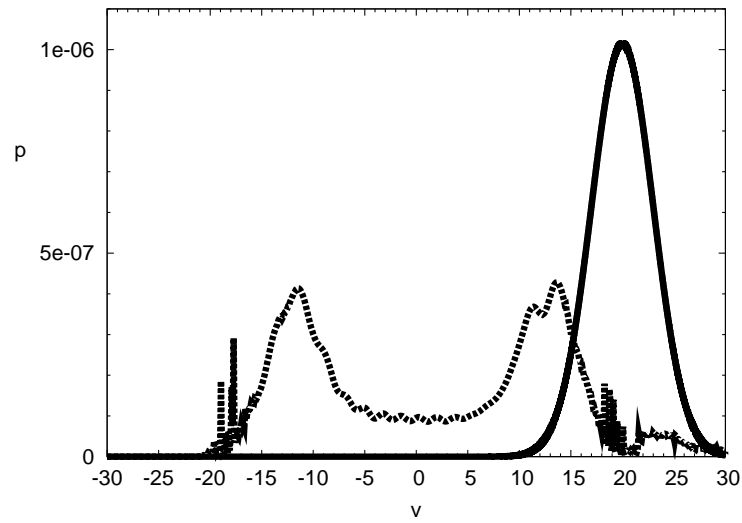


Figure 4.10: Quantum case: The initial velocity distribution (solid line) and final velocity distribution (dashed line) for an initial state (4.22) and the parameters in Table 4.4.

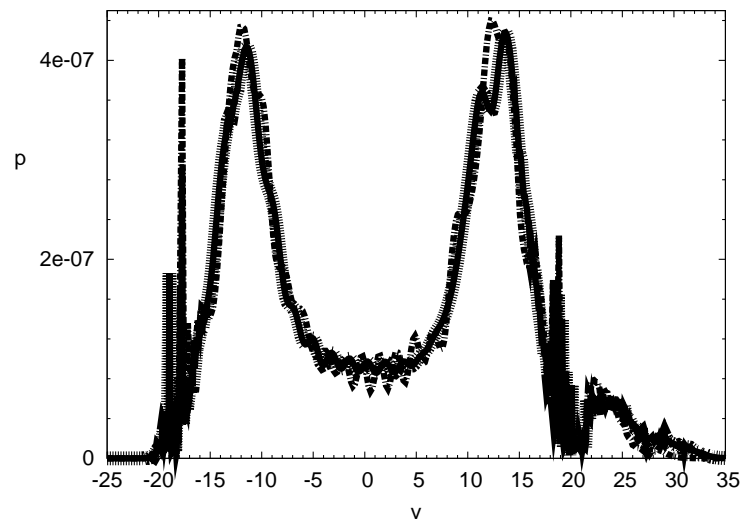


Figure 4.11: Quantum case: The final velocity distribution for 200 jumps (solid line) compared to those for 100 jumps (thick dashed line) with the same position step size and for 50 jumps with half the position step size (dotted dashed line) for an initial state (4.22) and the parameters in Table 4.4.

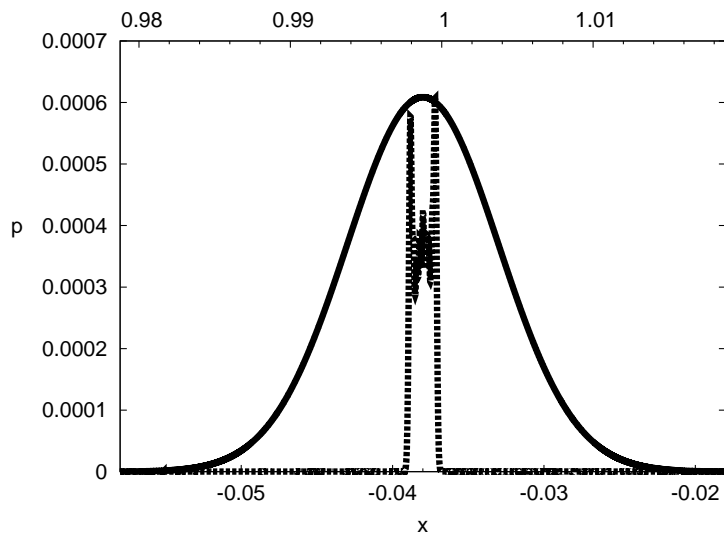


Figure 4.12: Quantum case: The initial position distribution (solid line) and final position distribution (dashed line) for an initial state (4.22) and the parameters in Table 4.6. The final distribution was shifted to fit it into the same graph. The actual position is given on the top axis.

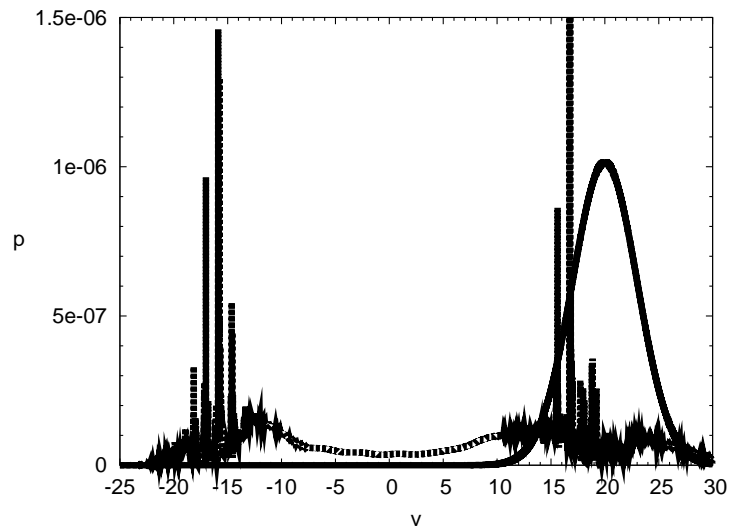


Figure 4.13: Quantum case: The initial velocity distribution (solid line) and final velocity distribution (dashed line) for an initial state (4.22) and the parameters in Table 4.6.

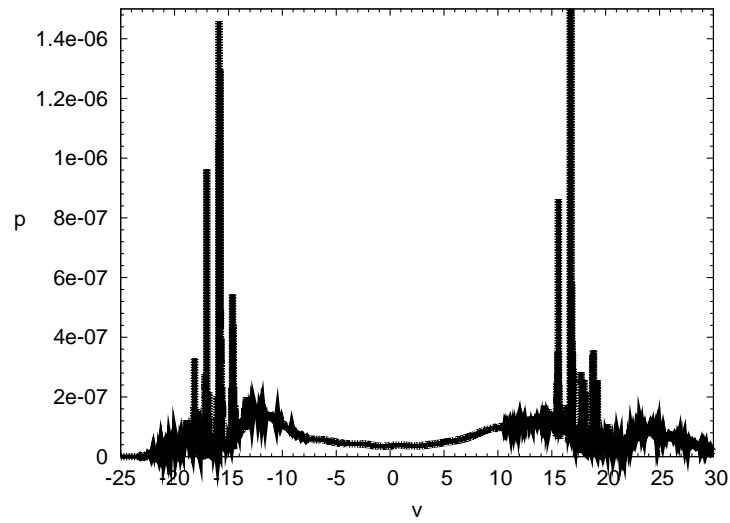


Figure 4.14: Quantum case: The final velocity distributions for 100 jumps (solid line) and 60 jumps (thick dashed line) for an initial state (4.22) and the parameters in Table 4.6.

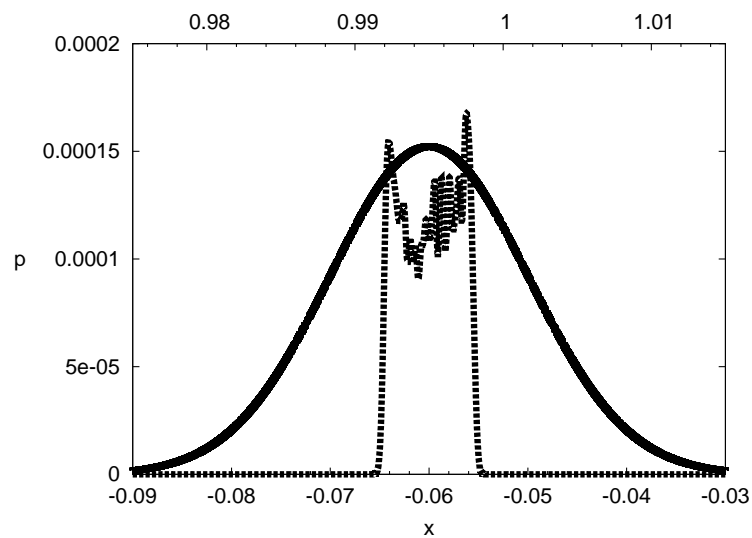


Figure 4.15: Quantum case: The initial position distribution (solid line) and final position distribution (dashed line) for an initial state (4.22) and the parameters in Table 4.8. The final distribution was shifted to fit it into the same graph. The actual position is given on the top axis.

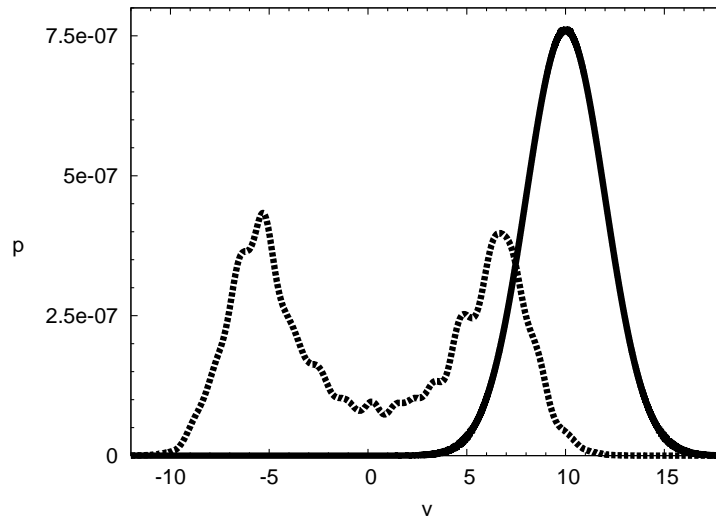


Figure 4.16: Quantum case: The initial velocity distribution (solid line) and final velocity distribution (dashed line) for an initial state (4.22) and the parameters in Table 4.8.

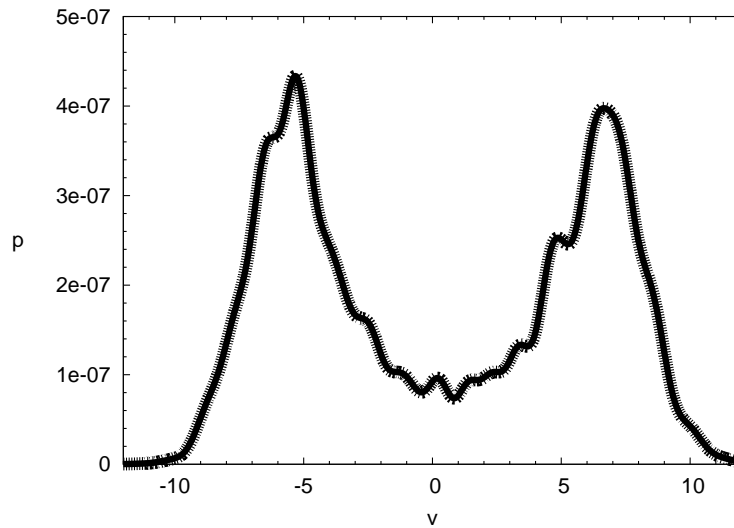


Figure 4.17: Quantum case: The final velocity distributions for 100 jumps (solid line) and 50 jumps (thick dashed line) for an initial state (4.22) and the parameters in Table 4.8.

4.4 Summary and Conclusion

In this chapter we proposed a new scheme for trapping and simultaneously cooling atoms by combining a moving atom diode and mirror, where the trajectory, inspired by the results in Chapter 3, is proportional to a square-root in time. We started with modelling the situation in an idealized classical setup for one particle moving to the right and, starting in front of the particle, two mirrors moving in the same direction. We assumed that the particle passes the first mirror from the left unaffected, which mimics the diodic behavior, such that the first collision occurs with the right mirror and the particle is trapped afterwards. Then we derived the important result that a classical particle in this setup is, as long as at least one collision occurs, always slower than it was initially. Furthermore, we derived expressions via which one can ensure a minimal velocity reduction. We continued by considering the case of a classical ensemble of non-interacting particles and gave a numerical example showing a reduction of the phase-space volume. Following the classical analysis we examined the problem in the quantum mechanical framework. We proposed a setup with which one can actually realize this scheme. This setup consists of a state selective mirror potential, followed by a pump laser and another mirror potential, all moving along a square-root in time trajectory. We derived the corresponding master-equation and solved it numerically via the quantum jump approach. The results actually showed a velocity reduction and confinement of the particles between the mirrors, especially resulting in a reduction of the phase-space volume. Finally the results showed the expected behaviour by reducing the initial distance and the mirror distance, i.e. we observed a larger reduction of the phase-space volume. Based on these results we conjecture that given suitable parameters much larger reductions can be achieved, which could not be examined numerically, because for these parameter ranges the problem was numerically not feasible anymore.

5 A Shortcut to Adiabaticity

The sciences do not try to explain, they hardly even try to interpret, they mainly make models. By a model is meant a mathematical construct which, with the addition of certain verbal interpretations, describes observed phenomena. The justification of such a mathematical construct is solely and precisely that it is expected to work - that is, correctly to describe phenomena from a reasonably wide area.

(John v. Neumann, The Unity of Knowledge)

5.1 Introduction

A standard operation to probe, control or prepare a quantum system, in particular in the realm of atomic and molecular science, consists in changing the external parameters of the Hamiltonian. In many cases the ideal transformations from an initial to a final parameter configuration are the ones that do not induce any transitions¹ [59, 60]. The standard solution to this requirement is to perform the changes “adiabatically”. Loosely speaking, an “adiabatic” process in quantum mechanics is a slow process where the system follows at all times the instantaneous eigenvalues and eigenstates of the time-dependent Hamiltonian. This is the content of the adiabatic theorem in quantum mechanics, whose original form [61] can loosely be stated as

A physical system remains in its instantaneous eigenstate if a given perturbation is acting on it slowly enough and if there is a gap between the eigenvalue and the rest of the Hamiltonian's spectrum.

That the adiabatic hypothesis holds in the region of the discrete spectrum of a Hamiltonian was already recognized in the early days of quantum mechanics, but it took over 20 years until a complete proof was found [62]. For more information on the adiabatic theorem in quantum mechanics we refer the reader also to [63]-[67]. In a more rigorous way the theorem states the following, where the subsequent presentation is based on [67]. Let $H(t)$ be a time-dependent Hamiltonian given by

$$H(t) = \sum_i e_i(t) P_i(t), \quad (5.1)$$

with $e_i(t)$ its i th eigenvalue at time t and $P_i(t)$ the projection onto the corresponding eigenspace. Introducing the scaling τ , the time-evolution $U_\tau(t)$ generated by $H(t/\tau)$ is given by

$$\frac{d}{dt} U_\tau(t) = -iH(t/\tau)U_\tau(t). \quad (5.2)$$

¹ As an example consider a system which is prepared at a certain location, but has to be transported to an appropriate location in order to perform further experiments.

Although in general the Hamiltonian is not covariant, i.e.

$$H(t/\tau) \neq U_\tau^{-1}(t)H(0)U_\tau(t), \quad (5.3)$$

in [62] it was shown that:

Theorem 2. For $U_\tau(t)$ given by eq. (5.2) one has

$$\lim_{\tau \rightarrow \infty} U_\tau^{-1}(\tau)P_i(0)U_\tau(\tau) = P_i(1), \quad (5.4)$$

where $P_i(0)$ and $P_i(1)$ are the initial and final projections onto the i th eigenspace.

Furthermore, for a mixed state $\rho(t/\tau)$ it was shown that it is adiabatically invariant in the nondegenerate case, i.e.

Theorem 3. For $U_\tau(t)$ given by eq. (5.2) and $\rho(t/\tau)$ a nondegenerate mixed state one has

$$\lim_{\tau \rightarrow \infty} U_\tau^{-1}(\tau)\rho(0)U_\tau(\tau) = \rho(1), \quad (5.5)$$

i.e. under sufficiently slow evolution the populations remain unchanged.

Although it should be clear that the Hamiltonian is in general not covariant, it is also straightforward to show this using Theorem 2. We have

$$\begin{aligned} \lim_{\tau \rightarrow \infty} U_\tau^{-1}(\tau)H(0)U_\tau(\tau) &= \lim_{\tau \rightarrow \infty} U_\tau^{-1}(\tau) \sum_i e_i(0)P_i(0)U_\tau(\tau) \\ &= \sum_i e_i(0) \lim_{\tau \rightarrow \infty} U_\tau^{-1}(\tau)P_i(0)U_\tau(\tau) = \sum_i e_i(0)P_i(1) \neq H(1), \end{aligned} \quad (5.6)$$

since generally $e_i(0) \neq e_i(1)$, as is the case for a harmonic oscillator with time dependent frequency. This change of energy eigenvalues is for example used to cool trapped atoms by lowering the trap frequency, which will be discussed in more detail in Section 5.3 where we will present a shortcut to adiabaticity for this method.

If in an experiment the change of the parameters happens sufficiently slowly, such that the adiabatic theorem approximately holds, the populations do not change and there is no heating or friction. The drawbacks are that the long times needed may render the operation useless or even impossible to implement, or quite simply a faster process is preferred, e.g. to increase the repetition rate of a cycle. There has recently been a surge of interest in adiabatic theory and applications [59, 68, 69, 70].

A highly desirable goal would therefore be the preparation of the same final states and energies of the adiabatic process in a given finite time t_f , without necessarily following the instantaneous eigenstates along the way, and where the procedure also ought to be robust with respect to arbitrary initial states, and realizable in practice.

If fulfilled, this goal [71] has important implications, since most of the current theoretical and experimental work with cold atoms involves an adiabatic tuning of the system (frequently an expansion or trap weakening) after a cooling phase [59], or as part of the

cooling process itself [72]. This adiabatic step has different objectives: the reduction of velocity dispersion and collisional shifts for spectroscopy and atomic clocks [73]; reaching extremely low temperatures inaccessible by standard cooling techniques [72]; or, in experiments with optical lattices, broadening the state before turning on the lattice [74]. These applications would benefit from a shortcut to adiabaticity, reducing the times by several orders of magnitude.

The above goal also includes a long standing question in the fields of optimal control theory and finite time thermodynamics, namely, how to optimize the passage between two thermal states of a system [75]-[84]. For time-dependent harmonic oscillators, minimal times have been established using “bang-bang” real-frequency processes believed up to now to be optimal [83], in which the frequencies are changed suddenly at certain instants but kept constant otherwise.

In this chapter we will present a solution to the stated general goal for different setups. The general method, which we will call the “inverse-invariant” or “inverse-engineering” method and which will be applied to different problems afterwards, is presented in Section 5.2. This method was developed using Lewis-Riesenfeld invariants [71] of motion and inverse scattering techniques [85]-[87]. In Section 5.3 we will consider the cooling of non-interacting atoms trapped in a harmonic potential by lowering the trap frequency and especially show the methods superiority over adiabatic following¹. In Section 5.4 we will then apply the method to the transport of a Bose-Einstein condensate in a rigid harmonic trap. Additionally we will give further optimality criteria for the family of solutions one derives with the proposed method and consider the effect of noise, which is treated as a deviation of the potential shape from that of a perfect harmonic one. These results were published in [2]-[4] and were obtained in collaboration with X. Chen, A. del Campo, S. Ibáñez, E. Torrontegui, M. Modugno, D. Guéry-Odelin, J. G. Muga and A. Ruschhaupt.

The two examples on their own are, also from an experimental point of view, already interesting and important, but the method’s application range much further. This is illustrated by subsequent publications, for example [88]-[96], which include applications of this method to cooling Bose-Einstein condensates in harmonic traps, the transport of non-interacting atoms, adiabatic passage in two- and three-level atoms, or using it as a toolbox for low-dimensional Bose-Einstein condensates. The success of this method was also already demonstrated in different experiments [97]-[99].

5.2 Inverse-Invariant Method

In this section we will give a general description of what we will call the “inverse-invariant” or “inverse-engineering” method, with which we achieve a shortcut to adiabaticity. We start by giving a short summary of the underlying idea, which will be explained in more detail afterwards.

¹ There exists other methods which overcome certain drawbacks of the adiabatic evolution. A comparison with these was made by other authors and shows the advantages of the inverse-invariant method. A brief discussion of these results can be found in the summary of this chapter.

We consider atoms initially in a certain state that we want to transfer to some desired final state. This transfer will be described by an explicitly time-dependent Hamiltonian $H(t)$, where the initial state is an eigenstate of this Hamiltonian at time $t = 0$ and the final state an eigenstate at time $t = t_f$. According to the adiabatic theorem this can be achieved via a sufficiently slow evolution, where the state is then an instantaneous eigenstate of $H(t)$ for all times. However, the requirement to remain in the same eigenstate for all times is not necessary in most cases, since one is often only interested in the populations at initial and final times. We will therefore design a method with which we obtain, up to a global phase, the instantaneous eigenstate of the Hamiltonian at the final time t_f , but during the process the state can deviate from the corresponding instantaneous eigenstates. We will achieve this by considering dynamical invariants of the Hamiltonian and choose suitable boundary conditions such that their initial and final eigenstates match those of the Hamiltonian. We then design a trajectory¹ for some auxiliary variable satisfying these boundary conditions, such that during the process the state evolves along the “invariants-basis”. This leads to a fast and perfect transfer, i.e. with fidelity one, between the final eigenstate of the invariant and the eigenstate of the Hamiltonian obtained by an adiabatic process. Therefore we achieve an adiabatic-like transfer in finite time, i.e. a “shortcut to adiabaticity”. For the theory of dynamical invariants of the Hamiltonian in the linear case, which we will discuss in the following, see [71, 107, 108, 109, 110]. Afterwards we will connect and partially extend these results to the Gross-Pitaevskii equation (GPE) and present our protocol using these invariants to achieve the shortcut to adiabaticity.

5.2.1 Invariants of the Hamiltonian

We briefly introduce the concept of invariants of the Hamiltonian for the SE, which we will need in Section 5.3 to apply our proposed “inverse-invariant method” to cooling of non-interacting atoms via trap expansion. Afterwards we will then apply this idea to the GPE [100]-[105], where the linear part, i.e. the corresponding SE, will admit the previously discussed invariants. We will need this in Section 5.4 where we will show a “shortcut to adiabaticity” for the transport of a BEC.

In general we consider the equation

$$i\hbar \frac{\partial}{\partial t} |\Psi\rangle = H(t) |\Psi\rangle, \quad (5.7)$$

where the explicitly time-dependent Hamiltonian $H(t)$ shall for now be linear, such that eq. (5.7) is the ordinary SE. Later we will extend the treatment by including a non-linearity, i.e. eq. (5.7) will be a GPE.

We consider dynamical invariants $I(t)$ of $H(t)$, i.e. $I(t)$ commutes with $i\hbar \frac{\partial}{\partial t} - H(t)$ and therefore its total derivative with respect to time vanishes, which is clear from

¹ To be more precise, a whole family of possible trajectories, which leaves a degree of freedom one can exploit to optimize the results with respect to different optimality criteria as we will see below.

Heisenberg's equation of motion

$$\frac{d}{dt}I(t) = \frac{\partial}{\partial t}I(t) + \frac{1}{i\hbar}[I(t), H(t)] = 0. \quad (5.8)$$

This means that if $|\Psi\rangle$ is a solution of the time-dependent SE (5.7), then $I(t)|\Psi\rangle$ is a solution too. $I(t)$ is called an invariant, because the expectation value $\langle\Psi|I|\Psi\rangle$ is constant in time, that is

$$\begin{aligned} \frac{\partial}{\partial t}\langle\Psi|I|\Psi\rangle &= \left(\frac{\partial}{\partial t}\langle\Psi|\right)I(t)|\Psi\rangle + \langle\Psi|\left(\frac{\partial}{\partial t}I(t)\right)|\Psi\rangle + \langle\Psi|I(t)\left(\frac{\partial}{\partial t}|\Psi\rangle\right) \\ &= -\frac{1}{i\hbar}\langle\Psi|H(t)I(t)|\Psi\rangle + \langle\Psi|\left(\frac{\partial}{\partial t}I(t)\right)|\Psi\rangle + \frac{1}{i\hbar}\langle\Psi|I(t)H(t)|\Psi\rangle \\ &= \langle\Psi|\left(\frac{\partial}{\partial t}I(t)\right)|\Psi\rangle + \frac{1}{i\hbar}\langle\Psi|[I(t), H(t)]|\Psi\rangle = 0. \end{aligned} \quad (5.9)$$

An important property of these dynamical invariants is the connection between their eigenstates and those of the Hamiltonian $H(t)$. In [71] it was shown that for every eigenstate of an invariant there exists a time-dependent and, which is important, position-independent (i.e. a global) phase-transformation such that the eigenstate becomes a solution of the SE. Furthermore this phase, which we will call the Lewis-Riesenfeld phase, is determined by a simple first-order differential equation (see eq. (5.16) and corresponding explanations). In the following we will give the explicit form of these invariants and their corresponding transformations for the class of Hamiltonians for which we want to achieve a shortcut to adiabaticity.

Invariants for the Schrödinger Equation

We consider eq. (5.7) with an explicitly time-dependent Hamiltonian

$$H(t) = \frac{\vec{p}^2}{2m} + V(\vec{q}, t), \quad (5.10)$$

with dimension $D = 1, 2, 3$. In [107] it was shown¹ that such a Hamiltonian has an invariant which is quadratic in momentum \vec{p} if and only if the potential has the form

$$V(\vec{q}, t) = -\vec{F}(t) \cdot \vec{q} + \frac{1}{2}m\omega^2(t)|\vec{q}|^2 + \frac{1}{b^2}U\left(\frac{\vec{q} - \vec{\alpha}}{b}\right) + f(t) \quad (5.11)$$

where $f = f(t)$ is arbitrary and U is an arbitrary potential function of the argument $\vec{\sigma} \equiv (\vec{q} - \vec{\alpha})/b$. In addition $\omega(t)$, the force $\vec{F}(t)$, $\vec{\alpha} = \vec{\alpha}(t)$ and the scaling function $b = b(t)$ satisfy the auxiliary equations

$$\frac{\omega_0^2}{b^3} = \ddot{b} + \omega^2(t)b, \quad (5.12)$$

¹ Actually it was only shown for one dimension, but the generalization for $D = 2, 3$ presented here is straightforward.

which is an Ermakov equation where real solutions must be chosen to make $I(t)$ hermitian [106] and

$$\frac{\vec{F}(t)}{m} = \ddot{\vec{\alpha}} + \omega^2(t)\vec{\alpha}, \quad (5.13)$$

where ω_0 is a constant and as usual the dots represent time derivatives. The physical meaning of $\vec{\alpha}$ and b depends on the process type and will be clarified below. Eqs. (5.12) and (5.13) just follow as additional constraints in the construction of the most general SE admitting a quadratic invariant in momentum.

Up to a constant factor, the dynamical invariant for the Hamiltonian (5.10) with potential (5.11) is given by [107]

$$I(t) = \frac{1}{2m}[b(\vec{p} - m\dot{\vec{\alpha}}) - m\dot{b}(\vec{q} - \vec{\alpha})]^2 + \frac{1}{2}m\omega_0^2 \left(\frac{\vec{q} - \vec{\alpha}}{b}\right)^2 + U\left(\frac{\vec{q} - \vec{\alpha}}{b}\right). \quad (5.14)$$

This result is straightforwardly derived by assuming an arbitrary invariant quadratic in \vec{p} for the Hamiltonian (5.10) satisfying eq. (5.8). An arbitrary solution $\psi(\vec{q}, t)$ of the time-dependent SE can be written as a linear combination of the eigenvectors ψ_n of $I(t)$ [71],

$$\psi(\vec{q}, t) = \sum_n c_n e^{i\alpha_n(t)} \psi_n(\vec{q}, t), \quad \text{with} \quad I(t)\psi_n(\vec{q}, t) = \lambda_n \psi_n(\vec{q}, t), \quad (5.15)$$

with a time-dependent phase-transformation $e^{i\alpha_n(t)}$ and where the amplitudes c_n and the eigenvalues λ_n are time-independent¹, so the c_n may be computed at $t = 0$. Here ψ_n is normalized to one, but continuum, delta-normalized states are also possible [71]. The Lewis-Riesenfeld phases $\alpha_n(t)$ satisfy [71, 108]

$$\hbar \frac{d}{dt} \alpha_n(t) = \left\langle \psi_n \left| i\hbar \frac{\partial}{\partial t} - H \right| \psi_n \right\rangle. \quad (5.16)$$

It follows from the Lewis-Riesenfeld invariant theory [71] that a single mode solution of the SE with Hamiltonian (5.10) can be written as

$$\begin{aligned} & e^{i\alpha_n(t)} \psi_n(\vec{q}, t) \\ &= b^{-D/2} e^{\frac{im}{\hbar b} [b|\mathbf{q}|^2/2 + (\dot{\vec{\alpha}}b - \vec{\alpha}\dot{b}) \cdot \mathbf{q}]} e^{-\frac{i}{\hbar} \int_0^t dt' \left\{ \frac{m[|\dot{\vec{\alpha}}b - \vec{\alpha}\dot{b}|^2 - \omega_0^2 |\vec{\alpha}|^2/b^2]}{2b^2} + f \right\}} \phi_n(\vec{\sigma}, \tau), \end{aligned} \quad (5.17)$$

where we have introduced a scaled time $\tau = \int_0^t dt' b^{-2}$ and $\phi_n(\vec{\sigma}, \tau)$ satisfies a SE with time-independent Hamiltonian given by

$$i\hbar \frac{\partial}{\partial \tau} \phi_n(\vec{\sigma}, \tau) = \left[-\frac{\hbar^2}{2m} \nabla_{\vec{\sigma}}^2 + \frac{m\omega_0^2}{2} |\vec{\sigma}|^2 + U(\vec{\sigma}) \right] \phi_n(\vec{\sigma}, \tau). \quad (5.18)$$

Note that eq. (5.18) is very general and applicable to compressions, expansions, or transport for harmonic or anharmonic potentials. As an example in Section 5.3 we will

¹ The time-independence of the invariant's eigenvalues λ_n is crucial and a non-trivial result.

therefore apply the inverse-invariant method to the problem of cooling non-interacting atoms via expansion of a harmonic trap.

Connection to the Gross-Pitaevskii Equation

We now proceed by considering the more general case of a GPE for potentials whose Schrödinger dynamics admit a quadratic invariant in momentum, which is given by [94, 107, 109, 111, 112]

$$\begin{aligned} i\hbar \frac{\partial \psi(\vec{q}, t)}{\partial t} &= \left[-\frac{\hbar^2}{2m} \nabla_{\mathbf{q}}^2 - \vec{F}(t) \cdot \vec{q} + \frac{1}{2} m \omega^2(t) |\vec{q}|^2 \right. \\ &\quad \left. + \frac{1}{b^2} U\left(\frac{\vec{q} - \vec{\alpha}}{b}\right) + g_D |\psi(\vec{q}, t)|^2 + f(t) \right] \psi(\vec{q}, t), \end{aligned} \quad (5.19)$$

i.e. its linear part ($g_D = 0$) is given by eq. (5.10) and eq. (5.11).

The results for the linear case can partially be generalized for the GPE, where the extent of the generalization depends on the process type as we will see below. We start by using eq. (5.17) as an ansatz for a time-dependent solution of eq. (5.19), where we restrict the following calculations to $D = 1$ and drop the index n to keep the notation clear. Setting

$$A := e^{\frac{im}{\hbar b} [bq^2/2 + (\dot{\alpha}b - \alpha\dot{b}) \cdot q]} e^{-\frac{i}{\hbar} \int_0^t dt' \left\{ \frac{m[|\dot{\alpha}b - \alpha\dot{b}|^2 - \omega_0^2 |\alpha|^2 / b^2]}{2b^2} + f \right\}},$$

we have for the derivatives

$$\begin{aligned} \frac{d}{dt} \psi &= -\frac{\dot{b}}{2b^{3/2}} A \phi + \frac{1}{b^{1/2}} \left[-\frac{i}{\hbar} \left(\frac{m(\dot{\alpha}b - \alpha\dot{b})^2 - \omega_0^2 \alpha^2 / b^2}{2b^2} + f \right) \right. \\ &\quad \left. + \frac{im}{\hbar} \left(-\frac{q^2 \dot{b}^2}{2b^2} - \frac{q\dot{b}(b\dot{\alpha} - \alpha\dot{b})}{b^2} + \frac{q^2 \ddot{b}}{2b} + \frac{q(b\ddot{\alpha} - \alpha\ddot{b})}{b} \right) \right] A \phi \\ &\quad + \frac{1}{b^{1/2}} \left[\frac{1}{b^2} \frac{\partial}{\partial \tau} \phi + \left(-\frac{\dot{\alpha}}{b} - \frac{(q - \alpha)\dot{b}}{b^2} \right) \frac{\partial}{\partial \sigma} \phi \right] A \\ \frac{d^2}{dq^2} \psi &= \frac{1}{b^{1/2}} \left\{ \left[\frac{im\dot{b}}{\hbar b} - \frac{m^2}{\hbar^2} \left(\frac{q\dot{b}}{b} + \frac{b\dot{\alpha} - \alpha\dot{b}}{b} \right)^2 \right] A \phi \right. \\ &\quad \left. + \left[\frac{2im}{\hbar b} \left(\frac{q\dot{b}}{b} + \frac{b\dot{\alpha} - \alpha\dot{b}}{b} \right) \right] A \frac{\partial}{\partial \sigma} \phi + \frac{1}{b^2} A \frac{\partial^2}{\partial \sigma^2} \phi \right\} \end{aligned}$$

and

$$|\psi|^2 = \frac{1}{b} |\phi|^2.$$

Inserting this in eq. (5.19) and cancelling terms appearing on both sides we obtain

$$\begin{aligned} & -\frac{m\omega_0^2}{b^{9/2}}\alpha^2\phi - \frac{m\ddot{b}}{2b^{3/2}}q^2\phi - \frac{m(b\ddot{\alpha} - \alpha\ddot{b})}{b^{3/2}}q\phi + i\hbar\frac{1}{b^{5/2}}\frac{\partial}{\partial\tau}\phi \\ = & -\frac{\hbar^2}{2m}\frac{1}{b^{5/2}}\frac{\partial^2}{\partial\sigma^2}\phi - \frac{F(t)}{b^{1/2}}q\phi + \frac{m\omega^2(t)}{2b^{1/2}}q^2\phi + \frac{1}{b^{5/2}}U(\sigma)\phi + \frac{g_1}{b^{3/2}}|\phi|^2\phi. \end{aligned}$$

Rearranging terms and sorting them with respect to powers of q we have

$$\begin{aligned} i\hbar\frac{\partial}{\partial\tau}\phi &= -\frac{\hbar^2}{2m}\frac{\partial^2}{\partial\sigma^2}\phi + U(\sigma)\phi + bg_1|\phi|^2\phi + m\left(\frac{\ddot{b}b}{2} + \frac{\omega^2(t)b^2}{2}\right)q^2\phi \\ &+ m\left(b(b\ddot{\alpha} - \alpha\ddot{b}) - \frac{F(t)}{m}b^2\right)q\phi + \frac{m\omega_0^2}{b^2}\alpha^2\phi. \end{aligned}$$

Now using eqs. (5.12) and (5.13) for the terms containing q and q^2 in a first step we obtain

$$\begin{aligned} i\hbar\frac{\partial}{\partial\tau}\phi &= -\frac{\hbar^2}{2m}\frac{\partial^2}{\partial\sigma^2}\phi + U(\sigma)\phi + bg_1|\phi|^2\phi + \frac{m\omega_0^2}{2b^2}q^2\phi \\ &+ mb^2\left(-\frac{\alpha\ddot{b}}{b} - \omega^2(t)\alpha\right)q\phi + \frac{m\omega_0^2}{b^2}\alpha^2\phi \end{aligned}$$

and applying eq. (5.12) a second time we have

$$i\hbar\frac{\partial}{\partial\tau}\phi = -\frac{\hbar^2}{2m}\frac{\partial^2}{\partial\sigma^2}\phi + U(\sigma)\phi + bg_1|\phi|^2\phi + \frac{m\omega_0^2}{2b^2}q^2\phi - \frac{m\omega_0^2}{b^2}\alpha q\phi + \frac{m\omega_0^2}{b^2}\alpha^2\phi.$$

Using $\sigma = \frac{q-\alpha}{b}$ this can be rewritten as

$$i\hbar\frac{\partial}{\partial\tau}\phi = -\frac{\hbar^2}{2m}\frac{\partial^2}{\partial\sigma^2}\phi + U(\sigma)\phi + bg_1|\phi|^2\phi + \frac{m\omega_0^2}{2}\sigma^2\phi + \frac{m\omega_0^2}{2b^2}\alpha^2\phi.$$

The term $\frac{m\omega_0^2}{2b^2}\alpha^2$ is not position dependent and can be neglected because it just corresponds to a shift of the energy origin. Therefore we finally have that $\phi = \phi_n(\sigma, \tau)$ has to solve the equation

$$i\hbar\frac{\partial}{\partial\tau}\phi_n(\sigma, \tau) = \left[-\frac{\hbar^2}{2m}\frac{\partial^2}{\partial\sigma^2} + \frac{m\omega_0^2}{2}\sigma^2 + U(\sigma) + bg_1|\phi_n(\sigma, \tau)|^2\right]\phi_n(\sigma, \tau). \quad (5.20)$$

An analogous calculation shows that in general for $D = 1, 2, 3$, $\phi_n(\vec{\sigma}, \tau)$ has to solve the equation

$$i\hbar\frac{\partial}{\partial\tau}\phi_n(\vec{\sigma}, \tau) = \left[-\frac{\hbar^2}{2m}\nabla_{\vec{\sigma}}^2 + \frac{m\omega_0^2}{2}|\vec{\sigma}|^2 + U(\vec{\sigma}) + b^{2-D}g_D|\phi_n(\vec{\sigma}, \tau)|^2\right]\phi_n(\vec{\sigma}, \tau). \quad (5.21)$$

As was discussed above, solving eq. (5.19) in the linear case ($g_D = 0$), that is the SE with potential (5.11), simplifies to a time-independent problem, since instead one can solve the now stationary equation (5.18). This solution can then be mapped via

eq. (5.17) to the time-dependent one. Unlike the linear case, for the GPE we cannot construct the general solution by linear superposition, so in this case we will restrict the treatment to a single mode, for example the ground state, and therefore we will drop the n subindex hereafter when dealing with the GPE. As in the linear case, eq. (5.21) is very general and also applicable to compressions, expansions, or transport for harmonic or anharmonic potentials. It is most useful when $b^{2-D}g_D$ does not depend on time, since then the time-dependent problem can again be mapped via eq. (5.17) to the solution of a much simpler stationary equation, as in the linear case. This happens in several physically relevant cases, in particular for expansions of BECs when $D = 2$, or by tuning g_D as a time-dependent coupling to cancel the time dependence of b^{2-D} [88]. Different time scalings combined with a Thomas-Fermi approximation also lead to a stationary equation [88]. Furthermore, as we will see in Section 5.4, in the case of the transport of a BEC in a rigid trap the problem always reduces to a stationary one independent of the dimension.

5.2.2 Inverse-Invariant Protocol

In the previous section we introduced the concept of dynamical invariants for the SE and partially generalized it to the GPE. This allows us to engineer eigenstates which are instantaneous eigenstates of the Hamiltonian at any given time. However, this method only provides the tools to obtain a shortcut to adiabaticity. How this concept can be used to achieve this goal remains to be explained. We now state the procedure in a general way before applying the method in Sections 5.3 and 5.4.

Protocol for the Inverse-Invariant Method

- Step 1: *Given a time-dependent Hamiltonian $H(t)$ construct the corresponding dynamical invariant $I(t)$ [71, 107].*
- Step 2: *Choose trajectories $b(t)$ and $\alpha(t)$, which obey the auxiliary eqs. (5.12) and (5.13), and boundary conditions for these trajectories, such that the eigenstates of $H(t)$ and $I(t)$ are, up to global phase, equal at initial and final time t_0 and t_f respectively. The latter can be ensured by using eq. (5.15) and corresponding ones.*
- Step 3: *Deduce the physical trajectories and forces from the auxiliary eqs. (5.12) and (5.13).*

This protocol coined the term “inverse-engineering” or “inverse-invariant” method, meaning that we inverse the procedure by first ensuring population preservation, but only at initial and final times, and then deducing the trajectories of the physical parameters. During the process the state evolves along the invariants basis and the populations are in general not preserved, thereby exploring a degree of freedom which is not given for the adiabatic evolution.

5.3 Applications: Cooling via Expansion of a Harmonic Trap

In this section we shall describe a “shortcut to adiabaticity” for cooling atoms trapped in a time-dependent harmonic oscillator via trap expansion, which applies both to equilibrium and non-equilibrium states. We achieve this goal by applying the inverse-invariant method introduced in the previous section. We shall for simplicity describe our method for states representing single atoms of mass m , but the same results are applicable to N -body non-interacting fermions or to a Tonks-Girardeau gas [113], and can be adapted to Bose-Einstein condensates in different dimensions [114].

After applying the protocol to this specific problem together with some general considerations, we will compare it with adiabatic following for a specific choice of the trajectory of the auxiliary variable, namely a polynomial. In order to give a first impression of the efficiency of the method, we will briefly state the result for this particular case, which will be presented in more detail below. In this exemplary case we consider the ground state and choose an initial trap frequency $\omega_0 = 250 \times 2\pi$ Hz as well as a final frequency $\omega_f = 2.5 \times 2\pi$. For the inverse-invariant method we consider expansion times down to $t_f = 2$ ms and obtain a perfect population preservation. In contrast, for the two trajectories we consider in the case of adiabatic following, namely a simple linear ramp, i.e. a linear in time change of the frequency from initial to final frequency, as well as an optimized trajectory given by a square-root in time, one needs $t_f = 6$ s and $t_f = 45$ ms respectively to achieve a relative error of 1% for the ground state energy.

5.3.1 General Considerations

Consider an effectively one-dimensional time-dependent harmonic oscillator,

$$H = \frac{\hat{p}^2}{2m} + \frac{m\omega^2(t)\hat{q}^2}{2}, \quad (5.22)$$

which has instantaneous eigenstates

$$u_n(t, x) = \left(\frac{m\omega(t)}{\pi\hbar} \right)^{1/4} \frac{1}{(2^n n!)^{1/2}} e^{-\frac{m}{2\hbar}\omega(t)x^2} \tilde{H}_n \left[\left(\frac{m\omega(t)}{\hbar} \right)^{1/2} x \right]. \quad (5.23)$$

We are interested in the situation with an initial angular frequency $\omega(0) > 0$ at time $t = 0$ and final frequency $0 < \omega_f = \omega(t_f) < \omega(0)$ at time t_f . When the Hamiltonian is constant we are used to thinking of temperature changes and “cooling” in terms of population changes. Note however that when the Hamiltonian changes with time the temperature may change even if the populations stay constant, because the eigenvalues change with time (see also eq. (5.6)). For a population preserving process involving canonical states $e^{-H/(kT)}/\text{tr} [e^{-H/(kT)}]$, the decrease in frequency may be considered as a “cooling” process since the initial and final partition functions are the same. Therefore

$$\frac{E_n(0)}{kT(0)} = \frac{E_n(t_f)}{kT(t_f)},$$

which, because of $E_n(t) = (n + 1/2)\hbar\omega(t)$, implies a temperature reduction

$$T(t_f) = T(0) \frac{\omega_f}{\omega(0)}. \quad (5.24)$$

Note that this process does not involve a phase-space compression, i.e. a process in which, in addition to a temperature decrease, there is phase-space compression¹.

The challenge is to find a trajectory $\omega(t)$ between these two frequency values so that the populations of the oscillator levels $n = 0, 1, 2, \dots$ at t_f are equal to the ones at $t = 0$. Our main tool to engineer $\omega(t)$ and the state dynamics will be the solution of the corresponding Schrödinger equation based on the invariants of motion we discussed in the previous section.

For the Hamiltonian (5.22) the invariant takes the form (see eq. (5.14)),

$$I(t) = \frac{1}{2} \left[\frac{1}{m} \hat{\pi}^2 + \frac{1}{b(t)^2} m \omega_0^2 \hat{q}^2 \right], \quad (5.25)$$

where $\hat{\pi} = b(t)\hat{p} - m\dot{b}(t)\hat{q}$ plays the role of a momentum conjugate to \hat{q}/b and the dots are as usual derivatives with respect to time. The scaling, dimensionless function $b = b(t)$ fulfills the auxiliary condition (5.12), i.e.

$$\ddot{b} + \omega^2(t)b = \frac{\omega_0^2}{b^3}. \quad (5.26)$$

and ω_0 is in principle an arbitrary constant, but it should be chosen to be real, because otherwise $I(t)$ is not hermitian. This constant is frequently rescaled to unity by a scale transformation of b [71]. Another convenient choice is $\omega_0 = \omega(0)$ as we shall see below. $I(t)$ also has the structure of a harmonic oscillator Hamiltonian (as long as $\omega_0^2 > 0$) with time-dependent eigenvectors $|n(t)\rangle$ and time-independent eigenvalues $(n + 1/2)\hbar\omega_0$. These are useful because the general solution of the Schrödinger equation $\psi(t, x)$ for the Hamiltonian (5.22) can be written as a superposition of orthonormal “expanding modes” (see Section 5.2)

$$\psi(t, x) = \sum_n c_n e^{i\alpha_n(t)} \langle x | n(t) \rangle = \sum_n c_n e^{i\alpha_n(t)} \psi_n(t, x). \quad (5.27)$$

The Lewis-Riesenfeld phases $\alpha_n(t)$ can be calculated via eq. (5.16) and we obtain $\alpha_n(t) = -(n + 1/2)\omega_0 \int_0^t dt' b^{-2}$. A complete single mode solution can be deduced from eq. (5.17) by solving the corresponding stationary equation (5.21). For $\omega_0^2 > 0$ we obtain

$$e^{i\alpha_n(t)} \psi_n(t, x) = \left(\frac{m\omega_0}{\pi\hbar} \right)^{1/4} \frac{e^{-i(n+1/2) \int_0^t dt' \frac{\omega_0}{b(t')^2}}}{(2^n n! b)^{1/2}} e^{i \frac{m}{2\hbar} \left(\frac{\dot{b}}{b(t)} + \frac{i\omega_0}{b^2} \right) x^2} \tilde{H}_n \left[\left(\frac{m\omega_0}{\hbar} \right)^{1/2} \frac{x}{b} \right], \quad (5.28)$$

where \tilde{H}_n are the Hermite polynomials.

¹ Such a process is sometimes called “brightening” or “true cooling” [48].

Average Energy and Moments

In the following we will derive the corresponding time-dependent average energy $\langle H(t) \rangle_n = \langle \psi_n | H(t) | \psi_n \rangle$. Using $\langle \psi_n | H(t) | \psi_n \rangle = i\hbar \langle \psi_n | \frac{\partial}{\partial t} | \psi_n \rangle$ and substituting $y = (m\omega_0/\hbar)^{1/2}x/b$ we obtain after a lengthy but elementary calculation

$$\begin{aligned} \langle H(t) \rangle_n = \frac{i\hbar}{\sqrt{\pi}2^n n!} \int dy \left[-\frac{\dot{b}}{2b} e^{-y^2} \tilde{H}_n^2(y) - i \left(n + \frac{1}{2} \right) \frac{\omega_0}{b^2} e^{-y^2} \tilde{H}_n^2(y) \right. \\ \left. + \frac{i}{2\omega_0} (\ddot{b}b - \dot{b}^2) y^2 e^{-y^2} \tilde{H}_n^2(y) + \frac{\dot{b}}{b} y^2 e^{-y^2} \tilde{H}_n^2(y) \right. \\ \left. - \frac{\dot{b}}{b} y e^{-y^2} \tilde{H}_n(y) \frac{\partial}{\partial y} \tilde{H}_n(y) \right]. \end{aligned} \quad (5.29)$$

Now, using orthogonality of the Hermite polynomials with respect to the weight function (or measure) e^{-y^2} [37], i.e.

$$\int dy \tilde{H}_m(y) \tilde{H}_n(y) e^{-y^2} = \sqrt{\pi} 2^n n! \delta_{nm}, \quad (5.30)$$

along with the recurrence relations

$$y \tilde{H}_n(y) = \frac{1}{2} \tilde{H}_{n+1}(y) + \frac{1}{2} \frac{\partial}{\partial y} \tilde{H}_n(y) \quad (5.31)$$

and

$$\frac{\partial}{\partial y} \tilde{H}_n(y) = 2n \tilde{H}_{n-1}(y) \quad (5.32)$$

we obtain for the integrals

$$\begin{aligned} \int dy \tilde{H}_n^2(y) e^{-y^2} &= \sqrt{\pi} 2^n n! \\ \int dy y^2 \tilde{H}_n^2(y) e^{-y^2} &= \sqrt{\pi} 2^n n! \left(n + \frac{1}{2} \right) \\ \int dy y \tilde{H}_n(y) \frac{\partial}{\partial y} \tilde{H}_n(y) e^{-y^2} &= \sqrt{\pi} 2^n n! n. \end{aligned} \quad (5.33)$$

Therefore eq. (5.29) reduces to

$$\begin{aligned} \langle H(t) \rangle_n &= i\hbar \left[-\frac{\dot{b}}{2b} - i \left(n + \frac{1}{2} \right) \frac{\omega_0}{b^2} + \frac{i}{2\omega_0} (\ddot{b}b - \dot{b}^2) \left(n + \frac{1}{2} \right) + \frac{\dot{b}}{b} \left(n + \frac{1}{2} \right) - \frac{\dot{b}}{b} n \right] \\ &= \hbar \left(n + \frac{1}{2} \right) \left(\frac{\omega_0}{b^2} - \frac{1}{2\omega_0} (\ddot{b}b - \dot{b}^2) \right). \end{aligned} \quad (5.34)$$

Using eq. (5.26) to replace \ddot{b} we finally obtain

$$\langle H(t) \rangle_n = \langle \psi_n | H(t) | \psi_n \rangle = \frac{(2n+1)\hbar}{4\omega_0} \left(\dot{b}^2 + \omega^2(t)b^2 + \frac{\omega_0^2}{b^2} \right). \quad (5.35)$$

Applying similar relations for the Hermite polynomials it is also straightforward to calculate the first and second position moments. The average position of an expanding mode is zero since applying the same substitution $y = (m\omega_0/\hbar)^{1/2}x/b$ as before one finds

$$\langle \psi_n | x | \psi_n \rangle = \int dx x |\psi_n|^2 \sim \int dy y \tilde{H}_n^2(y) e^{-y^2} = 0, \quad (5.36)$$

where the last step follows from eqs. (5.30) and (5.31). The second moment is of interest because it gives physical meaning to the scaling b . For the standard deviation we have

$$\begin{aligned} \sigma &= (\langle \psi_n | x^2 | \psi_n \rangle)^{1/2} = \left(\int dx x^2 |\psi_n|^2 \right)^{1/2} \\ &= \left(\frac{1}{\sqrt{\pi} 2^n n!} \frac{\hbar}{m\omega_0} b^2 \int dy y^2 \tilde{H}_n^2(y) e^{-y^2} \right)^{1/2}. \end{aligned} \quad (5.37)$$

Now using eq. (5.33) we obtain

$$\sigma = \left(\frac{(n+1/2)\hbar}{m\omega_0} \right)^{1/2} b, \quad (5.38)$$

i.e. the standard deviation is proportional to b . Therefore the scaling factor provides a measure of the state width along its evolution.

Direct Approach

We now come back to the design of the frequency $\omega(t)$ leading from some initial trap with frequency $\omega(0)$ to the desired final one with $\omega(t_f)$, and briefly review the common direct approach, i.e. designing the physical frequency $\omega(t)$ first.

A well studied case corresponds to the frequency scaling

$$\omega(t) = \frac{\omega(0)}{b^2} \quad (5.39)$$

with $b = (At^2 + 2Bt + C)^{1/2}$ [39, 115, 116], which includes a square-root in time scaling and leads to $\omega_0^2 = \omega(0)^2 + AC - B^2$ when substituted in eq. (5.26). Additionally the results in Chapter 3 and 4 motivated further investigation whether the square-root in time scaling might also be optimal for cooling with a harmonic trap, which was one starting point of the research finally leading to the “inverse-invariant method”.

For a hard wall trap, this scaling factor b ($A = 0$) has been shown to provide fast and efficient cooling [1, 42]. However, for harmonic traps, such time dependence leads to negative values of ω_0^2 even for modest cooling objectives. Note that, using eq. (5.39) at $t = 0$ and t_f with $A = 0$, it follows that

$$C = 1 \quad \text{and} \quad B = \frac{\omega(0) - \omega_f}{2t_f\omega_f}. \quad (5.40)$$

Thus ω_0^2 becomes negative easily by decreasing t_f and therefore $I(t)$ is not hermitian. This is cumbersome because the reference or auxiliary system provided by the invariant is not a harmonic oscillator with discretized levels but a harmonic repeller, so eq. (5.28)

becomes invalid. Moreover, instead of eq. (5.27), linear combinations of a continuum of non-square-integrable expanding modes would be needed to describe the evolution of any single eigenstate of the initial trap. However, this is of course only a drawback when calculating the dynamics using the invariant, and does not hinder the realization of the expansion in the laboratory. In fact for a negative ω_0^2 it is more convenient to use the adiabatic basis [117]. The numerical results show that, even though the square-root in time scaling is singularly efficient for adiabatic following, the cooling performance fails for very short expansion times t_f , as we will discuss below.

5.3.2 Inverse Engineering of Trajectories

Instead of the briefly discussed direct approach we now apply the inverse-invariant method to the procedure of cooling via trap expansion. We set $\omega_0 = \omega(0)$ (this will be the case hereafter), leaving $\omega(t)$ undetermined at first and imposing boundary conditions (BC) on $b(t)$ and its derivatives at $t = 0$ and t_f , to ensure:

(a) *that any eigenstate of $H(0)$ evolves as a single expanding mode.*

(b) *this expanding mode becomes, up to a position-independent phase factor, equal to the corresponding eigenstate of the Hamiltonian $H(t_f)$ of the final trap.*

In this way the populations in the instantaneous basis will be equal at initial and final times. The scaling $b(t)$ may be chosen as a real function satisfying the BC, for example a polynomial or some other convenient functional form with enough free parameters. One can explore this degree of freedom in the choice of the trajectory to find optimal trajectories for various constraints of interest, see also Section 5.5. After $b(t)$ has been engineered, the physical frequency $\omega(t)$ is given by eq. (5.26). The BC are determined in the following.

Boundary conditions for $t = 0$

We choose $b(0)$ and $\dot{b}(0)$ in such a way that $H(0)$ and $I(0)$ commute and have common eigenfunctions. Since $\omega_0 = \omega(0)$, this choice then also determines $\ddot{b}(0)$. This is guaranteed by the following BC, which can be easily checked by direct substitution in eq. (5.28) and comparison to the instantaneous eigenstates of the Hamiltonian given by eq. (5.23).

The initial boundary conditions are given by $b(0) = 1$, $\dot{b}(0) = 0$ and $\ddot{b}(0) = 0$.

These imply that any initial eigenstate of $H(0)$, which we call $u_n(0)$, will evolve according to the expanding mode (5.28) for all later times. In general $H(t)$ and $I(t)$ will not commute for $t > 0$, so that the expanding mode $\psi_n(t)$ may have more than one component in the ‘‘adiabatic basis’’ of instantaneous eigenstates of $H(t)$, $\{u_n(t)\}$, $n = 0, 1, 2, \dots$, where the $\{u_n(t)\}$ are given by eq. (5.23). Note that this is a consequence of the relaxed constraint that we only want to ensure that the initial and final states of $I(t)$ and $H(t)$ are the same, but not necessarily at any time during the process.

Boundary conditions for $t = t_f$

At time t_f we want $\psi_n(t_f)$ to be proportional, up to the global phase factor $e^{i\alpha_n(t_f)}$, to the corresponding eigenstate of the final trap $u_n(t_f)$. The BC which guarantee this can be derived in a straightforward way by matching eq. (5.28) with eq. (5.23) at time t_f . These BC then imply that the fidelity F , i.e. the overlap, between the final state of the invariant and the eigenstate of the Hamiltonian obtained after a perfect adiabatic process is one. To be more precise we have

Choosing the boundary conditions $b(t_f) = \gamma = (\omega_0/\omega_f)^{1/2}$, $\dot{b}(t_f) = 0$ and $\ddot{b}(t_f) = 0$, the final state $|\psi_{n,t_f}\rangle$ of the invariant is, up to a global phase, equal to the eigenstate $|u_{n,t_f}\rangle$ of the Hamiltonian obtained by a perfectly adiabatic process. For the fidelity F between these states we therefore have

$$F = |\langle \psi_{n,t_f} | u_{n,t_f} \rangle| = 1, \quad (5.41)$$

that is we obtain a perfect population preservation.

Average Energies of the Inverse-Invariant Process

It can be shown that these boundary conditions minimize the average energy. From eq. (5.35), one finds $\langle H(t_f) \rangle_n$ in terms of $b_f = b(t_f)$ and $\dot{b}_f = db(t)/dt|_{t=t_f}$,

$$\langle H(t_f) \rangle_n = \frac{(2n+1)\hbar}{4\omega_0} \left(\dot{b}_f^2 + \omega_f^2 b_f^2 + \frac{\omega_0^2}{b_f^2} \right). \quad (5.42)$$

Since b_f and \dot{b}_f can be set independently we can minimize the terms depending on them separately,

$$\frac{\partial \langle H(t_f) \rangle_n}{\partial \dot{b}_f} = \frac{(2n+1)\hbar}{2\omega_0} \dot{b}_f \stackrel{!}{=} 0, \quad (5.43)$$

$$\frac{\partial \langle H(t_f) \rangle_n}{\partial b_f} = \frac{(2n+1)\hbar}{4\omega_0} \left(2\omega_f^2 b_f - 2\frac{\omega_0^2}{b_f^3} \right) \stackrel{!}{=} 0. \quad (5.44)$$

These equations are satisfied for,

$$\dot{b}_f = 0, \quad (5.45)$$

$$\omega_f^2 = \frac{\omega_0^2}{b_f^4}. \quad (5.46)$$

Comparing eq. (5.46) with the Ermakov equation (5.26) at t_f , it follows that $\ddot{b}_f = 0$. In other words, the boundary conditions that we have imposed above correspond to the minimal possible average energy. Using $\ddot{b}_f = 0$, eqs. (5.46) and (5.45) in eq. (5.42), this turns out to be the adiabatic energy, i.e.

$$\langle H(t_f) \rangle_{n,\min} = \left(n + \frac{1}{2} \right) \hbar \omega_f. \quad (5.47)$$

Since this is true for all n this means that we cannot design any trajectory to achieve an average energy below the one provided by an adiabatic process. Any other choice of boundary conditions for b would necessarily produce excitations or “frictional heating”. It is interesting to compute the average energy as well for a density operator ρ that is stationary in the initial trap. This means that it is diagonal in the basis of the invariant,

$$\begin{aligned}\langle H(t) \rangle &= \text{tr}[\rho(t)H(t)] = \text{tr}\left[\sum_n p_n |\psi_n\rangle\langle\psi_n| H(t)\right] = \sum_n p_n \langle\psi_n| H(t) |\psi_n\rangle \\ &= \sum_n p_n \frac{(2n+1)\hbar}{4\omega_0} \left(\dot{b} + \omega^2(t)b^2 + \frac{\omega_0^2}{b^2} \right) = [2\langle n \rangle_{inv} + 1]E_0(t),\end{aligned}\quad (5.48)$$

where $E_0(t) = \hbar/(4\omega_0)(\dot{b} + \omega^2(t)b^2 + \omega_0^2/b^2)$ and $\langle n \rangle_{inv} = \sum_n n p_n$ is the average vibrational quantum number in the invariant basis. The latter does not change with time so it coincides with the initial average. Comparing this to the corresponding calculation in the adiabatic basis,

$$\begin{aligned}\langle H(t) \rangle &= \sum_n p_n^{ad}(t) \langle H(t) \rangle_n^{ad} = \sum_n p_n^{ad}(t) \left(n + \frac{1}{2} \right) \hbar\omega(t) = \left[\langle n(t) \rangle^{ad} + \frac{1}{2} \right] \hbar\omega(t) \\ &= [2\langle n(t) \rangle^{ad} + 1]E_0^{ad}(t),\end{aligned}\quad (5.49)$$

we may calculate the average excitation number in the adiabatic basis as a function of time,

$$2\langle n(t) \rangle^{ad} + 1 = \frac{\langle H(t) \rangle}{E_0^{ad}(t)} = \frac{2\langle H(t) \rangle}{\hbar\omega(t)} = [2\langle n \rangle_{inv} + 1] \frac{2E_0(t)}{\hbar\omega(t)}.\quad (5.50)$$

Example with a Polynomial Trajectory

We now proceed by giving an example of the efficiency of the inverse-invariant method by considering an explicit trajectory matching the BC given above, i.e. $b(0) = 1$, $\dot{b}(0) = 0$, $\ddot{b}(0) = 0$ and $b(t_f) = (\omega_0/\omega_f)^{1/2}$, $\dot{b}(t_f) = 0$, $\ddot{b}(t_f) = 0$. A simple choice is the polynomial ansatz $b(t) = \sum_{j=0}^5 a_j t^j$. The three initial and three final BC above give six equations that can be solved to provide the coefficients a_j and we obtain

$$b(t) = 6(b_f - 1)s^5 - 15(b_f - 1)s^4 + 10(b_f - 1)s^3 + 1,\quad (5.51)$$

where $b_f = b(t_f)$ as before and $s = t/t_f$. The universality of the solution indicates that there is no fundamental limitation on t_f as long as the potential is quadratic. We will investigate this question and the effect of noise later in this chapter. At initial and final times 0 and t_f , $\omega(t) = \omega_0/b^2(t)$, but, unlike in the treatment with square-root in time expansions, this relation does not hold in general for an arbitrary intermediate time. The above mentioned six conditions leave the time-dependent phases $e^{i\alpha_n(t)}$ undetermined, which are of no relevance regarding the population of the n th level. In particular stationary density operators with respect to $H(0)$ (e.g. a canonical state, or a pure state $|u_n(0)\rangle\langle u_n(0)|$) are mapped onto the corresponding stationary states of $H(t_f)$ with the phases canceled. In other cases the phases remain but the populations are preserved. Note that $e^{i\alpha_n(t)}$ is the phase factor that the initial state $u_n(0)$ would acquire in a virtual adiabatic process with adiabatic (instantaneous) energy $(n + 1/2)\hbar\omega_0/b^2$,

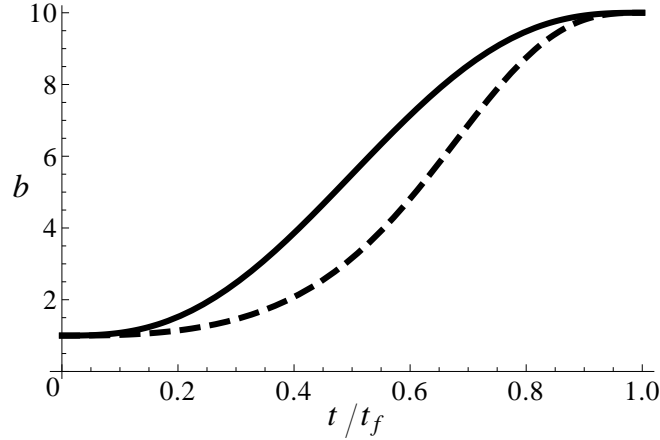


Figure 5.1: Examples of ansatz for b : A simple polynomial ansatz (solid line), and an exponential of a polynomial (dashed line, $\exp \sum_{j=0}^5 d_j t^j$), where we chose the parameters $\omega(0) = 250 \times 2\pi$ Hz, $\omega(t_f) = 2.5 \times 2\pi$ Hz, $\gamma = 10$.

see eq. (5.28). If desired, the trajectories may be designed to also control the phases by adding integral conditions, such as

$$\tau(t_f) = \int_0^{t_f} dt \frac{1}{b^2(t)} = \frac{\omega_f}{\omega_0} t', \quad (5.52)$$

where t' is some chosen time. This would require a more complicated ansatz for b , such as a polynomial of higher degree. Numerical examples of frequencies $\omega(t)$ and energies $\langle H(t) \rangle$ of several expansions that provide a shortcut to adiabaticity are given in Figs. 5.2 and 5.3, using the b shown in Fig. 5.1 for $\omega_0 = 250 \times 2\pi$ Hz and $\omega_f = 2.5 \times 2\pi$ Hz ($\gamma = 10$). These values are experimentally realisable [118]. We could formally study sub-hertz frequencies ω_f but they would render the trap very sensitive to low-frequency acoustic noise [119].

5.3.3 Comparison to Adiabatic Following

We will now compare the results obtained with the inverse-invariant method to those for adiabatic following. We start with the finite times considered in the examples above (from 2 to 25 ms) with the times $t_f^{(ad)}$ necessary for actual adiabatic following. To maintain adiabaticity during the expansion, the system should satisfy [42]

$$\left| \frac{\langle \tilde{n}(t) | \partial_t n(t) \rangle}{[E_{\tilde{n}}(t) - E_n(t)]/\hbar} \right| \ll 1, \quad (5.53)$$

where

$$\langle \tilde{n}(t) | \partial_t n(t) \rangle = \begin{cases} \frac{\dot{\omega}}{4\omega} \sqrt{n(n-1)} & \tilde{n} = n-2 \\ -\frac{\dot{\omega}}{4\omega} \sqrt{(n+1)(n+2)} & \tilde{n} = n+2 \\ 0 & \text{otherwise} \end{cases} .$$

For a linear ramp, $\omega(t) \rightarrow \omega_0 + (\omega_f - \omega_0)t/t_f$, the adiabaticity condition (5.53) for the harmonic oscillator becomes

$$\left| \frac{\sqrt{2}\dot{\omega}}{8\omega^2} \right| \ll 1. \quad (5.54)$$

This implies a very long time $t_f^{(ad)} \gg 1.1$ s for an initial frequency $\omega_0 = 250 \times 2\pi$ Hz, and final one $\omega_f = 2.5 \times 2\pi$ Hz. In practice 6 s are necessary to achieve a 1% relative error in the final energy of the ground state with the linear ramp. A much more efficient (still adiabatic) strategy is to distribute $\dot{\omega}/\omega^2$ uniformly along the trajectory, i.e., $\dot{\omega}/\omega^2 = c$, c being constant. Solving this differential equation and imposing $\omega_f = \omega(t_f)$ we have

$$\omega(t) = \frac{\omega_0}{\left[1 - \frac{(\omega_f - \omega_0)}{t_f \omega_f} t\right]}. \quad (5.55)$$

This corresponds to the case¹ $A = 0$, $2B = -(\omega_f - \omega_0)/(t_f \omega_f)$, $C = 1$, and implies $t_f^{(ad)} \gg 11$ ms for the given initial and final frequencies. With this optimized adiabatic trajectory a 1% error level for the ground state energy is achieved after 45 ms.

Let us now return to the fast-track trajectories designed with the invariant method. A prominent feature, see Fig. 5.2b, is that $\omega^2(t)$ may be negative during some time interval in which the potential becomes an expulsive parabola [120]. In general the (imaginary) frequency of the repulsive region increases for shorter cooling times as shown in Fig. 5.2b. For the regular Ermakov equation (5.26), a simple estimate for the polynomial ansatz is that the imaginary frequencies occur if $t_f < 1/(2\omega_f)$, the critical time is $t_c \approx 30$ ms for the final frequency of the examples. Note that this is different from the negativity of ω_0^2 commented above. Now ω_0^2 remains positive by construction and the invariant $I(t)$ hermitian. The transient energies may be below the final one, but they are a consequence of the repulsive regime and should not be interpreted as useful cooling in a time shorter than t_f . Since the “trap” is actually a repeller the kinetic energy would grow unboundedly if the potential were kept frozen at the time when the energy is minimal. Similarly, if the potential were suddenly changed into its final form, $V(t_f)$, the total energy would be higher than the adiabatic energy, i.e., the one for a population-preserving process. However, it is important to note that although during the process the potential occasionally becomes a repeller, the atoms always remain confined, since the second moment is bounded, see eq. (5.38) and also Fig. 5.4.

5.3.4 Remarks and Experimental Implementation

The shortcut to adiabaticity for the expansion of harmonic traps using invariants applies to arbitrary initial states, i.e. superpositions or mixed. Fig. 5.3 illustrates that the same $\omega(t)$ trajectories used before for the ground state also work for excited states. We propose an experimental realization based on a time-dependent far-off resonance optical dipole trap (red detuned) and an antitrap (blue detuned), which are not sensitive to the detailed internal states and in particular to Zeeman sublevels, if sufficiently detuned

¹ This means a square-root in time scaling factor, which shows its efficiency for adiabatic following.

from the atomic line resonance. This effective interaction can be made time dependent by varying the laser intensity, the frequency, or both [73], since the optical frequencies are many orders of magnitude larger than Rabi frequencies or detunings, and the changes will be slowly varying in the scale of optical periods. The intensity of a dipole trap can be changed by three or four orders of magnitude in 100 ns using acousto-optics or electro-optics modulators. We have so far considered the 1D case. Formally, the three coordinates in an ideal harmonic trap are uncoupled so the expansion processes can be treated independently. However, in practice changing the intensity of a laser beam affects simultaneously the longitudinal and transversal frequencies. To avoid this problem, the available degrees of freedom, namely the laser intensities and waists [121], may be used to satisfy the desired frequency trajectory in one coordinate, say longitudinal, while keeping the other frequency constant. It is also possible to leave the waists constant and add more lasers to compensate for the transversal frequency change. The problem was recently addressed in [122].

5.3.5 The Effect of Noise

In real experiments perfectly harmonic potentials cannot be designed, instead the potential is typically a Gaussian. The results above, e.g. the perfect fidelity, are a consequence of the harmonicity, because the most general potential admitting an invariant quadratic in momentum is of that form, see eq. (5.11). Therefore one cannot expect such properties to also hold when taking anharmonicities into account. What is important though is how crucial the harmonic shape is, i.e. how robust the proposed scheme is with respect to noise. If the efficiency would decrease drastically the scheme would not be useful for an actual application. Therefore in the above optical implementation of the potential we also have to take into account the anharmonicity and finite depth as they limit the possible excitation of the (initial and final) states.

A Gaussian potential $V_0(t)(1 - e^{-2x^2/w^2})$, induced by a laser with waist w , mimics the harmonic oscillator with frequency $\omega(t) = (2/w)\sqrt{V_0(t)/m}$ holding approximately $V_0(t)/(\hbar\omega)$ bound states. By making t_f smaller the anharmonicity effects become more important. We will examine these effects by using time-dependent perturbation theory and the polynomial ansatz in eq. (5.51) for b . There is a difference to the usual time-dependent problem treated with time-dependent perturbation theory, namely the Hamiltonian with known solutions is already time-dependent itself, but one can extend the treatment in a straightforward way (see Appendix C).

We consider the series expansion of the Gaussian potential up to second order to examine the effect of anharmonicity, i.e. we consider the potential

$$\begin{aligned} V(x,t) &= \underbrace{\left(\frac{2V_0(t)}{w^2}\right)}_{\frac{m\omega(t)^2}{2}}x^2 - \underbrace{\left(\frac{2V_0(t)}{w^4}\right)}_{\frac{m\omega(t)^2}{2w^2}}x^4 = \frac{m\omega(t)^2}{2}x^2 - \frac{1}{w^2}\frac{m\omega(t)^2}{2}x^4 \\ &= V_0(x,t) + V_1(x,t), \end{aligned} \tag{5.56}$$

where we set $V_0(x,t) := \frac{m\omega(t)^2}{2}x^2$ and $V_1(x,t) := -\frac{1}{w^2}\frac{m\omega(t)^2}{2}x^4$. The solution for the time-dependent harmonic oscillator, i.e. in the case that $V(x,t) = V_0(x,t)$, is known and given by eq. (5.28). The anharmonic term $V_1(x,t)$ will be treated as the perturbation. The quantity we are interested in is the fidelity F of the perturbed state, i.e. the overlap between the state of the perturbed Hamiltonian and the state of the time-dependent harmonic oscillator at time $t = t_f$, which is given by

$$F = |\langle \psi_s(t_f) | \tilde{\psi}_s(t_f) \rangle|. \quad (5.57)$$

$|\psi_s(t_f)\rangle$ is the exact solution for the harmonic oscillator and $|\tilde{\psi}_s(t_f)\rangle$ the solution for the perturbed Hamiltonian. The harmonic oscillator state at $t = t_f$ is, by construction with the inverse-invariant method, equal to the invariants state at time t_f up to a position-independent phase. We will now treat the problem perturbatively, using the formulas derived in the Appendix C for time-dependent perturbation theory with known solutions for an explicitly time-dependent part of the Hamiltonian. We assume that initially the states are the same, i.e. $\tilde{\psi}_s(t_0) = \psi_s(t_0)$, which is a good approximation especially for the lower eigenstates, and therefore, according to eq. (C.21) the zero-th order is given by $|\langle \psi_s(t_f) | U_0(t_f, t_0) \psi_s(t_0) \rangle|$. Since by construction the final states are the same, this overlap is one, i.e. $|\langle \psi_s(t_f) | U_0(t_f, t_0) \tilde{\psi}_s(t_0) \rangle| = 1$. The approximated fidelity F_a up to first order in $V_1(t)$ is then given by

$$F_a = |1 + F_{cor}| \geq 1 - |F_{cor}| \quad (5.58)$$

where we used the triangle inequality $|a + b| \geq ||a| - |b||$. The first order correction F_{cor} is, again according to eq. (C.21), given by

$$\begin{aligned} F_{cor} &= -\frac{i}{\hbar} \int_{t_0}^{t_f} dt' \langle \psi_s(t_f) | U_0(t_f, t') V_1(t') U_0(t', t_0) | \tilde{\psi}_s(t_0) \rangle \\ &= -\frac{i}{\hbar} \underbrace{\int_{t_0}^{t_f} dt' \langle \psi_s(t_f) | U_0(t_f, t') V_1(t') U_0(t', t_0) | \psi_s(t_0) \rangle}_{\text{I}} \end{aligned} \quad (5.59)$$

where we used again the assumption that initially the states are the same. According to eq. (5.58) we want to ensure that the absolute value of eq. (5.59) is small and determine how the waist w , the final frequency ω_f and the final time t_f have to be chosen with respect to each other to achieve this. We have

$$\begin{aligned} \text{I} &= \int_{t_0}^{t_f} dt' \underbrace{\langle \psi_s(t_f) | U_0(t_f, t')}_{\langle \psi_s(t') |} V_1(t') \underbrace{U_0(t', t_0) | \psi_s(t_0) \rangle}_{|\psi_s(t')\rangle} \\ &= -\frac{m}{2} \frac{1}{w^2} \int_{t_0}^{t_f} dt' \omega(t')^2 \langle \psi_s(t') | x^4 | \psi_s(t') \rangle. \end{aligned} \quad (5.60)$$

Using eq. (5.28) we obtain for the fourth moment

$$\langle \psi_s(t') | x^4 | \psi_s(t') \rangle = \left(\frac{m\omega_0}{\pi\hbar} \right)^{\frac{1}{2}} \int dx \frac{1}{2^n n! b} e^{-\frac{m\omega_0}{\hbar b^2} x^2} \tilde{H}_n \left[\left(\frac{m\omega_0}{\hbar} \right)^{\frac{1}{2}} \frac{x}{b} \right] x^4 \tilde{H}_n \left[\left(\frac{m\omega_0}{\hbar} \right)^{\frac{1}{2}} \frac{x}{b} \right].$$

Substituting $y = \left(\frac{m\omega_0}{\hbar}\right)^{\frac{1}{2}} \frac{x}{b}$ we have

$$\left(\frac{\hbar}{m\omega_0}\right)^2 \frac{1}{2^n n! \sqrt{\pi}} b^4 \int dy y^4 e^{-y^2} \mathbb{H}_n[y] \mathbb{H}_n[y]. \quad (5.61)$$

Using eqs. (5.30), (5.31) and (5.32) we obtain for the integral

$$\begin{aligned} \int dy y^4 e^{-y^2} \mathbb{H}_n[y] \mathbb{H}_n[y] &= \frac{1}{16} \int dy e^{-y^2} \mathbb{H}_{n+2}[y] \mathbb{H}_{n+2}[y] + n^2 \int dy e^{-y^2} \mathbb{H}_n[y] \mathbb{H}_n[y] \\ &+ n^4 \int dy e^{-y^2} \mathbb{H}_{n-2}[y] \mathbb{H}_{n-2}[y] \\ &= \frac{\sqrt{\pi}(n+2)(n+1)}{4} + n^2 + \frac{n^4}{4n(n-1)}. \end{aligned} \quad (5.62)$$

Performing some basic manipulations eq. (5.61) therefore reduces to

$$\left(\frac{\hbar}{m\omega_0}\right)^2 \frac{1}{2^n n! \sqrt{\pi}} b^4 \int dy y^4 e^{-y^2} \mathbb{H}_n[y] \mathbb{H}_n[y] = \left(\frac{\hbar}{m\omega_0}\right)^2 b^4 \frac{3}{4} [(n+1)^2 + n^2]. \quad (5.63)$$

Using this result in eq. (5.60) we therefore have

$$I = -\frac{m}{2} \frac{1}{w^2} \int_{t_0}^{t_f} dt' \omega(t')^2 \left(\frac{\hbar}{m\omega_0}\right)^2 b^4 \frac{3}{4} [(n+1)^2 + n^2].$$

According to eq. (5.58) we want to ensure that

$$\begin{aligned} &\left| \frac{\hbar}{2w^2\omega_0^2 m} \frac{3}{4} [(n+1)^2 + n^2] \int_{t_0}^{t_f} dt' \omega(t') b^4(t') \right| \ll 1 \\ \Leftrightarrow &\frac{\hbar}{2w^2\omega_0 m} \frac{3}{4} [(n+1)^2 + n^2] \left| \frac{1}{\omega_0} \int_{t_0}^{t_f} dt' \omega(t') b^4(t') \right| \ll 1. \end{aligned}$$

Using eq. (5.26) the integral can be rewritten such that

$$\frac{\hbar}{2w^2\omega_0 m} \frac{3}{4} [(n+1)^2 + n^2] \left| \frac{1}{\omega_0} \int_{t_0}^{t_f} dt' \left[\omega_0 - \frac{1}{\omega_0} b^3 \ddot{b} \right] \right| \ll 1. \quad (5.64)$$

Using for $b(t)$ the polynomial ansatz (5.51) and assuming $w_f \ll \omega_0$ we can approximate the integral by $\omega_0^2/(t_f \omega_f^2)$ and therefore it follows that

$$w^2 \gg \frac{3\hbar[(n+1)^2 + n^2]}{8mt_f \omega_f^2} \quad (5.65)$$

for a high fidelity of the vibrational state n . For the shortest time considered so far in the examples, $t_f = 2$ ms, and solving numerically the time-dependent Schrödinger equation with the mass of Rb-87, the fidelity for the ground state is 0.91 with $w = 50 \mu\text{m}$, and 0.99 with $w = 150 \mu\text{m}$. They decrease to 0.84 and 0.98 for $t_f = 1$ ms. Furthermore, in Fig. 5.4 an example for a fast optimal frictionless atom cooling is shown. Fig. 5.4(a) displays $b(t)$ and the resulting $\omega^2(t)$ leading to an optimal cooling in exact harmonic traps and Fig. 5.4(b) presents snapshots of the corresponding time evolution of the wave

function (dotted lines). In addition, the time evolution is presented if the harmonic potential is approximated by a Gaussian (solid lines). The final wave functions are nearly indistinguishable in the two cases. The fidelity between the final state for an exact harmonic potential and for a Gaussian is $F = 0.91$ in this case. We therefore conclude that the inverse-invariant method applied to cooling via expansion of a harmonic trap is also robust with respect to anharmonicities in the potential shape.

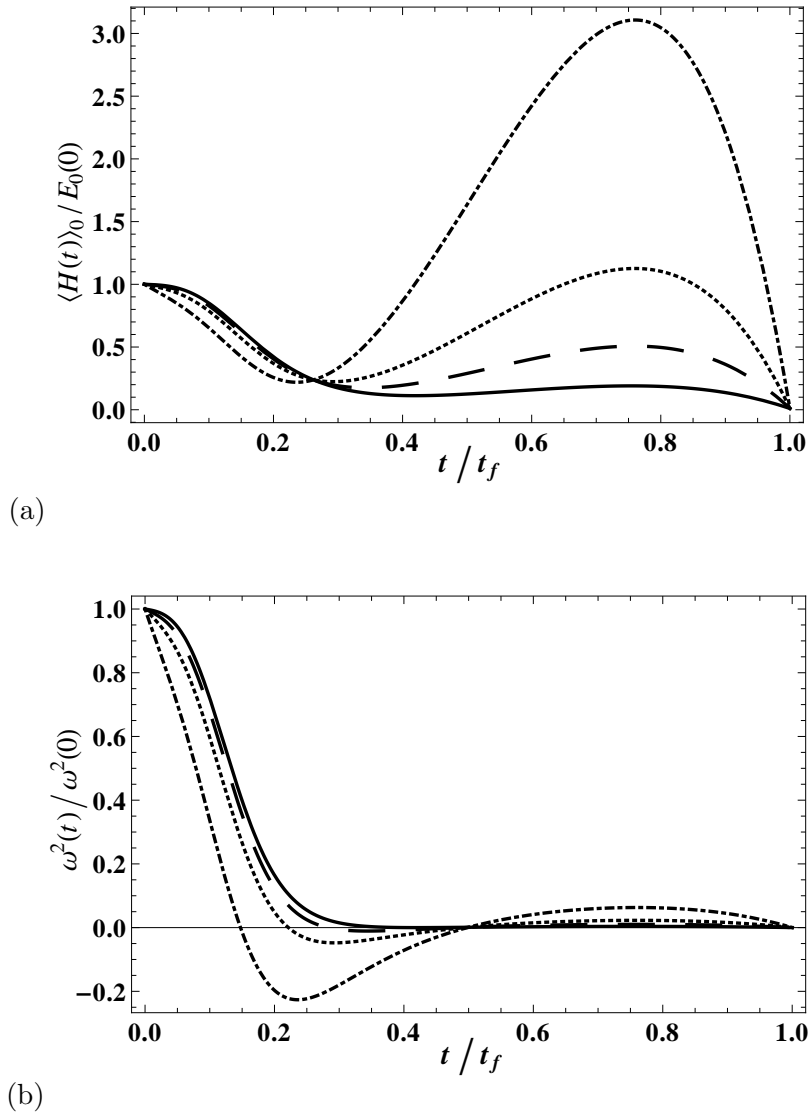


Figure 5.2: (a) The average energies of the ground state expanding mode for different final times t_f : $t_f = 25$ ms (solid), $t_f = 15$ ms (dashed), $t_f = 10$ ms (dotted), and $t_f = 6$ ms (dash-dotted). Other parameters are as in Fig. 5.1 (polynomial b) (b) The corresponding squared frequency $\omega^2(t)$.

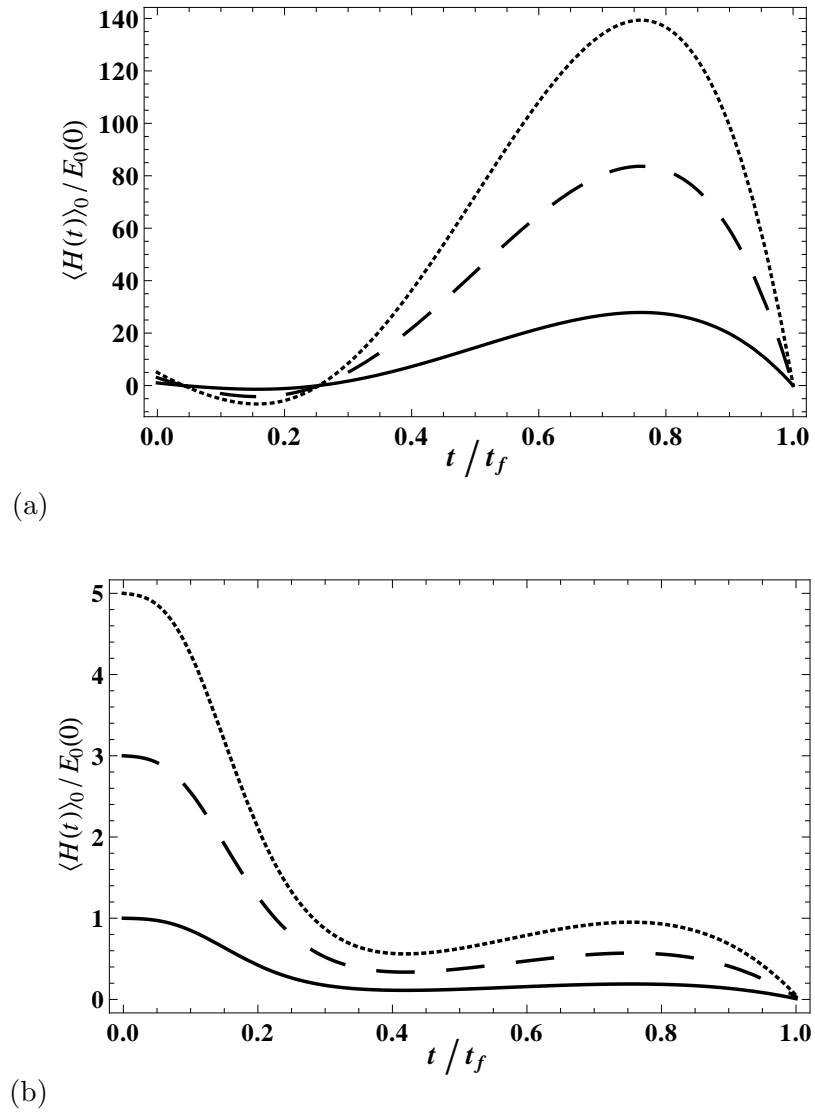
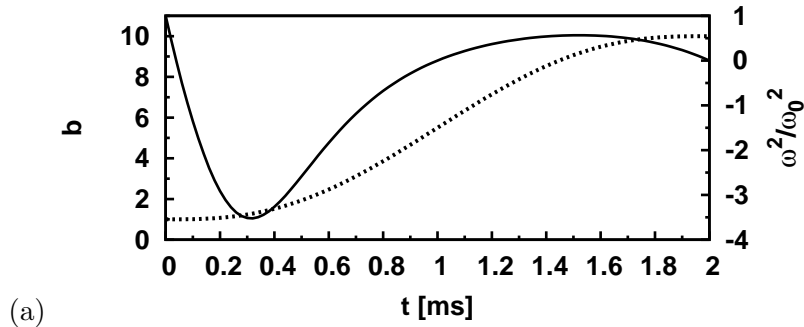
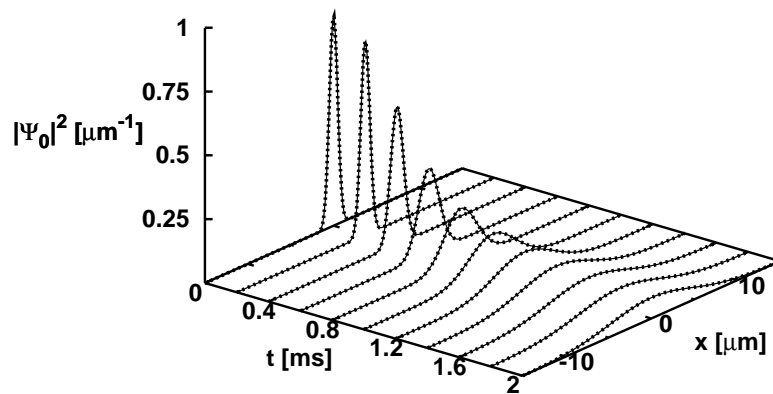


Figure 5.3: Average energies for expanding modes $n = 0$ (solid), $n = 1$ (dashed), and $n = 2$ (dotted). (a) $t_f = 2$ ms; (b) $t_f = 25$ ms. The other parameters are the same as in Fig. 5.1 (polynomial b).



(a)



(b)

Figure 5.4: Example of fast optimal frictionless atom cooling: $\omega_0 = 250 \times 2\pi$ Hz, $\omega_f = 2.5 \times 2\pi$ Hz, mass of Rb-87, and $t_f = 2$ ms. (a) $b(t)$ (dotted line, left axis) and $\omega^2(t)$ (solid line, right axis). (b) Time evolution of $|\psi_0(t,x)|^2$ with a harmonic potential $V(t,x) = \frac{m}{2}\omega^2(t)x^2$ (dotted line) and with a Gaussian potential $V(t,x) = \frac{mw^2}{4}\omega^2(t)\left(1 - \exp\left(-\frac{2x^2}{w^2}\right)\right)$ of width $w = 50 \mu\text{m}$ (solid line, indistinguishable from the dotted line); in both cases: the function $\omega^2(t)$ shown in (a) is used, the initial state at $t = 0$ is the ground state of the harmonic potential.

5.4 Applications: Transport of a Bose-Einstein Condensate

In Section 5.3 we applied the “inverse-invariant” method to cooling atoms via expansion of a harmonic trap and showed that it provides a “shortcut to adiabaticity”. However, as we already remarked, the proposed method is far from exhausted. The ability to manipulate Bose-Einstein condensates may be particularly rewarding, consider for example their potential in interferometric sensors, but it is also challenging, as their low temperatures make them more fragile than ordinary cold atoms. A basic operation is the transport of the condensate to appropriate locations such as a “science chamber”, or to launch or stop the atomic cloud. This transport has been performed with several techniques based on adiabatic, slow motion to avoid excitations and losses [123]-[126]. Long transport times, however, may be counterproductive since the condensate is more exposed to noise and decoherence, and also severely limit the repetition rates and signal to noise ratios. Fast, non-adiabatic but “faithful” transport of cold atoms, i.e., leading to the desired final state, has also been investigated experimentally [127] and theoretically [94, 128, 129]. For the Schrödinger equation the presented “inverse-invariant” method based on constructing Lewis-Riesenfeld invariants and corresponding dynamical modes (solutions of the SE formed by invariant eigenvectors times a phase factor) provides a “shortcut to adiabaticity” [2, 97], see Sections 5.2 and 5.3.

Nonetheless, as we have seen in Section 5.2, the invariant concept is not directly applicable to the non-linear Gross-Pitaevskii equation. In fact previous extensions of this inverse technique to expansions of condensates required special regimes or time-dependent Feshbach resonance control [88, 93, 98, 99].

In this section we will apply the “inverse-invariant” method to accelerate the adiabatic transport of a Bose-Einstein condensate without final excitation. We will see that this is generally possible in one, two or three dimensions without considering special regimes. This will be illustrated with a numerical example and compared with a direct (as opposed to “inverse”) approach. Furthermore, we will study the effect of anharmonicities in the potential and the effect of noise on the transport process. Finally, in the next section we shall optimize the trap trajectory according to several criteria, since the invariant-based inverse engineering provides a family of possible transport solutions.

In order to give a first impression of the efficiency of the method, we will again briefly state the result for the numerical example, which will be presented in more detail below. In this exemplary case we consider the ground state and choose a trap frequency $\omega_0 = 50 \times 2\pi$ Hz as well as a final distance $d = 1.6$ mm. In the inverse-invariant approach we consider transport times down to $t_f \approx 8$ ms and obtain by construction a perfect population preservation. In contrast, for the trajectory we consider in the direct approach, the smallest time which does not lead to excitations is $t_f = 30$ ms. However, in this case the transport is not adiabatic. Furthermore, this final time leading to no excitation is the minimal time in a discrete set, i.e. not only for smaller times, but generally a deviation from this final time necessarily leads to excitations. Therefore the result is not stable with respect to variations of the final time, whereas for the inverse-invariant method one obtains a perfect population preservation for all larger

final times too.

5.4.1 General Considerations

We are interested in the very important case of transport processes driven by a rigidly displaced harmonic potential, which means that the scaling $b(t)$ in eq. (5.19) is simply given by $b(t) = 1 \forall t$. For the scaled time we then have that $\tau = \int_0^t dt' b^{-2} = t$ (see e.g. eq. (5.17)), the frequency is time-independent and set to $\omega(t) = \omega_0$ ¹ and the coefficients in eq. (5.21) are time-independent. Furthermore, it is also useful to define $\phi(\vec{\sigma}, t) = e^{-i\mu t/\hbar} \chi(\vec{\sigma})$, where μ is the chemical potential and according to eq. (5.21) $\chi(\vec{\sigma})$ satisfies the **stationary GPE**

$$\left[-\frac{\hbar^2}{2m} \nabla_{\vec{\sigma}}^2 + \frac{m\omega_0^2}{2} |\vec{\sigma}|^2 + U(\vec{\sigma}) + g_D |\chi(\vec{\sigma})|^2 \right] \chi(\vec{\sigma}) = \mu \chi(\vec{\sigma}). \quad (5.66)$$

The physical solution of the time-dependent GPE for a single transport mode is

$$\psi(\vec{q}, t) = e^{\frac{i}{\hbar}(-\mu t + m\dot{\vec{q}}_c \cdot \vec{q}) - \frac{i}{\hbar} \int_0^t dt' \left[\frac{m}{2} (|\dot{\vec{q}}_c|^2 - \omega_0^2 |\vec{q}_c|^2) + f(t') \right]} \chi(\vec{\sigma}) \quad (5.67)$$

with $\vec{\sigma} = \vec{q} - \vec{q}_c$ and where we renamed $\vec{\alpha} \rightarrow \vec{q}_c$ for the transport because of its physical meaning clarified below, see eq. (5.17). Eq. (5.67) is of central importance, since it shows that this wave function is shape invariant and the only possible excitations associated with such a mode are center of mass oscillations with constant mean field energy. Since we are interested in the transport between an initial and final point, we restrict the analysis in the following to the one-dimensional transport scenario between these two points and omit the vector notation.

5.4.2 Inverse Engineering of Harmonic Transport

For a 1D, harmonic and horizontal transport of a condensate from 0 to d in a time t_f , with zero mean velocity at $t = 0$ and t_f , q_c (now a scalar function) must be chosen to match the transport mode (5.67) with the instantaneous eigenstates of the Hamiltonian, including the mean field term, at times $t = 0$ and $t = t_f$.

A concrete example will illustrate our method. Consider a ⁸⁷Rb BEC in the $F = 2$, $m_F = 2$ ground state formed of 3000 atoms [124]. The transport of BECs aided by microchips can use a “bucket chain” [130], or a single harmonic and frequency-stable bucket [131]. We assume here a single bucket with $\omega_0 = 2\pi \times 50$ Hz moved from $q_0(0) = 0$ at time $t = 0$ to $q_0(t_f) = d = 1.6$ mm at t_f . The time-dependent GPE for $\psi(q, t)$ is now

$$i\hbar \frac{\partial \psi}{\partial t}(q, t) = \left[-\frac{\hbar^2}{2m} \nabla_q^2 + \frac{m\omega_0^2}{2} (q - q_0)^2 + g_1 |\psi(q, t)|^2 \right] \psi(q, t), \quad (5.68)$$

¹ In accordance with the auxiliary eq. (5.12).

a particular case of eq. (5.19) with $\omega(t) = \omega_0$, $U = 0$, $F(t) = m\omega_0^2 q_0(t)$, $f(t) = m\omega_0^2 \dot{q}_0^2(t)/2$ and $b(t) = 1$. Therefore eq. (5.12) does not play any role and $q_c(t)$ has to satisfy

$$\ddot{q}_c(t) + \omega_0^2 [q_c(t) - q_0(t)] = 0, \quad (5.69)$$

the equation for a classical trajectory $q_c(t)$ in a moving harmonic potential¹. If we impose at $t = 0$ the initial conditions

$$q_c(0) = \dot{q}_c(0) = \ddot{q}_c(0) = 0, \quad (5.70)$$

the transport modes given by eq. (5.67) become equal to the instantaneous eigenstates of eq. (5.68) at $t = 0$. To solve eq. (5.68) we proceed in two different ways, namely using direct and inverse approaches.

Direct Approach

The first step of the direct approach is to fix the evolution of the center of the trap $q_0(t)$. In [124], for example, the evolution of $q_0(t)$ is determined by increasing $\dot{q}_0(t)$ linearly during a quarter of the transported distance $d/4$, then keeping it constant for $d/2$, and finally ramping $\dot{q}_0(t)$ back to zero during the last quarter, such that

$$q_0(t) = \begin{cases} \frac{v_m^2 t^2}{d}, & 0 < t < \frac{d}{2v_m} \\ v_m t - \frac{d}{4}, & \frac{d}{2v_m} < t < \frac{d}{v_m} \\ \frac{v_m}{2(d/v_m - t_f)}(t - t_f)^2 + d, & \frac{d}{v_m} < t < t_f \end{cases},$$

where $v_m = 3d/(2t_f)$ is the maximum trap velocity during the transport compatible with $q_0(t_f) = d$ in this scheme. Solving eq. (5.69) for the previous $q_0(t)$ with initial conditions $q_c(0) = \dot{q}_c(0) = 0$, and imposing continuity on $q_c(t)$ and $\dot{q}_c(t)$, we find

$$\begin{aligned} q_c(t_f) - q_0(t_f) &= 9d(1 - 2\cos\varphi)(\sin^2\varphi)/(\omega_0^2 t_f^2), \\ \dot{q}_c(t_f) - \dot{q}_0(t_f) &= \frac{9d}{2\omega_0 t_f^2}(\sin\varphi + \sin 2\varphi - \sin 3\varphi), \end{aligned} \quad (5.71)$$

where $\varphi = \omega_0 t_f/3$. The final state of the transported BEC is given by eqs. (5.67) and (5.71). In general some excitation is produced, except for the discrete set of final times $t_{f,N} = 3(2N + 1)\pi/\omega_0$, $N = 0, 1, 2, \dots$, for which

$$q_c(t_f) = d, \quad \dot{q}_c(t_f) = \ddot{q}_c(t_f) = 0, \quad (5.72)$$

and the transported state matches the eigenstate of the final Hamiltonian. The classically moving center of mass and the trap center stop at d , $\dot{q}_c(t_f) = 0$, $\dot{q}_0(t_f) = 0$, with zero (classical) energy $m\dot{q}_c(t_f)^2/2 + m\omega_0^2[d - q_c(t_f)]^2/2 = 0$. Using this direct approach, the minimal final time that does not produce an excitation is $t_{f,0} = 3\pi/\omega_0$ ($N = 0$), in our example $t_{f,0} = 30$ ms. For such short times the transport is not adiabatic.

¹ Note that for an abrupt shift of the trap one recovers the scaling for dipole oscillations [105].

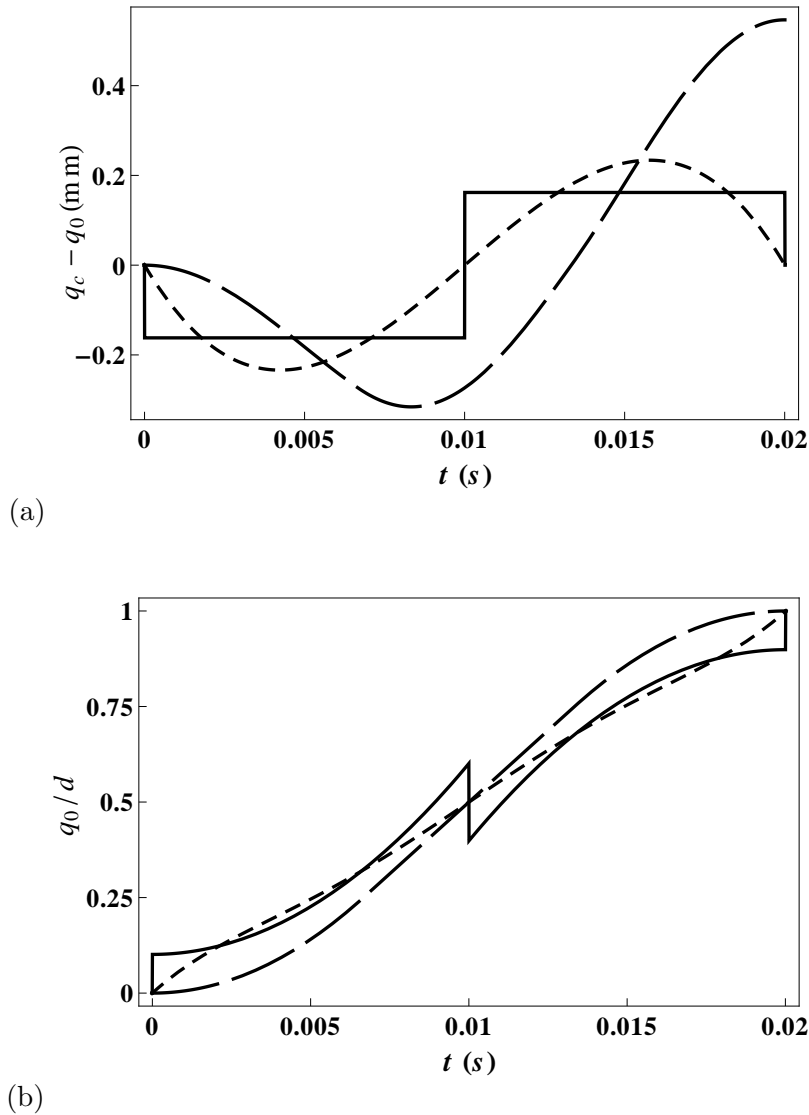


Figure 5.5: (a) Displacement $q_c - q_0$ versus time. Long dashed line: direct method, short dashed line: inverse method (polynomial). Solid line: inverse method + OCT. (b) Trap trajectories. Parameter values: $d = 1.6$ mm, $t_f = 20$ ms, $\delta \simeq 0.162$ mm, $\omega_0 = 2\pi \times 50$ Hz.

Inverse Approach

Due to the structure of the solution (5.67), we may apply a generalized inverse engineering method similar to the one for the linear case, see Sections 5.2 and 5.3 and [2, 88, 94]. The idea is again to design $q_c(t)$ first and deduce the transport protocol from it. We impose the conditions given by eqs. (5.70) and (5.72) at $t = 0$ and t_f , and interpolate q_c with a function, e.g. a polynomial with enough parameters to satisfy all these conditions. Then $q_0(t)$ is calculated via eq. (5.69). An example is shown in Fig. 5.5 where we have chosen $t_f = 20$ ms $< t_{f,0}$. By construction no final excitation is produced and, similarly

as for harmonic expansion (see Section 5.3), we therefore have

Choosing the boundary conditions $q_c(t_f) = d$ and $\dot{q}_c(t_f) = \ddot{q}_c(t_f) = 0$, the final state $|\psi_{t_f}\rangle$ of the invariant becomes, up to a global phase, equal to the eigenstate $|u_{t_f}\rangle$ of the Hamiltonian obtained by a perfectly adiabatic transport process. For the fidelity F between these states we therefore have

$$F = |\langle \psi_{t_f} | u_{t_f} \rangle| = 1, \quad (5.73)$$

that is we obtain a perfect population preservation.

Contrast this to the direct approach which, for $t_f = 20$ ms, produces more transient excitation and a final excited state with nearly zero fidelity.

In principle there is no lower limit to t_f with the inverse method, but in practice there are some limitations [94]. Smaller values of t_f increase the distance from the condensate to the trap center, see eq. (5.71), and the effect of anharmonicity. There could also be geometrical constraints: for short t_f , $q_0(t)$ could exceed the interval $[0, d]$. For the polynomial ansatz this happens [94] at $t_f = 2.505/\omega_0$, i.e. $t_f \approx 8$ ms for the parameters of the example. Optimal control theory (OCT) combined with the inverse method, see Section 5.5, provides a way to design trajectories taking these restrictions into account.

5.4.3 Anharmonic Transport

The inverse method can also be applied to anharmonic transport by means of a compensating force [94]. Let the anharmonic potential be $U(q)$ at time $t = 0$ and $U(q - d)$ at time t_f . The condensate starts in the ground state of the potential at time $t = 0$. We set $q_0(t) = q_c(t)$, $\omega(t) = \omega_0 = 0$, $f = 0$, and $F(t) = m\ddot{q}_0(t)$ in eq. (5.19), so the GPE for $\psi(q, t)$ becomes

$$i\hbar \frac{\partial \psi}{\partial t}(q, t) = \left[-\frac{\hbar^2}{2m} \nabla_q^2 - m\ddot{q}_0 q + U(q - q_c) + g_1 |\psi(q, t)|^2 \right] \psi(q, t),$$

and the auxiliary equations (5.12) and (5.13) are satisfied trivially. Here we impose

$$q_0(0) = 0, \quad \dot{q}_0(0) = 0, \quad q_0(t_f) = d, \quad \dot{q}_0(t_f) = 0.$$

Additionally we could impose $\ddot{q}_0(t) = 0$ at $t = 0$ and t_f . The function that must be interpolated is now $q_0(t)$ instead of $q_c(t)$, and again we may consider a polynomial. Note that the exact potential U could be unknown since $q_0(t)$ is independent of U . By implementing the compensating force $m\ddot{q}_0(t)$, we ensure that the condensate will be in the ground state of the moved trap at final time t_f .

As an example, let $t_f = 20$ ms and $d = 1.6$ mm. For the compensating acceleration we then obtain $\ddot{q}_0(t) \leq 23.1 \text{ m/s}^2$ for $0 \leq t \leq t_f$.

5.4.4 Effect of Perturbations

First we investigate the effect of anharmonicities when the harmonic transport protocol is applied. For a symmetrically perturbed potential

$$V = \frac{\omega_0^2 m}{2} \left[(q - q_0)^2 + \alpha (q - q_0)^4 \right], \quad (5.74)$$

the results can be seen in Fig. 5.6a. For small anharmonicity α we still attain a very high fidelity $\bar{F} = |\langle \psi_{\alpha=0}(t_f) | \psi_\alpha(t_f) \rangle|$. In general, the fidelity increases with increasing g_1 , as will be explained below. In a first step we derive an approximate solution of the time-dependent GPE with the potential given by eq. (5.74). Let us insert the ansatz

$$\tilde{\psi}(q,t) = \exp \left\{ \frac{i}{\hbar} \gamma [q - q_c(t) - \Delta(t), t] + \frac{im}{\hbar} \dot{\Delta}(t) q \right\} \psi [q - \Delta(t), t]$$

into the GPE (5.68) with the additional anharmonicity, where $\psi(q,t)$ is the solution with the harmonic potential, i.e. $\alpha = 0$, see eq. (5.67), and $\Delta(t)$ is some time-dependent shift. After a lengthy but elementary calculation we obtain

$$\begin{aligned} & \frac{\partial \gamma}{\partial t}(y,t) - i \frac{\hbar}{2m} \frac{\partial^2 \gamma}{\partial y^2}(y,t) + \frac{1}{2m} \left[\frac{\partial \gamma}{\partial y}(y,t) \right]^2 - \frac{i \hbar \frac{\partial \chi}{\partial y}(y)}{m \chi(y)} \frac{\partial \gamma}{\partial y}(y,t) \\ & + g_1 |\chi(y)|^2 \left[1 - e^{2\text{Im}\gamma(y,t)/\hbar} \right] - \tilde{\gamma}(t) \\ & = y \left[\left(\frac{6\alpha m \ddot{q}_c^2(t)}{\omega_0^2} + m \omega_0^2 \right) \Delta(t) - 6\alpha m \Delta^2(t) \ddot{q}_c(t) - \frac{2\alpha m \ddot{q}_c^3(t)}{\omega_0^4} \right. \\ & \left. + 2\alpha m \omega_0^2 \Delta^3(t) + m \ddot{\Delta}(t) \right] + \alpha y^2 [\dots] + \alpha y^3 [\dots] + \alpha y^4 [\dots] \end{aligned} \quad (5.75)$$

where we set $y := q - q_c(t) - \Delta(t) = \sigma - \Delta(t)$, $\tilde{\gamma}(t)$ is some function that depends only on time and $\chi(y) = \chi(\sigma - \Delta(t))$ is a solution of the stationary GPE (5.67). The position expectation value of $\chi(\sigma)$ is $\langle \sigma \rangle = 0$ and so the position expectation value of the unperturbed wavefunction $\psi(q,t)$ is $q_c(t)$, since

$$\int dq q |\psi(q,t)|^2 = \int dq q |\chi(\sigma)|^2 = \int d\sigma \sigma |\chi(\sigma)|^2 + q_c(t) \int d\sigma |\chi(\sigma)|^2 = q_c(t).$$

Let the position expectation value of the wavefunction with the perturbed potential be $q_c(t) + \Delta(t)$. We assume that the perturbed wavefunction is non-zero only for $q \approx q_c(t) + \Delta(t)$ and therefore we neglect contributions in the previous eq. (5.75) of the orders $\alpha y^2, \alpha y^3, \alpha y^4$. If $\Delta(t)$ is a solution of

$$\ddot{\Delta}(t) = -2\alpha \omega_0^2 \Delta^3(t) + 6\alpha \ddot{q}_c(t) \Delta^2(t) - \frac{\omega_0^4 + 6\alpha [\ddot{q}_c(t)]^2}{\omega_0^2} \Delta(t) + \frac{2\alpha [\ddot{q}_c(t)]^3}{\omega_0^4},$$

then the prefactor of y in eq. (5.75) is zero and the right hand side does not depend on y . Therefore $\gamma(t,y) = \int_0^y dt' \tilde{\gamma}(t') = \gamma(t)$ is an approximate solution of eq. (5.75). We

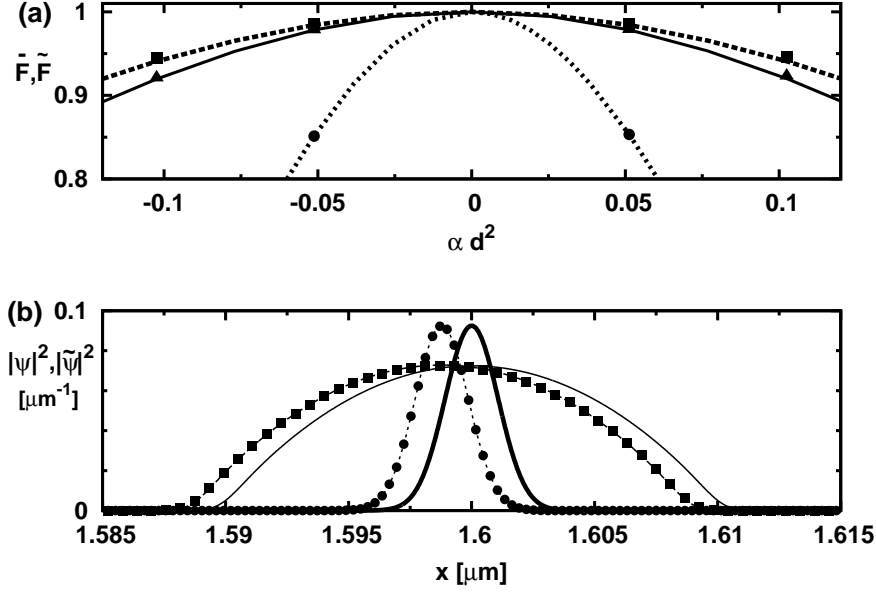


Figure 5.6: Effect of trap anharmonicity α on transport. (a) Exact fidelity \bar{F} (lines) and approximated fidelity \tilde{F} (symbols); $g_1 = 0$ (dotted lines and circles), $g_1/\hbar = 0.05$ m/s (solid lines and triangles), $g_1/\hbar = 0.1$ m/s (dashed lines and boxes). (b) Wave function at final time t_f ; $g_1 = 0, \alpha = 0$ (thick solid line, scaled by a factor of 4), $g_1 = 0, \alpha d^2 = 0.0512$ (exact result ψ : thin dashed line, approximation $\tilde{\psi}$: circles, scaled by a factor of 4), $g_1/\hbar = 0.1$ m/s, $\alpha = 0$ (thin solid line), $g_1/\hbar = 0.1$ m/s, $\alpha d^2 = 0.0512$ (exact result ψ : dashed line, indistinguishable in the scale of the figure from the approximation $\tilde{\psi}$: boxes); $d = 1.6$ mm, $t_f = 20$ ms, $\omega_0 = 2\pi \times 50$ Hz.

therefore have the approximate wavefunction for the perturbed potential

$$\tilde{\psi}(t, q) = \exp \left[\frac{i}{\hbar} \gamma(t) + \frac{im}{\hbar} \dot{\Delta}(t) q \right] \psi [t, q - \Delta(t)] .$$

The approximate perturbed wavefunction should coincide with the unperturbed initial wavefunction at $t = 0$. Therefore we demand the boundary conditions $\Delta(0) = 0, \dot{\Delta}(0) = 0$. Consequently the effect of the anharmonicity at final time t_f is approximately only a shift $d_{error} = \Delta(t_f)$ and this shift is independent of g_1 . The exact final perturbed wavefunction $\psi(q, t_f)$ for different g_1 is shown in Fig. 5.6b by lines. It coincides very well with the approximated final wavefunction $\tilde{\psi}(q, t_f)$ indicated by symbols. In Fig. 5.6b, it can also be seen that the width w of the wavefunction increases with increasing g_1 . Because of this the relative error d_{Error}/w is decreasing for increasing g_1 and this explains why the fidelity is increasing with increasing g_1 in Fig. 5.6a. Using $\tilde{\psi}$, we can approximate the fidelity. This can be further simplified by neglecting $\dot{\Delta}(t_f)$,

$$\tilde{F} = \left| \int dq \chi^*(q) \chi [q - \Delta(t_f)] \right|. \quad (5.76)$$

This is also shown in Fig. 5.6a by symbols, and agrees very well with the exact result.

Finally, we consider the effect of noise in harmonic transport. We assume that the center of the physical trap is randomly perturbed by the shift $\lambda\zeta(t)$ with respect to $q_0(t)$. For the shifted trap center, eq. (5.69) can be solved using the ansatz $\tilde{q}_c(t) = q_c(t) + \lambda\beta(t)$ such that

$$\beta(t) = \int_0^{\omega_0 t} d\tau \zeta(\tau) \sin(\omega_0 t - \tau), \quad \dot{\beta}(t) = \omega_0 \int_0^{\omega_0 t} d\tau \zeta(\tau) \cos(\omega_0 t - \tau),$$

with the solution still given by eq. (5.67). The fidelity at t_f is

$$\bar{F}_\zeta = \left| \int dq \exp\left[\frac{im}{\hbar}\lambda\dot{\beta}(t_f)q\right] \chi^*[q + \lambda\beta(t_f)] \chi(q) \right|. \quad (5.77)$$

Quite remarkably, eq. (5.77) is independent of d and the chosen $q_c(t)$. We assume now that $\zeta(t)$ is white Gaussian noise, and average the fidelity \bar{F}_ζ over different realizations of $\zeta(t)$. This exact result $\bar{F} = \langle \bar{F}_\zeta \rangle$ is shown in Fig. 5.7 by lines for three values of g_1 and two final times t_f . Note that the result is independent of d . By comparing Figs. 5.7a and 5.7b, we see that the fidelity increases for shorter times t_f . Heuristically this can be understood because the noise has less time to cause perturbations. Moreover, the fidelity increases for smaller couplings g_1 , unlike the previous results in Fig. 5.6a. This is because in the case of noisy perturbation the phase factor $\exp\left[\frac{im}{\hbar}\lambda\dot{\beta}(t_f)\right]$ in eq. (5.77) plays an essential role, while the phase factor is negligible in the anharmonic perturbation, see eq. (5.76). In the case of noisy perturbation, we may even obtain a good approximation for the fidelity by neglecting the shift $\lambda\beta(t_f)$ completely,

$$\tilde{F}_\zeta = \left| \int dq \exp\left[\frac{im}{\hbar}\lambda\dot{\beta}(t_f)q\right] \chi^*(q) \chi(q) \right|.$$

The average of this approximate fidelity $\tilde{F} = \langle \tilde{F}_\zeta \rangle$ is also shown in Fig. 5.7 by symbols and it is a very good approximation for $g_1 > 0$. The approximation $\tilde{F} \approx \bar{F}$ becomes better with increasing g_1 as the width of the wave function increases and therefore the shift (which is independent of g_1) becomes more and more negligible.

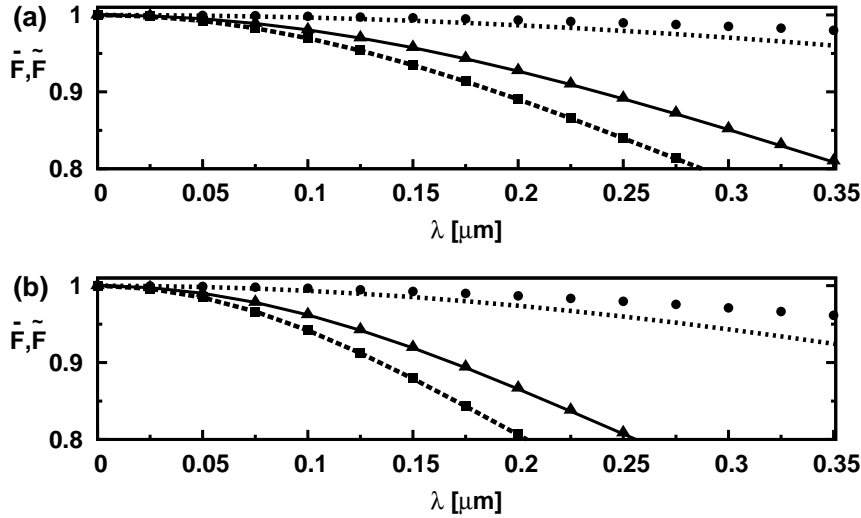


Figure 5.7: Average fidelity of harmonic transport versus noise intensity λ ; (a) $t_f = 10$ ms; (b) $t_f = 20$ ms. In both cases: exact result \bar{F} (lines), approximation \tilde{F} (symbols); $g_1 = 0$ (dotted lines and circles), $g_1/\hbar = 0.05$ m/s (solid lines and crosses), $g_1/\hbar = 0.1$ m/s (dashed lines and boxes). $\omega_0 = 2\pi \times 50$ Hz.

5.5 Optimal Control of Transport

We now utilize the degree of freedom left by the inverse method by combining it with optimal control theory (OCT) and design the trajectory according to relevant physical criteria. This framework has been successfully applied to various quantum dynamical problems [132]-[143]. For harmonic transport, we have imposed the boundary conditions (5.70) and (5.72) at $t = 0$ and $t = t_f$, but $q_0(t)$, and the polynomial ansatz for $q_c(t)$ are quite arbitrary. As an example of the possibilities of OCT we will examine two different constraints for which we deduce the optimal trajectory. The following derivations are based on the OCT treatment of cooling non-interacting atoms via the expansion of a harmonic trap in [141]-[143].

In an application of OCT one generally faces the problem of optimally transferring the initial state of a system to some final state that is subject to a number of constraints. The optimality criteria are specific to the given situation and must be defined accordingly. For a general introduction to optimal control theory we refer the reader to [144]. In the following we consider the special case of time-optimal problems and are therefore content with briefly introducing the concepts we will use. Loosely speaking our goal is to determine those admissible state transfers that take the least amount of time. Adapting the language of OCT, we consider state variables $\vec{x}(t) = (x_1(t), x_2(t))^T \in \mathbb{R}^2$ and a control $u(t)$, lying in some control set U . We determine the controls for which the initial state $\vec{x}(0)$ is transferred to the final one $\vec{x}(t_f)$ in minimal time. In our case the state variables will be given by the classical trajectory q_c and its time derivative, whereas the control will be defined according to the constraint we want to consider. The state variables and the control are then subject to a system of differential equations,

which in our case will be two-dimensional and take the form

$$\dot{\vec{x}} = \vec{f}(\vec{x}) + u\vec{g}(\vec{x}) \quad (5.78)$$

with vectorfields $\vec{f}(\vec{x}), \vec{g}(\vec{x}) \in \mathbb{R}^2$. We then define the control Hamiltonian [142, 143]

$$H_c = H_c(p_0, \vec{p}, \vec{x}, u) = p_0 + \langle \vec{p} | \vec{f}(\vec{x}) + u\vec{g}(\vec{x}) \rangle \quad (5.79)$$

with $p_0 \leq 0$ and a nonzero, absolutely continuous row vector function $\vec{p} = \vec{p}(t)$ ¹. To determine the time-optimal solution, we will then use the important Pontryagin maximum principle [142, 145, 146], which states that for a trajectory $\{u(t), \vec{x}(t)\}$ to be time-optimal, the following theorem must necessarily hold

Theorem 4. *Let $u_{op}(t), \vec{x}_{op}(t)$ be a time-optimal control transferring the initial state $\vec{x}(0)$ into the final state $\vec{x}(t_f)$. Then it is a necessary condition for optimality that there exists a constant $p_0 \leq 0$ and a nonzero, absolutely continuous row vector function $\vec{p} = \vec{p}(t)$, such that:*

(a) p satisfies the so-called adjoint equation

$$\begin{aligned} \dot{\vec{p}} &= -\frac{\partial}{\partial \vec{x}} H(p_0, \vec{p}, \vec{x}_{op}, u_{op}) \\ &= -\langle \vec{p} | \begin{pmatrix} \frac{\partial}{\partial x_1} f_1 & \frac{\partial}{\partial x_2} f_1 & \cdots \\ \frac{\partial}{\partial x_1} f_2 & \frac{\partial}{\partial x_2} f_2 & \cdots \\ \vdots & \vdots & \ddots \end{pmatrix} + u_{op} \begin{pmatrix} \frac{\partial}{\partial x_1} g_1 & \frac{\partial}{\partial x_2} g_1 & \cdots \\ \frac{\partial}{\partial x_1} g_2 & \frac{\partial}{\partial x_2} g_2 & \cdots \\ \vdots & \vdots & \ddots \end{pmatrix} \rangle \\ &= -\langle \vec{p} | D\vec{f}(\vec{x}_{op}) + u_{op} D\vec{g}(\vec{x}_{op}) \rangle. \end{aligned}$$

(b) For $0 \leq t \leq t_f$ the function $u \rightarrow H(p_0, \vec{p}, \vec{x}_{op}, u)$ attains its maximum over the control set U at $u = u_{op}$.

(c) $H(p_0, \vec{p}, \vec{x}_{op}, u_{op}) \equiv 0$.

Condition (a) together with the system (5.78) can be stated in an alternative and more natural way for physicists, namely

$$\dot{\vec{x}} = \frac{\partial}{\partial \vec{p}} H(p_0, \vec{p}, \vec{x}_{op}, u_{op}) \quad \dot{\vec{p}} = -\frac{\partial}{\partial \vec{x}} H(p_0, \vec{p}, \vec{x}_{op}, u_{op}), \quad (5.80)$$

where \vec{x} and \vec{p} are conjugate variables. The first equation gives eq. (5.78) and the second is the necessary condition (a) of the theorem.

A trajectory $\{u(t), \vec{x}(t)\}$ for which permissible multipliers p_0 and \vec{p} exist is called an *extremal*.

In the following we make the connection between these general definitions and our transport process and consider two different controls. In both applications we will

¹ \vec{p} plays the role of a Lagrangian multiplier.

assume $p_0 < 0$ and therefore rescale it w.l.o.g. to $p_0 = -1^1$.

Limiting the deviation of the condensate from the trap center

Suppose that we wish to limit the deviation of the condensate from the trap center according to $-\delta \leq q_c - q_0 \leq \delta$, $\delta > 0$, and find the minimal time t_f . This constraint is for example interesting if one wants to decrease the effect of anharmonicities. The transport process given by eqs. (5.67), (5.70) and (5.72) can be rewritten as a minimum-time optimal control problem by defining the state variables $x_1 = x_1(t)$ and $x_2 = x_2(t)$ and the control $u = u(t)$ as

$$x_1 = q_c, \quad x_2 = \dot{q}_c, \quad u = q_c - q_0. \quad (5.81)$$

Eq. (5.69) is then transformed into a system of equations

$$\dot{x}_1 = x_2, \quad \dot{x}_2 + \omega_0^2 u = 0 \quad (5.82)$$

that can be written in a more compact form as

$$\dot{\vec{x}} = \vec{f}(\vec{x}) + u\vec{g}. \quad (5.83)$$

The vector fields $\vec{f}(\vec{x})$ and \vec{g} are given by

$$\vec{f}(\vec{x}) = (x_2, 0)^T, \quad \vec{g} = (0, -\omega_0^2)^T, \quad (5.84)$$

$\vec{x} \in D = \{(x_1, x_2)^T \in \mathbb{R}^2\}$ and u is in the control set $U = [-\delta, \delta]$.

With these definitions the OCT problem can now be stated as follows

Find a trajectory $\{u(t), \vec{x}(t)\}$ with $-\delta \leq u(t) \leq \delta$, $u(0) = u(t_f) = 0$, $(x_1(0), x_2(0))^T = (0, 0)^T$, and $(x_1(t_f), x_2(t_f))^T = (d, 0)^T$ such that the transport occurs in minimal final time t_f .

According to eqs. (5.79), (5.83) and (5.84) the control Hamiltonian is given by

$$H_c = H_c(p_0, \vec{p}, \vec{x}, u) = p_0 + \langle \vec{p} | \vec{f}(\vec{x}) + u\vec{g} \rangle = p_0 + p_1 x_2 - p_2 \omega_0^2 u, \quad (5.85)$$

with p_0 a constant and multiplier $\vec{p} = \vec{p}(t) = (p_1(t), p_2(t))^T \in \mathbb{R}^2$. Before determining the optimal trajectory below, we first give the following definitions. If the control u switches between its boundary values we call this a *bang-bang switch* and therefore we call a trajectory $\{u(t), \vec{x}(t)\}$ with a bang-bang switch a *bang-bang trajectory* [83, 141, 143, 144]. We are now ready to prove the following:

Proposition 8. *For the OCT problem stated above, optimal controls are bang-bang.*

Proof. We first note that the Hamiltonian (5.85) is a linear function of u and since we consider a rigid harmonic trap we have $\omega_0^2 > 0$. Therefore, the sign of the coefficient

¹ An extremal with $p_0 = 0$ is called abnormal and would need a separate treatment which we omit here.

of u is determined by $-p_2$. The linearity of the Hamiltonian with respect to u and the necessary condition (b) in Theorem 4 imply that the optimal control is given by $u = -\delta$ if $-p_2$ is positive and $u = \delta$ if it is negative. It remains to show that the optimal control u switches between these values. Although in general the theorem does not tell anything about the control for those times at which p_2 vanishes, in the special case $p_2 = 0$ and $\dot{p}_2 \neq 0$, u switches between its boundary values, i.e. a bang-bang switch occurs. To complete the proof we will use this fact by considering the adjoint equation of our problem, which is given by

$$\begin{aligned} \dot{\vec{p}} &= -\vec{p} \left[\begin{pmatrix} \frac{\partial}{\partial x_1} f_1 & \frac{\partial}{\partial x_2} f_1 \\ \frac{\partial}{\partial x_1} f_2 & \frac{\partial}{\partial x_2} f_2 \end{pmatrix} + u \begin{pmatrix} \frac{\partial}{\partial x_1} g_1 & \frac{\partial}{\partial x_2} g_1 \\ \frac{\partial}{\partial x_1} g_2 & \frac{\partial}{\partial x_2} g_2 \end{pmatrix} \right] \\ &= -\vec{p} \left[\begin{pmatrix} 0 & 1 \\ 0 & 0 \end{pmatrix} + u \begin{pmatrix} 0 & 0 \\ 0 & 0 \end{pmatrix} \right] = \vec{p} \begin{pmatrix} 0 & -1 \\ 0 & 0 \end{pmatrix} \\ &= \vec{p} M = (0, -p_1)^T. \end{aligned} \quad (5.86)$$

From this equation it follows that $\dot{p}_2 = -p_1$. Now assume that $p_2 = 0$ for some time t . According to Theorem 4 the multiplier \vec{p} must be non-trivial, i.e. $\vec{p} \neq 0$. We have $-\dot{p}_2 = p_1$ and therefore $-\dot{p}_2 \neq 0$, i.e. p_2 changes sign and there is a bang-bang switch at time t . \square

Although we can classify time-optimal controls as bang-bang, we are yet to determine which controls lead to smaller final times t_f and are therefore optimal in this subset of admissible controls. In other words we still have to determine if for example one or multiple bang-bang switches are better. In the case of harmonic trap expansion it was shown out that more than one switching might be beneficial [142, 143]. However, the following proposition shows, that for the problem we consider exactly one switching is time-optimal.

Proposition 9. *For the OCT problem stated above the time-optimal control is bang-bang with exactly one switching.*

Proof. We already proved that optimal controls are bang-bang. It remains to show that exactly one switching is time-optimal. First note that for a switch to occur we necessarily have $p_2 = 0$. This follows from condition (c) of Theorem 4 where the Hamiltonian in eq. (5.85) gives

$$-p_0 = p_1(t \pm \epsilon)x_{op,2}(t \pm \epsilon) - \omega_0^2 p_2(t \pm \epsilon) \cdot \begin{cases} \delta \\ -\delta \end{cases}. \quad (5.87)$$

However, $\vec{p}(t)$ and $x_{op,2}(t)$ are continuous and therefore, because u changes discontinuously from δ to $-\delta$ (or vice versa), we necessarily have $p_2(t) = 0$ if a jump occurs. Now consider again the adjoint equation (5.86). From this equation it follows that $p_1 = c_1$, $c_1 \in \mathbb{R}$, and $p_2 = -c_1 t + c_2$, $c_2 \in \mathbb{R}$. Therefore p_2 has exactly one zero for some switching time t_1 and it follows that exactly one switching is optimal. \square

Combining the previous results we therefore have that the complete solution with one bang-bang switch is given by

$$u(t) = \begin{cases} 0, & t \leq 0 \\ \pm\delta, & 0 < t < t_1 \\ \mp\delta, & t_1 < t < t_f \\ 0, & t \geq t_f \end{cases},$$

where the initial and final discontinuities are chosen to satisfy the boundary conditions. This trajectory still contains the freedom of either starting with δ or $-\delta$. From a physical point of view, starting with $-\delta$ would be the natural choice, corresponding to the case the condensate is accelerated beyond the desired position and then decelerated such that it comes to rest afterwards. In the course of deriving explicit expressions for the switching and final times for these trajectories using the constants of motion (see below), we show that starting with $-\delta$ is also the only admissible optimal trajectory.

The switching time and the final time can be calculated by solving the system (5.82) and imposing continuity on x_1 and x_2 . We begin with the trajectory $-\delta$ and use the initial conditions $x_1(0) = 0$, $\dot{x}_1(0) = 0$. Therefore it follows that

$$x_1(t) = \frac{\omega_0^2 \delta}{2} t^2, \quad 0 < t < t_1 \quad (5.88)$$

with t_1 being the switching time. To calculate the trajectory after the switching it is more convenient to consider the backwards evolution, i.e. we impose the boundary conditions $x_1(t_f) = d$, $\dot{x}_1(t_f) = 0$ where d is the final distance at time t_f to obtain

$$x_1(t_f - t) = -\frac{\omega_0^2 \delta}{2} t^2 + d, \quad 0 < t < t_2 \quad (5.89)$$

with $t_f = t_1 + t_2$. We denote our switching point by (a, b) and use the constants of motion to determine t_1 and t_2 . We have

$$\frac{d}{dt} \left(\frac{x_2(t)^2}{2} \right) + \omega_0^2 u \frac{d}{dt} x_1(t) = 0 \quad (5.90)$$

since

$$\dot{x}_2(t)\dot{x}_1(t) = -\omega_0^2 u \dot{x}_1(t) \Leftrightarrow x_2(t)\dot{x}_2(t) = -\omega_0^2 u \dot{x}_1(t), \quad (5.91)$$

where u is constant and one of the extremal values. Integrating eq. (5.90) for the trajectory during t_1 to the switching point (a, b) we obtain

$$\frac{b^2}{2} - \omega_0^2 \delta a = 0 \quad (5.92)$$

where we have used $x_1(0) = 0$, $\dot{x}_1(0) = 0$. Similarly, for the trajectory during t_2 we find

$$\frac{b^2}{2} + \omega_0^2 \delta a = \omega_0^2 \delta d \quad (5.93)$$

since $x_1(t_f) = d$, $\dot{x}_1(t_f) = 0$. Combining these equations it follows that

$$a = \frac{d}{2}. \quad (5.94)$$

Considering eq. (5.88) on the other hand we have

$$a = \frac{\omega_0^2 \delta}{2} t_1^2. \quad (5.95)$$

Using eq. (5.94) we therefore obtain for the switching time t_1 for a trajectory starting with $-\delta$

$$t_1 = \left(\frac{d}{\delta}\right)^{\frac{1}{2}} \frac{1}{\omega_0}. \quad (5.96)$$

Due to the symmetry, i.e. the switching point being at $d/2$, we have

$$t_1 = \frac{t_f}{2}, t_f = 2 \left(\frac{d}{\delta}\right)^{\frac{1}{2}} \frac{1}{\omega_0}. \quad (5.97)$$

Using the same procedure we can determine the switching time for a trajectory starting with δ . Since $x_1(t)$, $\dot{x}_1(t)$ and the expressions for the constants of motion are linear in u , the terms containing δ simply switch sign and we again obtain

$$a = \frac{d}{2}. \quad (5.98)$$

Again according to eq. (5.88) we now have

$$a = -\frac{\omega_0^2 \delta}{2} t_1^2 \quad (5.99)$$

which leads to

$$d = -\omega_0^2 \delta t_1^2. \quad (5.100)$$

However, all the single factors are strictly positive and therefore we have a contradiction and can exclude the trajectory starting with δ . We now have our final expression for the time-optimal control

$$u(t) = \begin{cases} 0, & t \leq 0 \\ -\delta, & 0 < t < t_1 \\ \delta, & t_1 < t < t_f \\ 0, & t \geq t_f \end{cases}.$$

The corresponding trajectory can be deduced from eq. (5.81) which leads to

$$q_0(t) = \begin{cases} 0, & t \leq 0 \\ (1 + \omega_0^2 t^2 / 2) \delta, & 0 < t < t_1 \\ -[\omega_0^2 (t - t_f)^2 / 2 + 1] \delta + d, & t_1 < t < t_f \\ d, & t \geq t_f \end{cases},$$

where the switching and final time are given by eq. (5.97). In Fig. 5.5 the displacement of the center of mass with respect to the trap center and the trap trajectory are plotted for this optimal trajectory. We have chosen $\delta \simeq 0.162$ mm so that the minimal final time is $t_f = 20$ ms, as in the previous example.

Limiting the range for the center of the physical trap

We now consider another important constraint. Suppose we require the center of the physical trap to stay inside a given range (e.g. inside the vacuum chamber). Mathematically the constraint is then $q_{\downarrow} \leq q_0(t) \leq q_{\uparrow}$.

The first part of the following treatment will be analogous to the previous analysis. As before, for the transport process given by eqs. (5.67), (5.70) and (5.72), we define the control variables $x_1 = x_1(t)$, $x_2 = x_2(t)$ and $u = u(t)$ as

$$x_1 = q_c, \quad x_2 = \dot{q}_c, \quad u = q_0. \quad (5.101)$$

with $q_{\downarrow} \leq u \leq q_{\uparrow}$. Furthermore, because we consider a transport from 0 to d , the extremal values must satisfy $q_{\downarrow} < 0$ and $q_{\uparrow} > d$. Eq. (5.69) can now be rewritten as

$$\dot{\vec{x}} = \vec{f}(\vec{x}) + u\vec{g}, \quad (5.102)$$

where the vector fields $\vec{f}(\vec{x})$ and \vec{g} are given by

$$\vec{f}(\vec{x}) = (x_2, -\omega_0^2 x_1)^T, \quad \vec{g} = (0, \omega_0^2)^T, \quad (5.103)$$

$\vec{x} \in D = \{(x_1, x_2)^T \in \mathbb{R}^2\}$ and u is in the control set $U = [q_{\downarrow}, q_{\uparrow}]$.

The OCT problem can now be stated as follows

Find a trajectory $\{u(t), \vec{x}(t)\}$ with $q_{\downarrow} \leq u(t) \leq q_{\uparrow}$, $u(0) = u(t_f) = 0$, $(x_1(0), x_2(0))^T = (0, 0)^T$, and $(x_1(t_f), x_2(t_f))^T = (d, 0)^T$ such that the transport occurs in the minimum final time t_f .

According to eqs. (5.79), (5.83) and (5.84) the control Hamiltonian is similarly given by

$$H_c = H_c(p_0, \vec{p}, \vec{x}, u) = p_0 + \langle \vec{p} | \vec{f}(\vec{x}) + u\vec{g} \rangle = p_0 + p_1 x_2 - p_2 \omega_0^2 x_1 + p_2 \omega_0^2 u, \quad (5.104)$$

with p_0 a constant and multiplier $\vec{p} = \vec{p}(t) = (p_1(t), p_2(t))^T \in \mathbb{R}^2$ as before. Once more we have

Proposition 10. *For the OCT problem stated above, optimal controls are bang-bang.*

Proof. The proof is completely analogous to that of Proposition 8. □

As before we can prove that multiple switches are not beneficial and one switch is time-optimal. The proof, however, is not as straightforward as for the constraint above. Instead we will prove the result indirectly by showing that the sojourn time between switchings is too long for further switchings to be useful. By useful we mean that they might reduce the final time t_f of the whole process. For this we need the following

Proposition 11. *For the OCT problem stated above, time-optimal controls are bang-bang where the switching times t_n occur with periodicity π and the time between different switchings, the interswitching time t_s , is given by $t_s = \frac{n\pi}{\omega_0}$, $n \in \mathbb{N}_+$.*

Proof. As before it only remains to prove the second part of the proposition, i.e. the periodicity of the switching times and the time between switchings. In the following we will present two different ways (a) and (b) to prove this. The first (a), will be similar to the proof of Proposition 9 by considering the zeros of $p_2(t)$. The reason for the second proof (b) is that we can apply a slightly more general technique particularly suited to determining the interswitching times that can be applicable even if the zeros of $p_2(t)$ are not easily determined. This proof is closely related to the concept of a “conjugate point” [161, 162] which we will discuss in more detail in Appendix D.

(a) As in the proof of Proposition 9 we use the fact that p_2 has to be zero when a switching occurs. Using the adjoint equation we can again determine the explicit form of p_2 . We have

$$\begin{aligned}\dot{\vec{p}} &= -\vec{p} \left[\begin{pmatrix} 0 & 1 \\ -\omega_0^2 & 0 \end{pmatrix} + u \begin{pmatrix} 0 & 0 \\ 0 & 0 \end{pmatrix} \right] = -\vec{p} \begin{pmatrix} 0 & -1 \\ \omega_0^2 & 0 \end{pmatrix} \\ &= \vec{p} M = (\omega_0^2 p_2, -p_1)^T,\end{aligned}\tag{5.105}$$

i.e. componentwise we have $\dot{p}_1(t) = \omega_0^2 p_2(t)$ and $\dot{p}_2(t) = -p_1(t)$ and therefore $\ddot{p}_2 = -\omega_0^2 p_2(t)$. It follows that $p_2(t) = c_1 \sin(\omega_0 t + \phi)$ with $c_1 \in \mathbb{R}$ and $\phi \in [0, \pi[$. The zeros of $p_2(t)$ are therefore given by $t_n = \frac{1}{\omega_0}(n\pi - \phi)$ with $n \in \mathbb{N}_+$. For the relative time between switchings, i.e. the interswitching time t_s , we thus obtain $t_s = \frac{n\pi}{\omega_0}$ which proves the proposition.

(b) Consider two switching points \vec{a} and \vec{b} . Because we are only interested in the relative time between them we will assume w.l.o.g. that the trajectory passes \vec{a} at time $t = 0$ and \vec{b} at time $t_s > 0$. First note that at these points, because a bang-bang switch occurs, we necessarily have

$$\langle \vec{p}(0) | \vec{g}(\vec{a}) \rangle = 0 = \langle \vec{p}(t_s) | \vec{g}(\vec{b}) \rangle\tag{5.106}$$

due to condition (c) of Theorem 4¹. From the adjoint equation (5.105) we furthermore have

$$\dot{\vec{p}}^T = \vec{p}^T M \Leftrightarrow M^T \vec{p} = \dot{\vec{p}}.\tag{5.107}$$

Because M is independent of time we can write

$$\vec{p}(t_s) = e^{t_s M^T} \vec{p}(0).\tag{5.108}$$

Using this relation we obtain

$$0 = \langle \vec{p}(t_s) | \vec{g} \rangle = \langle e^{t_s M^T} \vec{p}(0) | \vec{g} \rangle = \langle \vec{p}(0) | e^{t_s M} \vec{g} \rangle.\tag{5.109}$$

¹ Here of course $\vec{g}(\vec{x}) = \vec{g}$ and we therefore omit the arguments in the following.

Combining eqs. (5.106) and (5.109) we therefore have

$$(\vec{p}(0) \perp \vec{g}) \wedge (\vec{p}(0) \perp e^{t_s M} \vec{g}). \quad (5.110)$$

Moreover, since we have a two-dimensional system this is possible if and only if

$$\vec{g} \parallel e^{t_s M} \vec{g}. \quad (5.111)$$

The matrix exponential $e^{t_s M}$ is easily computed and we obtain

$$e^{t_s M} = \begin{pmatrix} \cos(t_s \omega_0) & -\frac{\sin(t_s \omega_0)}{\omega_0} \\ \omega_0 \sin(t_s \omega_0) & \cos(t_s \omega_0) \end{pmatrix}. \quad (5.112)$$

With $g = (0, \omega_0^2)^T$ it follows for eq. (5.111) that

$$(0, \omega_0^2)^T \parallel (-\omega_0 \sin(t_s \omega_0), \cos(t_s \omega_0))^T \quad (5.113)$$

and therefore $\sin(t_s \omega_0) = 0$, i.e. $t_s = \frac{n\pi}{\omega_0}$, $n \in \mathbb{N}_+$ which proves the proposition. \square

We are yet to prove that the trajectory with one switching is time-optimal. Our next step toward such a proof is to determine the switching and final time in this case. Calculating the explicit form of these process times is of interest in its own right, since such a single switch trajectory would certainly be the natural first choice in an implementation. However, these expression will also enable us to show that a trajectory with exactly one switch is indeed the optimal choice.

To determine the switching and final time we again calculate the initial x_1 , which is simply the solution of the ODE (5.69), and which is in general given by

$$x_1(t) = A \sin(\omega_0 t) + B \cos(\omega_0 t) + q_{\downarrow, \uparrow}. \quad (5.114)$$

Similarly as before, choosing q_{\uparrow} as the initial control is the natural choice, because this describes the physical situation of initially accelerating the condensate as much as possible and then decelerating it by moving the trap to the lower bound q_{\downarrow} , leaving the condensate at rest at the final time t_f . In the following we will show that this is also the only admissible trajectory, because starting with q_{\downarrow} leads to a contradiction.

We first consider the case of an initial control q_{\uparrow} . Starting again at $t_0 = 0$ and using the initial conditions $x_1(0) = 0$, $\dot{x}_1(0) = 0$, for the trajectory during t_1 it follows that

$$x_1(t) = q_{\uparrow}(1 - \cos(\omega_0 t)), \quad 0 < t < t_1 \quad (5.115)$$

with t_1 being the switching time. We calculate the second trajectory again by considering the backwards evolution, i.e. as before we impose $x_1(t_f) = d$, $\dot{x}_1(t_f) = 0$ to obtain

$$x_1(t_f - t) = (d - q_{\downarrow}) \cos(\omega_0 t) + q_{\downarrow}, \quad 0 < t < t_2 \quad (5.116)$$

with $t_f = t_1 + t_2$. Again, we denote our switching point by (a, b) and use the constants of motion for this system, i.e.

$$\frac{d}{dt} \left(\frac{x_2^2}{2} \right) + \omega_0^2 \frac{d}{dt} \left(\frac{x_1^2}{2} \right) + \omega_0^2 u \frac{d}{dt} x_1 = 0 \quad (5.117)$$

which is due to

$$\dot{x}_1\dot{x}_2 = -\omega_0^2(\dot{x}_1x_1 + u\dot{x}_1) \Leftrightarrow x_2\dot{x}_2 = -\omega_0^2(\dot{x}_1x_1 + u\dot{x}_1), \quad (5.118)$$

where as before u is one of the constant extremal values. Integrating eq. (5.117) for the trajectory during t_1 to the switching point (a, b) and using the initial conditions $x_1(0) = 0, \dot{x}_1(0) = 0$ we have

$$\frac{b^2}{2} + \frac{\omega_0^2 a^2}{2} - \omega_0^2 q_\uparrow a = 0. \quad (5.119)$$

For the trajectory during t_2 obtain

$$\frac{b^2}{2} + \frac{\omega_0^2 a^2}{2} - \omega_0^2 q_\downarrow a = \frac{\omega_0^2 d^2}{2} - \omega_0^2 q_\downarrow d \quad (5.120)$$

after application of the initial conditions $x_1(t_f) = d, \dot{x}_1(t_f) = 0$. Combining these equations it follows that

$$\omega_0^2 q_\uparrow a = \omega_0^2 q_\downarrow a + \frac{\omega_0^2 d^2}{2} - \omega_0^2 q_\downarrow d \quad (5.121)$$

$$\Rightarrow a = \frac{\frac{d^2}{2} - q_\downarrow d}{q_\uparrow - q_\downarrow} \quad (5.122)$$

Using eq. (5.115) on the other hand we have

$$a = q_\uparrow(1 - \cos(\omega_0 t_1)) \quad (5.123)$$

and therefore

$$\cos(\omega_0 t_1) = 1 - \frac{\frac{d^2}{2} - q_\downarrow d}{q_\uparrow(q_\uparrow - q_\downarrow)}. \quad (5.124)$$

Similarly for the second trajectory we have

$$\kappa = q_\downarrow + (d - q_\downarrow)\cos(\omega_0 t_2) \quad (5.125)$$

and it follows that

$$\cos(\omega_0 t_2) = \frac{\frac{d^2}{2} - q_\downarrow d}{(d - q_\downarrow)(q_\uparrow - q_\downarrow)} - \frac{q_\downarrow}{d - q_\downarrow}. \quad (5.126)$$

As before $x_1(t), \dot{x}_1(t)$ and the expressions for the constants of motion are linear in u , and therefore in the formulas above q_\uparrow can be replaced by q_\downarrow and vice versa when starting with q_\downarrow . We therefore have

$$\cos(\omega_0 t_1) = 1 - \frac{\frac{d^2}{2} - q_\uparrow d}{q_\downarrow(q_\downarrow - q_\uparrow)} \quad (5.127)$$

and

$$\cos(\omega_0 t_2) = \frac{\frac{d^2}{2} - q_\uparrow d}{(d - q_\uparrow)(q_\downarrow - q_\uparrow)} - \frac{q_\uparrow}{d - q_\uparrow}. \quad (5.128)$$

To determine the different switching times we are left with verifying if the $\cos(\omega_0 t_{1,2})$ has a well-defined inverse for the given parameters. Using the natural assumptions $q_\downarrow < 0$ and $q_\uparrow > d$ stated in the beginning, we find that this is only the case for a trajectory starting with q_\uparrow . For a trajectory starting with q_\downarrow , we have a contradiction. Furthermore, the resulting times t_1 and t_2 for the admissible case are even bounded by $\pi/2$, a fact we will soon use to show that exactly one switching is optimal. Next we exclude the trajectory starting with q_\downarrow , which is a direct consequence of the following

Proposition 12. *For $q_\downarrow < 0$ and $q_\uparrow > d$, eqs. (5.127) and (5.128) for the switching times t_1 and t_2 for a trajectory starting with q_\downarrow lead to a contradiction.*

Proof. According to eq. (5.127) we have

$$\cos(\omega_0 t_1) = 1 - \frac{\frac{d^2}{2} - q_\uparrow d}{q_\downarrow(q_\downarrow - q_\uparrow)} = 1 + \frac{q_\uparrow d - \frac{d^2}{2}}{q_\downarrow(q_\downarrow - q_\uparrow)}. \quad (5.129)$$

But $q_\uparrow > d$ and therefore $q_\uparrow d - d^2/2 > d^2 - d^2/2 > 0$. Furthermore we have $q_\downarrow < 0$ and therefore $q_\downarrow(q_\downarrow - q_\uparrow) > 0$. We therefore obtain

$$\cos(\omega_0 t_1) > 1, \quad (5.130)$$

i.e. we have a contradiction. This is already enough to exclude this trajectory, but it is interesting to note that similar arguments also show a contradiction for eq. (5.128). \square

For the trajectory starting with q_\uparrow we have

Proposition 13. *For $q_\downarrow < 0$ and $q_\uparrow > d$, the $\cos(\omega_0 t_{1,2})$ in eqs. (5.124) and (5.126) is invertible and the corresponding times t_1 and t_2 are given by*

$$t_1 = \frac{1}{\omega_0} \cos^{-1} \left[1 - \frac{\frac{d^2}{2} - q_\downarrow d}{q_\uparrow(q_\uparrow - q_\downarrow)} \right]. \quad (5.131)$$

and

$$t_2 = \frac{1}{\omega_0} \cos^{-1} \left[\frac{\frac{d^2}{2} - q_\downarrow d}{(d - q_\downarrow)(q_\uparrow - q_\downarrow)} - \frac{q_\downarrow}{d - q_\downarrow} \right] \quad (5.132)$$

with $t_1 + t_2 = t_f$ where t_f is the total time of the transport process. Furthermore, we have $t_1 \in]0, \frac{\pi}{2\omega_0}[$ and $t_2 \in]0, \frac{\pi}{2\omega_0}[$.

Proof. The proof of this proposition is as straightforward as the previous one. We have

$$\frac{\frac{d^2}{2} - q_\downarrow d}{q_\uparrow(q_\uparrow - q_\downarrow)} = \frac{d}{q_\uparrow} \frac{\frac{d}{2} - q_\downarrow}{(q_\uparrow - q_\downarrow)} > 0 \quad (5.133)$$

since by assumption, all factors are larger than zero. We also have that

$$\frac{d}{q_{\uparrow}} \frac{\frac{d}{2} - q_{\downarrow}}{(q_{\uparrow} - q_{\downarrow})} < \frac{\frac{d}{2} - q_{\downarrow}}{(q_{\uparrow} - q_{\downarrow})} < 1. \quad (5.134)$$

due to the fact that $(q_{\uparrow} - q_{\downarrow}) > 0$ and $q_{\uparrow} > d > d/2$. Combining these inequalities we obtain

$$0 < 1 - \frac{\frac{d^2}{2} - q_{\downarrow}d}{q_{\uparrow}(q_{\uparrow} - q_{\downarrow})} < 1 \quad (5.135)$$

and therefore the inverse of $\cos(\omega_0 t_1)$ in eq. (5.124) is well-defined. Moreover, we have $t_1 \in]0, \frac{\pi}{2\omega_0}[$, where t_1 is given by eq. (5.131), which proves the proposition for t_1 . Similarly we show that

$$0 < \frac{\frac{d^2}{2} - q_{\downarrow}d}{(d - q_{\downarrow})(q_{\uparrow} - q_{\downarrow})} - \frac{q_{\downarrow}}{d - q_{\downarrow}} < 1. \quad (5.136)$$

The first inequality holds because the first summand is a product of strictly positive factors, whilst the second summand is negative because $q_{\downarrow} < 0$. The second inequality holds because

$$\begin{aligned} & \frac{\frac{d^2}{2} - q_{\downarrow}d}{(d - q_{\downarrow})(q_{\uparrow} - q_{\downarrow})} - \frac{q_{\downarrow}}{d - q_{\downarrow}} = \frac{\frac{d^2}{2} - q_{\downarrow}d - q_{\downarrow}(q_{\uparrow} - q_{\downarrow})}{(d - q_{\downarrow})(q_{\uparrow} - q_{\downarrow})} < 1 \\ \Leftrightarrow & \frac{d^2}{2} - q_{\downarrow}d - q_{\downarrow}(q_{\uparrow} - q_{\downarrow}) < (d - q_{\downarrow})(q_{\uparrow} - q_{\downarrow}) \Leftrightarrow \frac{d}{2} < q_{\uparrow} \end{aligned} \quad (5.137)$$

which is true by assumption. Therefore, we also have that the inverse of $\cos(\omega_0 t_2)$ in eq. (5.126) is well-defined, t_2 is given by eq. (5.132) and $t_2 \in]0, \frac{\pi}{2\omega_0}[$ which completes the proof. \square

To summarize, we have shown thus far that the only admissible trajectory with one switching is given by

$$q_0(t) = \begin{cases} 0, & t \leq 0 \\ q_{\uparrow}, & 0 < t < t_1 \\ q_{\downarrow}, & t_1 < t < t_f \\ d, & t \geq t_f \end{cases},$$

with

$$\begin{aligned} \omega_0 t_1 &= \arccos \left[1 - \frac{q_{\downarrow}d - d^2/2}{q_{\uparrow}(q_{\downarrow} - q_{\uparrow})} \right], \quad t_1 \in]0, \frac{\pi}{2\omega_0}[\\ \omega_0 t_f &= \omega_0 t_1 + \arccos \left[\frac{\frac{d^2}{2} - q_{\downarrow}d - q_{\downarrow}(q_{\uparrow} - q_{\downarrow})}{(d - q_{\downarrow})(q_{\uparrow} - q_{\downarrow})} \right], \quad t_f \in]0, \frac{\pi}{\omega_0}[. \end{aligned}$$

With the previous results we are now ready to prove that for this constraint $q_{\downarrow} \leq q_0(t) \leq q_{\uparrow}$ exactly one switching is time-optimal, that is

Proposition 14. *In the set of time-optimal controls, which are bang-bang, the control*

with exactly one switching is time-optimal, because it leads to a final time t_f strictly smaller than all final times $t_{f,ms}$ achieved with more than one switching, i.e. $t_f < t_{f,ms}$.

Proof. According to Proposition 13 we have $t_1 \in]0, \frac{\pi}{2\omega_0}[$ as well as $t_2 \in]0, \frac{\pi}{2\omega_0}[$ and therefore $t_f = t_1 + t_2 < \frac{\pi}{\omega_0}$. On the other hand according to Proposition 11 for the inter switching time t_s , we have $t_s \geq \frac{\pi}{\omega_0}$. The final time $t_{f,ms}$ for a process with n switchings, $n \in \mathbb{N}_+$, is given by $t_{f,ms} = t_r + (n-1)t_s$ where t_r is the time needed before the first and after the last switching and which is of course positive. For $n \geq 2$ we therefore have

$$t_{f,ms} = t_r + (n-1)t_s > (n-1)t_s \geq (n-1)\frac{\pi}{\omega_0} > t_f \quad (5.138)$$

which proves the proposition. □

5.6 Summary and Conclusion

In this chapter we presented the so called “inverse-invariant” method, which is based on dynamical invariants of the Hamiltonian and provides a “shortcut to adiabaticity”. Instead of deducing the physical trajectory for the process directly, we match the initial and final states of the invariant and the Hamiltonian and let the state evolve along the invariants basis by ensuring that certain auxiliary equations are fulfilled. From these auxiliary equations we then deduce the physical trajectory afterwards, i.e. “inversely”, and achieve an adiabatic like state transfer in less time.

We began by introducing the method in a general way, followed by two exemplary applications. First we showed that the “inverse-invariant” method provides a scheme to cool down atoms in a harmonic trap without phase-space compression as in a perfectly slow adiabatic expansion but in a much shorter time. An important feature is that for very short total expansion times this may require that the harmonic trap becomes transitorily an expulsive parabolic potential. However, this does not pose a problem, since we also showed that the atom remains confined during the whole process. Furthermore, we showed that the method is stable with respect to anharmonicities in the potential in the sense that we still obtain a high fidelity for the final state, which is important, since a perfect harmonic potential cannot be implemented experimentally. Second we showed that the “inverse-invariant” method can also be applied to the transport of Bose-Einstein condensates, for which we have provided efficient transport protocols and pointed out the effect of different perturbations. Extensions in several directions may be envisioned: the use of optimal control theory combined with inverse engineering techniques provides a powerful approach and we have given two possible examples minimizing the time for a bounded displacement of the condensate from the trap center or for a bounded accessible space. Furthermore, we studied both constraints in more detail and found in both cases that among optimal trajectories, which are bang-bang, the trajectory with exactly one switching is time-optimal and that only one of the two possible remaining trajectories in each case is admissible, i.e. we found a unique time-optimal solution for these constraints. There may also be many other physical constraints or conditions that could be also imposed depending on specific settings. A continued analysis for the displacement constraint can be found in [148]. A second important open question we leave for future work is to evaluate the effect of the approximate realization of the discontinuities found in some of the optimal (bang-bang) solutions. Moreover the results on transport processes may be extended to other physical scenarios like non-spherical traps, rotations, and launching/stopping condensates up to/from a determined velocity.

In addition to these results we like to point out some further work done by other authors based on the inverse-invariant method, e.g. in the context of cooling via harmonic trap expansion.

For example it was also shown that it is possible to take a Bose-Einstein condensate in a very short time from an initial harmonic trap to a final one without excitations, by the same technique [88].

Furthermore, in addition to the comparison of the inverse-invariant method with an adiabatic process presented here, which showed the formers superiority over the latter, its advantages with respect to other methods like real frequency bang-bang techniques and “transitionless-tracking” methods were examined too.

For example it was illustrated in [3] that a given cooling objective may be attained in less time with the inverse-invariant method than the minimal time required by real-frequency bang-bang trajectories, optimal among real-frequency trajectories [83]. Relaxing the positivity condition for the intermediate frequencies makes faster processes with $t_f < t_f^{min}$ possible, where t_f^{min} is the minimal time in a real-frequency bang-bang process. Moreover, the inverse-invariant method involves only finite frequencies, whereas t_f^{min} is obtained via a limiting process including one of the frequencies going to infinity. Since t_f^{min} has been used to justify a finite time version of the third principle and maximal cooling rates, these findings call for a revision of these conclusions [149, 150]. In [3] the inverse-invariant method was also compared to the “transitionless-tracking” method, which provides a different shortcut to adiabaticity, but the potential in the final Hamiltonian is a non-local operator. This is the main drawback for its physical implementation and its physical realizability remains an open question. The inverse-invariant method is clearly distinct from this method and implements a different Hamiltonian with a time-dependent, local, realizable potential.

As an outlook, similar techniques may be applied to the control of soliton dynamics of Bose-Einstein condensates [120, 151], pulsed beams [152] or adiabatic computing [69, 70]. Fast driven expansions may also offer an enlarged and faithful copy of the initial system that can be imaged on much shorter times than with the standard time-of-flight technique based on free expansions.

6 Conclusion and Outlook

We live on an island surrounded by a sea of ignorance. As our island of knowledge grows, so does the shore of our ignorance.

(John A. Wheeler)

In modern quantum optical experiments, the control of atomic motional states plays an essential role. In the present work we therefore proposed and studied three different schemes which provide new techniques for their manipulation.

One important scheme to reduce the atomic velocity is based on the atom's reflection from a moving potential barrier or mirror. Such a mirror can, for example, be realized with a detuned laser. However, one main drawback in most of the current applications is that the mirror potential moves with a constant velocity. For atoms in a pulse with a velocity distribution this only leads to a significant velocity reduction for atoms with a velocity close to half the mirror velocity. In **Chapter 3** we showed that in an idealized and classical description a mirror moving along a square-root in time trajectory stops particles irrespective of their initial velocity. Using more realistic conditions, like a finite width of the ensemble in position space, we showed that such a mirror trajectory stops atoms in a pulse significantly better than a mirror with constant velocity and leads to a narrow velocity distribution around zero. Furthermore, we showed how to reduce and, in a limit, even suppress effects due to e.g. the finite width of the pulse. Since a classical analysis is not sufficient, we then studied the problem also in the quantum mechanical framework, including the treatment of realistic Gaussian potentials. We presented both numerical and analytical results, showing that also in this framework a square-root in time mirror trajectory leads to a similar velocity reduction for atoms in a pulse. Moreover, we also considered a two-dimensional setting and different mirror geometries both in the classical and the quantum mechanical framework. Taking both velocity components into account, it emerged that atoms in a pulse can be stopped more efficiently with a mirror whose surface is given by a quadratic polynomial than with a flat mirror. In the quantum mechanical setting we additionally considered a mirror potential given by a ring whose radius increased along a square-root in time trajectory. We found that a ring with larger initial radius can be useful, since this might lead to a smaller final velocity if multiple collisions occur. Finally, we used the ring geometry to implement cooling cycles via a square-root in time expansion and a linear in time compression. Although a phase-space compression cannot be achieved with such a setup, i.e. without an irreversible step, we studied whether one could still obtain a reduction of the mean velocity. However, such a velocity reduction was not observed. Since we could show that the compression was adiabatic, we explained the former with an increase of the energy eigenvalue spacing due to the decreasing radius.

Motivated by the efficiency of a square-root in time trajectory for reducing the atomic

velocity, in **Chapter 4** we devised a scheme with which we not only achieve cooling and a phase-space compression of the atomic ensemble, but also trap the atoms during the process. We introduced the scheme in an idealized and one-dimensional classical setting, which consists of two mirrors moving along a square-root in time trajectory. The first mirror has the additional property that it lets the classical particle pass in the initial direction of movement, i.e. it mimics a diodic behaviour. We showed that such a scheme always leads to a reduction of the absolute value of the velocity and gave some bounds on the “worst case” velocity as well as how to decrease it. Following this we showed how to realize this scheme in the quantum mechanical framework. We combined an atom diode, i.e. a “one-way barrier”, with an atom mirror, which both have fixed distance and move along a square-root in time trajectory. This setup implements precisely the previously studied scheme in the classical case. Atoms in a pulse can pass the diode in one direction and become trapped between it and the following mirror. Since the first collision occurs with the mirror potential, the atoms are slowed and, depending on the initial width of the pulse, the ensemble is also compressed in space. This leads to a phase-space compression and cooling of the ensemble. We showed that this setup indeed leads to the desired effect by numerically solving the corresponding master-equation with the quantum jump approach. As expected from the classical considerations we were able to show that larger phase-space compressions can be achieved by, for example, decreasing the initial average ensemble and mirror distances.

In **Chapter 5** we proposed a “shortcut to adiabaticity”. An important and common technique used to manipulate atoms is state transfer via changing the parameters of some time-dependent Hamiltonian, with the objective to transfer some initial state to a desired final one, where both are instantaneous eigenstates of this Hamiltonian at the respective initial and final times. Although the adiabatic theorem provides a way to achieve this, in many cases one is interested in alternative methods, since the adiabatic approximation only holds for sufficiently slow evolution, whereas it would often be beneficial to perform such a process as fast as possible. A highly desirable goal would therefore be the preparation of the same final states as obtained in an adiabatic process, but in less time. In addition this procedure should be stable with respect to noise. This goal is achieved with the proposed shortcut to adiabaticity, which is based on invariants of the Hamiltonian. These invariants can be designed such that their eigenstates are, up to a global phase, also instantaneous eigenstates of the Hamiltonian at initial and final times. We then explore the degree of freedom that in general we do not require the state to be an eigenstate of the Hamiltonian at all times and let the state evolve along the invariants basis instead of the adiabatic basis. This can be achieved by fulfilling some auxiliary equations. Only afterwards we deduce the physical trajectories of the process. This “inverse” procedure coined the term “inverse-invariant” method. Applying this method we achieve much faster processes with fidelity equal to one as in a perfectly adiabatic process. We presented two applications of this protocol, namely the cooling of non-interacting atoms via harmonic trap expansion and the transport of Bose-Einstein condensates. In both cases we showed that the inverse-invariant method leads to a much faster process with perfect fidelity for a harmonic potential. Since a harmonic potential cannot be perfectly realized in an experiment, we also considered the effect of anharmonicities and showed that in both applications the scheme is stable. Since the auxiliary equations, which ensure an evolution along the invariants basis, do not lead to a unique trajectory, but rather a whole family of possible trajectories, we are left

with a degree of freedom to further optimize the process subject to different constraints. For the transport of a Bose-Einstein condensate we therefore applied optimal control theory and considered two different constraints, namely a bounded deviation of the ensemble from the trap center and a bounded shift of the trap, e.g. due to bounded space in a laboratory. In both cases we showed that so called “bang-bang” switches, i.e. discontinuous changes between the boundary values of these constraints, which are constant otherwise, are time-optimal and furthermore that among these exactly one switch leads to a minimal final time.

As might be expected, this work not only provided new insights and techniques to more efficiently control and manipulate atoms, but also provides new questions and possible extensions. We detail a selection of these in the following. Concerning the results in **Chapter 3** the following questions remain for future work:

- The appearance and width of the interference fringes occurring in the final position and momentum distributions in the quantum case are still to be explained in more detail. In the examples presented, the width in position space is antiproportional to the atom’s mass. To prove that this is generally the case as well as a thorough explanation for their appearance would be interesting. This could be studied by using the analytical solution we derived, and applying suitable approximations or considering appropriate limits.
- In the classical case a square-root in time trajectory is the optimal solution for stopping a particle with unknown velocity and we demonstrated its efficiency also in the quantum case. Furthermore, in the quantum case we were able to show that such a trajectory is at least optimal compared to any trajectory with an additional linear in time term. Here we mean by optimal that only for a pure square-root trajectory the energy expectation value goes to zero for infinite time. The reason for this restriction is that only for these trajectories the corresponding time-dependent Schrödinger equation is separable. In addition one can presumably also exclude trajectories leading to a positive mirror acceleration, which is evident in the classical case. Still there are arbitrary many other sublinear trajectories and a proof that the square-root in time trajectory is in general also optimal in the quantum case would be an interesting result. This might be accomplished using a different approach, e.g. optimal control theory and different optimality criteria.
- An important reason we considered the two different mirror geometries given by a quadratic polynomial and a ring is their symmetry and simplicity, both deemed necessary for a larger velocity reduction with respect to the setup considered. It would generally be interesting to consider other geometries too and furthermore to determine if there are better ones or even an optimal mirror geometry. Without any constraints on the geometry this problem does not seem to allow for a solution, but maybe appropriate constraints like certain symmetry assumptions might lead to a more tractable problem.
- Finally, it would be interesting to demonstrate the efficiency of the square-root in time trajectory also in a real experiment.

Chapter 4 poses the following questions:

- For the quantum catcher we showed that a classical particle is always slowed independent of its initial parameters and also determined some useful bounds on the velocities after subsequent collisions. The numerical results in the quantum case showed that this scheme still works, but an analytical treatment on the efficiency of this scheme and its dependence on the initial parameters would be desirable.
- As for the quantum stopper, an experimental realization of this scheme would be interesting, also to determine if, as we conjecture, larger phase-space compressions than in our numerical simulations would be achievable.

Finally, considering the results in **Chapter 5**, one could investigate the subsequent questions:

- Since the “inverse-invariant” method provides a whole family of possible trajectories, we used optimal control theory to determine the time-optimal solutions for the transport of Bose-Einstein condensates. However, these solutions have discontinuities, which apparently can only be approximately realized. It is therefore important to determine the effect due to these approximations. Moreover, it would not only be interesting to consider additional constraints, but also to consider different constraints simultaneously.
- We presented two examples of applications of the “inverse-invariant” method and publications by other authors show that its applications range even further. We assume that the method’s applications are still far from exhausted and that there exist other processes which could benefit from this method.

In this thesis we devised new laser-based techniques to more efficiently control and manipulate atomic motional states. All these techniques are in principle experimentally realisable with current technology and we are convinced that they will play an important role in future applications.

A Effective Potential for an Accelerated Laser

In Section 2.1 we showed that for large detuning the interaction between a laser and a two-level atom leads to an effective potential the atom experiences if it is in the ground state. However, the derivation was somewhat heuristic and in addition only valid for the case of a stationary laser. A more thorough derivation in the stationary case can be found in [9]. Since the proposals in Chapters 3 and 4 rely on such an effective potential induced by an accelerated laser, in the following we will give a derivation which is both more thorough and also applies to the case of an accelerated laser.

For simplicity we treat the problem in the following in a one-dimensional approximation by assuming that the atom impinges perpendicular on the laser field, i.e. $\vec{k}_L \vec{R} = 0$, though a generalization to three dimensions is straightforward. The derivations in Section 2.1 leading to the interaction Hamiltonian H_i given by eq. (2.26) for the atom-laser interaction are in principle still valid in this case. Considering an accelerated laser with trajectory $\sim \sqrt{t}$ only leads to a time-dependent Rabi frequency $\Omega(x,t) = \Omega(x - \sqrt{t})$ instead, which is straightforward to verify by considering the corresponding formulas and approximations leading to this Hamiltonian. Therefore the interaction Hamiltonian $H_i = H_i(t)$ is now given by

$$H_i = \frac{p^2}{2m} - \hbar\Delta|2\rangle\langle 2| - \frac{\hbar}{2} \left[|1\rangle\langle 2|\Omega(x - \sqrt{t}) + |2\rangle\langle 1|\Omega^*(x - \sqrt{t}) \right]. \quad (\text{A.1})$$

As before, the atom shall initially be in the ground state and the two-level Schrödinger equation for the Hamiltonian (A.1) is componentwise given by

$$\begin{aligned} i\hbar \frac{\partial}{\partial t} \Psi_t^1 &= \frac{p^2}{2m} \Psi_t^1 - \frac{\hbar}{2} \Omega(x - \sqrt{t}) \Psi_t^2 \\ i\hbar \frac{\partial}{\partial t} \Psi_t^2 &= \frac{p^2}{2m} \Psi_t^2 - \frac{\hbar}{2} \Omega^*(x - \sqrt{t}) \Psi_t^1 - \hbar\Delta \Psi_t^2 \end{aligned} \quad (\text{A.2})$$

with $\Psi_t^1 = \Psi^1(x,t)$ and $\Psi_t^2 = \Psi^2(x,t)$ the components corresponding to $|1\rangle$ and $|2\rangle$ respectively. It will become clear later why we keep the index t to denote the time-dependence. As in the stationary case we first consider the equation for the second component, which we rewrite as

$$\frac{\partial}{\partial t} \Psi_t^2 = -\frac{i}{\hbar} \left[\frac{p^2}{2m} - \hbar\Delta \right] \Psi_t^2 + \frac{i}{2} \Omega^*(x - \sqrt{t}) \Psi_t^1. \quad (\text{A.3})$$

In [153] it was shown that we can write the solution of this equation as¹

$$\begin{aligned}\Psi_t^2 &= e^{-\frac{i}{\hbar}[\frac{p^2}{2m}-\hbar\Delta]t}\Psi_0^2 + \int_0^t dt_1 e^{-\frac{i}{\hbar}[\frac{p^2}{2m}-\hbar\Delta](t-t_1)} \left[\left(-\frac{i}{\hbar}\right) \left(-\frac{\hbar}{2}\right) \Omega^*(x-\sqrt{t_1})\Psi_{t_1}^1 \right] \\ &= \int_0^t dt_1 e^{-\frac{i}{\hbar}[\frac{p^2}{2m}-\hbar\Delta](t-t_1)} \left[\frac{i}{2}\Omega^*(x-\sqrt{t_1})\Psi_{t_1}^1 \right],\end{aligned}\quad (\text{A.4})$$

since the atom is initially in the ground state, i.e. $\Psi_0^1 = 0$, and where $\left[\frac{i}{2}\Omega^*(x-\sqrt{t_1})\Psi_{t_1}^1\right]$ is the ‘‘memory kernel’’. We can also directly verify that this is indeed a solution via

$$\begin{aligned}\frac{\partial}{\partial t}\Psi_t^2 &= \frac{\partial}{\partial t} \int_0^t dt_1 e^{-\frac{i}{\hbar}[\frac{p^2}{2m}-\hbar\Delta](t-t_1)} \left[\frac{i}{2}\Omega^*(x-\sqrt{t_1})\Psi_{t_1}^1 \right] \\ &= \frac{\partial}{\partial t} e^{-\frac{i}{\hbar}[\frac{p^2}{2m}-\hbar\Delta]t} \int_0^t dt_1 e^{\frac{i}{\hbar}[\frac{p^2}{2m}-\hbar\Delta]t_1} \left[\frac{i}{2}\Omega^*(x-\sqrt{t_1})\Psi_{t_1}^1 \right] \\ &= -\frac{i}{\hbar} \left[\frac{p^2}{2m} - \hbar\Delta \right] e^{-\frac{i}{\hbar}[\frac{p^2}{2m}-\hbar\Delta]t} \int_0^t dt_1 e^{\frac{i}{\hbar}[\frac{p^2}{2m}-\hbar\Delta]t_1} \left[\frac{i}{2}\Omega^*(x-\sqrt{t_1})\Psi_{t_1}^1 \right] \\ &+ e^{-\frac{i}{\hbar}[\frac{p^2}{2m}-\hbar\Delta]t} e^{\frac{i}{\hbar}[\frac{p^2}{2m}-\hbar\Delta]t} \left[\frac{i}{2}\Omega^*(x-\sqrt{t})\Psi_t^1 \right] \\ &= -\frac{i}{\hbar} \left[\frac{p^2}{2m} - \hbar\Delta \right] \Psi_t^2 + \frac{i}{2}\Omega^*(x-\sqrt{t})\Psi_t^1.\end{aligned}$$

Using this result for the first component we therefore obtain

$$\frac{\partial}{\partial t}\Psi_t^1 = -\frac{i}{\hbar} \frac{p^2}{2m} \Psi_t^1 - \frac{\Omega(x-\sqrt{t})}{4} \int_0^t dt_1 e^{-\frac{i}{\hbar}[\frac{p^2}{2m}-\hbar\Delta](t-t_1)} \left[\Omega^*(x-\sqrt{t_1})\Psi_{t_1}^1 \right].$$

Setting $t_2 = t - t_1$ this can be rewritten as

$$\frac{\partial}{\partial t}\Psi_t^1 = -\frac{i}{\hbar} \frac{p^2}{2m} \Psi_t^1 - \frac{\Omega(x-\sqrt{t})}{4} \int_0^t dt_2 e^{-\frac{i}{\hbar}[\frac{p^2}{2m}-\hbar\Delta]t_2} \left[\Omega^*(x-\sqrt{t-t_2})\Psi_{t-t_2}^1 \right].$$

We now apply a form of Markov approximation to this expression by assuming that the detuning is much larger than the kinetic term, i.e. loosely speaking $|\hbar\Delta| \gg |\frac{p^2}{2m}|$. Then the integrand oscillates fast and gives only a significant contribution for $t_2 \approx 0$. In good approximation we can therefore extend the limit of integration to infinity. Additionally we can neglect the kinetic term in the exponent and obtain

$$\frac{\partial}{\partial t}\Psi_t^1 \approx -\frac{i}{\hbar} \frac{p^2}{2m} \Psi_t^1 - \frac{\Omega(x-\sqrt{t})}{4} \int_0^\infty dt_2 e^{i\Delta t_2} \left[\Omega^*(x-\sqrt{t-t_2})\Psi_{t-t_2}^1 \right].$$

1 The solution is actually derived for the stationary case, but it is straightforward to see that the result can be extended in this way since the generator of the unitary operator $e^{-\frac{i}{\hbar}[\frac{p^2}{2m}-\hbar\Delta]t}$ is time-independent.

Furthermore, since the integrand is rapidly damped we consider only the zeroth order of the series expansion of $\Omega^*(x - \sqrt{t-t_2})\Psi_{t-t_2}^1$ in t_2 and we therefore obtain

$$\begin{aligned} \frac{\partial}{\partial t}\Psi_t^1 &\approx -\frac{i}{\hbar}\frac{p^2}{2m}\Psi_t^1 - \frac{\Omega(x - \sqrt{t})}{4} \left[\int_0^\infty dt_2 e^{i\Delta t_2} \right] \Omega^*(x - \sqrt{t})\Psi_t^1 \\ &= -\frac{i}{\hbar}\frac{p^2}{2m}\Psi_t^1 + \frac{\Omega(x - \sqrt{t})}{4} \frac{1}{i\Delta} \Omega^*(x - \sqrt{t})\Psi_t^1. \end{aligned}$$

Since the detuning commutes with the Rabi frequency we finally obtain

$$i\hbar\frac{\partial}{\partial t}\Psi_t^1 \approx \left[\frac{p^2}{2m} + \frac{\hbar|\Omega(x - \sqrt{t})|^2}{4\Delta} \right] \Psi_t^1, \quad (\text{A.5})$$

i.e. the atom in the ground state experiences an effective potential which moves along a square-root in time trajectory. This potential is either attractive or repulsive depending on the detuning, see Section 2.1 for more details.

B Numerical Evolution of the Schrödinger Equation with Time-Dependent Potential

The numerical results for the quantum stopper in 1d for an infinitely high potential wall in Section 3.2, which was modelled by a time-dependent boundary condition, were obtained via the well known Crank-Nicholson method, see for example [154]. The results in the case of a more realistic Gaussian potential in the same section were obtained via time-evolution of the Schrödinger equation based on the also well known operator-splitting method and Fast Fourier Transform (FFT) [155]. Furthermore, the operator-splitting method was also used for the simulations in 2d in Section 3.3 as well as for the simulation of the quantum catcher in Chapter 4. The problem one faces when simulating the quantum stopper, and, in the case of the operator-splitting, also the quantum catcher, is, that the potentials are time-dependent, whereas the Crank-Nicholson method and the operator-splitting method are usually derived for and applied to time-independent potentials. It is not a priori clear if these methods are still applicable in the time-dependent case and, if so, how they might have to be altered. In the subsequent sections we will show that both can indeed be applied in the time-dependent case. In Appendix B.1 we will explicitly construct the Crank-Nicholson algorithm for a time-dependent boundary condition, showing that it provides the same accuracy as in the time-independent case, and in Appendix B.2 we will prove that the operator-splitting method for a time-dependent potential also gives the same accuracy as for a time-independent one.

The complete algorithms based on these methods to simulate the different physical situations are written in the programming language C and can be found in Appendix E. The actual implementation often allowed for a parallelized computation of some of the simulation steps. An example in the classical case are the calculations of the final parameters corresponding to a set of initial parameters given by the discretization in position and momentum space. For each point the corresponding equations can be solved independently and therefore these calculations can be carried out in parallel. For the algorithms in the quantum case using the operator-splitting for example the FFTW (“Fastest Fourier Transform in the West”) [156, 157], which is a C subroutine library to compute the discrete Fourier transform, includes routines to parallelize certain steps in the calculation of the Fourier transform. In addition to it various calculations necessary to perform one time step allow for parallelization. Examples are the computation of the respective exponential operators in position and momentum space for the discretized kinetic and potential terms, where especially the latter have to be calculated anew for each time-step since they are time-dependent, or the calculation of the wavefunction after such a time-step via multiplication with these operators.

On the working station we used to perform the simulations, 16 cores are available to carry

out certain computation steps in parallel, which already leads to a significant speed-up of the simulations. However, an even more significant speed-up was obtained by using the CUDA architecture developed by NVIDIA to carry out the performance intensive parts of the computation on a NVIDIA graphics card (or GPU) [158]. Computations usually performed by the CPU are transferred to the GPU instead, which allows for a massive parallelization. In our case for example 240 cores are available for parallel computing. This architecture is specifically designed to perform parallel computation and experiences an increasing number of applications in various fields like science, engineering and finance.

B.1 Crank-Nicholson Method for Time-Dependent Boundary Conditions

The Crank-Nicholson-Method is a second-order finite difference method implicit in time to solve certain partial differential equations, like the Schrödinger equation, with boundary conditions. The problem we are facing when simulating the quantum stopper in 1d is that we have to deal with time-dependent boundary conditions. In the following we will show by construction that we can still apply the Crank-Nicholson-Method and obtain the same accuracy as in the time-independent case.

We consider the Schrödinger equation for a free particle, which is given by

$$i \frac{\partial}{\partial t} \Psi(t, x) = -\frac{1}{2m} \frac{\partial^2}{\partial x^2} \Psi(t, x) \quad (\text{B.1})$$

with time-dependent boundary conditions

$$\Psi(t, \sqrt{t}) = \Psi(t, L + \sqrt{t}) = 0 \quad (\text{B.2})$$

and where we set $\hbar = 1$. It describes the time-evolution of particles in a moving box, where the walls move along a square-root in time trajectory. This situation is slightly more general than the situation considered in Chapter 3, but we can easily adjust it by a space translation $x \rightarrow x - L$ and choosing L to be large, such that only an interaction with the right boundary occurs. In the following derivation we will therefore only give the formulas corresponding to the right side of the box, while the ones corresponding to the left side can be derived analogously.

We can transform eqs. (B.1) and (B.2) to a problem with time-independent boundary conditions by setting $y = x - \sqrt{t}$ and $\Phi(t, y) = \Psi(t, y + \sqrt{t})$. This leads to the equation

$$i \frac{\partial}{\partial t} \Phi(t, y) = -\frac{1}{2m} \frac{\partial^2}{\partial y^2} \Phi(t, y) + \frac{i}{2\sqrt{t}} \frac{\partial}{\partial y} \Phi(t, y) \quad (\text{B.3})$$

with time-independent boundary conditions

$$\Phi(t, 0) = \Phi(t, L) = 0, \quad (\text{B.4})$$

which now describes the time evolution of the particles in the reference frame of the mirror. Note that this transformation is different to the one in Chapter 3, where we considered a scaling $\frac{x}{\sqrt{t}}$ for the analytical treatment of the quantum stopper in 1d.

The question is now how to discretize the time-evolution where we would like to achieve an accuracy of order $\mathcal{O}(\Delta t^3)$, which is the usual accuracy achieved with the Crank-Nicholson-Method. Important is that we have to ensure that the time-evolution is still unitary, i.e. the norm is conserved. The following proposition guarantees both requirements.

Proposition 15. *Given a time-dependent Hamiltonian $H(t)$, an approximate unitary time-evolution, approximating the exact time-evolution leading from the state $\psi(t)$ to the state $\psi(t + \Delta t)$ up to order $\mathcal{O}(\Delta t^3)$, is given by*

$$\left(\mathbb{1} + i \frac{\Delta t}{2} H \left(t + \frac{\Delta t}{2} \right) \right) |\psi(t + \Delta t)\rangle = \left(\mathbb{1} - i \frac{\Delta t}{2} H \left(t + \frac{\Delta t}{2} \right) \right) |\psi(t)\rangle + \mathcal{O}(\Delta t^3). \quad (\text{B.5})$$

Proof. The time-evolution is unitary, because

$$\begin{aligned} \langle \psi(t + \Delta t) | \psi(t + \Delta t) \rangle &= \langle \psi(t) | \frac{(\mathbb{1} + i \frac{\Delta t}{2} H(t + \frac{\Delta t}{2})) (\mathbb{1} - i \frac{\Delta t}{2} H(t + \frac{\Delta t}{2}))}{(\mathbb{1} - i \frac{\Delta t}{2} H(t + \frac{\Delta t}{2})) (\mathbb{1} + i \frac{\Delta t}{2} H(t + \frac{\Delta t}{2}))} | \psi(t) \rangle \\ &= \langle \psi(t) | \psi(t) \rangle. \end{aligned} \quad (\text{B.6})$$

In order to prove the accuracy we now expand $|\psi(t + \Delta t)\rangle$ in powers of Δt explicitly up to order $\mathcal{O}(\Delta t^2)$ and in this process we will also expand $H(t + \Delta t)$ in the integrals of the Dyson-series. We have

$$\begin{aligned} |\psi(t + \Delta t)\rangle &= \mathcal{T} \exp \left(-i \int_t^{t+\Delta t} dt' H(t') \right) |\psi(t)\rangle \\ &= |\psi(t)\rangle - i \int_t^{t+\Delta t} dt_1 H(t_1) |\psi(t)\rangle \\ &\quad - \int_t^{t+\Delta t} dt_1 \int_t^{t_1} dt_2 H(t_1) H(t_2) |\psi(t)\rangle \pm \dots \\ &= |\psi(t)\rangle - i \int_t^{t+\Delta t} dt_1 \left(H(t) + t_1 \dot{H}(t) + \frac{t_1^2}{2} \ddot{H}(t) + \dots \right) \\ &\quad - \int_t^{t+\Delta t} dt_1 \int_t^{t_1} dt_2 \left(H(t) + t_1 \dot{H}(t) + \frac{t_1^2}{2} \ddot{H}(t) + \dots \right) \\ &\quad \cdot \left(H(t) + t_2 \dot{H}(t) + \frac{t_2^2}{2} \ddot{H}(t) + \dots \right) |\psi(t)\rangle \pm \dots \\ &= |\psi(t)\rangle - i \Delta t H(t) |\psi(t)\rangle - i \frac{\Delta t^2}{2} \dot{H}(t) |\psi(t)\rangle - \frac{\Delta t^2}{2} H(t)^2 |\psi(t)\rangle \\ &\quad + \mathcal{O}(\Delta t^3), \end{aligned}$$

where \mathcal{T} denotes the time-ordering operator. Using this expansion we have

$$\begin{aligned}
& \left(\mathbb{1} + i \frac{\Delta t}{2} H \left(t + \frac{\Delta t}{2} \right) \right) |\psi(t + \Delta t)\rangle - \left(\mathbb{1} - i \frac{\Delta t}{2} H \left(t + \frac{\Delta t}{2} \right) \right) |\psi(t)\rangle \\
&= \left[\left(\mathbb{1} + i \frac{\Delta t}{2} \left(H(t) + \frac{\Delta t}{2} \dot{H}(t) \right) \right) \left(\mathbb{1} - i \Delta t H(t) - i \frac{\Delta t^2}{2} \dot{H}(t) - \frac{\Delta t^2}{2} H(0)^2 \right) \right. \\
&\quad \left. - \mathbb{1} + i \frac{\Delta t}{2} \left(H(t) + \frac{\Delta t}{2} \dot{H}(t) \right) \right] |\psi(t)\rangle + \mathcal{O}(\Delta t^3) \\
&= \left[\mathbb{1} - i \Delta t H(t) - i \frac{\Delta t^2}{2} \dot{H}(t) - \frac{\Delta t^2}{2} H(t)^2 + i \frac{\Delta t}{2} \left(H(t) + \frac{\Delta t}{2} \dot{H}(t) \right) + \frac{\Delta t^2}{2} H(t)^2 \right. \\
&\quad \left. + \mathcal{O}(\Delta t^3) - \mathbb{1} + i \frac{\Delta t}{2} H(t) + i \frac{\Delta t^2}{4} \dot{H}(t) \right] |\psi(t)\rangle + \mathcal{O}(\Delta t^3) \\
&= 0 + \mathcal{O}(\Delta t^3)
\end{aligned} \tag{B.7}$$

which proves eq. (B.5). \square

We will now apply this general result to our problem. According to eq. (B.3) the Hamiltonian $H(t)$ in our problem is given by

$$H(t) = -\frac{1}{2m} \frac{\partial^2}{\partial y^2} + \frac{i}{2\sqrt{t}} \frac{\partial}{\partial y}. \tag{B.8}$$

So far we derived an approximate expression for the time-evolution, but of course we also have to discretize the Hamiltonian in space. For the first and second derivatives we use a centered difference approximation, because this achieves an accuracy up to order $\mathcal{O}(\Delta y^2)$ instead of just $\mathcal{O}(\Delta y)$ for a naive approximation [154, 159]. To be more precise for a state $\Phi(t, y)$ we have

$$\begin{aligned}
\frac{\partial}{\partial y} \Phi(t, y) &= \frac{\Phi(t, y + \Delta y) - \Phi(t, y - \Delta y)}{2\Delta y} + \mathcal{O}(\Delta y^2) \\
\frac{\partial^2}{\partial y^2} \Phi(t, y) &= \frac{\Phi(t, y + \Delta y) - 2\Phi(t, y) + \Phi(t, y - \Delta y)}{\Delta y^2} + \mathcal{O}(\Delta y^2)
\end{aligned}$$

Combining this with eq. (B.3) and neglecting all terms of order $\mathcal{O}(\Delta t^3)$ and $\mathcal{O}(\Delta y^2)$, we obtain

$$\begin{aligned}
& \Phi(t + \Delta t, y) - i \frac{\Delta t}{4m} \left(\frac{\Phi(t + \Delta t, y + \Delta y) - 2\Phi(t + \Delta t, y) + \Phi(t + \Delta t, y - \Delta y)}{\Delta y^2} \right) \\
&- \frac{\Delta t}{4\sqrt{t + \frac{\Delta t}{2}}} \left(\frac{\Phi(t + \Delta t, y + \Delta y) - \Phi(t + \Delta t, y - \Delta y)}{2\Delta y} \right) \\
&= \Phi(t, y) + i \frac{\Delta t}{4m} \left(\frac{\Phi(t, y + \Delta y) - 2\Phi(t, y) + \Phi(t, y - \Delta y)}{\Delta y^2} \right) \\
&+ \frac{\Delta t}{4\sqrt{t + \frac{\Delta t}{2}}} \left(\frac{\Phi(t, y + \Delta y) - \Phi(t, y - \Delta y)}{2\Delta y} \right)
\end{aligned} \tag{B.9}$$

Rearranging these terms eq. (B.3) therefore finally becomes

$$\begin{aligned}
& \Phi(t + \Delta t, y) \left[1 + i \frac{\Delta t}{2m\Delta y^2} \right] - \Phi(t + \Delta t, y + \Delta y) \frac{\Delta t}{4\Delta y} \left[i \frac{1}{m\Delta y} + \frac{1}{2\sqrt{t + \frac{\Delta t}{2}}} \right] \\
& - \Phi(t + \Delta t, y - \Delta y) \frac{\Delta t}{4\Delta y} \left[i \frac{1}{m\Delta y} - \frac{1}{2\sqrt{t + \frac{\Delta t}{2}}} \right] \\
& = \Phi(t, y) \left[1 - i \frac{\Delta t}{2m\Delta y^2} \right] + \Phi(t, y + \Delta y) \frac{\Delta t}{4\Delta y} \left[i \frac{1}{m\Delta y} + \frac{1}{2\sqrt{t + \frac{\Delta t}{2}}} \right] \\
& + \Phi(t, y - \Delta y) \frac{\Delta t}{4\Delta y} \left[i \frac{1}{m\Delta y} - \frac{1}{2\sqrt{t + \frac{\Delta t}{2}}} \right]. \tag{B.10}
\end{aligned}$$

Now set $\beta := \frac{\Delta t}{4m\Delta y^2}$. Then it follows that

$$\begin{aligned}
& \Phi(t + \Delta t, y) [1 + 2i\beta] - \Phi(t + \Delta t, y + \Delta y) \left[i\beta + \frac{m\Delta y\beta}{2\sqrt{t + \frac{\Delta t}{2}}} \right] \\
& - \Phi(t + \Delta t, y - \Delta y) \left[i\beta - \frac{m\Delta y\beta}{2\sqrt{t + \frac{\Delta t}{2}}} \right] \\
& = \Phi(t, y) [1 - 2i\beta] + \Phi(t, y + \Delta y) \left[i\beta + \frac{m\Delta y\beta}{2\sqrt{t + \frac{\Delta t}{2}}} \right] \\
& + \Phi(t, y - \Delta y) \left[i\beta - \frac{m\Delta y\beta}{2\sqrt{t + \frac{\Delta t}{2}}} \right]. \tag{B.11}
\end{aligned}$$

Now define $y_j := j\Delta y$, $\Delta y := \frac{L}{m+1}$, $\Phi_j := \Phi(t, j\Delta y)$ and $\tilde{\Phi}_j := \Phi(t + \Delta t, j\Delta y)$. The boundary conditions are $\Phi_0 = \Phi(t, 0) = \Phi_{m+1} = \Phi(t, L) = 0$ and $\tilde{\Phi}_0 = \Phi(t + \Delta t, 0) =$

$\tilde{\Phi}_{m+1} = \Phi(t + \Delta t, L) = 0$. With these definitions it follows that

$$\begin{aligned}
& -\tilde{\Phi}_{j+1} \left[i\beta + \frac{m\Delta y\beta}{2\sqrt{t + \frac{\Delta t}{2}}} \right] + \tilde{\Phi}_j [1 + 2i\beta] - \tilde{\Phi}_{j-1} \left[i\beta - \frac{m\Delta y\beta}{2\sqrt{t + \frac{\Delta t}{2}}} \right] \\
= & \Phi_{j+1} \left[i\beta + \frac{m\Delta y\beta}{2\sqrt{t + \frac{\Delta t}{2}}} \right] + \Phi_j [1 - 2i\beta] + \Phi_{j-1} \left[i\beta - \frac{m\Delta y\beta}{2\sqrt{t + \frac{\Delta t}{2}}} \right] \\
\Leftrightarrow & \tilde{\Phi}_{j+1} - \tilde{\Phi}_j \left[\frac{1 + 2i\beta}{i\beta + \frac{m\Delta y\beta}{2\sqrt{t + \frac{\Delta t}{2}}}} \right] - \tilde{\Phi}_{j-1} \left[\frac{\left(i\beta - \frac{m\Delta y\beta}{2\sqrt{t + \frac{\Delta t}{2}}} \right)}{\frac{m^2\Delta y^2\beta^2}{4(t + \frac{\Delta t}{2}) + \beta^2}} \right] \\
= & -\Phi_{j+1} + \Phi_j \left[\frac{1 + 2i\beta}{i\beta + \frac{m\Delta y\beta}{2\sqrt{t + \frac{\Delta t}{2}}}} \right] + \Phi_{j-1} \left[\frac{\left(i\beta - \frac{m\Delta y\beta}{2\sqrt{t + \frac{\Delta t}{2}}} \right)}{\frac{m^2\Delta y^2\beta^2}{4(t + \frac{\Delta t}{2}) + \beta^2}} \right]. \tag{B.12}
\end{aligned}$$

Furthermore, by setting

$$\begin{aligned}
s & := \frac{1 + 2i\beta}{i\beta + \frac{m\Delta y\beta}{2\sqrt{t + \frac{\Delta t}{2}}}} = \frac{2\beta^2 + \frac{m\Delta y\beta}{2\sqrt{t + \frac{\Delta t}{2}}} + i \left(\frac{2m\Delta y\beta^2}{2\sqrt{t + \frac{\Delta t}{2}}} - \beta \right)}{\beta^2 + \frac{m^2\Delta y^2\beta^2}{4(t + \frac{\Delta t}{2})}} \\
r & := \frac{1 - 2i\beta}{i\beta + \frac{m\Delta y\beta}{2\sqrt{t + \frac{\Delta t}{2}}}} = \frac{-2\beta^2 + \frac{m\Delta y\beta}{2\sqrt{t + \frac{\Delta t}{2}}} - i \left(\frac{2m\Delta y\beta^2}{2\sqrt{t + \frac{\Delta t}{2}}} + \beta \right)}{\beta^2 + \frac{m^2\Delta y^2\beta^2}{4(t + \frac{\Delta t}{2})}} \\
w & := \frac{\left(i\beta - \frac{m\Delta y\beta}{2\sqrt{t + \frac{\Delta t}{2}}} \right)^2}{\beta^2 + \frac{m^2\Delta y^2\beta^2}{4(t + \frac{\Delta t}{2})}} = \frac{\frac{m^2\Delta y^2\beta^2}{4(t + \frac{\Delta t}{2})} - \beta^2 - \frac{im\Delta y\beta^2}{\sqrt{t + \frac{\Delta t}{2}}}}{\beta^2 + \frac{m^2\Delta y^2\beta^2}{4(t + \frac{\Delta t}{2})}} \tag{B.13}
\end{aligned}$$

and $\vec{\Phi} = (\Phi_1, \dots, \Phi_n)$ it follows that

$$M\vec{\Phi} = V\vec{\Phi}, \tag{B.14}$$

where

$$M = \begin{pmatrix} -s & 1 & 0 & \dots & 0 \\ -w & -s & 1 & 0 & \dots & \vdots \\ 0 & \ddots & \ddots & \ddots & & \\ \vdots & & & & & \\ 0 & \dots & & & -w & -s \end{pmatrix} \tag{B.15}$$

and

$$V = \begin{pmatrix} -r & -1 & 0 & \dots & 0 \\ w & -r & -1 & 0 & \dots & \vdots \\ 0 & \ddots & \ddots & \ddots & & \\ \vdots & & & & & \\ 0 & \dots & & & w & -r \end{pmatrix}. \quad (\text{B.16})$$

Now set $\vec{b} := V\vec{\Phi}$ with

$$\begin{aligned} b_1 &= -\Phi_2 - r\Phi_1 \\ b_j &= -\Phi_{j+1} - r\Phi_j + w\Phi_{j-1}, \quad j = 2, \dots, m-1. \\ b_m &= -r\Phi_m + w\Phi_{m-1} \end{aligned} \quad (\text{B.17})$$

Furthermore, we write

$$M = \begin{pmatrix} a_{11} & a_{12} & \dots \\ a_{21} & \ddots & \\ \vdots & & \end{pmatrix}, \quad (\text{B.18})$$

with

$$\begin{aligned} \alpha_{j+1,j} &= -w, \quad j = 1, \dots, m-1 \\ \alpha_{j-1,j} &= 1, \quad j = 2, \dots, m \end{aligned} \quad (\text{B.19})$$

and where all the other entries are zero. With all the definitions given above we therefore can finally state the Crank-Nicholson algorithm for time-dependent boundary conditions.

The Crank-Nicholson algorithm for time-dependent boundary conditions

Step 1: Forward substitution

$$\begin{aligned} \text{Calculate } \tilde{y}_1 &= \frac{b_1}{u_{11}} \text{ with } u_{11} = a_{11} = -s \text{ and } \tilde{y}_j = \frac{b_j - a_{j,j-1}\tilde{y}_{j-1}}{u_{jj}} \\ &= \frac{b_j + w\tilde{y}_{j-1}}{u_{jj}} \text{ with } u_{jj} = a_{jj} - a_{j-1,j}\frac{a_{j,j-1}}{u_{j-1,j-1}} = -s + \frac{w}{u_{j-1,j-1}}, \quad j = 2, \dots, m \end{aligned}$$

Step 2: Backward substitution

$$\begin{aligned} \text{Now calculate } \tilde{\Phi}_m &= \tilde{y}_m \text{ and } \tilde{\Phi}_j = \tilde{y}_j - \frac{a_{j,j+1}}{u_{jj}}\tilde{\Phi}_{j+1} = \tilde{y}_j - \frac{\tilde{\Phi}_{j+1}}{u_{jj}}, \\ &j = m-1, \dots, 1, \text{ and with } u_{jj} \text{ given as in step 1} \end{aligned}$$

Step 3: Repeat step 1 and step 2 with the updated values as new initial values until the desired evolution is complete.

B.2 Operator-Splitting for Time-Dependent Hamiltonians

When facing the task of solving a time-dependent Schrödinger equation numerically, the method of choice usually is the "splitting operator method" or just "operator-splitting" in the case that the Hamiltonian $H = T + V$ is time-independent. Using the series expansion of $e^{-i\Delta t H} = e^{-i\Delta t(T+V)}$, which describes the exact time-evolution during a time step Δt , it is straightforward to show that

$$e^{-i\Delta t(T+V)} - e^{-i\frac{\Delta t}{2}V} e^{-i\Delta t T} e^{-i\frac{\Delta t}{2}V} = 0 + \mathcal{O}(\Delta t^3). \quad (\text{B.20})$$

where again we set $\hbar = 1$. This approximation is useful since via the numerically powerful Fast Fourier Transform (FFT) the action of the single operators on the left hand side is just a multiplication in position or momentum space respectively. The whole algorithm implementing the time-evolution is then essentially given as a sequence of multiplications with matrix exponentials of the kinetic term and the potential with a FFT between each of these. The problem one now faces in the numerical simulations in Chapter 3 and 4 is that the Hamiltonian is time-dependent. Nevertheless, it would be desirable to obtain a similarly efficient way of simulating the time-evolution, but it is a priori not clear if one can still apply the operator-splitting and, if so, that it has the same accuracy as for a time-independent potential. In the following we will prove that the method is not only still applicable, but that it also provides the same accuracy, i. e. we will prove:¹

Proposition 16. *For a time-dependent Hamiltonian $H(t) = T + V(t)$ the exact time-evolution during a time step Δt given by*

$$\mathcal{T} e^{-i \int_{t_0}^{t_0+\Delta t} H(t') dt'} = \mathcal{T} e^{-i \int_{t_0}^{t_0+\Delta t} T+V(t') dt'}$$

can be approximated by

$$e^{-i\frac{\Delta t}{4}(V(t_0+\Delta t)+V(t_0))} e^{-i\Delta t T} e^{-i\frac{\Delta t}{4}(V(t_0+\Delta t)+V(t_0))}$$

with an accuracy of order $\mathcal{O}(\Delta t^3)$, i. e.

$$\begin{aligned} & \mathcal{T} e^{-i \int_{t_0}^{t_0+\Delta t} T+V(t') dt'} - e^{-i\frac{\Delta t}{4}(V(t_0+\Delta t)+V(t_0))} e^{-i\Delta t T} e^{-i\frac{\Delta t}{4}(V(t_0+\Delta t)+V(t_0))} \\ &= 0 + \mathcal{O}(\Delta t^3) \end{aligned}$$

Proof. The proof is straightforward by considering the series expansions of the single terms explicitly up to order $\mathcal{O}(\Delta t^2)$. W.l.o.g. we assume $t_0 = 0$. We have

$$\begin{aligned} e^{-i\frac{\Delta t}{4}(V(\Delta t)+V(0))} &= \mathbb{1} - i\frac{\Delta t}{4}[V(\Delta t) + V(0)] \\ &+ \frac{1}{2}(-i)^2 \frac{\Delta t^2}{16}[V(\Delta t) + V(0)]^2 + \mathcal{O}(\Delta t^3) \end{aligned}$$

¹ The symbol \mathcal{T} denotes the usual time-ordering operator.

and

$$e^{-i\Delta t T} = \mathbb{1} - i\Delta t T + (-i)^2 \frac{\Delta t^2}{2} T^2 + \mathcal{O}(\Delta t^3). \quad (\text{B.21})$$

Therefore we have

$$\begin{aligned} & e^{-i\Delta t T} e^{-i\frac{\Delta t}{4}(V(\Delta t)+V(0))} \\ &= \mathbb{1} - i\Delta t T - i\frac{\Delta t}{4}[V(\Delta t) + V(0)] - \frac{1}{2} \frac{\Delta t^2}{16} [V(\Delta t) + V(0)]^2 \\ & \quad - \frac{\Delta t^2}{4} (T[V(\Delta t) + V(0)] + [V(\Delta t) + V(0)]T) - \frac{\Delta t^2}{2} T^2 \\ & \quad + \mathcal{O}(\Delta t^3) \end{aligned}$$

and it follows that

$$\begin{aligned} & e^{-i\frac{\Delta t}{4}(V(\Delta t)+V(0))} e^{-i\Delta t T} e^{-i\frac{\Delta t}{4}(V(\Delta t)+V(0))} \\ &= \mathbb{1} - i\frac{\Delta t}{4}[V(\Delta t) + V(0)] - \frac{\Delta t^2}{32} [V(\Delta t) + V(0)]^2 \\ & \quad - i\Delta t T - \frac{\Delta t^2}{4} (T[V(\Delta t) + V(0)] + [V(\Delta t) + V(0)]T) - \frac{\Delta t^2}{2} T^2 \\ & \quad - \frac{\Delta t^2}{16} [V(\Delta t) + V(0)]^2 - \frac{\Delta t^2}{32} [V(\Delta t) + V(0)]^2 + \mathcal{O}(\Delta t^3) \\ &= \mathbb{1} - i\Delta t \left[T + \frac{1}{2}(V(\Delta t) + V(0)) \right] \\ & \quad - \Delta t^2 \left[\frac{1}{2} T^2 + \frac{1}{4} T(V(\Delta t) + V(0)) + \frac{1}{4} (V(\Delta t) + V(0))T \right. \\ & \quad \left. + \frac{1}{8} (V(\Delta t) + V(0))^2 \right] + \mathcal{O}(\Delta t^3). \quad (\text{B.22}) \end{aligned}$$

Now using the series expansion of $V(\Delta t)$ in the terms proportional to Δt^2 we obtain

$$e^{-i\frac{\Delta t}{4}(V(\Delta t)+V(0))} e^{-i\Delta t T} e^{-i\frac{\Delta t}{4}(V(\Delta t)+V(0))} \quad (\text{B.23})$$

$$\begin{aligned} &= \mathbb{1} - i\Delta t \left[T + \frac{1}{2}(V(\Delta t) + V(0)) \right] \\ & \quad - \frac{\Delta t^2}{2} \left[T^2 + TV(0) + V(0)T + V(0)^2 \right] + \mathcal{O}(\Delta t^3). \quad (\text{B.24}) \end{aligned}$$

For the exact time-evolution on the other hand we have

$$\begin{aligned} \mathcal{T} e^{-i \int_0^{\Delta t} T+V(t') dt'} &= \mathbb{1} + (-i) \int_0^{\Delta t} T + V(t_1) dt_1 \\ & \quad + (-i)^2 \int_0^{\Delta t} \int_0^{t_1} (T + V(t_1))(T + V(t_2)) dt_2 dt_1 + \mathcal{O}(\Delta t^3) \\ &= \mathbb{1} - i \int_0^{\Delta t} T + V(t_1) dt_1 \\ & \quad - \int_0^{\Delta t} \int_0^{t_1} T^2 + V(t_1)T + TV(t_2) + V(t_1)V(t_2) dt_2 dt_1 \\ & \quad + \mathcal{O}(\Delta t^3). \quad (\text{B.25}) \end{aligned}$$

We now evaluate the integrals containing the time-dependent potentials separately, by using the trapezium rule. For a rigorous mathematical derivation of the trapezium rule for bounded operators see for example [160]. We have

$$\begin{aligned}
\int_0^{\Delta t} V(t_1) dt_1 &= \frac{1}{2}(V(\Delta t) + V(0))\Delta t + \mathcal{O}(\Delta t^3) \\
\int_0^{\Delta t} \int_0^{t_1} V(t_1)T dt_2 dt_1 &= \int_0^{\Delta t} V(t_1)T t_1 dt_1 = V(t)T \frac{\Delta t^2}{2} + \mathcal{O}(\Delta t^3) \\
\int_0^{\Delta t} \int_0^{t_1} TV(t_2) dt_2 dt_1 &= \frac{1}{2} \int_0^{\Delta t} T(V(t_1) + V(0))t_1 dt_1 + \mathcal{O}(\Delta t^3) \\
&= TV(\Delta t) \frac{\Delta t^2}{4} + TV(0) \frac{\Delta t^2}{4} + \mathcal{O}(\Delta t^3) \\
\int_0^{\Delta t} \int_0^{t_1} V(t_1)V(t_2) dt_2 dt_1 &= \frac{1}{2} \int_0^{\Delta t} V(t_1)(V(t_1) + V(0))t_1 dt_1 + \mathcal{O}(\Delta t^3) \\
&= V(\Delta t)^2 \frac{\Delta t^2}{4} + V(\Delta t)V(0) \frac{\Delta t^2}{4} + \mathcal{O}(\Delta t^3).
\end{aligned}$$

For the expansion of the exact time-evolution up to order $\mathcal{O}(\Delta t^2)$ it therefore follows

$$\begin{aligned}
\mathcal{T}e^{-i \int_0^{\Delta t} T+V(t') dt'} &= \mathbb{1} - i\Delta t \left[T + \frac{1}{2}(V(\Delta t) + V(0)) \right] - \Delta t^2 \left[\frac{1}{2}T^2 + \frac{1}{2}V(\Delta t)T \right. \\
&\quad \left. + \frac{1}{4}TV(\Delta t) + \frac{1}{4}TV(0) + \frac{1}{4}V(\Delta t)^2 + \frac{1}{4}V(\Delta t)V(0) \right] \\
&\quad + \mathcal{O}(\Delta t^3). \tag{B.26}
\end{aligned}$$

Expanding $V(\Delta t)$ again around 0 in the terms proportional to Δt^2 we have

$$\begin{aligned}
\mathcal{T}e^{-i \int_0^{\Delta t} T+V(t') dt'} &= \mathbb{1} - i\Delta t \left[T + \frac{1}{2}(V(\Delta t) + V(0)) \right] \\
&\quad - \frac{\Delta t^2}{2} \left[T^2 + TV(0) + V(0)T + V(0)^2 \right] + \mathcal{O}(\Delta t^3). \tag{B.27}
\end{aligned}$$

Comparing eqs. (B.24) and (B.27) we finally obtain

$$\begin{aligned}
&\mathcal{T}e^{-i \int_0^{\Delta t} T+V(t') dt'} - e^{-i \frac{\Delta t}{4}(V(\Delta t)+V(0))} e^{-i\Delta t T} e^{-i \frac{\Delta t}{4}(V(\Delta t)+V(0))} \\
&= 0 + \mathcal{O}(\Delta t^3) \tag{B.28}
\end{aligned}$$

which proves the proposition. \square

C Perturbation Theory for Time-Dependent Hamiltonians

In time-dependent perturbation theory one usually considers the problem of finding the eigenfunctions and eigenvalues of a time-dependent Hamiltonian $H_s(t)$, which is given by

$$H_s(t) = H_0 + H_1(t), \quad (\text{C.1})$$

and where H_0 is a time-independent part for which the solutions are known [63, 64]. The time-dependent part $H_1(t)$ which is then treated as a perturbation. In the situation we consider on the other hand the part of the Hamiltonian with known solutions is already time-dependent itself and a time-dependent perturbation is added. Therefore it is not clear if standard results of time-dependent perturbation theory can be applied, since, for example, certain steps in their derivation rely on the time-independence of H_0 . In the following we will derive the formulas for time-dependent perturbation theory where the part with known solutions is itself time-dependent, i.e. $H_0(t)$. The proof evolves along the same lines as the standard one, but uses more fundamental properties of the operators involved.

We want to solve the Schrödinger equation

$$i\hbar \frac{\partial}{\partial t} |\psi_s(t)\rangle = H_s(t) |\psi_s(t)\rangle \quad (\text{C.2})$$

where

$$H_s(t) = H_0(t) + H_1(t) \quad (\text{C.3})$$

and the solutions of $H_0(t)$ are known. The index s denotes the Schrödinger picture. Eq. (C.2) is equivalent to

$$|\psi_s(t)\rangle = U(t, t_0) |\psi(t_0)\rangle \quad (\text{C.4})$$

with

$$i\hbar \frac{\partial}{\partial t} U(t, t_0) = H_s(t) U(t, t_0) \quad \text{and} \quad U(t_0, t_0) = \mathbb{1}. \quad (\text{C.5})$$

By repeated integration of this equation it follows that

$$U(t, t_0) = \mathbb{1} - \frac{i}{\hbar} \int_{t_0}^t dt' H_s(t') U(t', t_0) \quad (\text{C.6})$$

$$= \mathbb{1} - \frac{i}{\hbar} \int_{t_0}^t dt' H_s(t') \left[\mathbb{1} - \frac{i}{\hbar} \int_{t_0}^{t'} dt'' H_s(t'') U(t'', t_0) \right] \quad (\text{C.7})$$

$$= \dots \quad (\text{C.8})$$

$$= \sum_{n=0}^{\infty} \tilde{U}_n(t, t_0) \quad (\text{C.9})$$

with

$$\tilde{U}_n(t, t_0) = \left(-\frac{i}{\hbar} \right)^n \int_{t_0}^t dt_n \int_{t_0}^{t_n} dt_{n-1} \dots \int_{t_0}^{t_2} dt_1 H_s(t_n) \dots H_s(t_1), \quad \tilde{U}_0(t, t_0) = \mathbb{1}. \quad (\text{C.10})$$

and $t \geq t_n \geq t_{n-1} \geq \dots \geq t_1$. Therefore it follows that

$$U(t, t_0) = \exp \left(-\frac{i}{\hbar} \int_{t_0}^t dt' H_s(t') \right). \quad (\text{C.11})$$

We now change to the interaction picture. The state $|\psi_i(t)\rangle$ in the interaction picture is given by

$$\begin{aligned} |\psi_i(t)\rangle &:= \exp \left(\frac{i}{\hbar} \int_{t_0}^t dt' H_0(t') \right) |\psi_s(t)\rangle = U_0^\dagger(t, t_0) |\psi_s(t)\rangle \\ &= \exp \left(\frac{i}{\hbar} \int_{t_0}^t dt' H_0(t') \right) \exp \left(-\frac{i}{\hbar} \int_{t_0}^t dt' (H_0(t') + H_1(t')) \right) |\psi_s(t_0)\rangle \\ &= U_0^\dagger(t, t_0) U(t, t_0) |\psi_s(t_0)\rangle = U_1(t, t_0) |\psi_s(t_0)\rangle, \end{aligned} \quad (\text{C.12})$$

where $U_0(t, t_0) = \exp \left(-\frac{i}{\hbar} \int_{t_0}^t dt' H_0(t') \right)$ and $U_1(t, t_0) = \exp \left(-\frac{i}{\hbar} \int_{t_0}^t dt' H_1(t') \right)$ are just the time-evolution operators generated by the single Hamiltonians $H_0(t)$ and $H_1(t)$ respectively. We now proceed in the usual way by differentiating the state to obtain the Hamiltonian in the interaction picture, i.e.

$$\begin{aligned} i\hbar \frac{\partial}{\partial t} |\psi_i(t)\rangle &= i\hbar \frac{\partial}{\partial t} (U_0^\dagger(t, t_0) |\psi_s(t)\rangle) \\ &= \left(i\hbar \frac{\partial}{\partial t} U_0^\dagger(t, t_0) \right) |\psi_s(t)\rangle + U_0^\dagger(t, t_0) i\hbar \frac{\partial}{\partial t} |\psi_s(t)\rangle. \end{aligned} \quad (\text{C.13})$$

Using

$$\left(i\hbar \frac{\partial}{\partial t} U_0(t, t_0) \right)^\dagger = (H_0(t) U_0(t, t_0))^\dagger \Leftrightarrow -i\hbar \frac{\partial}{\partial t} U_0^\dagger(t, t_0) = U_0^\dagger(t, t_0) H_0(t) \quad (\text{C.14})$$

one obtains

$$\begin{aligned}
i\hbar \frac{\partial}{\partial t} |\psi_i(t)\rangle &= -U_0^\dagger(t, t_0) H_0(t) |\psi_s(t)\rangle + U_0^\dagger(t, t_0) i\hbar \frac{\partial}{\partial t} |\psi_s(t)\rangle \\
&= -U_0^\dagger(t, t_0) H_0(t) U_0(t, t_0) |\psi_i(t)\rangle + U_0^\dagger(t, t_0) H_s(t) |\psi_s(t)\rangle \\
&= -U_0^\dagger(t, t_0) H_0(t) U_0(t, t_0) |\psi_i(t)\rangle + U_0^\dagger(t, t_0) H_s(t) U_0(t, t_0) U_0^\dagger(t, t_0) |\psi_s(t)\rangle \\
&= -U_0^\dagger(t, t_0) H_0(t) U_0(t, t_0) |\psi_i(t)\rangle + U_0^\dagger(t, t_0) H_s(t) U_0(t, t_0) |\psi_i(t)\rangle. \quad (\text{C.15})
\end{aligned}$$

Therefore one has

$$i\hbar \frac{\partial}{\partial t} |\psi_i(t)\rangle = U_0^\dagger(t, t_0) \underbrace{(H_s(t) - H_0(t))}_{H_1(t)} U_0(t, t_0) |\psi_i(t)\rangle \quad (\text{C.16})$$

$$\begin{aligned}
&\underbrace{\hspace{10em}}_{H_i(t)} \\
&= H_i(t) |\psi_i(t)\rangle. \quad (\text{C.17})
\end{aligned}$$

Integrating eq. (C.17) with some initial condition $|\psi_i(t_0)\rangle$ it follows that

$$|\psi_i(t)\rangle = |\psi_i(t_0)\rangle - \frac{i}{\hbar} \int_{t_0}^t dt' H_i(t') |\psi_i(t')\rangle. \quad (\text{C.18})$$

Now we go back to the Schrödinger picture. Since $|\psi_i(t_0)\rangle = |\psi_s(t_0)\rangle$ we have

$$U_0^\dagger(t, t_0) |\psi_s(t)\rangle = |\psi_s(t_0)\rangle - \frac{i}{\hbar} \int_{t_0}^t dt' U_0^\dagger(t', t_0) H_1(t') \underbrace{U_0(t', t_0) U_0^\dagger(t', t_0)}_{\mathbb{1}} |\psi_s(t')\rangle.$$

For $|\psi_s(t)\rangle$ it therefore follows that

$$\begin{aligned}
|\psi_s(t)\rangle &= U_0(t, t_0) |\psi_s(t_0)\rangle - \frac{i}{\hbar} U_0(t, t_0) \int_{t_0}^t dt' U_0^\dagger(t', t_0) H_1(t') |\psi_s(t')\rangle \\
&= U_0(t, t_0) |\psi_s(t_0)\rangle - \frac{i}{\hbar} \int_{t_0}^t dt' U_0(t, t_0) U_0^\dagger(t', t_0) H_1(t') |\psi_s(t')\rangle \\
&= U_0(t, t_0) |\psi_s(t_0)\rangle - \frac{i}{\hbar} \int_{t_0}^t dt' U_0(t, t_0) U_0(t_0, t') H_1(t') |\psi_s(t')\rangle,
\end{aligned}$$

where we used $U_0^\dagger(t', t_0) = U_0^{-1}(t', t_0) = U_0(t_0, t')$. Furthermore, using $U_0(t, t_0) U_0(t_0, t') = U_0(t, t')$ this leads to

$$|\psi_s(t)\rangle = U_0(t, t_0) |\psi_s(t_0)\rangle - \frac{i}{\hbar} \int_{t_0}^t dt' U_0(t, t') H_1(t') |\psi_s(t')\rangle. \quad (\text{C.19})$$

Now let $H_1(t) = \lambda V(t)$ with $0 < \lambda \in \mathbb{R}$ the perturbation parameter. Substituting this in eq. (C.19) we obtain

$$|\psi_s(t)\rangle = U_0(t, t_0) |\psi_s(t_0)\rangle - \frac{i}{\hbar} \lambda \int_{t_0}^t dt' U_0(t, t') V(t') |\psi_s(t')\rangle. \quad (\text{C.20})$$

Inserting this again in $|\psi_s(t')\rangle$ and repeating this process we have

$$\begin{aligned}
|\psi_s(t)\rangle &= U_0(t,t_0) |\psi_s(t_0)\rangle \\
&+ \left(-\frac{i}{\hbar}\right) \lambda \int_{t_0}^t dt' U_0(t,t') V(t') U_0(t',t_0) |\psi_s(t_0)\rangle \\
&+ \left(-\frac{i}{\hbar}\right)^2 \lambda^2 \int_{t_0}^t dt' \int_{t_0}^{t'} dt'' U_0(t,t') V(t') U_0(t',t'') V(t'') |\psi_s(t_0)\rangle \\
&= \dots \\
&= \left[U_0(t,t_0) + \sum_{n=1}^{\infty} \lambda^n U_{0,n}(t,t_0) \right] |\psi_s(t_0)\rangle
\end{aligned} \tag{C.21}$$

where we set

$$\begin{aligned}
U_{0,n}(t,t_0) &= \left(-\frac{i}{\hbar}\right)^n \int_{t_0}^t dt_n \int_{t_0}^{t_n} dt_{n-1} \dots \int_{t_0}^{t_2} dt_1 U_0(t,t_n) V(t_n) U_0(t_n,t_{n-1}) \\
&\cdot \dots U_0(t_2,t_1) V(t_1) U_0(t_1,t_0).
\end{aligned} \tag{C.22}$$

We finally obtain that given an initial state $|\psi_s(t_0)\rangle$ and time-dependent Hamiltonian $H(t) = H_0(t) + \lambda V(t)$, the state at time $t > t_0$ is given by

$$|\psi_s(t)\rangle = \left[U_0(t,t_0) + \sum_{n=1}^{\infty} \lambda^n U_{0,n}(t,t_0) \right] |\psi_s(t_0)\rangle \tag{C.23}$$

where $U_0(t,t_0)$ is the time-evolution generated by $H_0(t)$ and $U_{0,n}(t,t_0)$ is given by eq. (C.22).

D Interswitching Time via “Conjugate Point” Method in Optimal Control Theory

In the following we will give an alternative proof of Proposition 11 in Chapter 5, Section 5.5, using the concept of a “conjugate point”, which we will briefly introduce hereafter. This concept was originally defined by Sussmann in [161, 162], and it is, amongst other things, a useful method to determine the interswitching times for time-optimal controls. The following description is guided by a similar discussion for the expansion of a harmonic trap in [142]. This concept is closely related to the technique applied in the proof (b) of Proposition 11 in Section 5.5, but the following considerations are more general.

We consider two switching points which we shall denote by $\vec{a} = (a_1, a_2)$ and $\vec{b} = (b_1, b_2)$. Let t_s be the time to reach \vec{b} from \vec{a} , i.e. t_s is the interswitching time¹. We will denote the trajectory between the switching points \vec{a} and \vec{b} as A-trajectory, e.g. for the second constraint in Section 5.5 a trajectory with constant control $q_{\downarrow, \uparrow}$.

W.l.o.g. we assume the trajectory passes through \vec{a} at time 0 and is at \vec{b} at time t_s . Since \vec{a} and \vec{b} are switching points the corresponding multipliers, due to condition (c) in Theorem 4, must be orthogonal to the control vector fields, i.e. we have $\langle \vec{p}(0) | \vec{g}(\vec{a}) \rangle = 0$ and $\langle \vec{p}(t_s) | \vec{g}(\vec{b}) \rangle = 0$. We continue by computing what the last condition implies at time 0. This is done by moving the vector field along the respective trajectory backwards from \vec{b} to \vec{a} . To achieve this we use the solution $\vec{\lambda}(t)$ of the variational equation along this trajectory with initial condition $\vec{\lambda}(t_s) = \vec{g}(\vec{b})$. The variational equation is represented by the linear system $\dot{\vec{\lambda}} = \vec{\lambda}M$, where M is the matrix of the adjoint equation of Theorem 4. Let us symbolically denote the value of the A-trajectory at time t , starting at \vec{a} at time 0, by e^{tA} and by e_{ad}^{-tA} the backwards evolution under the variational equation. Using this notation we can represent the solution as

$$\vec{\lambda}(0) = e_{ad}^{-t_s A} \vec{\lambda}(t_s) = e^{-t_s A} \vec{g}(\vec{b}) = e_{ad}^{-t_s A} \vec{g}(e^{t_s A}(\vec{a})). \quad (\text{D.1})$$

The vector field $e_{ad}^{-t_s A} \circ \vec{g} \circ e^{t_s A}(\vec{a})$ is also called the dragged field. Since the adjoint equation in Theorem 4 is precisely the adjoint equation to the variational equation, the function $t \rightarrow \langle \vec{p}(t) | \vec{\lambda}(t) \rangle$ is constant along the A-trajectory. Therefore $\langle \vec{p}(t_s) | \vec{g}(\vec{b}) \rangle = 0$

¹ Do not confuse these switching points with the components of the one-switching point (a, b) considered in Section 5.5, here \vec{a} and \vec{b} are different switching points.

implies

$$\langle \vec{p}(0) | \vec{\lambda}(0) \rangle = \langle \vec{p}(0) | e_{ad}^{-t_s A} \vec{g} \left(e^{t_s A}(\vec{a}) \right) \rangle = 0. \quad (\text{D.2})$$

This means that the multiplier $\vec{p}(0)$ is orthogonal to both $\vec{g}(\vec{a})$ and $\vec{\lambda}(0)$. Since the system is two-dimensional this is only possible if $\vec{g}(\vec{a})$ and $\vec{\lambda}(0)$ are parallel, i.e.

$$\vec{g}(\vec{a}) \parallel \vec{\lambda}(0) \Leftrightarrow \vec{g}(\vec{a}) \parallel e_{ad}^{-t_s A} \vec{g} \left(e^{t_s A}(\vec{a}) \right). \quad (\text{D.3})$$

This relation defines the interswitching time t_s . We therefore have to compute $\vec{\lambda}(0)$, which can be done by using the relation

$$e_{ad}^{-t_s A} \circ \vec{g} \circ e^{t_s A}(\vec{a}) = e^{t_s adA}(\vec{g}) \quad (\text{D.4})$$

where the operator adA is defined as $adA(\vec{g}) = [A, \vec{g}]$ and $[V, W]$ denotes the Lie bracket of the vector fields V and W [163, 164], which is componentwise defined by

$$[V, W]_a = \sum_b (V^b \partial_b W^a - W^b \partial_b V^a). \quad (\text{D.5})$$

The relation in eq. (D.4) is a consequence of the fact that the derivative of the function $\sigma : t \rightarrow e_{ad}^{-t_s A} \vec{g} \left(e^{t_s A}(\vec{a}) \right)$ at $t = 0$ is given by $[A, \vec{g}](\vec{a})$ and iteratively the higher order derivatives of σ at $t = 0$ are given by $\sigma^{(n)}(0) = ad^n A(\vec{g})$ where inductively $ad^n A(\vec{g}) = [A, ad^{n-1} A(\vec{g})]$. To summarize the interswitching time t_s can be determined by first computing $\vec{\lambda}(0)$ via eqs. (D.1) and (D.4) and then using the necessary condition that $\vec{\lambda}(0)$ and the control vector field $\vec{g}(\vec{a})$ at time $t = 0$ have to be parallel.

In what follows we will apply this method to provide an alternative proof of Proposition 11 in Section 5.5, where we will use a rescaled time $\omega_0 t \rightarrow t$ during the calculations and rescale the result in the end accordingly.

Proof. For our system, the Lie algebra L generated by the fields $f = (x_2, -x_1)^T$ and $g = (0, 1)^T$ is finite dimensional. We will first calculate $[f, g](x)$. Componentwise we have

$$\begin{aligned} [f, g](x)_1 &= (f^1 \partial_{x_1} g^1 + f^2 \partial_{x_2} g^1 - g^1 \partial_{x_1} f^1 - g^2 \partial_{x_2} f^1) \\ &= -1 \end{aligned}$$

and

$$\begin{aligned} [f, g](x)_2 &= (f^1 \partial_{x_1} g^2 + f^2 \partial_{x_2} g^2 - g^1 \partial_{x_1} f^2 - g^2 \partial_{x_2} f^2) \\ &= 0. \end{aligned}$$

Therefore we obtain

$$[f, g](x) = (-1, 0)^T. \quad (\text{D.6})$$

Furthermore, we will need $[f,[f,g]](x)$ and $[g,[f,g]](x)$. We have

$$\begin{aligned} [f,[f,g]](x)_1 &= (f^1 \partial_{x_1} [f,g]_1 + f^2 \partial_{x_2} [f,g]_1 - [f,g]_1 \partial_{x_1} f^1 - [f,g]_2 \partial_{x_2} f^1) \\ &= 0 \end{aligned}$$

and

$$\begin{aligned} [f,[f,g]](x)_2 &= (f^1 \partial_{x_1} [f,g]_2 + f^2 \partial_{x_2} [f,g]_2 - [f,g]_1 \partial_{x_1} f^2 - [f,g]_2 \partial_{x_2} f^2) \\ &= -\omega_0^2 \end{aligned}$$

such that

$$[f,[f,g]](x) = (0, -1)^T = -g. \quad (\text{D.7})$$

Similarly one obtains

$$[g,[f,g]](x) = (0,0)^T. \quad (\text{D.8})$$

We now consider the case q_\uparrow and call the trajectory a F-trajectory. With the previous calculations we can now deduce $e^{tadF}(g)$ in closed form via the expansion

$$e^{t_s adF}(g) = \sum_{n=0}^{\infty} \frac{t_s^n}{n!} ad^n F(g). \quad (\text{D.9})$$

We have

$$\begin{aligned} adF &= [F,g] = [f + q_\uparrow g, g] = [f,g] + q_\uparrow \underbrace{[g,g]}_{=0} = [f,g] \\ ad^2 F &= [F,[f,g]] = [f + q_\uparrow g, [f,g]] = [f,[f,g]] + q_\uparrow [g,[f,g]] = -g \\ ad^3 F &= [F, ad^2 F] = [f + q_\uparrow g, -g] = [f, -g] = -[f,g] \\ ad^4 F &= [F, ad^3 F] = [f + q_\uparrow g, -[f,g]] = [f, -[f,g]] - q_\uparrow [g,[f,g]] = g. \end{aligned} \quad (\text{D.10})$$

This suggests that

$$ad^{2n+1} F = (-1)^n [f,g] \quad \text{and} \quad ad^{2n+2} F = (-1)^{n+1} g, \quad n \in \mathbb{N}. \quad (\text{D.11})$$

The proof is straightforwardly done by induction. For $n = 0$ and $n = 1$ the statement is true. Now assume that $ad^{2n-1} F = (-1)^{n-1} [f,g]$ and $ad^{2n} F = (-1)^n g$ are true, then

$$\begin{aligned} ad^{2n+1} F &= [F, ad^{2n} F] = [F, [F, ad^{2n-1} F]] = [F, [F, (-1)^{n-1} [f,g]]] \\ &= [f + q_\uparrow g, [f + q_\uparrow g, (-1)^{n-1} [f,g]]] \\ &= (-1)^{n-1} [f, [f, [f,g]]] + q_\uparrow (-1)^{n-1} [f, [g, [f,g]]] \\ &+ q_\uparrow (-1)^{n-1} [g, [f, [f,g]]] + q_\uparrow^2 (-1)^{n-1} [g, [g, [f,g]]] \\ &= (-1)^{n-1} [f, -g] + q_\uparrow (-1)^{n-1} [f, 0] + q_\uparrow (-1)^{n-1} [g, -g] + q_\uparrow^2 (-1)^{n-1} [g, 0] \\ &= (-1)^n [f,g] \end{aligned} \quad (\text{D.12})$$

which is what we wanted to prove. Similarly

$$\begin{aligned}
ad^{2n+2}F &= [F,[F,ad^{2n}F]] = [F,[F,(-1)^n g]] \\
&= (-1)^n [f,[f,g]] + q_{\uparrow}(-1)^n [f,[g,g]] + q_{\uparrow}^2(-1)^n [g,[f,g]] \\
&= (-1)^n (-g) = (-1)^{n+1} g.
\end{aligned} \tag{D.13}$$

Using these these relations we obtain

$$\begin{aligned}
e^{t_s ad F}(g) &= \sum_{n=0}^{\infty} \frac{t_s^n}{n!} ad^n F(g) = g + \sum_{n=0}^{\infty} \frac{t_s^{2n+1}}{(2n+1)!} (-1)^n [f,g] + \sum_{n=0}^{\infty} \frac{t_s^{2n+2}}{(2n+2)!} (-1)^{n+1} g \\
&= g + \sin(t_s) [f,g] - (1 - \cos(t_s)) g = \sin(t) [f,g] + \cos(t) g.
\end{aligned} \tag{D.14}$$

Therefore $\lambda(0)$ is parallel to $g = (0,1)^T$ if and only if the first component of (D.14) is zero. Since $[f,g] = (-1,0)^T$ this means that $\sin(t_s) = 0$ and hence $t_s = k\pi$ with $k \in \mathbb{Z}/\{0\}$, because we have $t_s \neq 0$. Rescaling $t_s \rightarrow \omega_0 \cdot t_s$ then proves the proposition for a F-trajectory.

Similar calculations show that for q_{\downarrow} , which we call a B-trajectory, one obtains the same results, i.e. using $[f,g](x) = (-1,0)^T$, $[f,[f,g]](x) = -g$ and $[g,[f,g]](x) = (0,0)^T$ as before we obtain

$$ad^{2n+1}B = (-1)^n [f,g] \quad \text{and} \quad ad^{2n+2}B = (-1)^{n+1} g, \quad n \in \mathbb{N}. \tag{D.15}$$

This is clear because the result for the F-trajectory does not depend on q_{\uparrow} and therefore we have

$$e^{t_s ad B}(g) = \sin(t_s) [f,g] + \cos(t_s) g. \tag{D.16}$$

With the same arguments as before and after rescaling one again obtains that $t_s = k\pi/\omega_0$ with $k \in \mathbb{Z}/\{0\}$ for a B-trajectory, which completes the proof. \square

E Source Codes for Time-Evolution

In this section we provide the source codes developed to perform the simulations with which we obtained the numerical results in Chapters 3 and 4. However, since some situations we model are extensions of situations we studied in preceding chapters or sections, the corresponding algorithms are likewise extensions. For instance the time-evolution of an atom interacting with a Gaussian potential in 1d can be deduced from the corresponding algorithms in 2d simply by neglecting one dimension. Therefore we will only include the most general versions of similar algorithms and are content with giving a reference to these from which the simplified versions can be derived. All the algorithms will contain certain numerical values for the parameters. These do not necessarily correspond to any examples presented in this theses, but are only specified to illustrate possible choices.

The source codes also include some libraries and routines for example to use the FFTW [156, 157] or to perform the simulations on a NVIDIA graphics card (or GPU) using the CUDA architecture [158]. Since these are not necessary and do not alter the principle workings of the algorithms, but their sole purpose is to speed-up the computations, we refer the reader to the corresponding manuals for explanations and definitions of the various functions.

E.1 Quantum Stopper 1d

E.1.1 Classical Particles

The algorithm to simulate the quantum stopper in 1d in the classical case can straightforwardly be deduced from the algorithm simulating the 2d classical case with a mirror whose surface is given by quadratic polynomial and which can be found in Section E.2. Essentially this only requires to neglect one dimension and change the respective equations for the final positions and velocities.

E.1.2 Quantum Particles: Crank-Nicholson

```
// With this program we calculate the final position and velocity
// probability distribution for a wavepackage interacting with an
// infinitely high potential, which moves along a square-root in time
// trajectory via the Crank Nicholson method
```

```
#include <stdio.h>
#include <stdlib.h>           // stdlib included because of
#include <math.h>            // void exit(int fehlernummer)
#include <complex.h>
```

```

#define max_dateiname 100
#define max_schritte 400000 // im Raum

const int False = (1==0);
const int True = (1==1);

const double Pi = 3.141592653589793238462643383279502884197169399375105
820974944592307816406286208998628034825342117068;

// Here the important variables are declared, i.e. the wavefunction,
// the arrays for the Crank-Nicholson algorithm, the stepsize for time
// and position, the length of the box. Dim indicates that
// corresponding variables are dimensionless

double complex wave [max_schritte];
double complex psi2 [max_schritte];
double complex u [max_schritte];

double delta_t, delta_x, delta_t_dim, delta_x_dim;
int schritte_x;

double param_L_dim;
double param_m_dim;
double param_sigma_dim;
double param_v0_dim;
double param_x0_dim;
double param_t0_dim = 0.0;
double param_test = 1.0;
double complex y [max_schritte];

// This function calculates the square of the absolute value of a
// complex number
double cabs2 (double complex z)
{
    double re = creal (z), im = cimag (z);
    return re*re + im*im;
}

// This function calculates the Fourier transform via
// Fast Fourier Transform (FFT)
// This formulation is a standard one and can for example be found
// in the Numerical Recipes in C.
void fouriertransformation (double complex psi [max_schritte],
int max_laenge, int inverse_fft)

```

```
{
  int laenge, i, j, n, m, vorzeichen;
  double r;
  complex double temp, temp1, temp2, wn, w;

  for (j=0; j < max_laenge;j++)
    psi2 [j] = psi [j];

  if (inverse_fft)
    vorzeichen = 1;
  else
    vorzeichen = -1;

  j=0;
  for (i=1;i<max_laenge-1;i++)
  {
    m = max_laenge / 2;
    while (m >= 2 && j >= m)
    {
      j -= m;
      m = m / 2;
    }
    j += m;

    if (j > i)
    {
      temp = psi2 [i];
      psi2 [i] = psi2 [j];
      psi2 [j] = temp;
    }
  }

  laenge = 2;

  while (max_laenge >= laenge)
  {
    w = cexp(vorzeichen * I * 2.0 * Pi/laenge);
    wn = 1.0;
    for (n=0; n<laenge/2; n++)
    {
      for (i=n; i < max_laenge; i += laenge)
      {
        temp1 = psi2 [i] + wn * psi2 [i + laenge/2];
        temp2 = psi2 [i] - wn * psi2 [i + laenge/2];
        psi2 [i] = temp1;
        psi2 [i + laenge/2] = temp2;
      }
    }
  }
}
```

```

        }
        wn = wn * w;
    }
    laenge = laenge * 2;
}

r = (param_L_dim * sqrt(param_m_dim)) / (sqrt(2*Pi*max_laenge));
for (n=0; n<max_laenge; n++)
    psi2 [n] = psi2 [n] * r;
}

```

```

// This function calculates one time step via the Crank-Nicholson
// method, which is described explicitly in Appendix A
void einen_zeitschritt (double t_dim)
{

```

```

    double t_dim_x = param_t0_dim + t_dim + delta_t_dim/2.0;

    double complex dp = 1.0 + I *delta_t_dim/(2.0 * param_m_dim
    * delta_x_dim * delta_x_dim);
    double complex dm = 1.0 - I *delta_t_dim/(2.0 * param_m_dim
    * delta_x_dim * delta_x_dim);
    double complex cp = delta_t_dim/(4.0*delta_x_dim)
    * (I/(param_m_dim * delta_x_dim)
    + param_test/(2.0 * sqrt(t_dim_x)));
    double complex cm = delta_t_dim/(4.0*delta_x_dim)
    * (I/(param_m_dim * delta_x_dim)
    - param_test/(2.0 * sqrt(t_dim_x)));

    double complex b;
    int j;

    u [0] = dp;
    for (j=1; j<schritte_x; j++)
        u [j] = dp - cp * cm/u[j-1];

    // 1. partial step
    b = dm * wave [0] + cp * wave [1];
    y [0] = b/u[0];
    for (j=1; j < schritte_x - 1; j++)
    {
        b = cm * wave [j-1] + dm * wave [j] + cp * wave [j+1];
        y [j] = (b + cm * y[j-1])/ u[j];
    }
    b = cm * wave [schritte_x-2] + dm * wave [schritte_x - 1];

```

```

y [schritte_x - 1] = (b + cm * y [schritte_x - 2])
/ u [schritte_x -1];

// 2. partial step
wave [schritte_x - 1] = y [schritte_x - 1];
for (j=schritte_x - 2; j >= 0; j--)
    wave [j] = y [j] + cp * wave [j+1] / u [j];
}

// This function initialises the wavefunction, which is a Gaussian
void wave_initialisieren ()
{
    int j;
    double x_dim;
    double c = 1.0/(sqrt(param_sigma_dim)*sqrt(sqrt(2*Pi)));

    for (j=0; j < schritte_x; j++)
    {
        x_dim = (j+1) * delta_x_dim - param_L_dim
        + param_test * sqrt(param_t0_dim);
        wave [j] = c * cexp (-(x_dim-param_x0_dim)*(x_dim-param_x0_dim)
        /(4.0*param_sigma_dim * param_sigma_dim)
        + I * param_v0_dim * param_m_dim * x_dim);
    }
}

// This function writes the results in an output file. The results
// in momentum space are of course obtained via the previously defined
// Fourier transform
void wave_in_datei (FILE *datei_wave_ort, FILE *datei_wave_impuls,
double t_dim)
{
    int nr;
    double dk = 2.0 * Pi/param_L_dim;
    double k_dim;
    for (nr=0; nr < schritte_x; nr++)
        fprintf (datei_wave_ort, "%e %e %e\n", t_dim, (nr+1)
        * delta_x_dim - param_L_dim + param_test
        * sqrt(param_t0_dim + t_dim), cabs2 (wave [nr]));
    fprintf (datei_wave_ort, "\n\n");

    fouriertransformation (wave, schritte_x, False);
}

```

```

for (nr=schritte_x/2; nr < schritte_x; nr++)
{
    k_dim = (nr-schritte_x) * dk;
    fprintf (datei_wave_impuls, "%e %e %e\n", t_dim,
            k_dim/param_m_dim, cabs2 (psi2 [nr]));
}

for (nr=0; nr < schritte_x/2; nr++)
{
    k_dim = nr * dk;
    fprintf (datei_wave_impuls, "%e %e %e\n", t_dim,
            k_dim/param_m_dim, cabs2 (psi2 [nr]));
}

fprintf (datei_wave_impuls, "\n\n");
}

// This function calculates the time-evolution of the wavepackage
void wave_entwicklung (char *dateiname1, char *dateiname2,
int anzahl_x_schritte, int anzahl_t_schritte)
{
    // Here the important parameters are initialised and it is
    // checked if the files were opened successfully
    FILE *datei_wave_ort = fopen (dateiname1, "w");
    FILE *datei_wave_impuls = fopen (dateiname2, "w");
    int nr, nr2;
    double t_dim;

    if ((datei_wave_ort == NULL) || (datei_wave_impuls == NULL))
    {
        printf ("Fehler bei Dateioeffnung");
        exit (EXIT_FAILURE);
    }

    schritte_x = anzahl_x_schritte;

    delta_t_dim = 10.0 / anzahl_t_schritte;
    delta_x_dim = param_L_dim/(anzahl_x_schritte + 1);

    t_dim = 0.0;

    wave_initialisieren ();

    wave_in_datei (datei_wave_ort, datei_wave_impuls, t_dim);
}

```



```

// In the for loop the actual time-evolution is performed by making
// anzahl_t_schritte time steps in total, and writing a certain
// fraction into the output file
for (nr = 1; nr <= anzahl_t_schritte/62500; nr++)
{
    printf ("t = %f\n", t_dim);
    for (nr2=0; nr2 < 62500; nr2++)
    {
        einen_zeitschritt (t_dim);
        t_dim += delta_t_dim;
    }

    wave_in_datei (datei_wave_ort, datei_wave_impuls, t_dim);

}
fclose (datei_wave_ort);
fclose (datei_wave_impuls);
}

int main ()
{
    // Here the necessary parameters are initialised
    param_L_dim = 4.0;
    param_m_dim = 134578.0;
    param_sigma_dim = 0.0003;
    param_v0_dim = 3.0;
    param_x0_dim = -0.003;
    param_t0_dim = 0.0;
    param_test = 1.0;

    wave_entwicklung ("filename.dat", anzahl_x_schritte,
anzahl_t_schritte);

    return 0;
}

```

E.1.3 Quantum Particles: Operator-Splitting

The algorithm to simulate the quantum stopper in 1d in the quantum case can straightforwardly be deduced from the algorithm simulating the 2d quantum case with a mirror whose surface is given by quadratic polynomial (or of course also the one simulating the expansion and compression of a ring, but then a few more changes are necessary) and which can be found in Section E.2. Essentially this only requires to neglect one dimension and change the potential accordingly.

E.2 Quantum Stopper 2d

E.2.1 Classical Particles

```
// With this program we can calculate the final phase-space density of
// an ensemble of classical particles colliding with a wall whose
// surface is given by a quadratic polynomial and which moves along
// a trajectory proportional to the square-root in time
```

```
#include <stdio.h>
#include <stdlib.h>
#include <complex.h>
#include <math.h>
#include <omp.h>           // omp included in order to parallelize
                          // certain steps via #pragma omp parallel

#include "base_int_2d.c"   // these are routines for integration in
#include "base_nullstelle.c" // 2d and finding zeros of a polynomial

double Pi = 3.14159265358979323846264338327950288419716939937510582097
4944592307816406286208998628034825342117068;

double param_tf = 7.03e-3;

// Initial parameters: average velocities, positions, and variances in
// x and y direction, and the degree of freedom alpha of the
// square-root in time trajectory
double v01 = 0.3552;
double v02 = 0.0;
double x01 = -0.00002;
double x02 = 0.0;
double alpha = 0.00596338;
double dx1 = 0.000004;
double dx2 = 0.000004;
double dv1 = 0.1421;
double dv2 = 0.02;

// Parameters for the mirror whose surface is given by a quadratic
// polynomial and where c0,c1,c2 are its coefficients
double c0 = 0.0;
double c1 = 0.0;
double c2 = -1.0;

// Parameters for the integration.
double x1_start = -0.1;
double x1_ende = 0.1;
double x2_start = -0.1;
```

```
double x2_ende = 0.1;
int     x1_schritte = 2000;
int     x2_schritte = 1000;

double v1_start = -0.3;
double v1_ende = 1.0;
double v2_start = -0.4;
double v2_ende = 0.4;
int     v1_schritte = 2000;
int     v2_schritte = 1000;

#define max_punkte 2000

double wkeit1 [max_punkte][max_punkte];
double wkeit2 [max_punkte][max_punkte];

// This function writes the important parameters into the output file
void dateikopf_schreiben (FILE *datei)
{
    fprintf (datei, "# tf           = %e\n", param_tf);
    fprintf (datei, "# Startfunktion:\n");
    fprintf (datei, "# x01          = %e\n", x01);
    fprintf (datei, "# dx1          = %e\n", dx1);
    fprintf (datei, "# x02          = %e\n", x02);
    fprintf (datei, "# dx2          = %e\n", dx2);
    fprintf (datei, "# v01          = %e\n", v01);
    fprintf (datei, "# dv1          = %e\n", dv1);
    fprintf (datei, "# v02          = %e\n", v02);
    fprintf (datei, "# dv2          = %e\n", dv2);
    fprintf (datei, "# Wall:\n");
    fprintf (datei, "# c0           = %e\n", c0);
    fprintf (datei, "# c1           = %e\n", c1);
    fprintf (datei, "# c2           = %e\n", c2);
    fprintf (datei, "# Integrationsparameter:\n");
    fprintf (datei, "# x1_start     = %e\n", x1_start);
    fprintf (datei, "# x1_ende     = %e\n", x1_ende);
    fprintf (datei, "# x1_schritte = %e\n", x1_schritte);
    fprintf (datei, "# x2_start     = %e\n", x2_start);
    fprintf (datei, "# x2_ende     = %e\n", x2_ende);
    fprintf (datei, "# x2_schritte = %e\n", x2_schritte);
    fprintf (datei, "# v1_start     = %e\n", v1_start);
    fprintf (datei, "# v1_ende     = %e\n", v1_ende);
    fprintf (datei, "# v1_schritte = %e\n", v1_schritte);
    fprintf (datei, "# v2_start     = %e\n", v2_start);
    fprintf (datei, "# v2_ende     = %e\n", v2_ende);
    fprintf (datei, "# v2_schritte = %e\n", v2_schritte);
}
```

```

    fprintf (datei, "# x1_start    = %e\n", x1_start);
}

// This function calculates the shape of the potential
double wall_fkt (double x2)
{
    return c2*x2*x2 + c1*x2 + c0;
}

// This function calculates the partial derivative in x2 direction
// which is necessary to determine the normal vector
double wall_fkt_abl (double x2)
{
    return 2.0*c2*x2 + c1;
}

// This function decides whether a given point is in the allowed region
int point_valid (double x1, double x2, double tf)
{
    return x1 < (wall_fkt (x2) + alpha * sqrt(tf));
}

// This function calculates the collision time as the solution of a
// quartic equation. If no collision occurs it returns -1
double time_collision (double x1, double x2, double v1, double v2,
double tf)
{
    double z;

    z = nullstelle (c2*v2*v2, -v1+c1*v2-2.0*c2*tf*v2*v2+2.0*c2*v2*x2,
alpha, tf*v1-x1+c0-c1*tf*v2+c2*tf*tf*v2*v2+c1*x2-2.0*c2*tf*v2*x2
+c2*x2*x2, tf);

    if (z >= 0)
        return z*z;
    else
        return -1;
}

// This function calculates the initial probability distribution
// given by a Gaussian
double wkeit_start (double x1, double x2, double v1, double v2)
{
    return exp(-1.0/(2.0*dv1*dv1)*Power(v1-v01,2)
-1.0/(2.0*dx1*dx1)*Power(x1-x01,2)
-1.0/(2.0*dv2*dv2)*Power(v2-v02,2)

```

```

        -1.0/(2.0*dx2*dx2)*Power(x2-x02,2));
    }

// This function calculates the final positions and velocities
void wkeit_ende (double x1e, double x2e, double v1e, double v2e,
double *erg)
{
    double tf = param_tf;
    double tc, n2, abs2, mv1,hh;
    double x1 = x1e, x2 = x2e, v1=v1e, v2=v2e;

    if (!point_valid (x1, x2, tf)) // Check if the point is valid
    {
        *erg = 0.0;
        return;
    }

    tc = time_collision (x1, x2, v1, v2, tf);
    if (isnan (tc))
        printf ("NAN: tc\n");

    // In the loop the new position and velocity are calculated for all
    // the collisions occuring for the given parameters. The derivation
    // of these equations can be found in Chapter 3
    while (tc > 0.0) // The > is important, since tc == 0.0
        // can cause errors
    {
        n2 = -wall_fkt_abl (x2-v2*tf+v2*tc);
        abs2 = 1.0 + n2*n2;
        mv1 = alpha/(2.0 * sqrt(tc)); // Problem if tc=0

        x2= x2 - v2*(tf-tc);
        x1= wall_fkt (x2) + alpha * sqrt(tc) - eps;
        hh=v1;
        v1= mv1 + (-(v1-mv1)*(1-n2*n2)-2.0*v2*n2)/abs2;
        v2= (-2.0*(hh-mv1)*n2 + v2*(1.0-n2*n2))/abs2;

        tf = tc;
        tc = time_collision (x1, x2, v1, v2, tf);
        if (isnan (tc))
            printf ("NAN: tc\n");
    }
    x1 = x1 - v1 * tf;
    x2 = x2 - v2 * tf;

    *erg = wkeit_start (x1, x2, v1, v2);

```

```
    if (isnan (*erg))
        printf ("NAN: Ende: %e %e %e %e, Start: %e %e %e %e\n",x1e,x2e,v1e,
            v2e,x1,x2,v1,v2);
}

// This function is used to calculate the velocity distribution instead
// of the position distribution by just reversing the order and
// therefore the integration variables
void wkeit_ende_reverse (double v1, double v2, double x1, double x2,
double *erg)
{
    wkeit_ende (x1,x2,v1,v2, erg);
}

// This function calculates the final probability distribution
// in position space
void ges_wkeit_ort (double x1, double x2, double *erg1, double *erg2)
{
    int_w1_start = v1_start;
    int_w1_ende  = v1_ende;
    int_w2_start = v2_start;
    int_w2_ende  = v2_ende;
    int_1_schritte = v1_schritte;
    int_2_schritte = v2_schritte;

    berechne_integral_bode_2d (x1, x2, erg1, erg2, wkeit_ende);
}

// This function calculates the final probability distribution in
// momentum space
void ges_wkeit_geschw (double v1, double v2, double *erg1,
double *erg2)
{
    int_w1_start = x1_start;
    int_w1_ende  = x1_ende;
    int_w2_start = x2_start;
    int_w2_ende  = x2_ende;
    int_1_schritte = x1_schritte;
    int_2_schritte = x2_schritte;

    berechne_integral_bode_2d (v1, v2, erg1, erg2, wkeit_ende_reverse);
}

// This function just calculates the normalisation
void wkeit_norm (int punkte1, int punkte2, double *sum1, double *sum2)
{
```

```

int nr1, nr2;

*sum1 = 0.0;
*sum2 = 0.0;
for (nr1=0; nr1 <= punkte1; nr1++)
  for (nr2=0; nr2 <= punkte2; nr2++)
  {
    *sum1 += wkeit1 [nr1][nr2];
    *sum2 += wkeit2 [nr1][nr2];
  }
}

// This function writes the final position distribution into a file
void wkeit_ort_in_datei (char *dateiname, double out_x1_start,
double out_x1_ende, int punkte1, double out_x2_start,
double out_x2_ende, int punkte2)
{
  double dx1 = (x1_ende - x1_start) / (punkte1 * 1.0);
  double dx2 = (x2_ende - x2_start) / (punkte2 * 1.0);
  double norm1, norm2;

  int nr1, nr2;

  FILE *datei = fopen (dateiname,"w");
  fprintf (datei, "# Ortsverteilung\n");
  dateikopf_schreiben (datei);

  if ((punkte1 > max_punkte) || (punkte2 > max_punkte))
  {
    printf ("Zu viele Punkte!\n");
    exit (EXIT_FAILURE);
  }

#pragma omp parallel for private(nr1,nr2)

  for (nr1=0; nr1 <= punkte1; nr1++)
  {
    printf ("nr1 = %d\n", nr1);
    for (nr2=0; nr2 <= punkte2; nr2++)
    {
      ges_wkeit_ort(x1_start+nr1*dx1,x2_start+nr2 * dx2,
      &(wkeit1 [nr1][nr2]),&(wkeit2 [nr1][nr2]));
    }
  }

  wkeit_norm (punkte1, punkte2, &norm1, &norm2);
  norm1 *= dx1 * dx2;

```

```

norm2 *= dx1 * dx2;

for (nr1=0; nr1 <= punkte1; nr1++)
{
  for (nr2=0; nr2 <= punkte2; nr2++)
  {
    fprintf (datei, "%e %e %e %e\n",x1_start+nr1*dx1,
            x2_start+nr2*dx2,wkeit1[nr1][nr2]/norm1,
            wkeit2[nr1][nr2]/norm2);
  }
  fprintf (datei, "\n");
}
fclose (datei);
}

// This function writes the final momentum distribution into a file
void wkeit_geschw_in_datei (char *dateiname, double out_v1_start,
double out_v1_ende, int punkte1, double out_v2_start,
double out_v2_ende, int punkte2)
{
  double dv1 = (v1_ende - v1_start) / (punkte1 * 1.0);
  double dv2 = (v2_ende - v2_start) / (punkte2 * 1.0);
  double norm1 = 1.0, norm2 = 1.0;

  int nr1, nr2;

  FILE *datei = fopen (dateiname,"w");
  fprintf (datei, "# Geschwindigkeitsverteilung\n");
  dateikopf_schreiben (datei);

  if ((punkte1 > max_punkte) || (punkte2 > max_punkte))
  {
    printf ("Zu viele Punkte!\n");
    exit (EXIT_FAILURE);
  }

#pragma omp parallel for private(nr1,nr2)

  for (nr1=0; nr1 <= punkte1; nr1++)
  {
    printf ("nr1=%d\n", nr1);
    for (nr2=0; nr2 <= punkte2; nr2++)
    {
      ges_wkeit_geschw(v1_start+nr1*dv1,v2_start+nr2*dv2,
        &(wkeit1 [nr1][nr2]),&(wkeit2 [nr1][nr2]));
    }
  }
}

```



```

wkeit_norm (punkte1, punkte2, &norm1, &norm2);
norm1 *= dv1 * dv2;
norm2 *= dv1 * dv2;

for (nr1=0; nr1 <= punkte1; nr1++)
{
  for (nr2=0; nr2 <= punkte2; nr2++)
  {
    fprintf (datei, "%e %e %e %e\n",v1_start+nr1*dv1,
            v2_start+nr2*dv2,wkeit1[nr1][nr2]/norm1,
            wkeit2[nr1][nr2]/norm2);
  }
  fprintf (datei, "\n");
}
fclose (datei);
}

// This function writes the complete final distribution into a file
void wkeit_in_datei (char *dateiname, int punktex1, int punktex2,
int punktev1, int punktev2)
{
  double dv1 = (v1_ende - v1_start) / (punktev1 * 1.0);
  double dv2 = (v2_ende - v2_start) / (punktev2 * 1.0);

  double dx1 = (x1_ende - x1_start) / (punktex1 * 1.0);
  double dx2 = (x2_ende - x2_start) / (punktex2 * 1.0);

  double norm1, norm2, erg;

  int xnr1, xnr2, vnr1, vnr2;

  FILE *datei = fopen (dateiname,"w");

  for (xnr1=0; xnr1 <= punktex1; xnr1++)
    for (xnr2=0; xnr2 <= punktex2; xnr2++)
      for (vnr1=0; vnr1 <= punktev1; vnr1++)
        for (vnr2=0; vnr2 <= punktev2; vnr2++)
          {
            wkeit_ende (x1_start+xnr1*dx1,x2_start+xnr2*dx2,
            v1_start+vnr1*dv1,v2_start+vnr2*dv2,&erg);
            fprintf (datei, "%e %e %e %e %e\n",x1_start+xnr1*dx1,
            x2_start+xnr2*dx2,v1_start+vnr1*dv1,
            v2_start+vnr2*dv2, erg);
          }

  fclose (datei);
}

```

```

}

/*
Compiling with GNU Compiler
cc filename.c -lm -fopenmp -lpthread -lgsl -lgslcblas -o name.out

Compiling with Intel Compiler
icc filename.c -lm -openmp -lpthread -lgsl -lgslcblas -o name.out
*/

int main ()
{
    double erg;

    param_tf = 0.02;

    c2 = 1.0e-2;

    wkeit_ort_in_datei ("filename.dat", out_x1_start, out_x1_ende,
punkte1, out_x2_start, out_x2_ende, punkte2);
    wkeit_geschw_in_datei ("filename.dat",out_v1_start, out_v1_ende,
punkte1, out_v2_start, out_v2_ende, punkte2);
    wkeit_in_datei ("filename.dat", punktex1, punktex2, punktev1,
punktev2);

    return 0;
}

```

E.2.2 Quantum Particles: Operator-Splitting

```

// With this program we calculate the time-evolution of a wavepackage
// in 2d interacting with a Gaussian mirror potential whose surface is
// given by quadratic polynomial
// hbar = 1, m = 0,5

#include <stdio.h>
#include <stdlib.h>
#include <math.h>
#include <complex.h>
#include <string.h>

```

```
#define PP_CUDA
#include "pptools_v3.h" // This provides the necessary functions to
                        // perform parts of the simulation on the GPU

#define max_dateiname 100

const int FALSE = (1==0);
const int TRUE = (1==1);

const float Pi = 3.141592653589793238462643383279502884197169399375105
820974944592307816406286208998628034825342117068;

// Pointer declarations for the wavefunction, the potential and the
// kinetic term, whose respective values will be stored in an array

float complex *wave;
float complex *exp_V;
float complex *exp_H0;
float complex *exp_H0_2;

// Declaration and partially definition of the variables used for the
// wavefunction, the potential as well as the evolution time, the
// length of the box and the time and space discretization
float delta_x, delta_y;
const int schritte_x = 4096*1;
const int schritte_y = 4096*2;
float param_v0x, param_v0y;
float param_m;
float param_hbar = 1.0;
float param_t_init;
float param_t_ende = 1.0;

float param_x0, param_y0;
float param_delta_x, param_delta_y;
float param_delta_vx, param_delta_vy;
int ausgabe_step_x, ausgabe_step_y;

float param_x0_pot;
float param_y0_pot;
float c_poly;
float param_pot_sigma_xy;

float param_pot_hoehe;
float param_pot_r_start;
```

```

//float param_pot_sigma_x, param_pot_sigma_y;
float param_pot_sigma_r;
float param_rand_min_x, param_rand_max_x;
float param_rand_min_y, param_rand_max_y;
float param_L_x, param_L_y;

float beta;
float zeit_interv_1;
float zeit_interv_2;

int bild_nummer;

int nkuehl_ende;

// GPU/CUDA
// These pointers are declared to carry out the computation on the GPU

cuFloatComplex *gpu_wave;
cuFloatComplex *gpu_exp_H0;
cuFloatComplex *gpu_exp_H0_2;
cuFloatComplex *gpu_exp_V;

// GPU

// This function allocates the necessary memory in order
// to carry out the computation on the GPU
void variable_initialisieren ()
{
    printf ("Variable initialisieren Start\n");
    printf ("Size: cuFloatComplex = %d\n", sizeof (cuFloatComplex));
    printf ("Size: complex float = %d\n", sizeof (complex float));
    printf ("Size: cuDoubleComplex = %d\n", sizeof (cuDoubleComplex));
    printf ("Size: complex double = %d\n", sizeof (complex double));

    pp_MemAlloc ((void **)&wave, (void **)&gpu_wave,
        sizeof(cuFloatComplex) * schritte_x * schritte_y);
    pp_MemAlloc ((void **)&exp_H0, (void **)&gpu_exp_H0,
        sizeof(cuFloatComplex) * schritte_x * schritte_y);
    pp_MemAlloc ((void **)&exp_H0_2, (void **)&gpu_exp_H0_2,
        sizeof(cuFloatComplex) * schritte_x * schritte_y);
    pp_MemAlloc ((void **)&exp_V, (void **)&gpu_exp_V,
        sizeof(cuFloatComplex) * schritte_x * schritte_y);

    pp_fourier_initialisieren_2df (gpu_wave, schritte_x, schritte_y);
    printf ("Variable initialisieren Ende\n");
}

```

```
// This function then deallocates the memory
void variable_freigeben ()
{
    pp_MemFree (wave, gpu_wave);
    pp_MemFree (exp_H0, gpu_exp_H0);
    pp_MemFree (exp_H0_2, gpu_exp_H0_2);
    pp_MemFree (exp_V, gpu_exp_V);

    pp_fourier_beenden ();
}

// This function calculates the absolute value squared of a complex
// number z
float cabs2 (float complex z)
{
    float re = crealf (z), im = cimagf (z);
    return re*re + im*im;
}

// This function writes the results into a binary file. It obtains the
// "raw" binary data from the GPU and performs Fourier transforms in
// order to get the results in position and momentum space
void wave_in_datei_binary (FILE *datei_binary_ort,
FILE *datei_binary_impuls)
{
    pp_fourier_2df (TRUE);

    pp_MemcpyToHost (wave, gpu_wave, schritte_x * schritte_y
* sizeof (cuFloatComplex));

    fwrite (wave, sizeof (cuFloatComplex), schritte_x * schritte_y,
datei_binary_ort);

    pp_fourier_2df (FALSE);

    pp_MemcpyToHost (wave, gpu_wave, schritte_x * schritte_y
* sizeof (cuFloatComplex));

    fwrite (wave, sizeof (cuFloatComplex), schritte_x * schritte_y,
datei_binary_impuls);
}

// This function writes the results into a data file. Therefore some
// manipulations are necessary like determining the actual positions
// and velocities
```

```

void wave_in_datei (FILE *datei_ort, FILE *datei_impuls, float t)
{
    int nr, mr;
    float vx, vy;
    float param_L_x = param_rand_max_x - param_rand_min_x;
    float param_L_y = param_rand_max_y - param_rand_min_y;
    float dkx = 2.0 * Pi / param_L_x;
    float dky = 2.0 * Pi / param_L_y;
    float cx = param_L_x * param_L_x * param_m / (2.0 * Pi * schritte_x
    * schritte_x);
    float cy = param_L_y * param_L_y * param_m / (2.0 * Pi * schritte_y
    * schritte_y);

    float summe;

    printf ("Ortsdarstellung in Datei\n");
    // Fourier Impuls -> Ort
    pp_fourier_2df (TRUE);

    pp_MemcpyToHost (wave, gpu_wave, schritte_x * schritte_y
    * sizeof (cuFloatComplex));

    summe = 0.0;

    fprintf (datei_ort, "# INDEX = %d\n", bild_nummer);
    for (nr=0; nr < schritte_x; nr++)
    {
        for (mr=0; mr < schritte_y; mr++)
        {
            if (nr % ausgabe_step_x == 0)
            {
                if (mr % ausgabe_step_y == 0)
                {
                    fprintf (datei_ort, "%e %e %e %e\n", t,
                    nr * delta_x + param_rand_min_x,
                    mr * delta_y + param_rand_min_y,
                    cabs2 (wave [nr * schritte_y + mr]));
                }
            }
            summe += cabs2 (wave [nr * schritte_y + mr]);
        }
    }
    fprintf (datei_ort, "\n\n");
    fflush (datei_ort); // neu

    printf ("Ort: Norm = %e\n", summe * delta_x * delta_y);
}

```

```

printf ("Impulsdarstellung in Datei\n");
pp_fourier_2df (FALSE);

pp_MemcpyToHost (wave, gpu_wave, sizeof(float complex) * schritte_x
* schritte_y);

summe = 0.0;

fprintf (datei_impuls, "# INDEX = %d\n", bild_nummer);
for (nr=schritte_x/2; nr < schritte_x; nr++)
{
  for (mr=schritte_y/2; mr < schritte_y; mr++)
  {
    if (nr % ausgabe_step_x == 0)
    {
      if (mr % ausgabe_step_y == 0)
      {
        vx = (nr-schritte_x) * dkx/param_m;
        vy = (mr-schritte_y) * dky/param_m;

        fprintf (datei_impuls, "%e %e %e %e\n", t, vx, vy,
cabs2 (wave [nr * schritte_y + mr])*cx*cy);
      }
    }
    summe += cabs2 (wave[nr * schritte_y + mr])*cx*cy;
  }
}

for (nr=schritte_x/2; nr < schritte_x; nr++)
{
  for (mr=0; mr < schritte_y/2; mr++)
  {
    if (nr % ausgabe_step_x == 0)
    {
      if (mr % ausgabe_step_y == 0)
      {
        vx = (nr-schritte_x) * dkx/param_m;
        vy = mr * dky/param_m;

        fprintf (datei_impuls, "%e %e %e %e\n", t, vx, vy,
cabs2 (wave [nr * schritte_y + mr])*cx*cy);
      }
    }
    summe += cabs2 (wave[nr * schritte_y + mr])*cx*cy;
  }
}

```

```

for (nr=0; nr < schritte_x/2; nr++)
{
  for (mr=schritte_y/2; mr < schritte_y; mr++)
  {
    if (nr % ausgabe_step_x == 0)
    {
      if (mr % ausgabe_step_y == 0)
      {
        vx = nr * dkx/param_m;
        vy = (mr-schritte_y) * dky/param_m;

        fprintf (datei_impuls, "%e %e %e %e\n", t, vx, vy,
          cabs2 (wave [nr * schritte_y + mr])*cx*cy);
      }
    }
    summe += cabs2 (wave[nr * schritte_y + mr])*cx*cy;
  }
}

for (nr=0; nr < schritte_x/2; nr++)
{
  for (mr=0; mr < schritte_y/2; mr++)
  {
    if (nr % ausgabe_step_x == 0)
    {
      if (mr % ausgabe_step_y == 0)
      {
        vx = nr * dkx/param_m;
        vy = mr * dky/param_m;

        fprintf (datei_impuls, "%e %e %e %e\n", t, vx, vy,
          cabs2 (wave [nr * schritte_y + mr])*cx*cy);
      }
    }
    summe += cabs2 (wave[nr * schritte_y + mr])*cx*cy;
  }
}

printf ("Geschw.: Norm = %e\n", summe * dkx*dky/(param_m*param_m));
printf ("Geschw.: Norm = %e\n", summe);

fprintf (datei_impuls, "\n\n");
fflush (datei_impuls); // neu

bild_nummer++;
}

```



```

// This function calculates the potential, which is here given by a
// quadratic polynomial with Gaussian profile in the direction
// of movement. Here and in the following the additional parameter
// nkuehl can be ignored and set to one. This parameter makes it
// possible to generalize this code e.g. to perform cooling cycles
// by changing the potential shape to a ring. The corresponding
// code which actually implements this can be found in the next
// subsection
float potential (float x, float y, float t, int nkuehl)
{
    float pos;
    pos = param_x0_pot + param_y0_pot + sqrt(t);
    return param_pot_hoehe * exp(-(x + c_poly*y*y - pos)
    *(x+c_poly*y*y-pos)/(2.0*param_pot_sigma_xy*param_pot_sigma_xy));
}

// This function calculates the exponential of the potential
void exp_V_berechnen (float t, float delta_t, int nkuehl)
{
    int j,l;
    float v1;
    float v2;

#pragma omp parallel for private (j,l,v1,v2)
for (j=0; j < schritte_x; j++)
    {
        for (l=0; l < schritte_y; l++)
            {
                v1 = potential (j * delta_x + param_rand_min_x,
                l * delta_y + param_rand_min_y, t, nkuehl);
                v2 = potential (j * delta_x + param_rand_min_x,
                l * delta_y + param_rand_min_y, t + delta_t, nkuehl);
                exp_V [j*schritte_y+l] = cexpf (-I/param_hbar
                * delta_t * 0.5 * (v1 + v2));
            }
        }
    pp_MemcpyToDevice (gpu_exp_V, exp_V, sizeof(float complex)
    * schritte_x * schritte_y);
}

// This function calculates the exponential of the kinetic term both
// for one and two time steps, since from one step of the time-
// evolution to the next we have a concatenation of these
// exponentials, and therefore we can reduce the number of
// calculations. The value for one time step is only needed at
// the beginning and the end

```

```

void exp_H0_berechnen (float delta_t)
{
    int n,m;
    float kx, ky;
    float param_L_x = param_rand_max_x - param_rand_min_x;
    float param_L_y = param_rand_max_y - param_rand_min_y;
    float dkx = 2.0 * Pi / param_L_x;
    float dky = 2.0 * Pi / param_L_y;

#pragma omp parallel for private (n,m,kx,ky)
    for (n=0; n < schritte_x/2; n++)
    {
        for (m=0; m < schritte_y/2; m++)
        {
            kx = n * dkx;
            ky = m * dky;
            exp_H0 [n*schritte_y+m] = cexpf (-I * (kx * kx + ky * ky)
            / (2.0 * param_m) * delta_t);
            exp_H0_2 [n*schritte_y+m] = cexpf (-I * (kx * kx + ky * ky)
            / (2.0 * param_m) * 0.5 * delta_t);
        }
    }

#pragma omp parallel for private (n,m,kx,ky)
    for (n=0; n < schritte_x/2; n++)
    {
        for (m=schritte_y/2; m < schritte_y; m++)
        {
            kx = n * dkx;
            ky = (m-schritte_y) * dky;
            exp_H0 [n * schritte_y + m] = cexpf (-I * param_hbar
            * (kx * kx + ky * ky) / (2.0 * param_m) * delta_t);
            exp_H0_2 [n * schritte_y + m] = cexpf (-I * param_hbar
            * (kx * kx + ky * ky) / (2.0 * param_m) * 0.5 * delta_t);
        }
    }

#pragma omp parallel for private (n,m,kx,ky)
    for (n=schritte_x/2; n < schritte_x; n++)
    {
        for (m=0; m < schritte_y/2; m++)
        {
            kx = (n-schritte_x) * dkx;
            ky = m * dky;
            exp_H0 [n * schritte_y + m] = cexpf (-I * param_hbar
            * (kx * kx + ky * ky) / (2.0 * param_m) * delta_t);
            exp_H0_2 [n * schritte_y + m] = cexpf (-I * param_hbar

```

```

        * (kx * kx + ky * ky)/(2.0 * param_m) * 0.5 * delta_t);
    }
}

#pragma omp parallel for private (n,m,kx,ky)
for (n=schritte_x/2; n < schritte_x; n++)
{
    for (m=schritte_y/2; m < schritte_y; m++)
    {
        kx = (n-schritte_x) * dkx;
        ky = (m-schritte_y) * dky;
        exp_H0 [n * schritte_y + m] = cexp (-I * param_hbar
        * (kx * kx + ky * ky)/(2.0 * param_m) * delta_t);
        exp_H0_2 [n * schritte_y + m] = cexp (-I * param_hbar
        * (kx * kx + ky * ky)/(2.0 * param_m) * 0.5 * delta_t);
    }
}

pp_MemcpyToDevice (gpu_exp_H0, exp_H0, sizeof(float complex)
* schritte_x * schritte_y);
pp_MemcpyToDevice (gpu_exp_H0_2, exp_H0_2, sizeof(float complex)
* schritte_x * schritte_y);
}

// This function initialises the wavefunction
void wave_initialisieren ()
{
    int j,l;
    float cx,cy, x,y;
    float tx, ty, x0, y0, norm2 = 0.0;
    complex float c1x, c2x, c1y, c2y;

    printf ("Wave initialisieren Start\n");
    //printf ("v dimensionslos = %f\n", param_v0);
    //printf ("p dimensionslos = %f\n", param_v0 * param_m);
    //printf ("kmin = %f\n",-schritte_x/2 * alpha * sqrt(t_ende)
    /* 2.0 * Pi/L);
    //printf ("kmax = %f\n",(schritte_x/2-1) * alpha * sqrt(t_ende)
    /* 2.0 * Pi/L);

    cx = 4.0*param_delta_x * param_delta_x - 1.0/(param_delta_vx
    * param_delta_vx * param_m * param_m); //Uncertainty relation
    if (cx<0.0)
    {
        printf ("Unschaerferelation in x verletzt!\n");
        exit (EXIT_FAILURE);
    }
}

```

```

cy = 4.0*param_delta_y * param_delta_y - 1.0/(param_delta_vy
* param_delta_vy * param_m * param_m); //Uncertainty relation
if (cy<0.0)
{
    printf ("Unschaerferelation in y verletzt!\n");
    exit (EXIT_FAILURE);
}
tx = sqrtf(cx)/(2.0 * param_delta_vx);
ty = sqrtf(cy)/(2.0 * param_delta_vy);
x0 = param_x0 - tx * param_v0x;
y0 = param_y0 - ty * param_v0y;

c1x=sqrtf(sqrtf(2.0/Pi))/csqrtf(1.0/(param_delta_vx * param_m)
+ 2.0*I*param_delta_vx * tx);
c2x = param_m/(2.0 * (1.0 + 2.0*I*param_delta_vx *param_delta_vx
*param_m * tx));

c1y=sqrtf(sqrtf(2.0/Pi))/csqrtf(1.0/(param_delta_vy * param_m)
+ 2.0*I*param_delta_vy * ty);
c2y = param_m/(2.0 * (1.0 + 2.0*I*param_delta_vy *param_delta_vy
*param_m * ty));

for (j=0; j < schritte_x; j++)
{
    for (l=0; l < schritte_y; l++)
    {
        x = j * delta_x + param_rand_min_x;
        y = l * delta_y + param_rand_min_y;
        wave [j * schritte_y + l] = c1x * cexpf (-c2x*(2.0
*param_delta_vx*param_delta_vx*param_m*((x-x0)*(x-x0)
+2.0*tx*param_v0x*x0) + I*param_v0x * (tx*param_v0x
-2.0*x))) * c1y * cexpf (-c2y*(2.0*param_delta_vy
*param_delta_vy*param_m*((y-y0)*(y-y0)+2.0*ty*param_v0y*y0)
+ I*param_v0y * (ty*param_v0y-2.0*y)));

        norm2 += cabs2(wave [j * schritte_y + l]);
    }
}

norm2 *= delta_x * delta_y;
printf ("Anfangsnorm Ort = %e\n", norm2);

pp_MemcpyToDevice (gpu_wave, wave, schritte_x * schritte_y
* sizeof (cuFloatComplex));

pp_fourier_2df (FALSE);

```

```
    printf ("Wave ist initialisiert\n");
}

// This function calculates multiple steps of the time-evolution
// on the GPU
void mehrere_zeitschritte (int anzahl, float *t, float delta_t,
int nkuehl)
{
    int nr;

    // Here exp_H0_2 has to be calculated once in advance as was
    // discussed above
    pp_Mul_2df (gpu_wave, gpu_exp_H0_2, schritte_x, schritte_y);

    for (nr=1; nr <= anzahl-1; nr++)
    {
        pp_fourier_2df (TRUE);

        // exp_V
        exp_V_berechnen (*t, delta_t, nkuehl);
        pp_Mul_2df (gpu_wave, gpu_exp_V, schritte_x, schritte_y);

        pp_fourier_2df (FALSE);

        // exp_H0
        pp_Mul_2df (gpu_wave, gpu_exp_H0, schritte_x, schritte_y);

        printf ("t = %f\n", *t);
        *t += delta_t;
    }

    pp_fourier_2df (TRUE);

    // exp_V
    exp_V_berechnen (*t, delta_t, nkuehl);
    pp_Mul_2df (gpu_wave, gpu_exp_V, schritte_x, schritte_y);

    pp_fourier_2df (FALSE);

    // Here exp_H0_2 has to be calculated once more as was
    // discussed above
    pp_Mul_2df (gpu_wave, gpu_exp_H0_2, schritte_x, schritte_y);
    *t += delta_t;
}

// This function writes the chosen parameters into the file
void param_in_datei (FILE *datei)
```

```

{
    fprintf (datei, "# pot_hoehe           = %e\n",param_pot_hoehe);
    fprintf (datei, "# pot_sigma_r       = %e\n",param_pot_sigma_r);
    fprintf (datei, "# x0                = %e\n",param_x0);
    fprintf (datei, "# delta_x          = %e\n",param_delta_x);
    fprintf (datei, "# v0x             = %e\n",param_v0x);
    fprintf (datei, "# delta_vx        = %e\n",param_delta_vx);
    fprintf (datei, "# y0                = %e\n",param_y0);
    fprintf (datei, "# delta_y          = %e\n",param_delta_y);
    fprintf (datei, "# v0y             = %e\n",param_v0y);
    fprintf (datei, "# delta_vy        = %e\n",param_delta_vy);
    fprintf (datei, "# m                = %e\n",param_m);
    fprintf (datei, "# Lx               = %e\n",param_L_x);
    fprintf (datei, "# Ly               = %e\n",param_L_y);
    fprintf (datei, "# ausgabe_step_x   = %d\n",ausgabe_step_x);
    fprintf (datei, "# ausgabe_step_y   = %d\n",ausgabe_step_y);
    fprintf (datei, "# c_poly           = %e\n",c_poly);
}

// This function calculates the actual time-evolution of the
// wavefunction
void wave_entwicklung (char *dateiname1, char *dateiname2, char
*dateiname_binary1, char *dateiname_binary2, int anzahl_t_schritte,
int anzahl_bilder, int anzahl_ausgabe_x, int anzahl_ausgabe_y)
{
    FILE *datei_ort = fopen (dateiname1, "w");
    FILE *datei_impuls = fopen (dateiname2, "w");
    FILE *datei_binary_ort = fopen (dateiname_binary1, "w");
    FILE *datei_binary_impuls = fopen (dateiname_binary2, "w");
    int nr, nr2, nr_step_bild,j, nkuehl;
    float t, delta_t;

    if ((datei_ort == NULL) || (datei_impuls == NULL))
    {
printf ("Fehler bei Dateioeffnung");
exit (EXIT_FAILURE);
    }

    delta_t = param_t_ende / anzahl_t_schritte;
    printf ("delta_t = %e\n", delta_t);
    delta_x = (param_rand_max_x - param_rand_min_x)/(schritte_x * 1.0);
    delta_y = (param_rand_max_y - param_rand_min_y)/(schritte_y * 1.0);

    ausgabe_step_x = schritte_x/anzahl_ausgabe_x;
    ausgabe_step_y = schritte_y/anzahl_ausgabe_y;
}

```

```
if (ausgabe_step_x == 0)
    ausgabe_step_x = 1;

if (ausgabe_step_y == 0)
    ausgabe_step_y = 1;

variable_initialisieren ();
bild_nummer = 0;

param_in_datei (datei_ort);
param_in_datei (datei_impuls);
//param_in_datei (datei_binary_ort);
//param_in_datei (datei_binary_impuls);

t = param_t_init;

nkuehl = 1;

wave_initialisieren ();

nr_step_bild = anzahl_t_schritte / anzahl_bilder;

wave_in_datei (datei_ort, datei_impuls, t);
wave_in_datei_binary (datei_binary_ort, datei_binary_impuls);

exp_H0_berechnen (delta_t);

for (nr = 1; nr <= anzahl_t_schritte / nr_step_bild; nr++)
{
    mehrere_zeitschritte (nr_step_bild, &t, delta_t, nkuehl);
    wave_in_datei (datei_ort, datei_impuls, t);
    wave_in_datei_binary (datei_binary_ort, datei_binary_impuls);

    printf ("t = %f\n", t);
}

variable_freigeben ();

fclose (datei_ort);
fclose (datei_impuls);
fclose (datei_binary_ort);
fclose (datei_binary_impuls);
}

/*

Compiling with Intel Compiler
```

```

icc kuehlung.c cutools_v3.o -I /usr/local/cuda/include -L
/usr/local/cuda/lib64 -lcuda -lcufft -openmp -O3 -o cuda.out

*/

int main (int argc, char *argv[])
{
    char prg [200];
    int param_nr;

    /*strcpy (prg, argv[0]); // Security check, can be useful
    printf ("Programmname %s wird ausgefuehrt (Parameter=%d)!\n", prg,
    argc);

    if (argc < 2)
    {
        printf ("Zuwenige Parameter: Parameternr erwartet!\n");
        exit (EXIT_FAILURE);
    }
    sscanf(argv[1], "%d", &param_nr);*/

    param_pot_hoehe = 60000.0;
    param_pot_sigma_xy = 0.01;
    param_x0_pot = 0.0;
    param_y0_pot = 0.0;
    param_rand_min_x = -1.0;
    param_rand_max_x = 1.1;
    param_rand_min_y = -1.5;
    param_rand_max_y = 1.5;
    param_L_x = param_rand_max_x-param_rand_min_x;
    param_L_y = param_rand_max_y-param_rand_min_y;
    param_m = 296.033;
    param_x0 = -0.023715-4*0.00474299;
    param_delta_x = 0.00474299;
    param_v0x = 5.0;
    param_delta_vx = 1.2;
    param_y0 = 0.0;
    param_delta_y = 0.00474299;
    param_v0y = 0.0;
    param_delta_vy = 0.474299;
    param_t_init = 0.0;
    c_poly = 3.5;

    float param_L_x = param_rand_max_x - param_rand_min_x;
    float param_L_y = param_rand_max_y - param_rand_min_y;
    float dkx = 2.0 * Pi / param_L_x;

```



```

float dky = 2.0 * Pi / param_L_y;
printf ("v_max = %e\n", dkx * schritte_x/2/param_m);
param_t_ende = 1.0;

wave_entwicklung ("datafilename_position.dat",
"datafilename_momentum.dat", "binaryfilename_position.bin",
"binaryfilename_momentum.bin", anzahl_t_schritte, anzahl_bilder,
anzahl_ausgabe_x, anzahl_ausgabe_y);

return 0;
}

```

E.3 Quantum Stopper 2d: Expansion and Compression

E.3.1 Classical Particles

We will not present the code for the classical one particle case, because it is very simple and its implementation straightforward. Since we only presented this case in the classical treatment and immediately moved on to a simulation of the quantum mechanical situation, we will not include a code for a classical ensemble inside a ring which is expanded and compressed afterwards either. This code though could in principle be easily derived by changing the respective equations for the collision time and the final position as well as velocity in the corresponding code for a mirror whose surface is given by a quadratic polynomial to the corresponding equations for a ring. In a next step one would then have to include the compression, which is analogous to the implementation of the expansion. The necessary equations both for the expansion and compression can be found in Section 3.4.

E.3.2 Quantum Particles: Operator-Splitting

```

// With this program we calculate the time-evolution of a wavepackage
// in 2d interacting with a Gaussian mirror potential with ring shape
// which is expanded along a square-root in time trajectory and
// compressed linearly in time
// hbar = 1, m = 0,5

#include <stdio.h>
#include <stdlib.h>
#include <math.h>
#include <complex.h>
#include <string.h>

#define PP_CUDA
#include "pptools_v3.h" // This provides the necessary functions to
// perform parts of the calculation on the GPU

```

```

#define max_dateiname 100

const int FALSE = (1==0);
const int TRUE = (1==1);

const float Pi = 3.141592653589793238462643383279502884197169399375105
820974944592307816406286208998628034825342117068;

// Pointer declarations for the wavefunction, the potential and the
// kinetic term, whose respective values will be stored in an array

float complex *wave;
float complex *exp_V;
float complex *exp_H0;
float complex *exp_H0_2;

// Declaration and partially definition of the variables used for the
// wavefunction, the potential as well as the evolution time, the
// length of the box and the time and space discretization
float delta_x, delta_y;
const int schritte_x = 4096;//4096*2;
const int schritte_y = 4096;//4096*2;
float param_v0x, param_v0y;
float param_m;
float param_hbar = 1.0;
float param_t_init;
float param_t_ende = 1.0;//0.1;//1.0;

float param_x0, param_y0;
float param_delta_x, param_delta_y;
float param_delta_vx, param_delta_vy;
int ausgabe_step_x, ausgabe_step_y;

float param_pot_hoehe;
float param_pot_r_start;
//float param_pot_sigma_x, param_pot_sigma_y;
float param_pot_sigma_r;
float param_rand_min_x, param_rand_max_x;
float param_rand_min_y, param_rand_max_y;
float param_L_x, param_L_y;

float beta;
int zeit_interv_1; // use int, because quantity later calculated
int zeit_interv_2; // via double variable, such that it will be
// cut appropriately to be used for counting
int bild_nummer;

```

```
int nkuehl_ende;

// GPU/CUDA
// These pointers are declared to carry out the computation on the GPU

cuFloatComplex *gpu_wave;
cuFloatComplex *gpu_exp_H0;
cuFloatComplex *gpu_exp_H0_2;
cuFloatComplex *gpu_exp_V;

// GPU

// This function allocates the necessary memory in order
// to carry out the computation on the GPU
void variable_initialisieren ()
{
    printf ("Variable initialisieren Start\n");
    printf ("Size: cuFloatComplex = %d\n", sizeof (cuFloatComplex));
    printf ("Size: complex float = %d\n", sizeof (complex float));
    printf ("Size: cuDoubleComplex = %d\n", sizeof (cuDoubleComplex));
    printf ("Size: complex double = %d\n", sizeof (complex double));

    pp_MemAlloc ((void **)&wave, (void **)&gpu_wave,
                sizeof(cuFloatComplex) * schritte_x * schritte_y);
    pp_MemAlloc ((void **)&exp_H0, (void **)&gpu_exp_H0,
                sizeof(cuFloatComplex) * schritte_x * schritte_y);
    pp_MemAlloc ((void **)&exp_H0_2, (void **)&gpu_exp_H0_2,
                sizeof(cuFloatComplex) * schritte_x * schritte_y);
    pp_MemAlloc ((void **)&exp_V, (void **)&gpu_exp_V,
                sizeof(cuFloatComplex) * schritte_x * schritte_y);

    pp_fourier_initialisieren_2df (gpu_wave, schritte_x, schritte_y);
    printf ("Variable initialisieren Ende\n");
}

// This function then deallocates the memory
void variable_freigegeben ()
{
    pp_MemFree (wave, gpu_wave);
    pp_MemFree (exp_H0, gpu_exp_H0);
    pp_MemFree (exp_H0_2, gpu_exp_H0_2);
    pp_MemFree (exp_V, gpu_exp_V);

    pp_fourier_beenden ();
}
```

```

// This function calculates the absolute value squared of a complex
// number z
float cabs2 (float complex z)
{
    float re = crealf (z), im = cimagf (z);
    return re*re + im*im;
}

// This function writes the results into a binary file. It obtains the
// "raw" binary data from the GPU and performs Fourier transforms in
// order to get the results in position and momentum space
void wave_in_datei_binary (FILE *datei_binary_ort,
FILE *datei_binary_impuls)
{
    pp_fourier_2df (TRUE);

    pp_MemcpyToHost (wave, gpu_wave, schritte_x * schritte_y
* sizeof (cuFloatComplex));

    fwrite (wave, sizeof (cuFloatComplex), schritte_x * schritte_y,
datei_binary_ort);

    pp_fourier_2df (FALSE);

    pp_MemcpyToHost (wave, gpu_wave, schritte_x * schritte_y
* sizeof (cuFloatComplex));

    fwrite (wave, sizeof (cuFloatComplex), schritte_x * schritte_y,
datei_binary_impuls);
}

// This function writes the results into a data file. Therefore some
// manipulations are necessary like determining the actual positions
// and velocities. Furthermore, wer das hier liest ist doof and it
// also determines the corresponding expectation values and variances,
// although it is certainly nicer to do this with a seperate code and
// then also using the binary data, which was done for the results in
// this theses.
void wave_in_datei (FILE *datei_ort, FILE *datei_impuls,
FILE *datei_exp_var_ort, FILE *datei_exp_var_impuls, float t)
{
    int nr, mr;
    float vx, vy;
    float param_L_x = param_rand_max_x - param_rand_min_x;
    float param_L_y = param_rand_max_y - param_rand_min_y;
    float dkx = 2.0 * Pi / param_L_x;

```

```

float dky = 2.0 * Pi / param_L_y;
float cx = param_L_x * param_L_x * param_m / (2.0 * Pi * schritte_x
* schritte_x);
float cy = param_L_y * param_L_y * param_m / (2.0 * Pi * schritte_y
* schritte_y);

float summe;

float exp_x, exp_y, x_quad, y_quad, var_x, var_y, exp_vx_1,
exp_vy_1, exp_vx_2, exp_vy_2, exp_vx_3, exp_vy_3, exp_vx_4,
exp_vy_4, vx_quad_1, vy_quad_1, vx_quad_2, vy_quad_2, vx_quad_3,
vy_quad_3, vx_quad_4, vy_quad_4, exp_vx, exp_vy, vx_quad, vy_quad,
var_vx, var_vy;

printf ("Ortsdarstellung in Datei\n");
// Fourier Impuls -> Ort
pp_fourier_2df (TRUE);

pp_MemcpyToHost (wave, gpu_wave,
schritte_x * schritte_y * sizeof (cuFloatComplex));

summe=exp_x=exp_y=x_quad=y_quad=var_x=var_y=exp_vx=exp_vy=vx_quad=
vy_quad=var_vx=var_vy=exp_vx_1=exp_vy_1=vx_quad_1=vy_quad_1=
exp_vx_2=exp_vy_2=vx_quad_2=vy_quad_2=exp_vx_3=exp_vy_3=vx_quad_3=
vy_quad_3=exp_vx_4=exp_vy_4=vx_quad_4=vy_quad_4=0.0;

fprintf (datei_ort, "# INDEX = %d\n", bild_nummer);
for (nr=0; nr < schritte_x; nr++)
{
for (mr=0; mr < schritte_y; mr++)
{
if (nr % ausgabe_step_x == 0)
{
if (mr % ausgabe_step_y == 0)
{
fprintf (datei_ort, "%e %e %e %e\n", t,
nr * delta_x + param_rand_min_x,
mr * delta_y + param_rand_min_y,
cabs2 (wave [nr * schritte_y + mr]));
}
}
exp_x += (nr*delta_x + param_rand_min_x)
*cabs2 (wave[nr * schritte_y + mr]);
exp_y += (mr*delta_y + param_rand_min_y)
*cabs2 (wave[nr * schritte_y + mr]);
x_quad += (nr*delta_x + param_rand_min_x)*(nr*delta_x

```

```

    + param_rand_min_x)*cabs2 (wave[nr * schritte_y + mr]);
    y_quad += (mr*delta_y + param_rand_min_y)*(mr*delta_y
    + param_rand_min_y)*cabs2 (wave[nr * schritte_y + mr]);

    summe += cabs2 (wave[nr * schritte_y + mr]);
  }
}
exp_x = exp_x * delta_x * delta_y;
exp_y = exp_y * delta_x * delta_y;
x_quad = x_quad * delta_x * delta_y;
y_quad = y_quad * delta_x * delta_y;
var_x = sqrtf(x_quad-exp_x*exp_x);
var_y = sqrtf(y_quad-exp_y*exp_y);

fprintf (datei_exp_var_ort, "%e %e %e %e \n", exp_x, exp_y, var_x,
var_y);
fprintf (datei_exp_var_ort, "\n\n");

fprintf (datei_ort, "\n\n");
fflush (datei_ort); // neu
fflush (datei_exp_var_ort);

printf ("Ort: Norm = %e\n", summe * delta_x * delta_y);

printf ("Impulsdarstellung in Datei\n");
pp_fourier_2df (FALSE);

pp_MemcpyToHost (wave, gpu_wave,
  sizeof(float complex) * schritte_x * schritte_y);

summe = 0.0;

fprintf (datei_impuls, "# INDEX = %d\n", bild_nummer);
for (nr=schritte_x/2; nr < schritte_x; nr++)
{
  for (mr=schritte_y/2; mr < schritte_y; mr++)
  {
    if (nr % ausgabe_step_x == 0)
    {
      if (mr % ausgabe_step_y == 0)
      {
        vx = (nr-schritte_x) * dkx/param_m;
        vy = (mr-schritte_y) * dky/param_m;

        fprintf (datei_impuls, "%e %e %e %e\n", t, vx, vy,
          cabs2 (wave [nr * schritte_y + mr])*cx*cy);
      }
    }
  }
}

```

```

    }
    }
    exp_vx_1 += (nr-schritte_x) * dkx/param_m
    * cabs2 (wave [nr * schritte_y + mr])*cx*cy;
    exp_vy_1 += (mr-schritte_y) * dky/param_m
    * cabs2 (wave [nr * schritte_y + mr])*cx*cy;
    vx_quad_1 += (nr-schritte_x) * dkx/param_m * (nr-schritte_x)
    * dkx/param_m * cabs2 (wave [nr * schritte_y + mr])*cx*cy;
    vy_quad_1 += (mr-schritte_y) * dky/param_m * (mr-schritte_y)
    * dky/param_m * cabs2 (wave [nr * schritte_y + mr])*cx*cy;

    summe += cabs2 (wave[nr * schritte_y + mr])*cx*cy;
}
}

for (nr=schritte_x/2; nr < schritte_x; nr++)
{
    for (mr=0; mr < schritte_y/2; mr++)
    {
        if (nr % ausgabe_step_x == 0)
        {
            if (mr % ausgabe_step_y == 0)
            {
                vx = (nr-schritte_x) * dkx/param_m;
                vy = mr * dky/param_m;

                fprintf (datei_impuls, "%e %e %e %e\n", t, vx, vy,
                    cabs2 (wave [nr * schritte_y + mr])*cx*cy);
            }
        }
        exp_vx_2 += (nr-schritte_x) * dkx/param_m
        * cabs2 (wave [nr * schritte_y + mr])*cx*cy;
        exp_vy_2 += mr * dky/param_m
        * cabs2 (wave [nr * schritte_y + mr])*cx*cy;
        vx_quad_2 += (nr-schritte_x) * dkx/param_m * (nr-schritte_x)
        * dkx/param_m * cabs2 (wave [nr * schritte_y + mr])*cx*cy;
        vy_quad_2 += mr * dky/param_m * mr * dky/param_m
        * cabs2 (wave [nr * schritte_y + mr])*cx*cy;

        summe += cabs2 (wave[nr * schritte_y + mr])*cx*cy;
    }
}

for (nr=0; nr < schritte_x/2; nr++)
{
    for (mr=schritte_y/2; mr < schritte_y; mr++)
    {

```

```

if (nr % ausgabe_step_x == 0)
{
    if (mr % ausgabe_step_y == 0)
    {
        vx = nr * dkx/param_m;
        vy = (mr-schritte_y) * dky/param_m;

        fprintf (datei_impuls, "%e %e %e %e\n", t, vx, vy,
                cabs2 (wave [nr * schritte_y + mr])*cx*cy);
    }
}
exp_vx_3 += nr * dkx/param_m
* cabs2 (wave [nr * schritte_y + mr])*cx*cy;
exp_vy_3 += (mr-schritte_y) * dky/param_m
* cabs2 (wave [nr * schritte_y + mr])*cx*cy;
vx_quad_3 += nr * dkx/param_m * nr * dkx/param_m
* cabs2 (wave [nr * schritte_y + mr])*cx*cy;
vy_quad_3 += (mr-schritte_y) * dky/param_m * (mr-schritte_y)
* dky/param_m * cabs2 (wave [nr * schritte_y + mr])*cx*cy;

summe += cabs2 (wave[nr * schritte_y + mr])*cx*cy;
}
}

for (nr=0; nr < schritte_x/2; nr++)
{
    for (mr=0; mr < schritte_y/2; mr++)
    {
        if (nr % ausgabe_step_x == 0)
        {
            if (mr % ausgabe_step_y == 0)
            {
                vx = nr * dkx/param_m;
                vy = mr * dky/param_m;

                fprintf (datei_impuls, "%e %e %e %e\n", t, vx, vy,
                        cabs2 (wave [nr * schritte_y + mr])*cx*cy);
            }
}
exp_vx_4 += nr * dkx/param_m
* cabs2 (wave [nr * schritte_y + mr])*cx*cy;
exp_vy_4 += mr * dky/param_m
* cabs2 (wave [nr * schritte_y + mr])*cx*cy;
vx_quad_4 += nr * dkx/param_m * nr * dkx/param_m
* cabs2 (wave [nr * schritte_y + mr])*cx*cy;
vy_quad_4 += mr * dky/param_m * mr * dky/param_m
* cabs2 (wave [nr * schritte_y + mr])*cx*cy;
}
}

```



```

        summe += cabs2 (wave[nr * schritte_y + mr])*cx*cy;
    }
}
exp_vx = (exp_vx_1 + exp_vx_2 + exp_vx_3 + exp_vx_4)
* dkx*dky/(param_m*param_m);
exp_vy = (exp_vy_1 + exp_vy_2 + exp_vy_3 + exp_vy_4)
* dkx*dky/(param_m*param_m);
vx_quad = (vx_quad_1 + vx_quad_2 + vx_quad_3 + vx_quad_4)
* dkx*dky/(param_m*param_m);
vy_quad = (vy_quad_1 + vy_quad_2 + vy_quad_3 + vy_quad_4)
* dkx*dky/(param_m*param_m);

var_vx = sqrtf(vx_quad - exp_vx*exp_vx);
var_vy = sqrtf(vy_quad - exp_vy*exp_vy);

printf ("Geschw.: Norm = %e\n", summe * dkx*dky/(param_m*param_m));

fprintf (datei_impuls, "\n\n");

fprintf (datei_exp_var_impuls, "%e %e %e %e\n", exp_vx, exp_vy,
var_vx, var_vy);
fprintf (datei_exp_var_impuls, "\n\n");

fflush (datei_impuls); // neu
fflush (datei_exp_var_impuls);

bild_nummer++;

}

// This function calculates the potential, which is here given by a ring
// with Gaussian profile. Depending on the parameter nkuehl the potential
// is expanded along a square-root in time trajectory or compressed
// linearly in time and therefore allows for expansion and compression
// cycles
float potential (float x, float y, float t, int nkuehl)
{
    float radius, radius_rueck, r;

    r = sqrtf(x*x + y*y);
    if (nkuehl %2 == 1)
    {
        radius = sqrtf(t + param_t_init);
        //radius = param_pot_r_start + sqrtf(t);
    }
}

```

```

else
{
    radius = - beta*t + sqrtf(param_t_ende + param_t_init);
}
return param_pot_hoehe * expf(-(r - radius)*(r - radius)/
    (2.0*param_pot_sigma_r*param_pot_sigma_r));
}

// This function calculates the exponential of the potential
void exp_V_berechnen (float t, float delta_t, int nkuehl)
{
    int j,l;
    float v1;
    float v2;

#pragma omp parallel for private (j,l,v1,v2)
    for (j=0; j < schritte_x; j++)
    {
        for (l=0; l < schritte_y; l++)
        {
            v1 = potential (j * delta_x + param_rand_min_x,
                l * delta_y + param_rand_min_y, t, nkuehl);
            v2 = potential (j * delta_x + param_rand_min_x,
                l * delta_y + param_rand_min_y, t + delta_t, nkuehl);
            exp_V [j*schritte_y+l] = cexpf (-I/param_hbar * delta_t
                * 0.5 * (v1 + v2));
        }
    }
    pp_MemcpyToDevice (gpu_exp_V, exp_V, sizeof(float complex)
        * schritte_x * schritte_y);
}

// This function calculates the exponential of the kinetic term both
// for one and two time steps, since from one step of the time-
// evolution to the next we have a concatenation of these
// exponentials, and therefore we can reduce the number of
// calculations. The value for one time step is only needed at
// the beginning and the end
void exp_H0_berechnen (float delta_t)
{
    int n,m;
    float kx, ky;
    float param_L_x = param_rand_max_x - param_rand_min_x;
    float param_L_y = param_rand_max_y - param_rand_min_y;
    float dkx = 2.0 * Pi / param_L_x;
    float dky = 2.0 * Pi / param_L_y;

```

```
#pragma omp parallel for private (n,m,kx,ky)
  for (n=0; n < schritte_x/2; n++)
  {
    for (m=0; m < schritte_y/2; m++)
    {
      kx = n * dkx;
      ky = m * dky;
      exp_H0 [n*schritte_y+m] = cexpf (-I * (kx * kx + ky * ky)
        /(2.0 * param_m) * delta_t);
      exp_H0_2 [n*schritte_y+m] = cexpf (-I * (kx * kx + ky * ky)
        /(2.0 * param_m) * 0.5 * delta_t);
    }
  }

#pragma omp parallel for private (n,m,kx,ky)
  for (n=0; n < schritte_x/2; n++)
  {
    for (m=schritte_y/2; m < schritte_y; m++)
    {
      kx = n * dkx;
      ky = (m-schritte_y) * dky;
      exp_H0 [n*schritte_y+m] = cexpf (-I * (kx * kx + ky * ky)
        /(2.0 * param_m) * delta_t);
      exp_H0_2 [n*schritte_y+m] = cexpf (-I * (kx * kx + ky * ky)
        /(2.0 * param_m) * 0.5 * delta_t);
    }
  }

#pragma omp parallel for private (n,m,kx,ky)
  for (n=schritte_x/2; n < schritte_x; n++)
  {
    for (m=0; m < schritte_y/2; m++)
    {
      kx = (n-schritte_x) * dkx;
      ky = m * dky;
      exp_H0 [n*schritte_y+m] = cexpf (-I * (kx * kx + ky * ky)
        /(2.0 * param_m) * delta_t);
      exp_H0_2 [n*schritte_y+m] = cexpf (-I * (kx * kx + ky * ky)
        /(2.0 * param_m) * 0.5 * delta_t);
    }
  }

#pragma omp parallel for private (n,m,kx,ky)
  for (n=schritte_x/2; n < schritte_x; n++)
  {
    for (m=schritte_y/2; m < schritte_y; m++)
```

```

    {
        kx = (n-schritte_x) * dkx;
        ky = (m-schritte_y) * dky;
        exp_H0 [n*schritte_y+m] = cexp (-I * (kx * kx + ky * ky)
        /(2.0 * param_m) * delta_t);
        exp_H0_2 [n*schritte_y+m] = cexp (-I * (kx * kx + ky * ky)
        /(2.0 * param_m) * 0.5 * delta_t);
    }
}

pp_MemcpyToDevice (gpu_exp_H0, exp_H0, sizeof(float complex)
* schritte_x * schritte_y);
pp_MemcpyToDevice (gpu_exp_H0_2, exp_H0_2, sizeof(float complex)
* schritte_x * schritte_y);
}

// This function initialises the wavefunction
void wave_initialisieren ()
{
    int j,l;
    float cx,cy, x,y;
    float tx, ty, x0, y0, norm2 = 0.0;
    complex float c1x, c2x, c1y, c2y;

    printf ("Wave initialisieren Start\n");
    //printf ("v dimensionslos = %f\n", param_v0);
    //printf ("p dimensionslos = %f\n", param_v0 * param_m);
    //printf ("kmin = %f\n",-schritte_x/2 * alpha * sqrt(t_ende)
    /* 2.0 * Pi/L);
    //printf ("kmax = %f\n",(schritte_x/2-1) * alpha * sqrt(t_ende)
    /* 2.0 * Pi/L);

    cx = 4.0*param_delta_x * param_delta_x - 1.0/(param_delta_vx
    * param_delta_vx * param_m * param_m); // Uncertainty relation
    if (cx<0.0)
    {
        printf ("Unschaerferelation in x verletzt!\n");
        exit (EXIT_FAILURE);
    }

    cy = 4.0*param_delta_y * param_delta_y - 1.0/(param_delta_vy
    * param_delta_vy * param_m * param_m); // Uncertainty relation
    if (cy<0.0)
    {
        printf ("Unschaerferelation in y verletzt!\n");
        exit (EXIT_FAILURE);
    }
}

```

```

tx = sqrtf(cx)/(2.0 * param_delta_vx);
ty = sqrtf(cy)/(2.0 * param_delta_vy);
x0 = param_x0 - tx * param_v0x;
y0 = param_y0 - ty * param_v0y;

c1x=sqrtf(sqrtf(2.0/Pi))/csqrtf(1.0/(param_delta_vx * param_m)
+ 2.0*I*param_delta_vx * tx);
c2x = param_m/(2.0 * (1.0 + 2.0*I*param_delta_vx *param_delta_vx
*param_m * tx));

c1y=sqrtf(sqrtf(2.0/Pi))/csqrtf(1.0/(param_delta_vy * param_m)
+ 2.0*I*param_delta_vy * ty);
c2y = param_m/(2.0 * (1.0 + 2.0*I*param_delta_vy *param_delta_vy
*param_m * ty));

for (j=0; j < schritte_x; j++)
{
    for (l=0; l < schritte_y; l++)
    {
        x = j * delta_x + param_rand_min_x;
        y = l * delta_y + param_rand_min_y;
        wave [j * schritte_y + l] = c1x * cexpf(-c2x*(2.0
*param_delta_vx*param_delta_vx*param_m*((x-x0)*(x-x0)+2.0*tx
*param_v0x*x0) + I*param_v0x*(tx*param_v0x-2.0*x))) * c1y
* cexpf(-c2y*(2.0*param_delta_vy*param_delta_vy*param_m
*((y-y0)*(y-y0)+2.0*ty*param_v0y*y0) + I*param_v0y
* (ty*param_v0y-2.0*y)));

        norm2 += cabs2(wave [j * schritte_y + l]);
    }
}

norm2 *= delta_x * delta_y;
printf ("Anfangsnorm Ort = %e\n", norm2);

pp_MemcpyToDevice (gpu_wave, wave, schritte_x * schritte_y
* sizeof (cuFloatComplex));

pp_fourier_2df (FALSE);
printf ("Wave ist initialisiert\n");
}

// This function calculates multiple steps of the time-evolution
// on the GPU
void mehrere_zeitschritte (int anzahl, float *t, float delta_t,
int nkuehl)
{

```

```

int nr;

// Here exp_H0_2 has to be calculated once in advance as was
// discussed above
pp_Mul_2df (gpu_wave, gpu_exp_H0_2, schritte_x, schritte_y);

for (nr=1; nr <= anzahl-1; nr++)
{
    pp_fourier_2df (TRUE);

    // exp_V
    exp_V_berechnen (*t, delta_t, nkuehl);
    pp_Mul_2df (gpu_wave, gpu_exp_V, schritte_x, schritte_y);

    pp_fourier_2df (FALSE);

    // exp_H0
    pp_Mul_2df (gpu_wave, gpu_exp_H0, schritte_x, schritte_y);

    printf ("t = %f\n", *t);
    *t += delta_t;
}

pp_fourier_2df (TRUE);

// exp_V
exp_V_berechnen (*t, delta_t, nkuehl);
pp_Mul_2df (gpu_wave, gpu_exp_V, schritte_x, schritte_y);

// Fourier Ort -> Impuls
pp_fourier_2df (FALSE);

// Here exp_H0_2 has to be calculated once more as was
// discussed above
pp_Mul_2df (gpu_wave, gpu_exp_H0_2, schritte_x, schritte_y);
*t += delta_t;
}

// This function writes the chosen parameters into the file
void param_in_datei (FILE *datei)
{
    fprintf (datei, "# pot_hoehe           = %e\n", param_pot_hoehe);
    fprintf (datei, "# pot_sigma_r       = %e\n", param_pot_sigma_r);
    fprintf (datei, "# x0                 = %e\n", param_x0);
    fprintf (datei, "# delta_x           = %e\n", param_delta_x);
    fprintf (datei, "# v0x               = %e\n", param_v0x);
    fprintf (datei, "# delta_vx          = %e\n", param_delta_vx);
}

```

```

    fprintf (datei, "# y0                = %e\n",param_y0);
    fprintf (datei, "# delta_y          = %e\n",param_delta_y);
    fprintf (datei, "# v0y              = %e\n",param_v0y);
    fprintf (datei, "# delta_vy         = %e\n",param_delta_vy);
    fprintf (datei, "# m                = %e\n",param_m);
    fprintf (datei, "# Lx              = %e\n",param_L_x);
    fprintf (datei, "# Ly              = %e\n",param_L_y);
    fprintf (datei, "# ausgabe_step_x   = %d\n",ausgabe_step_x);
    fprintf (datei, "# ausgabe_step_y   = %d\n",ausgabe_step_y);
}

// This function defines the header for the file containing
// the expectation values and variances in order to
// identify them later
void param_in_datei_exp_var (FILE *datei1, FILE *datei2)
{
    fprintf (datei1, " Erwartungswert x  Erwartungswert y  Varianz x
    Varianz y \n\n");
    fprintf (datei2, "Erwartungswert vx  Erwartungswert vy  Varianz vx
    Varianz vy \n\n");
}

// This function calculates the actual time-evolution of the
// wavefunction
void wave_entwicklung (char *dateiname1, char *dateiname2,
char *dateiname3, char *dateiname4, char *dateiname_binary1,
char *dateiname_binary2, int anzahl_t_schritte, int anzahl_bilder,
int anzahl_ausgabe_x, int anzahl_ausgabe_y)
{
    FILE *datei_ort = fopen (dateiname1, "w");
    FILE *datei_impuls = fopen (dateiname2, "w");
    FILE *datei_exp_var_ort = fopen (dateiname3, "w");
    FILE *datei_exp_var_impuls = fopen (dateiname4, "w");
    FILE *datei_binary_ort = fopen (dateiname_binary1, "w");
    FILE *datei_binary_impuls = fopen (dateiname_binary2, "w");
    int nr, nr2, nr_step_bild, nr_step_bild_1, nr_step_bild_2, j,
    nkuehl, anzahl_t_schritte_1, anzahl_t_schritte_2;
    float t, delta_t, delta_t_1, delta_t_2;

    if ((datei_ort == NULL) || (datei_impuls == NULL) ||
(datei_exp_var_ort == NULL) || (datei_exp_var_impuls == NULL))
    {
        printf ("Fehler bei Dateioeffnung");
        exit (EXIT_FAILURE);
    }

    //schritte_x = anzahl_x_schritte;

```

```
//schritte_y = anzahl_y_schritte;

delta_t = param_t_ende / anzahl_t_schritte;
printf ("delta_t = %e\n", delta_t);
delta_x = (param_rand_max_x - param_rand_min_x)/(schritte_x * 1.0);
delta_y = (param_rand_max_y - param_rand_min_y)/(schritte_y * 1.0);

anzahl_t_schritte_1 = anzahl_t_schritte * zeit_interv_1;
anzahl_t_schritte_2 = anzahl_t_schritte * zeit_interv_2;

ausgabe_step_x = schritte_x/anzahl_ausgabe_x;
ausgabe_step_y = schritte_y/anzahl_ausgabe_y;

if (ausgabe_step_x == 0)
    ausgabe_step_x = 1;

if (ausgabe_step_y == 0)
    ausgabe_step_y = 1;

variable_initialisieren ();
bild_nummer = 0;

param_in_datei (datei_ort);
param_in_datei (datei_impuls);

param_in_datei_exp_var (datei_exp_var_ort, datei_exp_var_impuls);

t = 0.0;

nkuehl = 1;

wave_initialisieren ();

nr_step_bild = anzahl_t_schritte / anzahl_bilder;
nr_step_bild_1 = anzahl_t_schritte_1 / anzahl_bilder;
nr_step_bild_2 = anzahl_t_schritte_2 / anzahl_bilder;

wave_in_datei (datei_ort, datei_impuls, datei_exp_var_ort,
datei_exp_var_impuls, t);
wave_in_datei_binary (datei_binary_ort, datei_binary_impuls);

for (nkuehl = 1; nkuehl <=nkuehl_ende; nkuehl++)
{
    if (nkuehl % 2==1) // Expansion
    {
        //delta_t_1 = delta_t * zeit_interv_1;
```



```

        exp_H0_berechnen (delta_t); // Calculation for every Cycle
        t=0.0;
        for (nr = 1; nr <= anzahl_t_schritte_1 / nr_step_bild_1;
            nr++)
        {
            mehrere_zeitschritte (nr_step_bild_1, &t, delta_t,
                nkuehl);
            wave_in_datei (datei_ort, datei_impuls,
                datei_exp_var_ort, datei_exp_var_impuls,t);
            wave_in_datei_binary (datei_binary_ort,
                datei_binary_impuls);

            printf ("t = %f\n", t);
        }
    }

else // Compression
{
    //delta_t_2 = delta_t * zeit_interv_2;
    exp_H0_berechnen (delta_t);
    t=0.0;
    for (nr = 1; nr <= anzahl_t_schritte_2 / nr_step_bild_2;
        nr++)
    {
        mehrere_zeitschritte (nr_step_bild_2, &t, delta_t,
            nkuehl);
        wave_in_datei (datei_ort, datei_impuls,
            datei_exp_var_ort, datei_exp_var_impuls,t);
        wave_in_datei_binary (datei_binary_ort,
            datei_binary_impuls);

        printf ("t = %f\n", t);
    }
}

variable_freigeben ();

fclose (datei_ort);
fclose (datei_impuls);
fclose (datei_exp_var_ort);
fclose (datei_exp_var_impuls);
fclose (datei_binary_ort);
fclose (datei_binary_impuls);
}

/*

```

Compiling with Intel Compiler

```
icc kuehlung.c cutools_v3.o -I /usr/local/cuda/include -L /usr/local/cuda/lib64 -lcuda -l
```

```
*/
```

```
int main (int argc, char *argv[])
{
    char prg [200];
    int param_nr;

    /*strcpy (prg, argv[0]); // Security check, can be useful
    printf ("Programmname %s wird ausgefuehrt (Parameter=%d)!\n", prg,
    argc);

    if (argc < 2)
    {
        printf ("Zuwenige Parameter: Parameternr erwartet!\n");
        exit (EXIT_FAILURE);
    }
    sscanf(argv[1], "%d", &param_nr);*/

    param_pot_hoehe = 30000.0;
    param_pot_sigma_r = 0.01;
    param_pot_r_start = 0.04
    param_rand_min_x = -1.2;
    param_rand_max_x = 1.2;
    param_rand_min_y = -1.2;
    param_rand_max_y = 1.2;
    param_L_x = param_rand_max_x-param_rand_min_x;
    param_L_y = param_rand_max_y-param_rand_min_y;
    param_m = 296.033;
    param_x0 = 0.0;
    param_delta_x = 0.00474299;
    param_v0x = 5.0;
    param_delta_vx = 1.2;
    param_y0 = 0.0;
    param_delta_y = 0.00474299;
    param_v0y = 5.0;
    param_delta_vy = 1.2;
    param_t_init = 0.004;
    nkuehl_ende = 2;
    beta = 0.001;
    zeit_interv_1=1;
    zeit_interv_2=1/beta*(sqrtf(param_t_ende + param_t_init)
    -sqrtf(param_t_init))/param_t_ende;
```

```

printf ("zeit_interv_2 = %d \n", zeit_interv_2);

float param_L_x = param_rand_max_x - param_rand_min_x;
float param_L_y = param_rand_max_y - param_rand_min_y;
float dkx = 2.0 * Pi / param_L_x;
float dky = 2.0 * Pi / param_L_y;
printf ("v_max = %e\n", dkx * schritte_x/2/param_m);
param_t_ende = 1.0;

wave_entwicklung ("datafilename_position.dat",
"datafilename_momentum.dat",
"datafilename_position_expectation_variance.dat",
"datafilename_momentum_expectation_variance.dat",
"binaryfilename_position.bin", "binaryfilename_momentum.bin",
anzahl_t_schritte, anzahl_bilder, anzahl_ausgabe_x,
anzahl_ausgabe_y);

return 0;
}

```

E.4 Quantum Catcher

E.4.1 Classical Particles

```

// With this program we calculate the final phase-space distribution
// of an ensemble of classical particles becoming trapped between two
// mirror potentials both moving along a square-root in time
// trajectory, after the particle could pass the first mirror
// potential once coming from the left. Afterwards the particles
// undergo repeated reflections

#include <stdio.h>
#include <stdlib.h>
#include <complex.h>
#include <math.h>
#include <omp.h>
#include <string.h>

double Pi = 3.14159265358979323846264338327950288419716939937510582097
4944592307816406286208998628034825342117068;

const int TRUE = (1==1);
const int FALSE = (1==0);

double param_tf;
double x_md;

```

```
// These are the parameters for the initial Gaussian distribution
// and the degree of freedom alpha for the square-root in time
// trajectory in SI units
double sv0;
double sx0;
double alpha;
double sdx;
double sdv;

// These are the values for the integration
double x_ende;
double x_start;
double delta_x;
int schritte_x;

double v_start;
double v_ende;
double delta_v;
int schritte_v;

#define max_punkte 10000

double wkeit [max_punkte][max_punkte];
// wkeit_sonstiges measures how much is lost for given integration
// parameters
double wkeit_sonstiges;

// This function just sets back the probabilities
void wkeit_zuruecksetzen ()
{
    int nrx, nrv;
    for (nrx=0; nrx < schritte_x; nrx++)
        for (nrv=0; nrv < schritte_v; nrv++)
            wkeit [nrx][nrv] = 0.0;
    wkeit_sonstiges = 0.0;
}

// This function writes the important parameters into the output file
void dateikopf_schreiben (FILE *datei)
{
    fprintf (datei, "# tf          = %e\n", param_tf);
    fprintf (datei, "# alpha       = %e\n", alpha);
    fprintf (datei, "# x_md        = %e\n", x_md);
    fprintf (datei, "# Startfunktion:n");
    fprintf (datei, "# sx0         = %e\n", sx0);
}
```

```

fprintf (datei, "# sdx          = %e\n", sdx);
fprintf (datei, "# sv0          = %e\n", sv0);
fprintf (datei, "# sdv          = %e\n", sdv);
fprintf (datei, "# Integrationsparameter:\n");
fprintf (datei, "# x_start      = %e\n", x_start);
fprintf (datei, "# x_ende        = %e\n", x_ende);
fprintf (datei, "# x_schritte    = %d\n", schritte_x);
fprintf (datei, "# v_start      = %e\n", v_start);
fprintf (datei, "# v_ende        = %e\n", v_ende);
fprintf (datei, "# v_schritte    = %d\n", schritte_v);
}

// This function calculates the initial coordinates by choosing random
// numbers
void start_koordinaten (double *xs, double *vs)
{
    double x, y, s, dx, dy;
    do
    {
        do
        {
            x = 2.0*rand()/(1.0*RAND_MAX) - 1.0;
            y = 2.0*rand()/(1.0*RAND_MAX) - 1.0;
            s = x*x + y*y;
        }
        while ((s == 0.0) || (s >= 1.0));
        dx = sqrt(-2.0*log(s)/s);
        dy = sqrt(-2.0*log(s)/s);
        *xs = dx*x * sdx + sx0;
        *vs = dy*y * sdv + sv0;
    }
    while (*xs >= 0.0); // this produces a restart if one is on the right
                       // side of the mirror
}

// This function calculates the mirror or diode collision time depending
// on a parameter x_shift by solving the corresponding algebraic
// equations which can be found in the corresponding chapter
double tcollision_allgemein (double x0, double v0, double t0, double tf,
double x_shift)
{
    double xrel, trel, r, z1, z2;
    double arg_sqrt;

    xrel = x0 - x_shift;

```

```

if (v0 == 0.0)
{
    z1 = z2 = xrel/alpha;
}
else
{
    arg_sqrt = 1.0 - 4 * (xrel - v0 * t0)*v0/(alpha*alpha);
    if (arg_sqrt < 0.0)
        z1 = z2 = -1;
    else
    {
        r = sqrt(arg_sqrt);
        z1 = alpha/(2*v0) * (1 + r);
        z2 = alpha/(2*v0) * (1 - r);
    }
}
if ((z1 < 0.0) || (z1*z1 <= t0) || (z1*z1 >= tf))
    z1 = -1;
if ((z2 < 0) || (z2*z2 <= t0) || (z2*z2 >= tf))
    z2 = -1;
if ((z1 > 0) && (z2 > 0))
{
    if (z1 > z2) // Minimum
        return z2*z2;
    else
        return z1*z1;
}
else if (z1 > 0)
    return z1*z1;
else if (z2 > 0)
    return z2*z2;
else
    return -1;
}

// This function calculates the appropriate collision time by calling
// the latter function by turns with the appropriate shift
double tcollision (double x0, double v0, double t0, double tf,
int col_mirror)
{
    double z;
    if (col_mirror)
        return tcollision_allgemein (x0, v0, t0, tf, 0.0);
    else
        return tcollision_allgemein (x0, v0, t0, tf, x_md);
}

```

```
}

// Based on the initial coordinates this function calculates the final
// coordinates.
void end_koordinaten (double x0, double v0, double *xf, double *vf)
{
    int col_mirror;
    double akt_t, td, tm;
    double tc;
    double x, v;

    if (x0 >= 0.0) // If the initial value is on the right side of the
                  // mirror the program stops
    {
        printf (" rechts vom Mirror\n");
        exit (EXIT_FAILURE);
    }

    if (x0 <= x_md) // On the left side of the mirror
        col_mirror = TRUE; // First a mirror collision
    else
    {
        tm = tcollision (x0, v0, 0.0, param_tf, TRUE);
        td = tcollision (x0, v0, 0.0, param_tf, FALSE);
        printf ("tm=%e ms, td=%e ms\n", tm, td);
        if (tm >= 0.0)
            col_mirror = (td < 0.0) || (td > tm);
        else
            col_mirror = FALSE;
    }

    akt_t = 0.0;
    x = x0; v = v0;

    tc = tcollision (x, v, akt_t, param_tf, col_mirror);

    while (tc > 0.0) // Calculating the position and velocity
                   // backwards for all collisions which occur
    {
        x = x + v * (tc - akt_t);
        v = - v + alpha/sqrt(tc);

        akt_t = tc;

        col_mirror = !col_mirror;

        tc = tcollision (x, v, akt_t, param_tf, col_mirror);
    }
}
```

```

    }
    x = x + v * (param_tf - akt_t);

    *xf = x;
    *vf = v;
}

// This function calculates the position and velocity for one particle
void ein_teilchen (int startverteilung)
{
    double xs, vs, xf, vf;
    int nrx, nrv;

    start_koordinaten (&xs, &vs);
    if (startverteilung)
    {
        xf=xs; vf=vs;
    }
    else
        end_koordinaten (xs, vs, &xf, &vf);

    nrx = (xf - x_start)/delta_x;
    nrv = (vf - v_start)/delta_v;

    if ((nrx >= 0) && (nrx < schritte_x) && (nrv >= 0) &&
        (nrv < schritte_v))
    {
#pragma omp atomic
        wkeit [nrx] [nrv]++;
    }
    else
    {
        printf ("Aussen-Ziel: xs=%e mum, vs=%e cm/s, xf=%e mum,
            vf=%e cm/2\n", xs*1e6, vs*1e2, xf*1e6, vf*1e2);
#pragma omp atomic
        wkeit_sonstiges++;
    }
}

// This function calculates the whole final probability distribution
// based on one particle trajectories and writes it into a file
void wkeit_in_datei (char *dateiname, int punktex, int punktev,
    int anzahl_N, int startverteilung)
{
    schritte_x = punktex;
    schritte_v = punktev;
    delta_v = (v_ende - v_start) / (punktev * 1.0);

```



```

delta_x = (x_ende - x_start) / (punktex * 1.0);

int nr, xnr, vnr;
double r;
FILE *datei = fopen (dateiname,"w");

srand(time(NULL));

fprintf (datei, "# Phasenraumdichte\n");
dateikopf_schreiben (datei);

wkeit_zuruecksetzen ();
#pragma omp parallel for private(nr)
for (nr=0; nr < anzahl_N; nr++)
{
    printf ("n=%d\n", nr);
    ein_teilchen (startverteilung);
}

r = 1.0/(1.0*anzahl_N)/(delta_x*delta_v);

for (xnr=0; xnr < punktex; xnr++)
{
    for (vnr=0; vnr < punktev; vnr++)
    {
        if (wkeit [xnr][vnr] > 0)
        {
            // The scaling vor micrometer and cm/s is commented out
            /*fprintf (datei, "%e %e %e\n", (x_start + xnr
            * delta_x)*1e6,(v_start + vnr * delta_v)*1e2,
            wkeit [xnr][vnr]*r);*/
            fprintf (datei, "%e %e %e\n", (x_start+xnr*delta_x),
            (v_start + vnr * delta_v), wkeit [xnr][vnr]*r);
        }
    }
}

fprintf (datei, "# Sonstige Wkeit: %e\n", wkeit_sonstiges
/(1.0*anzahl_N));
printf ("Sonstige Wkeit: %e\n", wkeit_sonstiges/(1.0*anzahl_N));

fclose (datei);
}

/*

Compiling with GNU Compiler

```

```
cc filename.c -lm -fopenmp -lpthread -lgsl -lgslcblas -o name.out

Compiling with Intel Compiler

icc filename.c -lm -openmp -lpthread -lgsl -lgslcblas -o name.out

*/

int main ()
{
    // final time is always 1 sec
    param_tf = 1.0;
    // diode position, whose absolute value is also the distance to
    // the mirror
    x_md = -1e-6;

    // initial parameters: average velocity and position, variances,
    // and the degree of freedom alpha for the square-root trajectory
    sv0 = 10.0;
    sx0 = -2e-6;
    alpha = 1.0;
    sdx = 0.2e-6;
    sdv = 1.0e0;

    // The boundaries for the grid in position and velocity space
    // Depending on what is commented out either the initial
    // (startverteilung -> TRUE) or final (startverteilung -> FALSE)
    // distribution are calculated and written into a file
    x_start = -2e-5;
    x_ende = 0.0;
    v_start = 0.0;
    v_ende = 20.0;
    //wkeit_in_datei ("datafilename.dat", punktex, punktev, anzahl_N,
    //TRUE);

    v_start = -20.0;
    v_ende = 20.0;
    x_start = -2e-5;
    x_ende = 1.0;
    wkeit_in_datei ("datafilename.dat", punktex, punktev, anzahl_N, FALSE);

    return 0;
}
```

E.4.2 Quantum Particles: Quantum Jump Approach

```
// This program calculates the time evolution of an ensemble of non-  
// interacting three level atoms with positive momenta first interacting  
// with a quench laser and, after the excitation, interacting with two  
// mirror potentials moving along a trajectory proportional to the  
// square-root in time such that the atoms become trapped and slowed due  
// to subsequent collisions. The solution is derived via the quantum  
// jump approach. This algorithm was written such that it runs on a  
// NVIDIA graphics card
```

```
#include <stdio.h>  
#include <stdlib.h> // stdlib included because of  
#include <time.h> // void exit(int fehlernummer)  
#include <math.h>  
#include <complex.h>  
#include <string.h>  
#include "pptools_v2.h"  
  
#define max_dateiname 100  
#define max_schritte 1200000  
  
const int FALSE = (1==0);  
const int TRUE = (1==1);  
  
const double Pi = 3.141592653589793238462643383279502884197169399375105  
820974944592307816406286208998628034825342117068;  
  
// Declaring the necessary variables, pointers and arrays, i.e. the  
// wavefunction, the time-evolution operators, the parameters for time,  
// position and velocity, the potential parameters like height, width,  
// position and finally the boundaries of the box for the simulation  
// and the number of trajectories. Since in this setting only one jump  
// occurs, the maximum number of trajectories is called jumps  
  
//double complex wave [max_schritte];  
double complex *wave;  
cuDoubleComplex *gpu_wave;  
  
//double complex exp_V [max_schritte];  
double complex *exp_H0;  
cuDoubleComplex *gpu_exp_H0;  
  
double complex *exp_H0_2;  
cuDoubleComplex *gpu_exp_H0_2;  
  
double complex *exp_V;
```

```

cuDoubleComplex *gpu_exp_V;

double param_t_ende;
//double delta_t;
double delta_x;
int schritte_x;
double param_v0;
double param_m;

double param_x0;
double param_delta_x;
double param_delta_v;
int ausgabe_step;

double param_coupling_strength;
double param_pot_hoehe;
double x_m, x_d, x_p;
double param_gamma;
double param_pump_sigma, param_mirror_sigma, param_diode_sigma;
double param_rand_min, param_rand_max;
double param_L;

int zeit_interv;
int jumps;

// This function calculates the absolute value squared of a complex
// number z
double cabs2 (double complex z)
{
    double re = creal (z), im = cimag (z);
    return re*re + im*im;
}

// This function calculates the potential induced by the quenching laser
double omega (double x, double t)
{
    double pos_p;

    pos_p = x_p + sqrt(t);
    return param_coupling_strength*exp(-(x-pos_p)*(x-pos_p)
    /(2*param_pump_sigma*param_pump_sigma));
}

// This function calculates the complex potential which reduces the norm
// of the wavefunction where the reduction of norm is used to decide

```

```

// whether a jump occurred or not
double complex potential_coupling (double x, double t)
{
    return -I/2 * omega(x,t)*omega(x,t)/(param_gamma);
}

// This function calculates the two potentials the atoms interact with
// after the jump
double potential_trapped (double x, double t)
{
    double pos_m, pos_d;

    pos_m = x_m + sqrt(t);
    pos_d = x_d + sqrt(t);
    return param_pot_hoehe * (exp(-(x-pos_m)*(x-pos_m)
    /(2.0*param_mirror_sigma*param_mirror_sigma)) + exp(-(x-pos_d)
    *(x-pos_d)/(2.0*param_diode_sigma*param_diode_sigma)));
}

// This function allocates the necessary memory on the GPU for those
// arrays whose calculation is performed on it
// Additionally it also initializes the Fourier transform
void variable_initialisieren (int anzahl)
{
    pp_MemAlloc ((void **)&exp_H0_2, (void **)&gpu_exp_H0_2,
    sizeof (cuDoubleComplex) * anzahl);
    pp_MemAlloc ((void **)&exp_H0, (void **)&gpu_exp_H0,
    sizeof (cuDoubleComplex) * anzahl);

    pp_MemAlloc ((void **)&exp_V, (void **)&gpu_exp_V,
    sizeof (cuDoubleComplex) * (anzahl + 256));
    pp_MemAlloc ((void **)&wave, (void **)&gpu_wave,
    sizeof (cuDoubleComplex) * (anzahl + 256));

    pp_fourier_initialisieren (gpu_wave, anzahl);
}

// This function deallocates the memory again
void variable_freigeben ()
{
    pp_fourier_beenden ();

    pp_MemFree (exp_H0_2, gpu_exp_H0_2);
    pp_MemFree (exp_H0, gpu_exp_H0);
    pp_MemFree (wave, gpu_wave);
    pp_MemFree (exp_V, gpu_exp_V);
}

```

```

// This function calculates the evolution operator for the respective
// potentials before and after a jump. To further reduce the computation
// time, we calculate it just once for the initial time. The change due
// to the time dependence is then done by picking different array
// entries at different times. This is possible since the shape of the
// potential does not change, but only the position
void exp_V_berechnen (double t, double delta_t, int i)
{
    int j;
    double complex v1;
    double complex v2;

// The if condition is there to choose the correct potential depending
// on if a jump occurred or not. The calculation is parallelized, since it
// is not done on the GPU, because it has to be calculated only once
    if (i==0)
    {
#pragma omp parallel for private (j,v1,v2)
        for (j=0; j < schritte_x; j++)
        {
            v1 = potential_coupling (j * delta_x + param_rand_min, 0);
            exp_V [j] = cexp (-I * delta_t * 0.25 * v1);
        }
    }
    else
    {
#pragma omp parallel for private (j,v1,v2)
        for (j=0; j < schritte_x; j++)
        {
            v1 = potential_trapped (j * delta_x + param_rand_min, 0);
            exp_V [j] = cexp (-I * delta_t * 0.25 * v1);
        }
    }
    pp_MemcpyToDevice (gpu_exp_V, exp_V, schritte_x
    * sizeof (cuDoubleComplex));
}

// This function calculates the evolution operator for the kinetic
// term. After the calculation it is copied to the GPU for the time-
// evolution
void exp_H0_ausfuehren (double delta_t)
{
    int n;
    double k;
    double param_L = param_rand_max - param_rand_min;
    double dk = 2.0 * Pi / param_L;

```

```

for (n=0; n < schritte_x/2; n++)
{
    k = n * dk;
    exp_H0_2 [n] = cexp(-I*0.5*k*k/(2.0*param_m)*delta_t);
    exp_H0 [n] = cexp(-I*k*k/(2.0*param_m)*delta_t);
}
for (n=schritte_x/2; n < schritte_x; n++)
{
    k = (n-schritte_x) * dk;
    exp_H0_2 [n] = cexp(-I*0.5*k*k/(2.0*param_m)*delta_t);
    exp_H0 [n] = cexp(-I*k*k/(2.0*param_m)*delta_t);
}

pp_MemcpyToDevice (gpu_exp_H0_2, exp_H0_2, schritte_x
* sizeof (cuDoubleComplex));
pp_MemcpyToDevice (gpu_exp_H0, exp_H0, schritte_x
* sizeof (cuDoubleComplex));
}

// This function calculates one time step of the evolution. This is done
// on the GPU. Additionally depending on the time the correct array
// entry of the potential is chosen via the offset variables ofs, which
// mimics the the time dependence of the potential but has the advantage
// that the potential has to be calculated only once
void einen_zeitschritt (double t, double delta_t)
{
    int ofs_1, ofs_2, a, b;

    double delta_x = param_L/(1.0 * schritte_x);

    ofs_1 = floor(sqrt(t)/delta_x);
    ofs_2 = floor(sqrt(t+delta_t)/delta_x);

    a = ceil((schritte_x - ofs_1)/256.) * 256;
    b = ceil((schritte_x - ofs_2)/256.) * 256;

    pp_Mul (gpu_wave + ofs_1, gpu_exp_V, a);
    pp_Mul (gpu_wave + ofs_2, gpu_exp_V, b);

    pp_fourier (FALSE);

    pp_Mul (gpu_wave, gpu_exp_H0, schritte_x);

    pp_fourier (TRUE);
}

```

```

pp_Mul (gpu_wave + ofs_1, gpu_exp_V, a);
pp_Mul (gpu_wave + ofs_2, gpu_exp_V, b);

}

// This function initializes the wavefunction, which is a Gaussian, but
// not necessarily a minimal uncertainty one
void wave_initialisieren ()
{
    int j;
    double c, x;
    double t, x0;
    complex double c1, c2;
    double delta_x = param_L/(1.0*schritte_x);
    double norm, norm2;

    norm = 0.0;
    norm2 = 0.0;

    c = 4.0*param_delta_x * param_delta_x - 1.0/(param_delta_v
    * param_delta_v * param_m * param_m); // Uncertainty relation
    if (c<0.0)
    {
        printf ("Unschaerferelation verletzt!\n");
        exit (EXIT_FAILURE);
    }
    t = sqrt(c)/(2.0 * param_delta_v);
    x0 = param_x0 - t * param_v0;

    c1=sqrt(sqrt(2.0/Pi))/csqrt(1.0/(param_delta_v * param_m)
    + 2.0*I*param_delta_v * t);
    c2 = param_m/(2.0 * (1.0 + 2.0*I*param_delta_v *param_delta_v
    *param_m * t));

    for (j=0; j < schritte_x; j++)
    {
        x = j * delta_x + param_rand_min;
        wave [j] = c1 * cexp (-c2*(2.0*param_delta_v*param_delta_v
        *param_m*((x-x0)*(x-x0)+2.0*t*param_v0*x0)
        + I*param_v0 * (t*param_v0-2.0*x)));
        norm += cabs2 (wave [j]);
    }
    printf("Norm zu Beginn = %e \n", norm);
    for (j=0; j < schritte_x; j++)
    {

```



```

        wave[j] = wave[j]/sqrt(norm);
    }
    for (j=0; j < schritte_x; j++)
    {
        norm2 += cabs2 (wave [j]);
    }
    printf("Norm2 zu Beginn = %e \n", norm2); // Normalisation

    pp_MemcpyToDevice (gpu_wave, wave, schritte_x
    * sizeof (cuDoubleComplex));

}

// This function writes the important parameters into the output file
void param_in_datei (FILE *datei)
{
    fprintf (datei, "# pot_hoehe           = %e\n",param_pot_hoehe);
    fprintf (datei, "# coupling strength = %e\n",
    param_coupling_strength);
    fprintf (datei, "# mirror_sigma       = %e\n",param_mirror_sigma);
    fprintf (datei, "# diode_sigma        = %e\n",param_diode_sigma);
    fprintf (datei, "# pump_sigma         = %e\n",param_pump_sigma);
    fprintf (datei, "# xm                = %e\n",x_m);
    fprintf (datei, "# xd                = %e\n",x_d);
    fprintf (datei, "# xp                = %e\n",x_p);
    fprintf (datei, "# x0                = %e\n",param_x0);
    fprintf (datei, "# delta_x           = %e\n",param_delta_x);
    fprintf (datei, "# v0                = %e\n",param_v0);
    fprintf (datei, "# delta_v           = %e\n",param_delta_v);
    fprintf (datei, "# m                 = %e\n",param_m);
    fprintf (datei, "# gamma             = %e\n",param_gamma);
    fprintf (datei, "# jumps              = %d\n",jumps);
    fprintf (datei, "# rand min           = %e\n",param_rand_min);
    fprintf (datei, "# rand max           = %e\n",param_rand_max);
    fprintf (datei, "# L                  = %e\n",param_L);
    fprintf (datei, "# ausgabe_step       = %d\n",ausgabe_step);
    fprintf (datei, "# t_ende             = %e\n",param_t_ende);
    fprintf (datei, "# schritte_x        = %d\n",schritte_x);
}

// This function writes final results in position and momentum space
// in separate files. For this the results have to be copied from the
// GPU and a Fourier transformation is necessary for the results in
// momentum space
void wave_in_datei (FILE *datei_ort, FILE *datei_impuls, double t,
int trap)
{

```

```

int nr;
double param_L = param_rand_max - param_rand_min;
double v;
double dk = 2.0 * Pi / param_L;
double c = param_L * param_L * param_m / (2.0 * Pi * schritte_x
* schritte_x);

double summe;

summe = 0.0;

pp_MemcpyToHost (wave, gpu_wave, schritte_x
* sizeof (cuDoubleComplex));

for (nr=0; nr < schritte_x; nr++)
{
    if (nr % ausgabe_step == 0)
        fprintf (datei_ort, "%d %e %e %e\n", trap, t, nr * delta_x
+ param_rand_min, cabs2 (wave [nr]));
    summe += cabs2 (wave[nr]);
}
fprintf (datei_ort, "\n\n");
fflush (datei_ort);
printf ("Ort: Norm = %e\n", summe * delta_x);

pp_fourier (FALSE);

pp_MemcpyToHost (wave, gpu_wave, schritte_x
* sizeof (cuDoubleComplex));

summe = 0.0;
for (nr=schritte_x/2; nr < schritte_x; nr++)
{
    if (nr % ausgabe_step == 0)
    {
        v = (nr-schritte_x) * dk/param_m;
        fprintf (datei_impuls, "%d %e %e %e\n", trap, t, v,
cabs2 (wave [nr])*c);
    }
    summe += cabs2 (wave[nr])*c;
}

for (nr=0; nr < schritte_x/2; nr++)
{
    if (nr % ausgabe_step == 0)
    {
        v = nr * dk/param_m;

```

```

        fprintf (datei_impuls, "%d %e %e %e\n", trap, t, v,
                cabs2 (wave [nr])*c);
    }
    summe += cabs2 (wave[nr])*c;
}

fprintf (datei_impuls, "\n\n");
fflush (datei_impuls);

pp_fourier (TRUE);
}

// This function does the same as the previous one, but takes the "raw"
// binary data for higher precision
void wave_in_datei_binary (FILE *datei_binary_ort,
FILE *datei_binary_impuls, int trap)
{
    pp_MemcpyToHost (wave, gpu_wave, schritte_x
    * sizeof (cuDoubleComplex));

    fwrite (wave, sizeof(wave[0]), sizeof(wave)/sizeof(wave[0]),
    datei_binary_ort);

    pp_fourier (FALSE);

    pp_MemcpyToHost (wave, gpu_wave, schritte_x
    * sizeof (cuDoubleComplex));

    fwrite (wave, sizeof(wave[0]), sizeof(wave)/sizeof(wave[0]),
    datei_binary_impuls);

    pp_fourier (TRUE);
}

// This function writes the wavefunction in position and momentum
// representation immediately after the jump into a file. This is done
// to check if has approximately the same shape before and directly
// after the jump, i.e. if the results are ok
void wave_in_datei_quench (FILE *datei_quench_ort,
FILE *datei_quench_impuls, double t, int trap)
{
    int nr;
    double param_L = param_rand_max - param_rand_min;
    double v;
    double dk = 2.0 * Pi / param_L;
    double c = param_L * param_L * param_m / (2.0 * Pi * schritte_x
    * schritte_x);

```

```

double summe;

summe = 0.0;

pp_MemcpyToHost (wave, gpu_wave, schritte_x
* sizeof (cuDoubleComplex));

for (nr=0; nr < schritte_x; nr++)
{
    if (nr % ausgabe_step == 0)
        fprintf (datei_quench_ort, "%d %e %e %e\n", trap, t,
            nr * delta_x + param_rand_min, cabs2 (wave [nr]));
    summe += cabs2 (wave[nr]);
}
fprintf (datei_quench_ort, "\n\n");
fflush (datei_quench_ort);
printf ("Ort: Norm = %e\n", summe * delta_x);

pp_fourier (FALSE);

pp_MemcpyToHost (wave, gpu_wave, schritte_x
* sizeof (cuDoubleComplex));

summe = 0.0;
for (nr=schritte_x/2; nr < schritte_x; nr++)
{
    if (nr % ausgabe_step == 0)
    {
        v = (nr-schritte_x) * dk/param_m;
        fprintf (datei_quench_impuls, "%d %e %e %e\n", trap, t, v,
            cabs2 (wave [nr])*c);
    }
    summe += cabs2 (wave[nr])*c;
}

for (nr=0; nr < schritte_x/2; nr++)
{
    if (nr % ausgabe_step == 0)
    {
        v = nr * dk/param_m;
        fprintf (datei_quench_impuls, "%d %e %e %e\n", trap, t, v,
            cabs2 (wave [nr])*c);
    }
    summe += cabs2 (wave[nr])*c;
}

```

```
fprintf (datei_quench_impuls, "\n\n");
fflush (datei_quench_impuls);

pp_fourier (TRUE);
}

// This function calculates the time-evolution of the wavefunction
void wave_entwicklung (char *dateiname1, char *dateiname2,
char *dateiname_binary1, char *dateiname_binary2,
char *dateiname_quench1, char *dateiname_quench2,
int anzahl_x_schritte, int anzahl_t_schritte, int anzahl_bilder,
int anzahl_ausgabe)
{
FILE *datei_ort = fopen (dateiname1, "w");
FILE *datei_impuls = fopen (dateiname2, "w");
FILE *datei_binary_ort = fopen (dateiname_binary1, "w");
FILE *datei_binary_impuls = fopen (dateiname_binary2, "w");
FILE *datei_quench_ort = fopen (dateiname_quench1, "w");
FILE *datei_quench_impuls = fopen (dateiname_quench2, "w");
int nr, nr2, nr3, nr4, nr_step_bild, trapped, jump,
anzahl_t_schritte_jump;
double t, delta_t, coupling, randomnr, norm, new_norm, norm_ort,
norm_atomic_1, norm_atomic_2;

norm = 0.0;
new_norm = 0.0;
anzahl_t_schritte_jump = 0;
trapped = 0;

// Check if there is a problem with opening the files
if ((datei_ort == NULL) || (datei_impuls == NULL) ||
(datei_binary_ort == NULL) || (datei_binary_impuls == NULL))
{
printf ("Fehler bei Dateioeffnung");
exit (EXIT_FAILURE);
}

schritte_x = anzahl_x_schritte;

delta_t = param_t_ende / anzahl_t_schritte;
delta_x = param_L/(anzahl_x_schritte * 1.0);

ausgabe_step = anzahl_x_schritte/anzahl_ausgabe;
if (ausgabe_step == 0)
ausgabe_step = 1;
```

```

variable_initialisieren (schritte_x);

param_in_datei (datei_ort);
param_in_datei (datei_impuls);

// Here the calculation of the trajectories starts, which have to
// be averaged in the end. Since in this setting only one jump
// occurs, the maximum number of trajectories is called jumps
for (jump = 1; jump <= jumps; jump++)
{
    // Again necessary initialisations, but these have to be done
    // for every trajectory again
    norm = 0.0;
    new_norm = 0.0;
    wave_initialisieren ();

    exp_H0_ausfuehren(delta_t);

    t = 0.0;
    trapped = 0;
    nr = 0;
    randomnr = rand ()/((double)RAND_MAX + 1);
    printf ("Randomnumber = %e \n", randomnr);

    exp_V_berechnen (t, delta_t, trapped);

    // In this while loop the first part of the evolution takes
    // place, that is the atoms interacts with the quenching laser
    // until a jump occurs or until the final time is reached
    while ((trapped == 0) && (nr < anzahl_t_schritte))
    {
        einen_zeitschritt (t, delta_t);

        t += delta_t;

        // The coupling is updated for every time step, measuring
        // the reduction of the norm
        coupling = 1 - pp_NormQ(gpu_wave, schritte_x);

        // When the norm decreased sufficiently the wavefunction
        // is normalised again and the first part of the evolution
        // is complete
        if (coupling > randomnr)
        {
            pp_MemcpyToHost (wave, gpu_wave, schritte_x
                * sizeof (cuDoubleComplex));

```

```

        new_norm = 0.0;

        for (nr3 = 0; nr3 < schritte_x; nr3++)
        {
            wave[nr3] = -I*omega(param_rand_min+nr3*delta_x,t)
                /param_gamma*wave[nr3];
            new_norm += cabs2(wave[nr3]);
        }

        for (nr3 = 0; nr3 < schritte_x; nr3++)
        {
            wave[nr3] = wave[nr3]/sqrt(new_norm);
        }
        pp_MemcpyToDevice (gpu_wave, wave, schritte_x
            * sizeof (cuDoubleComplex));

        trapped = 1;
        printf("Jump erfolgt \n");
    }

    nr++;
}

wave_in_datei_quench (datei_quench_ort, datei_quench_impuls, t,
trapped);

exp_V_berechnen (t, delta_t, trapped);

// Now the second part of the evolution starts, if there is
// time left. The atoms now interact with the two mirrors
if (nr < anzahl_t_schritte)
{
    for (nr2 = nr; nr2 < anzahl_t_schritte; nr2++)
    {
        einen_zeitschritt (t, delta_t);
        t += delta_t;
    }
}

wave_in_datei (datei_ort, datei_impuls, t, trapped);
wave_in_datei_binary (datei_binary_ort, datei_binary_impuls,
trapped);

}

variable_freigeben ();

```

```
fclose (datei_ort);
fclose (datei_impuls);
fclose (datei_binary_ort);
fclose (datei_binary_impuls);
fclose (datei_quench_ort);
fclose (datei_quench_impuls);

}

/*

Compiling with GNU Compiler

gcc filename.c -openmp cutools_v3.o -I /usr/local/cuda/include -L
/usr/local/cuda/lib64 -lcuda -lcufft -o name.out

Compiling with Intel Compiler

icc filename.c -openmp cutools_v3.o -I /usr/local/cuda/include -L
/usr/local/cuda/lib64 -lcuda -lcufft -o name.out

*/

int main ()
{
    // The parameters for the wavefunction, the potentials, the
    // trajectories and the box are initialised

    srand ( (unsigned) time(NULL) );

    param_pot_hoehe = 200000.0;
    param_coupling_strength = 200.0;
    x_m=0.0;
    x_d=-2.5e-3;
    x_p=(x_m+x_d)/2.0;
    param_pump_sigma = 2.5e-4;
    param_mirror_sigma = 2.5e-4;
    param_diode_sigma = 2.5e-4;
    param_rand_min = -0.5;
    param_rand_max = 1.5;
    param_L = param_rand_max - param_rand_min;
    param_m = 1000.0;
    param_x0 = -3.8e-2;
    param_delta_x = 5e-3;
    param_v0 = 20.0;
}
```



```
param_delta_v = 3.0;
zeit_interv = 1;
param_gamma = 1.0;
jumps = 200;

param_t_ende = 1.0;

double dk = 2.0 * Pi / param_L;
// Check if the potentials are high enough by calculating the
// maximal velocity
printf ("v_max = %e\n", dk * 4096*16/2/param_m);

wave_entwicklung ("datafilename_position.dat",
"datafilename_momentum.dat", "binaryfilename_position.bin",
"binaryfilename_momentum.bin", "datafilename_position_quench.dat",
"datafilename_momentum_quench.dat", anzahl_x_schritte,
anzahl_t_schritte, anzahl_bilder, anzahl_ausgabe);

return 0;
}
```


List of Figures

3.1	Scheme of the stopping of classical particles: a hard wall moving with trajectory $x_m(t) = d\sqrt{t/t_f}$ (solid line); examples of two particle trajectories with different initial velocities (dashed lines).	29
3.2	Scheme of the transformation between initial parameters and final parameters, the wall is indicated by the black box, the dark grey region is for free motion, and the light gray region for motion with collision. The symbols provide examples connecting final and initial parameters: $x_s/d = \chi_s = 0, v_s/v_b = \nu_s = 0 \rightarrow x_f/d = \chi_f = 0, v_f/v_b = \nu_f = 0$ (free motion, circles); $\chi_s = 0, \nu_s = 1 \rightarrow \chi_f = 1, \nu_f = 1$ (free motion, boxes); $\chi_s = 0, \nu_s = 2 \rightarrow \chi_f = 1/2, \nu_f = 0$ (collision, triangles).	29
3.3	The final velocity $\chi_f(\chi_s, \nu_s) = v_f(x_s, v_s)/v_b(x_s, v_s)$ depending on the initial position and velocity. The line at $\nu_s = 1 - \chi_s$ separates the regions with or without a collision before $\tau = 1$	31
3.4	Classical particles, $x_0/d = -0.04, \Delta x/d = 0.008, v_0/v_b = 5.0$ and $\Delta v/v_b = 2.0$; the p in the vertical axis is shorthand for the different probability densities, multiplied by d or v_b to obtain a dimensionless quantity. (a) Initial joint probability density of position and velocity p_s (solid graph) and final probability density p_f (striped graph); (b) Position distributions: initial ($p_{x,s}$, solid line, scaled by a factor of $1/50$), final ($p_{x,f}$, dashed line), and final for a mirror with constant velocity ($\bar{p}_{x,f}$, thick dotted line); (c) Velocity distributions: initial ($p_{v,s}$, solid line), final ($p_{v,f}$, dashed line), and final for constant-velocity mirror $\bar{p}_{v,f}$ (thick dotted line).	33
3.5	Classical particles, $x_0/d = -0.003, \Delta x/d = 0.0003, v_0/v_b = 3.0$ and $\Delta v/v_b = 1.24$; as in the previous figure, the p in the vertical axis represents the different probability densities, multiplied by d or v_b to obtain a dimensionless quantity. (a) Position distributions: initial ($p_{x,s}$, solid line, scaled by a factor of $1/400$), final ($p_{x,f}$, dashed line) and final for constant-velocity mirror ($\bar{p}_{x,f}$, thick dotted line); (b) Velocity distributions: initial ($p_{v,s}$, solid line), final ($p_{v,f}$, dashed line, scaled by a factor of $1/40$), and final for a constant-velocity mirror ($\bar{p}_{v,f}$, thick dotted line).	34
3.6	Scheme of a particle which would have started behind the mirror at time $t = 0$. Changing coordinates such that the particle starts at time t' , this situation can equivalently be described by an altered mirror trajectory $\alpha\sqrt{t' + t_0}$ and is therefore different from the one considered so far.	36
3.7	The second collision time t_{c2} depending on the initial time t_0 and v_s for a particle moving between two mirror potentials. We set the parameter $\alpha = 1$	39

- 3.8 Plot of the strictly positive part of the difference between the first and second final velocity $|v_{f1}(1, v_s)| - |v_{f2}(1 + \epsilon, v_s)|$ depending on ϵ and v_s for a particle moving between two mirror potentials. We set the parameter $\alpha = 1$ 40
- 3.9 The absolute value of the final velocity $|v_f|$ depending on v_s and t_0 for a particle moving between two mirror potentials moving apart in opposite directions along a trajectory $\sqrt{t + t_0}$. For the final time we always set $t_f = 1$, such that the mirrors final distance increases with increasing t_0 , i.e. $d_f = \sqrt{1 + t_0}$ 41
- 3.10 The absolute value of the final velocity $|v_f|$ depending on v_s and t_0 for a particle moving between two mirror potentials moving apart in opposite directions along a trajectory $\sqrt{t + t_0}$. For the final time we set $t_f = 1 - t_0$, such that the mirrors final distance is always $d_f = 1$ 42
- 3.11 Quantum particle, see Table 3.1 for parameters; (a) Position distributions: $p_{x,s}$ ($t = 0$, solid line, scaled by a factor of $1/40$), $p_{x,f}$ with an ideal wall ($t = t_f$, thick dashed line), $p_{x,f}$ with a Gaussian wall ($t = t_f$, thin dashed line); (b) Velocity distributions: $p_{v,s}$ ($t = 0$, solid line, scaled by a factor of 4), $p_{v,f}$ with an ideal wall ($t = t_f$, thick dashed line) and $p_{v,f}$ with a Gaussian wall ($t = t_f$, thin dashed line). 45
- 3.12 Quantum particle, see Table 3.2 for parameters; (a) Position distributions: $p_{x,s}$ ($t = 0$, dotted line, scaled by a factor of $1/100$), $p_{x,f}$ with a Gaussian wall ($t = t_f$, $t_0 = 0.01 t_f$, solid line); (b) Velocity distributions: $p_{v,s}$ ($t = 0$, dotted line, scaled by a factor of 100), $p_{v,f}$ with a Gaussian wall ($t = t_f$, $t_0 = 0.01 t_f$, solid line). 45
- 3.13 Black curve: The potential $V(y)$ the particles interact with in the mirror reference frame, where we chose the parameters $m = 1/2$, $\alpha = 1$, so that $V(y) = -\frac{1}{16}y^2$. The black vertical line indicates the boundary condition at $y = 1 \Leftrightarrow x = \alpha\sqrt{t}$ 53
- 3.14 Initial distribution $\rho(\lambda)$ for the parameters in Table 3.1. 56
- 3.15 (a) Final position distribution $|\Psi(x, t_f)|^2$ and (b) final velocity distribution $|\Psi(v, t_f)|^2$ for the parameters in Table (3.1) derived with the analytical solution (3.73). For the initial distributions see Fig. 3.11. 57
- 3.16 (a) Initial distribution $\rho(\lambda)$, (b) final position distribution $|\Psi(x, t_f)|^2$ and (c) final velocity distribution $|\Psi(v, t_f)|^2$ (c) for mass $m=2.5$, where we chose units such that $\hbar = 1$ 58
- 3.17 (a) Initial distribution $\rho(\lambda)$, (b) final position distribution $|\Psi(x, t_f)|^2$ and (c) final velocity distribution $|\Psi(v, t_f)|^2$ for mass $m=5$, where we chose units such that $\hbar = 1$ 59
- 3.18 (a) Initial distribution $\rho(\lambda)$, (b) final position distribution $|\Psi(x, t_f)|^2$ and (c) final velocity distribution $|\Psi(v, t_f)|^2$ for mass $m=7.5$, where we chose units such that $\hbar = 1$ 60
- 3.19 (Thin black line) The exact final velocity distribution for the parameters in Table (3.1). (Thick black dashed line) The final velocity distribution calculated with (3.78) for the same parameters. 61

- 3.20 Schematic picture of the situation considered in this section. Particles start at some initial position \vec{x}_s with some initial velocity \vec{v}_s and collide with a mirror whose static shape is given by a quadratic polynomial and which moves along a square-root in time trajectory. 66
- 3.21 **Classical Case.** The surface of the mirror potential is given by a quadratic polynomial. (a) The (dashed) initial and (solid) final position probability distributions $p_{s,f}(x_1, x_2)$, where the initial distribution is given by eq. (3.103) with the parameters in Table 3.3 and $\kappa = 1.5$. Additionally the final mirror position is plotted. (b) The corresponding initial and final velocity probability distributions $p_{s,f}(v_1, v_2)$. The initial distribution was scaled by a factor 30. 69
- 3.22 **Classical Case.** The surface of the mirror potential is given by a quadratic polynomial. (a) The final velocity marginals $p_f(v_1)$ for the parameters in Table 3.3. (b) The final velocity marginals $p_f(v_2)$ for the parameters in Table (3.3). 70
- 3.23 **Classical Case.** The surface of the mirror potential is given by a quadratic polynomial. (a) The velocity marginals $p_f(v_1)$ for the parameters in Table 3.3 for $\kappa = 0$ (flat wall), $\kappa = 1$ and $\kappa = 3.5$ compared to the initial distribution. (b) The velocity marginals $p_f(v_2)$ for the parameters in Table 3.3 for $\kappa = 0$ (flat wall), $\kappa = 1$ and $\kappa = 3.5$ compared to the initial distribution. 71
- 3.24 **Quantum Case.** The mirror potential is given by eq. (3.108). (a) The (dashed) initial and (solid) final position probability distributions $p_{s,f}(x_1, x_2)$ for an initial wavefunction (3.107) with the parameters in Table 3.5 and $\kappa = 1.5$. Additionally the potential is plotted at $t_f = 1$. (b) The initial and final velocity probability distributions $p_{s,f}(v_1, v_2)$ for an initial wavefunction (3.107) with the parameters in Table 3.5 and $\kappa = 1.5$. The initial distribution was scaled by a factor 50. 76
- 3.25 **Quantum Case.** The mirror potential is given by eq. (3.108). (a) The final velocity marginals $p_f(v_1)$ for the parameters in Table 3.5. (b) The final velocity marginals $p_f(v_2)$ for the parameters in Table 3.5. 77
- 3.26 **Quantum Case.** The mirror potential is given by eq. (3.108). (a) The velocity marginals $p_f(v_1)$ for the parameters in Table 3.5 for flat wall ($\kappa = 0$), $\kappa = 1$ and $\kappa = 3.5$ compared to the initial distribution. (b) The velocity marginals $p_f(v_2)$ for the parameters in Table 3.5 for flat wall ($\kappa = 0$), $\kappa = 1$ and $\kappa = 3.5$ compared to the initial distribution. 78
- 3.27 The velocity marginals $p_f(v_1)$ and $p_f(v_2)$ in the quantum case for the parameters in Table 3.5 and $\kappa = 3.5$ (solid line) as well as for $m = 600$ (thick dashed line) compared to the corresponding classical results (dotted dashed line). (a) The velocity marginals $p_f(v_1)$. (b) The velocity marginals for $p_f(v_2)$ 79
- 3.28 Schematic picture of the situation considered in this section. Particles start at some initial position \vec{x}_s with some initial velocity \vec{v}_s and collide with a ring shaped mirror whose radius increases with a square-root in time. 80

- 3.29 **Quantum Case.** The mirror potential is given by eq. (3.109). (a) The (dashed) initial and (solid) final position probability distribution $p_{s,f}(x_1, x_2)$ for an initial wavefunction (3.107) with the parameters in Table 3.8 and $t_0 = 0.004$. Additionally the potential is plotted for $t_f = 1$. (b) The initial and final velocity probability distributions $p_{s,f}(v_1, v_2)$ for an initial wavefunction (3.107) with the parameters in Table 3.8 and $t_0 = 0.004$. The initial distribution was scaled by a factor 20. 83
- 3.30 **Quantum Case.** The mirror potential is given by eq. (3.109). The final velocity marginals $p_f(v_1)$ and $p_f(v_2)$, which are equal due to the symmetry of the situation, for the parameters in Table 3.8. 84
- 3.31 **Quantum Case.** The mirror potential is given by eq. (3.109). The velocity marginals $p_f(v_1)$ and $p_f(v_2)$, which are equal due to the symmetry of the situation, for the parameters in Table 3.8 and for $t_0 = 0.003$, $t_0 = 0.005$ as well as $t_0 = 0.01$ compared to the initial distribution. . . . 84
- 3.32 **Quantum Case.** The mirror potential is given by eq. (3.109). The velocity marginals $p_f(v_1)$ for the parameters in Table 3.5 for $t_0 = 0.005$ and $x_{s1} = 0.0025$ as well as $x_{s1} = 0.005$. Due to the symmetry the results for $p_f(v_2)$ with $x_{s2} = 0.0025$ as well as $x_{s2} = 0.005$ instead are the same. 85
- 3.33 **Quantum Case.** The mirror potential is given by eq. (3.109). The velocity marginals $p_f(v_2)$ for the parameters in Table 3.5 for $t_0 = 0.005$ and $x_{s1} = 0.0025$ as well as $x_{s1} = 0.005$. Due to the symmetry the results for $p_f(v_1)$ with $x_{s2} = 0.0025$ as well as $x_{s2} = 0.005$ instead are the same. 85
- 3.34 **Quantum Case.** The mirror potential is given by eq. (3.109). The velocity marginals $p_f(v_1)$ and $p_f(v_2)$, which are the same due to the symmetry of the situation, for the parameters in Table 3.5 for $t_0 = 0.005$ and $x_{s1} = x_{s2} = 0.0025$ as well as $x_{s1} = x_{s2} = 0.005$ 86
- 3.35 Schematic pictures of the situation considered in this section. Particles start at some initial position \vec{x}_s with some initial velocity \vec{v}_s and collide with a ring shaped mirror whose radius (a) first increases with a square-root in time and (b) after some expansion time decreases linearly with velocity β . (c) Additionally the time evolution of the radius is schematically depicted. First an expansion occurs along a square-root in time until some expansion time t_{exp} which is then followed by a linear compression until some final time t_f 88
- 3.36 Expansion and compression of a ring for one classical particle. The results are independent of the relative angle. (a) The dependence of the ratio of the final velocity $|\vec{v}_{f,comp}|$ after the compression and the absolute value of the initial velocity $|\vec{v}_s|$ on the components of the initial velocity for $\beta = 0.001$. (b) The dependence of the ratio of the final velocity $|\vec{v}_{f,comp}|$ after the compression and the absolute value of the initial velocity $|\vec{v}_s|$ on the initial velocity and β 90

- 3.37 **Quantum Case.** The mirror potential is given by eq. (3.115). (a) The final position probability distribution $p_f(x_1, x_2)$ after a square-root in time expansion and a linear in time compression for an initial wavefunction (3.107) for the parameters in Table 3.8 and $t_0 = 0.004$. Additionally the potential is plotted for $t_f = 10.4$. (b) The final velocity probability distributions $p_{s,f}(v_1, v_2)$ after a square-root in time expansion and a linear compression for an initial wavefunction (3.107) for the parameters in Table 3.8 and $t_0 = 0.004$ 93
- 3.38 **Quantum Case.** (Solid line) The energy expectation value E during the compression of the ring with velocity $\beta = 0.1$ over the inverse of the squared radius. (Dashed line) As a reference a straight line was added. 94
- 4.1 The figure schematically shows the setup considered in this chapter. The two mirrors both move along a trajectory $\alpha\sqrt{t}$, where the first mirror (thick dashed/solid line) lets the particle pass if it comes from the left, i.e. it acts as an atom diode, such that the particle is first reflected from the second mirror (thick solid line). The particle's trajectory is $\sim t$ (straight dotted-dashed lines) and the particle undergoes subsequent collisions while being trapped between both mirrors, thereby being effectively slowed, which is indicated by the decreasing slope. 99
- 4.2 **Classical Case:** One particle. The dependence of the ratio of the "worst case" velocity $v_{i,3}$ and the initial velocity $v_{i,1}$ on the initial particle distance $x_{i,1}$ and α for a fixed mirror distance $x_{m,l} = -1$ and $v_{i,1} = 5$ 104
- 4.3 **Classical Case:** One particle. The dependence of the absolute final velocity $|v_f|$ on the initial particle velocity $v_{i,1}$ and distance $x_{i,1}$ for a fixed mirror distance $x_{m,l} = -0.01$ and $t_f = 1$. Note that we ensured that the last collision always occurs with the right mirror. 105
- 4.4 **Classical Case:** The initial and final phase-space density of particles in a pulse becoming confined between two accelerated mirror potentials and undergoing subsequent collisions for the parameters in Table 4.1. (a) Initial phase space density. (b) Final phase space density. 106
- 4.5 (a) Schematic picture of the level scheme considered and the corresponding state-dependent potentials the atom experiences in the respective states. We have a groundstate $|1\rangle$, which is coupled to a fastly decaying excited state $|3\rangle$ via the pumping laser with frequency Ω_p . The state $|3\rangle$ then decays with high rate γ_3 (inverse life-time) to the metastable state $|2\rangle$. (b) Schematic picture of the atom, described as a three-level system, interacting with the three lasers. At the beginning the atom is in the ground-state $|1\rangle$, passing the left potential W_l unaffected (dashed Gaussian), but not the right one W_r (solid Gaussian). In the region between the mirrors it gets excited by the pump laser (solid arrow) to the state $|3\rangle$ and decays afterwards to the metastable state $|2\rangle$. In this state it will now also be reflected by W_l (now solid), but it will not interact with the pump laser anymore (now grey arrow). Therefore the atom is trapped between both mirrors and undergoes repeated reflections. 108

4.6	Quantum case: The initial position distribution (solid line) and final position distribution (dashed line) for an initial state (4.22) and the parameters in Table 4.2. The final distribution was shifted to fit it into the same graph. The actual position is given on the top axis.	115
4.7	Quantum case: The initial velocity distribution (solid line) and final velocity distribution (dashed line) for an initial state (4.22) and the parameters in Table 4.2.	115
4.8	Quantum case: The final velocity distribution for 200 jumps (solid line) compared to those for 100 jumps (thick dashed line) for an initial state (4.22) and the parameters in Table 4.2.	116
4.9	Quantum case: The initial position distribution (solid line) and final position distribution (dashed line) for an initial state (4.22) and the parameters in Table 4.4. The final distribution was shifted to fit it into the same graph. The actual position is given on the top axis.	116
4.10	Quantum case: The initial velocity distribution (solid line) and final velocity distribution (dashed line) for an initial state (4.22) and the parameters in Table 4.4.	117
4.11	Quantum case: The final velocity distribution for 200 jumps (solid line) compared to those for 100 jumps (thick dashed line) with the same position step size and for 50 jumps with half the position step size (dotted dashed line) for an initial state (4.22) and the parameters in Table 4.4.	117
4.12	Quantum case: The initial position distribution (solid line) and final position distribution (dashed line) for an initial state (4.22) and the parameters in Table 4.6. The final distribution was shifted to fit it into the same graph. The actual position is given on the top axis.	118
4.13	Quantum case: The initial velocity distribution (solid line) and final velocity distribution (dashed line) for an initial state (4.22) and the parameters in Table 4.6.	118
4.14	Quantum case: The final velocity distributions for 100 jumps (solid line) and 60 jumps (thick dashed line) for an initial state (4.22) and the parameters in Table 4.6.	119
4.15	Quantum case: The initial position distribution (solid line) and final position distribution (dashed line) for an initial state (4.22) and the parameters in Table 4.8. The final distribution was shifted to fit it into the same graph. The actual position is given on the top axis.	119
4.16	Quantum case: The initial velocity distribution (solid line) and final velocity distribution (dashed line) for an initial state (4.22) and the parameters in Table 4.8.	120
4.17	Quantum case: The final velocity distributions for 100 jumps (solid line) and 50 jumps (thick dashed line) for an initial state (4.22) and the parameters in Table 4.8.	120
5.1	Examples of ansatz for b : A simple polynomial ansatz (solid line), and an exponential of a polynomial (dashed line, $\exp \sum_{j=0}^5 d_j t^j$), where we chose the parameters $\omega(0) = 250 \times 2\pi$ Hz, $\omega(t_f) = 2.5 \times 2\pi$ Hz, $\gamma = 10$	139

- 5.2 (a) The average energies of the ground state expanding mode for different final times t_f : $t_f = 25$ ms (solid), $t_f = 15$ ms (dashed), $t_f = 10$ ms (dotted), and $t_f = 6$ ms (dash-dotted). Other parameters are as in Fig. 5.1 (polynomial b) (b) The corresponding squared frequency $\omega^2(t)$ 145
- 5.3 Average energies for expanding modes $n = 0$ (solid), $n = 1$ (dashed), and $n = 2$ (dotted). (a) $t_f = 2$ ms; (b) $t_f = 25$ ms. The other parameters are the same as in Fig. 5.1 (polynomial b). 146
- 5.4 Example of fast optimal frictionless atom cooling: $\omega_0 = 250 \times 2\pi$ Hz, $\omega_f = 2.5 \times 2\pi$ Hz, mass of Rb-87, and $t_f = 2$ ms. (a) $b(t)$ (dotted line, left axis) and $\omega^2(t)$ (solid line, right axis). (b) Time evolution of $|\psi_0(t,x)|^2$ with a harmonic potential $V(t,x) = \frac{m}{2}\omega^2(t)x^2$ (dotted line) and with a Gaussian potential $V(t,x) = \frac{mw^2}{4}\omega^2(t) \left(1 - \exp\left(-\frac{2x^2}{w^2}\right)\right)$ of width $w = 50 \mu\text{m}$ (solid line, indistinguishable from the dotted line); in both cases: the function $\omega^2(t)$ shown in (a) is used, the initial state at $t = 0$ is the ground state of the harmonic potential. 147
- 5.5 (a) Displacement $q_c - q_0$ versus time. Long dashed line: direct method, short dashed line: inverse method (polynomial). Solid line: inverse method + OCT. (b) Trap trajectories. Parameter values: $d = 1.6$ mm, $t_f = 20$ ms, $\delta \simeq 0.162$ mm, $\omega_0 = 2\pi \times 50$ Hz. 151
- 5.6 Effect of trap anharmonicity α on transport. (a) Exact fidelity \bar{F} (lines) and approximated fidelity \tilde{F} (symbols); $g_1 = 0$ (dotted lines and circles), $g_1/\hbar = 0.05$ m/s (solid lines and triangles), $g_1/\hbar = 0.1$ m/s (dashed lines and boxes). (b) Wave function at final time t_f ; $g_1 = 0, \alpha = 0$ (thick solid line, scaled by a factor of 4), $g_1 = 0, \alpha d^2 = 0.0512$ (exact result ψ : thin dashed line, approximation $\tilde{\psi}$: circles, scaled by a factor of 4), $g_1/\hbar = 0.1$ m/s, $\alpha = 0$ (thin solid line), $g_1/\hbar = 0.1$ m/s, $\alpha d^2 = 0.0512$ (exact result ψ : dashed line, indistinguishable in the scale of the figure from the approximation $\tilde{\psi}$: boxes); $d = 1.6$ mm, $t_f = 20$ ms, $\omega_0 = 2\pi \times 50$ Hz. 154
- 5.7 Average fidelity of harmonic transport versus noise intensity λ ; (a) $t_f = 10$ ms; (b) $t_f = 20$ ms. In both cases: exact result \bar{F} (lines), approximation \tilde{F} (symbols); $g_1 = 0$ (dotted lines and circles), $g_1/\hbar = 0.05$ m/s (solid lines and crosses), $g_1/\hbar = 0.1$ m/s (dashed lines and boxes). $\omega_0 = 2\pi \times 50$ Hz. 156

List of Tables

3.1	Set of parameters in the quantum case corresponding to the results shown in Fig. 3.11.	44
3.2	Set of parameters in the quantum case corresponding to the results shown in Fig. 3.12.	46
3.3	Dimensionless parameters for the simulations with a polynomial mirror in the classical case.	66
3.4	Expectation values and standard deviations of the final velocity distributions for a polynomial mirror and the parameters in Table 3.3 in the classical case.	67
3.5	Dimensionless parameters for the simulations with a polynomial mirror in the quantum case.	73
3.6	Example of dimensioned parameters corresponding to the dimensionless ones in Table 3.5 for Lithium.	74
3.7	Expectation values and standard deviations of the final velocity distributions for a polynomial mirror and the parameters in Table 3.5 in the quantum case.	74
3.8	Dimensionless parameters for the simulations with a ring in the quantum setting.	81
3.9	Expectation values and standard deviations of the absolute value of the final velocities for a ring and the parameters in Table 3.8 and $t_0 = 0.003$, $t_0 = 0.005$ and $t_0 = 0.01$ in the quantum case.	81
3.10	Dimensionless parameters for the simulations of a ring used to reduce the velocity of one classical particle via expansion and compression.	89
3.11	Dimensionless parameters for the simulations of a ring used to cool via expansion and compression in the quantum case.	91
4.1	Dimensionless parameters for the simulations of a particle confined between two accelerated mirrors in the classical case.	106
4.2	Dimensionless parameters for the simulations of the quantum catcher shown in Figs. 4.6, 4.7 and 4.8.	111
4.3	Initial and final expectation values and variances corresponding to the results for the quantum catcher shown in Figs. 4.6, 4.7 and 4.8.	111
4.4	Dimensionless parameters for the simulations of the quantum catcher shown in Figs. 4.9, 4.10 and 4.11.	112
4.5	Initial and final expectation values and variances corresponding to the results for the quantum catcher shown in Figs. 4.9, 4.10 and 4.11.	112
4.6	Dimensionless parameters for the simulations of the quantum catcher shown in Figs. 4.12, 4.13 and 4.14.	112

4.7	Initial and final expectation values and variances corresponding to the results for the quantum catcher shown in Figs. 4.12, 4.13 and 4.14. . . .	113
4.8	Dimensionless parameters for the simulations of the quantum catcher shown in Figs. 4.15, 4.16 and 4.17.	113
4.9	Initial and final expectation values and variances corresponding to the results for the quantum catcher shown in Figs. 4.15, 4.16 and 4.17. . . .	113
4.10	Example of dimensioned parameters for the results shown in Figs. 4.9, 4.10 and 4.11 and corresponding to the dimensionless parameters in Table 4.4.	114

List of Publications

- [1] **S. Schmidt**, J. G. Muga, and A. Ruschhaupt: *Stopping particles of arbitrary velocities with an accelerated wall*, Phys. Rev. A, 80, 023406 (2009)
- [2] X. Chen, A. Ruschhaupt, **S. Schmidt**, A. del Campo, D. Guéry-Odelin, and J. G. Muga: *Fast Optimal Frictionless Atom Cooling in Harmonic Traps: Shortcut to Adiabaticity*, Phys. Rev. Lett., 104, 063002 (2010)
- [3] X. Chen, A. Ruschhaupt, **S. Schmidt**, S. Ibáñez, and J. G. Muga: *Shortcut to adiabaticity in harmonic traps*, J. At. Mol. Sci., 1, 1-17 (2010)
- [4] E. Torrontegui, X. Chen, M. Modugno, **S. Schmidt**, A. Ruschhaupt, and J. G. Muga: *Fast transport of Bose-Einstein condensates*, New. J. Phys., 14, 013031 (2012)

Bibliography

- [5] W. P. Schleich: *Quantum Optics in Phase Space*, Wiley-VCH Verlag (2001)
- [6] L. Mandel, and E. Wolf: *Optical coherence and quantum optics*, Cambridge University Press (1995)
- [7] D. F. Walls, and G. J. Milburn: *Quantum Optics*, Springer-Verlag Berlin Heidelberg (2008)
- [8] J. P. Gordon, and A. Ashkin: *Motion of atoms in a radiation trap*, Phys. Rev. A, 21, 1606-1617 (1980)
- [9] A. Ruschhaupt, J. A. Damborenea, B. Navarro, J. G. Muga, and G. C. Hegerfeldt: *Exact and approximate complex potentials for modelling time observables*, Europhys. Lett., 67, 1-7 (2004)
- [10] H. J. Metcalf, and P. v.d. Straten: *Laser Cooling and Trapping*, Springer-Verlag New York (1999)
- [11] H. J. Metcalf, and P. v.d. Straten: *Laser cooling and trapping of atoms*, J. Opt. Soc. Am. B, 20, 887 (2003)
- [12] Tamás Sándor Biró: *Is There a Temperature*, Springer-Verlag (2011)

-
- [13] H. Carmichael: *An Open Systems Approach to Quantum Optics*, Springer-Verlag Berlin Heidelberg (1993)
- [14] H. Carmichael: *Statistical Methods in Quantum Optics: Master equations and Fokker-Planck equations*, Springer-Verlag Berlin Heidelberg (1998)
- [15] H. Carmichael: *Statistical Methods in Quantum Optics 2*, Springer-Verlag Berlin Heidelberg (2007)
- [16] G. Lindblad: *On the Generators of Quantum Dynamical Semigroups*, Commun. Math. Phys., 48, 119 (1976)
- [17] G. C. Hegerfeldt: *How to reset an atom after a photon detection: Applications to photon-counting processes*, Phys. Rev. A, 47, 449-455 (1993)
- [18] J. Dalibard, Y. Castin, and K. Mølmer: *Wave-function approach to dissipative processes in quantum optics*, Phys. Rev. Lett., 68, 580-583 (1992)
- [19] M. H. A. Davis: *Markov Models and Optimization*, Chapman and Hall (1993)
- [20] A. Steyerl, H. Nagel, F.-X. Schreiber, K.-A. Steinhauser, R. Gähler, W. Gäser, P. Ageron, J. M. Astruc, W. Drexel, G. Gervais, and W. Mampe: *A new source of cold and ultracold neutrons*, Phys. Lett. A, 116, 347 (1986)
- [21] V. I. Balykin, V. S. Letokhov, Y. B. Ovchinnikov, and A. I. Sidorov: *Quantum state-selective reflection of atoms by laser light*, Phys. Rev. Lett., 60, 2137-2149 (1988)
- [22] A. Steane, P. Szriftgiser, P. Desbiolles, and J. Dalibard: *Phase Modulation of Atomic de Broglie Waves*, Phys. Rev. Lett., 74, 4972 (1995)
- [23] M. Arndt, P. Szriftgiser, J. Dalibard, and A.M. Steane: *Atom optics in the time domain*, Phys. Rev. A, 53, 3369 (1996)
- [24] A. Libson, M. Riedel, G. Bronshtein, E. Narevicius, U. Even, and M. G. Raizen: *Towards coherent control of supersonic beams: a new approach to atom optics*, New. J. Phys., 8, 77 (2006)
- [25] E. Narevicius, A. Libson, M. F. Riedel, C. G. Parthey, I. Chavez, U. Even, and M. G. Raizen: *Coherent Slowing of a Supersonic Beam with an Atomic Paddle*, Phys. Rev. Lett., 98, 103201 (2007)
- [26] G. Reinaudi, Z. Wang, A. Couvert, T. Lahaye, and D. Guéry-Odelin: *A moving magnetic mirror to slow down a bunch of atoms*, Eur. Phys. J. D., 40, 405 (2006)
- [27] J. J. Thorn, E. A. Schoene, T. Li, and D. Steck: *Dynamics of cold atoms crossing a one-way barrier*, Phys. Rev. A, 79, 063402 (2009)
- [28] P. Berman: *Atom Interferometry*, Academic Press, London (1997)
- [29] A. del Campo, J. G. Muga, and M. Kleber: *Quantum matter-wave dynamics with moving mirrors*, Phys. Rev. A, 77, 013608 (2008)

-
- [30] M. Reed, and B. Simon: *Methods of Modern Mathematical Physics III: Scattering Theory*, Academic Press, Inc. (1979)
- [31] S. W. Doescher, and M. H. Rice: *Infinite Square-Well Potential with a Moving Wall*, Am. J. Phys., 37, 1246 (1969)
- [32] A. Munier, J. R. Burgan, M. Feix, and E. Fijalkow: *Schrödinger equation with time-dependent boundary conditions*, J. Math. Phys., 22, 1219 (1981)
- [33] A. J. Makowski, and S. T. Dembinski: *Exact propagators for time-dependent Coulomb, delta and other potentials*, Phys. Lett. A, 154, 217 (1991)
- [34] V. V. Dodonov, A. B. Klimov, and D. E. Nikonov: *Quantum particle in a box with moving walls*, J. Math. Phys., 34, 3391 (1993)
- [35] C.L. Ho, and C.C. Lee: *Stabilizing quantum metastable states in a time-periodic potential*, Phys. Rev. A, 71, 012102 (2005)
- [36] T.K. Jana, and P. Roy: *A class of exactly solvable Schrödinger equation with moving boundary condition*, Phys. Lett. A, 372, 2368-2373 (2008)
- [37] M. Abramowitz, and I. A. Stegun: *Handbook of Mathematical Functions*, Dover Publications, Inc., New York (1972)
- [38] A. F. Nikiforov, and V. B. Uvarov: *Special Functions of Mathematical Physics*, Birkhäuser Verlag, Basel (1988)
- [39] M. V. Berry, and G. Klein: *Newtonian trajectories and quantum waves in expanding force fields*, J. Phys. A, 17, 1805 (1984)
- [40] R. Folman, P. Krueger, J. Schmiedmayer, J. Denschlag, and C. Henkel: *Microscopic Atom Optics: From Wires to an Atom Chip*, Adv. Atomic Mol. Opt. Phys., 48, 263 (2002)
- [41] D. Schneble, M. Hasuo, T. Anker, T. Pfau, and J. Mlynek: *Integrated atom-optical circuit with continuous-wave operation*, J. Opt. Soc. Am. B, 20, 648 (2003)
- [42] X. Chen, J. G. Muga, A. del Campo, and A. Ruschhaupt: *Atom cooling by non-adiabatic expansion*, Physical Review A, 80, 024036 (2009)
- [43] G. Klein, and H. P. Mulholland: *Repeated elastic reflexions of a particle in an expanding sphere*, Proc. R. Soc. Lond. A, 361, 447-461 (1978)
- [44] G. Klein: *An invariant for repeated reflections in an expanding ellipsoid*, Proc. R. Soc. Lond. A, 396, 217-226 (1984)
- [45] Y. Kozawa, and S. Fato: *Focusing property of a double-ring-shaped radially polarized beam*, Optics Letters, 31, 820 (2006)
- [46] Y. Kozawa, and S. Fato: *Dark-spot formation by vector beam*, Optics Letters, 33, 2326 (2008)

- [47] Y. Kozawa, and S. Fato: *Dark Spot Trapping using a Double-Ring-Shaped Radially Polarized Beam*, Optical Molecular Probes, Imaging and Drug Delivery (2011)
- [48] W. Ketterle, and D. E. Pritchard: *Atom cooling by time-dependent potentials*, Phys. Rev. A, 46, 4051 (1992)
- [49] Carl W. David: *The Particle in a Box (and in a Circular Box)*, Chemistry Education Materials, Paper 12 (2006)
- [50] A. Ruschhaupt, and J. G. Muga: *Atom diode: a laser device for a unidirectional transmission of ground-state atoms*, Phys. Rev. A, 70, 061604(R) (2004)
- [51] A. Ruschhaupt, and J. G. Muga: *Adiabatic interpretation of a two-level atom diode, a laser device for unidirectional transmission of ground-state atoms*, Phys. Rev. A, 73, 013608 (2006)
- [52] A. Ruschhaupt, J. G. Muga, and M. G. Raizen: *Improvement by laser quenching of an 'atom diode': a one-way barrier for ultra-cold atoms*, J. Phys. B: At. Mol. Opt. Phys., 39, L 133-138 (2006)
- [53] A. Ruschhaupt, J. G. Muga, and M. G. Raizen: *One-photon atomic cooling with an optical Maxwell's demon valve*, J. Phys. B: At. Mol. Opt. Phys., 39, 3833-3838 (2006)
- [54] A. Ruschhaupt, and J. G. Muga: *Three-dimensional effects in atom diodes: Atom-optical devices for one-way motion*, Phys. Rev. A, 76, 013619 (2007)
- [55] A. Ruschhaupt, and J. G. Muga: *The atom diode - A one-way laser barrier for cooling atoms*, Eur. Phys. J. Special Topics, 159, 127-134 (2008)
- [56] A. Ruschhaupt, and J. G. Muga: *Control of atomic motion with an atom-optical diode on a ring*, J. Phys. B: At. Mol. Opt. Phys., 41, 205503 (2008)
- [57] S. Choi, B. Sundaram, and M. G. Raizen: *Single-photon cooling in a wedge billiard*, Phys. Rev. A, 82, 033415 (2010)
- [58] E. A. Schoene, J. J. Thorn, and D. A. Steck: *Cooling atoms with a moving one-way barrier*, Phys. Rev. A, 82, 023419 (2010)
- [59] M. V. Berry: *Transitionless quantum driving*, J. Phys. A: Math. Theor., 42, 365303 (2009)
- [60] Y. Rezek, and R. Kosloff: *Irreversible performance of a quantum harmonic heat engine*, N. J. Phys., 8, 83 (2006)
- [61] M. Born, and V. A. Fock: *Beweis des Adiabaticensatzes*, Zeitschrift für Physik A, 51 (3-4), 165-180 (1928)
- [62] T. Kato: *On the Adiabatic Theorem of Quantum Mechanics*, J. Phys. Soc. Japan, 5 (6), 435-439 (1950)
- [63] A. Galindo, and P. Pascual: *Quantum Mechanics II*, Springer-Verlag Berlin Heidelberg (1991)

- [64] L. Ballentine: *Quantum Mechanics: A Modern Development*, World Scientific Publishing Co. Pte. Ltd (1998)
- [65] G. Nenciu: *On the adiabatic theorem of quantum mechanics*, J. Phys. A: Math. Gen., 13, L15-L18 (1980)
- [66] H. Narnhofer, and W. Thirring: *Adiabatic theorem in quantum statistical mechanics*, Phys. Rev. A, 26, 6 (1982)
- [67] J. E. Avron, R. Seiler, and L. G. Yaffe: *Adiabatic Theorems and Applications to the Quantum Hall Effect*, Commun. Math. Phys., 110, 33-49 (1987)
- [68] A. Polkovnikov, and V. Gritsev: *Breakdown of the adiabatic limit in low-dimensional gapless systems*, Nature Physics, 4, 477 (2008)
- [69] D. Aharonov, W. v. Dam, J. Kempe, Z. Landau, S. Lloyd, and O. Regev: *Adiabatic Quantum Computation is Equivalent to Standard Quantum Computation*, SIAM J. Comput., 37, 166 (2007)
- [70] A. T. Rezakhani, W.-J. Kuo, A. Hamma, D. A. Lidar, and P. Zanardi: *Quantum Adiabatic Brachistochrone*, Phys. Rev. Lett., 103, 080502 (2009)
- [71] H. R. Lewis, and W. B. Riesenfeld: *An Exact Quantum Theory of the Time-Dependent Harmonic Oscillator and of a Charged Particle in a Time-Dependent Electromagnetic Field*, J. Math. Phys., 10, 1458 (1969)
- [72] A. Leanhardt, T. A. Pasquini, M. Saba, A. Schirotzek, Y. Shin, D. Kielpinski, D. E. Pritchard, and W. Ketterle: *Cooling Bose-Einstein Condensates Below 500 Picokelvin*, Science, 301, 1513 (2003)
- [73] S. Bize, P. Laurent, M. Abgrall, H. Marion, I. Maksimovic, L. Cacciapuoti, J. Grünert, C. Vian, F. Pereira d. Santos, P. Rosenbusch, P. Lemonde, G. Santarelli, P. Wolf, A. Clairon, A. Luiten, M. Tobar, and C. Salomon: *Cold atom clocks and applications*, J. Phys. B: At. Mol. Opt. Phys., 38, S449 (2005)
- [74] A. K. Tuchman, W. Li, H. Chien, S. Dettmer, and M. A. Kasevich: *Localization and anomalous transport in a 1D soft boson optical lattice*, New J. Phys., 8, 311 (2006)
- [75] A. Bulatov, B. Vugmeister, and H. Rabitz: *Nonadiabatic cooling and optimal control in off-resonance dipole optical potentials*, Phys. Rev. A, 58, 1346 (1998)
- [76] A. Bulatov, B. E. Vugmeister, and H. Rabitz: *Nonadiabatic control of Bose-Einstein condensation in optical traps*, Phys. Rev. A, 60, 4875-4881 (1999)
- [77] T. Feldmann, and R. Kosloff: *Performance of discrete heat engines and heat pumps in finite time*, Phys. Rev. E, 61, 4774 (2000)
- [78] R. Kosloff, R. E. Geva, and J. M. Gordon: *Quantum refrigerators in quest of the absolute zero*, J. Appl. Phys., 87, 8093 (2000)
- [79] J. P. Palao, R. Kosloff, and J. M. Gordon: *Quantum thermodynamic cooling cycle*, Phys. Rev. E, 64, 056130 (2001)

- [80] T. Feldmann, and R. Kosloff: *Quantum four-stroke heat engine: Thermodynamic observables in a model with intrinsic friction*, Phys. Rev. E, 68, 016101 (2003)
- [81] L. Diósi, T. Feldmann, and R. Kosloff: *On the exact identity between thermodynamic and informatic entropies in a unitary model of friction*, Int. J. Quant. Inf., 4, 99-104 (2006)
- [82] T. Feldmann, and R. Kosloff: *Quantum lubrication: Suppression of friction in a first-principles four-stroke heat engine*, Phys. Rev. E, 73, 025107(R) (2006)
- [83] P. Salamon, K. H. Hoffmann, Y. Rezek, and R. Kosloff: *Maximum work in minimum time from a conservative quantum system*, Phys. Chem. Chem. Phys., 11, 1027 (2009)
- [84] Y. Rezek, P. Salamon, K. H. Hoffmann, and R. Kosloff: *The quantum refrigerator: The quest for absolute zero*, EPL, 85, 30008 (2009)
- [85] S. Brouard S, D. Macías, and J. G. Muga: *Perfect absorbers for stationary and wavepacket scattering*, J. Phys. A: Math. Gen., 27, L439 (1994)
- [86] J. P. Palao, J. G. Muga, and R. Sala: *Composite Absorbing Potentials*, Phys. Rev. Lett., 80, 5469 (1998)
- [87] A. Ruschhaupt, B. Navarro, and J. G. Muga: *Perfect detection of ultra-cold atoms by laser-induced ionization*, J. Phys. B: At. Mol. Opt. Phys., 37 L313 (2004)
- [88] J. G. Muga, X. Chen, A. Ruschhaupt, and D. Guéry-Odelin: *Frictionless dynamics of Bose-Einstein condensates under fast trap variations*, J. Phys. B: At. Mol. Opt. Phys., 42, 241001 (2009)
- [89] J. G. Muga, X. Chen, S. Ibáñez, I. Lizuain, and A. Ruschhaupt: *Transitionless quantum drivings for the harmonic oscillator*, J. Phys. B: At. Mol. Opt. Phys., 43, 085509 (2010)
- [90] X. Chen, I. Lizuain, A. Ruschhaupt, D. Guéry-Odelin, and J. G. Muga: *Shortcut to adiabatic passage in two and three level atoms*, Phys. Rev. Lett., 105, 123003 (2010)
- [91] X. Chen, and J. G. Muga: *Transient energy excitation in shortcuts to adiabaticity for the time dependent harmonic oscillator*, Phys. Rev. A, 82, 053403 (2010)
- [92] X. Chen, E. Torrontegui, and J. G. Muga: *Lewis-Riesenfeld invariants and transitionless quantum driving*, Phys. Rev. A, 83, 062116 (2011)
- [93] A. del Campo: *Fast frictionless dynamics as a toolbox for low-dimensional Bose-Einstein condensates*, EPL, 96, 60005 (2011)
- [94] E. Torrontegui, S. Ibáñez, A. Ruschhaupt, D. Guéry-Odelin, and J. G. Muga: *Fast atomic transport without vibrational heating*, Phys. Rev. A, 83, 013415 (2011)
- [95] S. Ibáñez, X. Chen, E. Torrontegui, A. Ruschhaupt, and J. G. Muga: *Multiple Schrödinger pictures and dynamics in shortcuts to adiabaticity*, arXiv:1112.5522v1 (2011)

-
- [96] A. del Campo, and M. G. Boshier: *Shortcuts to adiabaticity in a time-dependent box*, arXiv:1201.6627 (2012)
- [97] J.-F. Schaff, X.-L. Song, P. Vignolo, and G. Labeyrie: *Fast optimal transition between two equilibrium states*, Phys. Rev. A, 82, 033430 (2010)
- [98] J.-F. Schaff, X.-L. Song, P. Capuzzi, P. Vignolo, and G. Labeyrie: *Shortcut to adiabaticity for an interacting Bose-Einstein condensate*, EPL 93, 23001 (2011)
- [99] J.-F. Schaff, P. Capuzzi, G. Labeyrie, and P. Vignolo: *Shortcuts to adiabaticity for trapped ultracold gases*, New J. Phys., 13, 113017 (2011)
- [100] E. P. Gross: *Structure of a quantized vortex in boson systems*, Il Nuovo Cimento, 20, 454-457 (1961)
- [101] L. P. Pitaevskii: *Vortex Lines in an Imperfect Bose Gas*, Soviet Physics JETP, 13, 451-454 (1961)
- [102] C. J. Pethick, and H. Smith: *Bose-Einstein Condensation in Dilute Gases*, Cambridge University Press (2002)
- [103] L. P. Pitaevskii, and S. Stringari: *Bose-Einstein Condensation*, Oxford Clarendon Press (2003)
- [104] L. Erdős, B. Schlein, and H.-T. Yau: *Rigorous Derivation of the Gross-Pitaevskii Equation*, Phys. Rev. Lett., 98, 040404 (2007)
- [105] F. Dalfovo, S. Giorgini, L. P. Pitaevskii, and S. Stringari: *Theory of Bose-Einstein condensation in trapped gases*, Rev. Mod. Phys, 71, 463 (1999)
- [106] J. G. Hartley, and J. R. Ray: *Ermakov systems and quantum-mechanical superposition laws*, Phys. Rev. A, 24, 2873 (1981)
- [107] H. R. Lewis, and P. G. Leach: *A direct approach to finding exact invariants for onedimensional time dependent classical Hamiltonians*, J. Math. Phys., 23, 2371 (1982)
- [108] A. K. Dhara, and S. V. Lawande: *Feynman propagator for time-dependent Lagrangians possessing an invariant quadratic in momentum*, J. Phys. A: Math. Gen., 17, 2423 (1984)
- [109] M. A. Lohe: *Exact time dependence of solutions to the time-dependent Schrödinger equation*, J. Phys. A: Math. Theor., 42, 035307 (2009)
- [110] J.-Y. Ji, J. K. Kim, and S. P. Kim: *Heisenberg-picture approach to the exact quantum motion of a time-dependent harmonic oscillator*, Phys. Rev. A, 51, 4268-4271 (1995)
- [111] D. Y. Song: *Collective motions of a quantum gas confined in a harmonic trap*, Phys. Rev. A, 72, 023614 (2005)
- [112] D. Y. Song: *Exact coherent states of a noninteracting Fermi gas in a harmonic trap*, Phys. Rev. A, 74, 051602 (2006)

- [113] A. Minguzzi, and D. M. Gangardt: *Exact Coherent States of a Harmonically Confined Tonks-Girardeau Gas*, Phys. Rev. Lett. 94, 240404 (2005)
- [114] Y. Kagan, E. L. Surlov, and G. V. Shlyapnikov: *Evolution of a Bose-condensed gas under variations of the confining potential*, Phys. Rev. A, 54, R1753 (1996)
- [115] V. V. Dodonov, A. B. Klimov and D. E. Nikonov: *Quantum particle in a box with moving walls*, J. Math. Phys., 34, 3391-3404 (1993)
- [116] O. Ciftja: *A simple derivation of the exact wavefunction of a harmonic oscillator with time-dependent mass and frequency*, J. Phys. A: Math. Gen, 32, 6385 (1999)
- [117] S. W. Doescher, and M. H. Rice: *Infinite Square-Well Potential with a Moving Wall*, Am. J. Phys., 37, 1246 (1969)
- [118] S. B. Papp, J. M. Pino, and C. E. Wieman: *Tunable Miscibility in a Dual-Species Bose-Einstein Condensate*, Phys. Rev. Lett., 101, 040402 (2008)
- [119] T. A. Savard, K. M. OHara, and J. E. Thomas: *Laser-noise-induced heating in far-off resonance optical traps*, Phys. Rev. A, 56, R1095 (1997)
- [120] L. Khaykovich, F. Schreck, G. Ferrari, T. Bourdel, J. Cubizolles, L. D. Carr, Y. Castin, and C. Salomon: *Formation of a Matter-Wave Bright Soliton*, Science, 296, 1290 (2002)
- [121] T. Kinoshita, T. Wenger, and D. S. Weiss: *All-optical Bose-Einstein condensation using a compressible crossed dipole trap*, Phys. Rev. A, 71, 011602 (2005)
- [122] E. Torrontegui, X. Chen, M. Modugno, A. Ruschhaupt, D. Guéry-Odelin, and J. G. Muga: *Fast transitionless expansions of cold atoms in optical Gaussian beam traps*, Phys. Rev. A, 85, 033605 (2012)
- [123] T. L. Gustavson, A. P. Chikkatur, A. E. Leanhardt, A. Görlitz, S. Gupta, D. E. Pritchard, and W. Ketterle: *Transport of Bose-Einstein Condensates with Optical Tweezers*, Phys. Rev. Lett, 88, 020401 (2002)
- [124] W. Hänsel, P. Hommelhoff, T. W. Hänsch, and J. Reichel: *Bose-Einstein condensation on a microelectronic chip*, Nature, 413, 498-501 (2001)
- [125] S. Schmid, G. Thalhammer, K. Winkler, F. Lang, and J. H. Denschlag: *Long distance transport of ultracold atoms using a 1D optical lattice*, New J. Phys., 8, 159 (2006)
- [126] D. Xiong, P. Wang, Z. Fu, and J. Zhang: *Transport of Bose-Einstein condensate in QUIC trap and separation of trapping spin states*, Opt. Express, 18, 1649 (2010)
- [127] A. Couvert, T. Kawalec, G. Reinaudi, and D. Guéry-Odelin: *Optimal transport of ultracold atoms in the non-adiabatic regime*, EPL. 83, 13001 (2008)
- [128] M. Murphy, L. Jiang, N. Khaneja, and T. Calarco: *High-fidelity fast quantum transport with imperfect controls*, Phys. Rev. A, 79, 020301 (2009)

- [129] S. Masuda, and K. Nakamura: *Fast-forward of adiabatic dynamics in quantum mechanics*, Proc. R. Soc. A, 466, 1135 (2010)
- [130] W. Hänsel, J. Reichel, P. Hommelhoff, and T. W. Hänsch: *Magnetic Conveyor Belt for Transporting and Merging Trapped Atom Clouds*, Phys. Rev. Lett., 86, 608 (2001)
- [131] A. Günther, M. Kemmler, S. Kraft, C. J. Vale, C. Zimmermann, and J. Fortagh: *Combined chips for atom optics*, Phys. Rev. A, 71, 63619 (2005)
- [132] T.-J. Tarn, G. Huang, and J. W. Clark: *Modelling of quantum mechanical control systems*, Mathematical Modelling, 1, 109 (1980)
- [133] A. Pierce, M. Dahleh, and H. Rabitz: *Optimal control of quantum-mechanical systems: Existence, numerical approximation, and applications*, Phys. Rev. A, 37, 4950 (1988)
- [134] L. Shen, and H. Rabitz: *Optimal Control of Molecular Rotation in the Sudden Limit*, J. Phys. Chem., 95, 1047-1053 (1991)
- [135] L. Shen, S. Shi, and H. Rabitz: *Optimal Control of Coherent Wave Functions: A Linearized Quantum Dynamical View*, J. Phys. Chem., 97, 12114-12121 (1993)
- [136] S. Lloyd, and L. Viola: *Engineering quantum dynamics*, Phys. Rev. A, 65, 010101(R) (2001)
- [137] D. Stefanatos, N. Khaneja, and S. J. Glaser: *Optimal control of coupled spins in the presence of longitudinal and transverse relaxation*, Phys. Rev. A, 69, 022319 (2004)
- [138] I. I. Maximov, Z. Tošner, and N. C. Nielsen: *Optimal control design of NMR and dynamic nuclear polarization experiments using monotonically convergent algorithms*, J. Chem. Phys., 128, 184505 (2008)
- [139] J.-S. Li, J. Ruths, and D. Stefanatos: *A pseudospectral method for optimal control of open quantum systems*, J. Chem. Phys., 131, 164110 (2009)
- [140] T. Schulte-Herbrüggen, S. J. Glaser, G. Dirr, and U. Helmke: *Gradient Flows for Optimization in Quantum Information and Quantum Dynamics: Foundations and Applications*, Rev. Math. Phys., 22, 597 (2010)
- [141] D. Stefanatos, J. Ruths, and J.-S. Li: *Frictionless atom cooling in harmonic traps: A time-optimal approach*, Phys. Rev. A, 82, 063422 (2010)
- [142] D. Stefanatos, H. Schaettler, and J.-S. Li: *Minimum-time frictionless atom cooling in harmonic traps*, SIAM J. Control Optim., 49, 2440-2462 (2010)
- [143] D. Stefanatos, and J.-S. Li: *The role of Singular Control in Frictionless Atom Cooling in a Harmonic Trapping Potential*, arXiv:1103.1665 (2011)
- [144] Donald E. Kirk: *Optimal Control Theory*, Dover Publications Inc., Mineola, New York (2004)

- [145] V. G. Boltyanskii, R. V. Gamkrelidze, and L. S. Pontryagin: *Towards a theory of optimal processes*, (Russian), Reports Acad. Sci. USSR, Vol. 110(1) (1956)
- [146] L. S. Pontryagin, V. G. Boltyanskii, R. V. Gamkrelidze, and E. F. Mishchenko: *The Mathematical Theory of Optimal Processes*, (Russian), English translation: Interscience 1962, ISBN 2881240771 and ISBN 978-2881240775 Dover Publications, Inc., Mineola, New York (2004)
- [147] D. Stefanatos, and J.-S. Li: *Minimum-Time Quantum Transport with Bounded Trap Velocity*, arXiv:1107.1691 (2011)
- [148] X. Chen, E. Torrontegui, D. Stefanatos, J.-S. Li, and J. G. Muga: *Optimal trajectories for efficient atomic transport without final excitation*, Phys. Rev. A, 84, 043415 (2011)
- [149] K. H. Hoffmann, P. Salamon, Y. Rezek, and R. Kosloff: *Time-optimal controls for frictionless cooling in harmonic traps*, EPL, 96, 60015 (2011)
- [150] Y. Rezek: *Reflections on Friction in Quantum Mechanics*, Entropy, 12 8, 1885-1901 (2010)
- [151] V. M. Pérez-García, P. J. Torres, and V. V. Konotop: *Similarity transformations for nonlinear Schrödinger equations with time-dependent coefficients*, Physica D, 221, 31 (2006)
- [152] S. Y. T. v.d. Meerakker, H. L. Bethlem, and G. Meijer: *Taming molecular beams*, Nature Physics, 4, 595 (2008)
- [153] R. Zwanzig: *Ensemble Method in the Theory of Irreversibility*, J. Chem. Phys., 33, 5 (1960)
- [154] J.W. Thomas: *Numerical Partial Differential Equations: Finite Difference Methods*, Texts in Applied Mathematics, 22, Springer Verlag (1995)
- [155] W. H. Press, S. A. Teukolsky, W. T. Vetterling, and B. P. Flannery: *Numerical Recipes in C*, Cambridge University Press (1997)
- [156] M. Frigo, and S. G. Johnson: *The Design and Implementation of FFTW3*, Proceedings of the IEEE, Vol. 93 No. 2, 216-231 (2005)
- [157] <http://www.fftw.org/>
- [158] http://www.nvidia.com/object/cuda_home_new.html
- [159] P.J. Davis, and P. Rabinowitz: *Methods of Numerical Integration*, Dover Publications. Inc., 2nd Edition (2007)
- [160] V. Hutson, J. S. Pym, and M. Cloud: *Applications of functional analysis and operator theory*, Mathematics in Science and Engineering, Vol. 200, Elsevier (2005)
- [161] H. J. Sussmann: *Time-optimal control in the plane*, Feedback Control of Linear and Nonlinear Systems, Lecture Notes in Control and Information Sciences, Vol. 39, 244-260, Springer-Verlag, Berlin (1982)

-
- [162] H. J. Sussmann: *The structure of time-optimal trajectories for single-input systems in the plane: the C^∞ nonsingular case*, SIAM J. Control Optim., 25, 433-465 (1987)
- [163] B. Simon: *Representations of Finite and Compact Groups*, Oxford University Press (1995)
- [164] A. Baker: *Matrix Groups: An Introduction to Lie Group Theory*, Springer-Verlag London (2002)

Curriculum Vitae

Dipl.-Phys. Sönke Schmidt

Ungerstraße. 26
30451 Hannover

Biographische Daten

Geburtstag: 08.09.1982
Geburtstort: Bremerhaven
Staatsangehörigkeit: deutsch

Wissenschaftlicher Werdegang

07/2002 Abitur am Niedersächsischen Internatsgymnasium in
Bad Bederkesa

2002 - 2008 Studium der Physik an der Technischen Universität Carolo-
Wilhelmina zu Braunschweig. Diplomarbeit am Institut für
Mathematische Physik unter Anleitung von
Prof. Dr. A. Ruschhaupt und Prof. Dr. R. F. Werner.

09/2004 Vordiplom in Physik

04/2008 Diplom in Physik

04/2008 - 04/2009 Promotion am Institut für Mathematische Physik an der
Technischen Universität Carolo-Wilhelmina zu Braunschweig
unter Anleitung von Prof. Dr. A. Ruschhaupt in der Arbeits-
gruppe "Quanteninformationstheorie" unter der Leitung
von Prof. Dr. R. F. Werner.

04/2009 Promotion am Institut für Theoretische Physik an der
Gottfried Wilhelm Leibniz Universität Hannover unter
Anleitung von Prof. Dr. A. Ruschhaupt in der Arbeitsgruppe
"Quanteninformationstheorie" unter der Leitung von
Prof. Dr. R. F. Werner.